Development of green sample preparation methods for the analysis of organic substances in aqueous matrices with gas chromatography mass spectrometry

Dissertation

zur Erlangung des akademischen Grades eines
Doktors der Naturwissenschaften
-Dr. rer. Nat.-

vorgelegt von

Lucie Katharina Tintrop

geboren in Oberhausen

Lehrstuhl für Instrumentelle Analytische Chemie
der Universität Duisburg-Essen

2023

Die vorliegende Arbeit wurde im Zeitraum von November 2020 bis Oktober 2023 am Lehrstuhl für Instrumentelle Analytische Chemie von Prof. Dr. Torsten C. Schmidt angefertigt.

Tag der Disputation: 26.01.2024

Gutachter: Prof. Dr. Torsten C. Schmidt
Prof. Dr. Oliver J. Schmitz

Vositzender: Prof. Dr. Mathias Ropohl

DOI: 10.17185/duepublico/81764
URN: urn:nbn:de:hbz:465-20240320-080826-2

Danksagung

Ich möchte bei allen bedanken die mich während der langen drei Jahre fachlich als auch emotional unterstützt haben und somit nachhaltig zu dieser Arbeit beigetragen haben. Besonders möchte ich mich bei meiner Familie und meinen Freunden bedanken.

Zudem danke ich meinen Studierenden, die bei mir ihre Praktika oder Abschlussarbeiten absolviert haben und mit großen Interesse und Erfolg mit mir zusammen geforscht haben: Thomas Beesley, Jana Lieske-Overgrand, Kaliyani Wickneswaran, Willi Eßer und Leonardo Solazzo. Des Weiteren danke ich meiner langjährigen wissenschaftlichen Hilfskraft Rukiyye Abis für die viele Laborarbeit die sie mir gewissenhaft abgenommen hat.

In der Instrumentellen Analytischen Chemie danke ich allen Mitarbeitern für die großartige Zeit die ich bereits seit meiner Bachelorarbeit mit euch verbringen durfte. Mein besonderer Dank gilt Klaus Kerpen, Simone Bettinger, Sasho Joksimoski, Max Reuschenbach und Robert Marks für die technische Unterstützung im GC-Labor und die fachlichen Diskussionen.

Für ihre fachliche Expertise im Bereich der Mikroextraktionsmethoden für die Gas Chromatographie möchte ich besonders Maik A. Jochmann, Amir Salemi und Werner Engewald danken, ich fand es sehr spannend mit euch zusammenzuarbeiten und habe viel von euch lernen können.

Meinen Kooperationspartnern Ruth Brunstermann vom Fachbereich Siedlungswasser- und Abfallwirtschaft der Universität Duisburg-Essen, Stefan Cretnik und Günther Böhm von CTC Analytics, Beat Schilling von BGB Analytik und Sonja Klee, Steffen Bräkling und Marleen Vetter von Tofwerk danke ich für die Unterstützung und dafür, dass ihr mir eure Projekte anvertraut habt. Es hat mir viel Freude gemacht mit euch zu arbeiten.

Mein besonderer Dank gilt Torsten C. Schmidt dafür, dass er mir das Vertrauen geschenkt hat meine Arbeit an seinem Lehrstuhl durchführen zu können, mir den Freiraum gelassen hat mich weiterzuentwickeln und meine eigenen Ideen zu erarbeiten, für die fachlichen Diskussionen und die großartige Unterstützung.

Abstract

The demand for green analytical methods is increasing. Microextraction methods pose the green alternative to large-scale extractions in research as well as in standard methods. The world's most used and well-accepted microextraction technique, solid-phase microextraction (SPME), is solvent-free, miniaturized, simple to handle, and automatable. The drawbacks of SPME, such as the poor mechanical resilience and small phase volume, were rectified by its further development SPME arrow. For water analysis using gas chromatography mass spectrometry (GC-MS), the choice of the extraction method is a critical step in terms of analytical performance and greenness. Nevertheless, the standardization of microextraction methods is still lacking. Therefore, this thesis investigates the applicability of SPME and SPME arrow for GC-MS water analysis in the fields of industrial process surveillance for the analysis of fatty acids and fatty acid methyl esters and non-targeted wastewater monitoring. Moreover, several challenges such as the combination of microextraction and derivatization, fiber cleaning, and extraction of analytes with different polarities are addressed. The optimization of the critical extraction parameters, such as time, temperature, and pH, by design of experiments significantly increased the gained response in all the applications and is discussed in detail to minimize the effort for future use and development of the methods. A chemical-thermal fiber cleaning procedure was developed, which substantially reduced the carry-over effect. The method detection limits obtained in this study ranged from low ng L^{-1} to low µg L^{-1}, which is lower than achieved by several research studies. With SPME headspace operation, no pre-treatment was necessary, even though the samples possess complex matrices. Additional reduction of sample matrix-based analysis interferences for target analysis was implemented by selective tandem mass spectrometry. A non-target approach using GC time-of-flight mass spectrometry with parallel electron ionization (EI) and chemical ionization (CI) was tested in combination with a prototype hydrophilic-lipophilic balanced (HLB) SPME with special focus laid on the identification of substances using the complementary dataset from EI and CI. The approach extracted and analyzed analytes with very different polarities resulting in the expectation that the HLB could become the new use-one-for-all material in SPME. For the investigated research fields, SPME and SPME arrow performed well, consequently their future implementation in standard methods is supported by the obtained results.

Zusammenfassung

Die Nachfrage nach grünen Analysemethoden steigt. Mikroextraktionsverfahren sind die grüne Alternative zu groß angelegten Extraktionen in der Forschung und Standardmethoden. Die weltweit am häufigsten verwendete und akzeptierte Mikroextraktionstechnik, die Festphasenmikroextraktion (SPME), ist lösungsmittelfrei, miniaturisiert, einfach zu handhaben und automatisierbar. Die Nachteile der SPME, wie die geringe mechanische Belastbarkeit und das kleine Phasenvolumen, wurden durch die Weiterentwicklung SPME Arrow verbessert. In der Wasseranalytik mittels Gaschromatographie Massenspektrometrie (GC-MS) ist die Wahl der Extraktionsmethode ein entscheidender Schritt in Bezug auf die analytische Performance und Umweltfreundlichkeit. Die Standardisierung von Mikroextraktionsmethoden ist jedoch noch nicht weit fortgeschritten. Daher wird in dieser Arbeit die Anwendbarkeit von SPME und SPME Arrow für die Wasseranalytik mittels GC-MS in den Bereichen der industriellen Prozessüberwachung zur Analyse von Fettsäuren und Fettsäuremethylestern und der Non-Target Abwasserüberwachung untersucht. Darüber hinaus werden verschiedene Herausforderungen wie die Kombination von Mikroextraktion und Derivatisierung, die Faserreinigung und die Extraktion von Analyten mit unterschiedlichen Polaritäten untersucht. Die Optimierung der kritischen Extraktionsparameter, wie Zeit, Temperatur und pH-Wert, durch statistische Versuchsplanung steigerte die gewonnenen Ergebnisse in allen Anwendungen erheblich und wird ausführlich diskutiert, um den Aufwand für die zukünftige Nutzung und Entwicklung der Methoden zu minimieren. Es wurde ein chemisch-thermisches Faserreinigungsverfahren entwickelt, das den Verschleppungseffekt erheblich reduziert. Die in dieser Studie erzielten Nachweisgrenzen reichten von niedrigen ng L^{-1} bis zu niedrigen µg L^{-1}, und liegen unter denen anderer Forschungsstudien. Durch die SPME Headspace Anreicherung war keine Vorbehandlung erforderlich, obwohl die Proben komplexe Matrices aufweisen. Eine zusätzliche Verringerung der durch die Probenmatrix induzierten Interferenzen für die Target-Analyse wurde durch selektive Tandem-Massenspektrometrie erreicht. Ein Non-Target-Ansatz unter Verwendung der GC-Flugzeit-Massenspektrometrie mit paralleler Elektronenionisation (EI) und chemischer Ionisation (CI) wurde in Kombination mit dem Prototyp einer hydrophil-lipophilen balancierten (HLB) SPME getestet, wobei der Schwerpunkt auf der Identifizierung von Substanzen unter Verwendung des komplementären Datensatzes von EI und CI lag.

Diese Anwendung extrahierte und analysierte Analyten mit sehr unterschiedlichen Polaritäten, sodass HLB das neue "Eins-für-alles"-Material für SPME werden könnte. Für die untersuchten Forschungsbereiche haben SPME und SPME Arrow gut abgeschnitten, sodass ihre künftige Implementierung in Standardmethoden durch die generierten Ergebnisse unterstützt wird.

Contents

1 General introduction

Water analysis of organic compounds holds immense significance due to the prevalence of aqueous processes in various sectors, including environmental monitoring in aquatic bodies [1, 2], industrial process surveillance [3], and wastewater treatment [4]. The Water Framework Directive (European Directive 2000/60/EC) [5] poses the main law of the European Union for water protection. Next to guiding community action for obtaining a “good ecological and chemical status” of surface waters, it lists priority substances that should not exceed specific threshold values. Industrial production accounts for a large share of environmental pollution worldwide. Many industrial processes involve water as a solvent or reactant, therefore in the European Union, the Industrial Emissions Directive [6] regulates the wastewater discharge of industrial production plants next to air emissions and waste generation.
In addition to environmental protection and pollution prevention, water analysis in industry is applied to monitor processes and improve their effectiveness. For example, bioreactors can be used to produce useful chemical products or biodiesel from waste or wastewater [7, 8]. The feed of bioreactors is heterogeneous and complex and deployed microorganisms are potentially sensitive to changes in conditions, so the production process is not uniform. Hence, the yields of the converted products and consumed substrates in the bioreactor need to be monitored to supervise effectiveness and discover occurring problems. [9] Fatty acids (FAs) and fatty acid methyl esters (FAMEs) are desired bioreactor products for large-scale industrial production. [10] On the other hand, specific FAMEs and FAs are known to interfere with relevant anaerobic digestion processes e.g., in wastewater treatment or biodiesel production, so their monitoring is of high relevance. [11-13]

These above-mentioned applications provide the impetus for the development and implementation of robust analytical techniques to detect and quantify organic compounds in water. Gas chromatography (GC) is a widely employed analytical technique due to its ability to separate volatile to semi-volatile organic compounds in complex matrices or as complex mixtures based on their vapor pressure and retention on the chromatographic column. In the context of water analysis, GC is less commonly applied compared to high-performance liquid chromatography (HPLC) but is essential for the analysis of certain substance classes and offers additional advantages. For

example, the resolution of GC is higher than of HPLC, due to smaller peak widths. GC coupled to a single-quadrupole mass spectrometer (MS) and tandem mass spectrometer (MS/MS) are very common approaches for the qualification and quantification of target compounds. Some standard methods utilize GC-MS for water analysis such as United States Environmental Protection Agency (USEPA) method 8272 [14] and International Organization for Standardization (ISO) method 12010 [15]. MS/MS is used in target analysis to gain a higher selectivity and exclude disturbing substances or matrix constituents by utilizing, for example, a second fragmentation and a second mass filter for each compound, which is the so-called multiple reaction monitoring (MRM). The substances are ionized and/or fragmented generating fragmentation patterns leading to unique mass spectra that are used for compound identification. Especially electron ionization (EI), generates fingerprint-like spectra for each compound, which contain valuable information about the substance at hand, for example, heteroatoms, isotopic patterns, and structural information, and can also be matched with database spectra. Chemical ionization (CI) is considered a “soft” ionization approach, which generates less to almost no fragmentation pattern in the mass spectra and hence is often used to receive molecular ion information of the substance, whereas, in EI, the molecular ion is often absent or low abundant. For non-target analysis (NTA), a common approach is high-resolution mass spectrometry (HRMS), which enables enhanced compound identification, due to the determination of the exact mass of fragment ions, molecular ions, and adduct ions.

Effective sample preparation is indispensable in water analysis using GC. Aqueous samples pose challenges such as the presence of water, dissolved solids, and matrix constituents that can interfere with the separation and detection of the analytes. Sample pretreatment steps are essential to concentrate target compounds, eliminate matrix components, and reduce potential interferences. Microextraction techniques offer valuable solutions to these challenges and gained prominence in analytical chemistry in recent years. Microextraction methods are characterized by their ability to extract trace-level analytes from small sample volumes, minimizing the need for extensive sample handling and reducing solvent consumption. The most prominent microextraction technique, SPME involves the use of a coated fiber to selectively sorb analytes from the sample matrix. This solvent-free approach reduces the risk of analyte losses and contamination during extraction. [16] Microextraction techniques align with

the principles of Green Analytical Chemistry (GAC) by reducing the use of solvents, minimizing waste generation, and allowing automation. [17, 18] The miniaturization inherent to these methods also aligns with the trend toward analytical portability and field-based analyses. [19] Additionally, microextraction techniques offer high extraction efficiency, enhanced sensitivity, and selectivity, even for analytes present in low concentrations in water samples. [20]

Recently, a lot of effort has been made to develop and validate novel extraction materials. [21-25] The demand for new materials usually results from the need for either greener materials [26, 27], very specific and selective materials [28, 29], or biocompatible materials [30]. In water analysis, the coverage of a wide polarity range is so far insufficient by the commercially available microextraction options. The classical phase materials for SPME such as polydimethylsiloxane (PDMS) and carbon wide range (CWR) are applied for nonpolar molecules and in combination with divinylbenzene (DVB) for polar molecules to non-polar molecules. A relatively new material in SPME to cover lipophilic as well as hydrophilic molecules is the hydrophilic-lipophilic balanced (HLB) material which contains both polar and nonpolar groups. [31]

Sample preparation depends on various physical and chemical parameters. To develop a method with optimal sample preparation conditions, such as extraction and derivatization, and consequently gain the highest response possible, an optimization strategy must be applied. One-factor-at-a-time (OFAT) describes the strategy to optimize one factor after another, which is easy to operate but requires more laboratory work, generates a large dataset, spends a lot of measurements, and is prone to miss an optimum if parameters interact. Another approach that is in perfect agreement with GAC is statistical experimental planning also called the design of experiments (DOE). By applying a DOE approach, several parameters can be optimized at the same time by using a multi-dimensional factor combination approach, which requires fewer measurements than an OFAT approach. Additionally, factor combinations such as dependence on extraction temperature and extraction time are observed. However, a DOE approach is more complex in operation and data evaluation as several parameter combinations are measured. An automated sample preparation setup (xyz-autosamples) is favored for DOE rendering almost no laboratory work, otherwise, the parameters have to be changed manually for each run, which would not be feasible. [32, 33]

As the analytical landscape continues to evolve, the integration of GC with microextraction techniques holds promise for enhancing water analysis and contributing to a greener analytical future.

2 Scope and aim

Analysis of aqueous samples is important in various application fields. Gas chromatography (GC) coupled with mass spectrometry (MS), tandem mass spectrometry (MS/MS), or high-resolution mass spectrometry (HRMS) combined with microextractions offer several advantages. Microextractions are miniaturized, automatable, and use low amounts to no solvents. In recent years the demand for greener chemistry and consequently greener analytical methods rapidly increased and surely will further increase in the next years. However, the application of microextractions in official analytical standard methods is still lacking. Therefore, this work aims to establish a basis for the standardization of microextractions combined with GC-MS for water analysis. For this purpose, new methods supporting microextraction techniques were developed, validated, and tested for different applications, and a novel extraction material was characterized. An overview of the covered topics is presented in Figure 2.1.

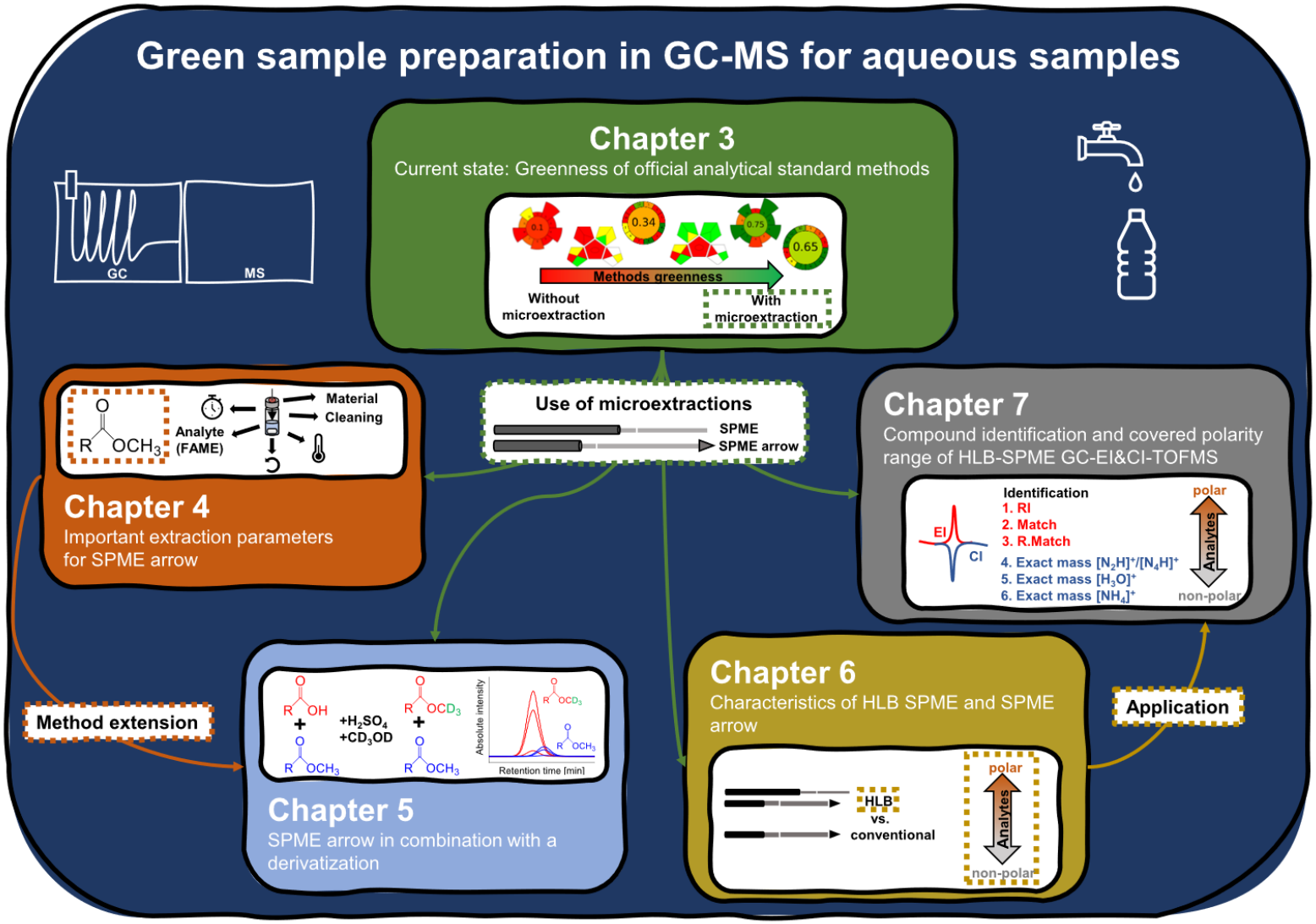

Figure 2.1 Graphical overview of the covered topics of this thesis. Thematical relationships of the chapters are displayed by colored arrows and dashed boxes.

To give an insight into the current state and how standard analytical methods can be improved in terms of greenness and sustainability using microextractions, a critical literature review is presented in Chapter 3. The most common microextraction methods are discussed and compared based on their greenness and standard analytical methods from the United States Environmental Protection Agency are evaluated with greenness evaluation tools and compared to published replacement methods using microextractions. Based on the review's conclusions all following chapters included microextractions.

Chapter 4 deals with a basic investigation on what are the important parameters influencing SPME arrow extraction applied to a simple headspace extraction of fatty acid methyl esters from aqueous samples. For a basic understanding of microextraction processes, it is important to investigate how the extraction parameters influence analytical performance, which helps to identify and overcome the limitations. The optimized and automated method finds application for the analysis of aqueous samples from a bioreactor.

Although derivatizations should be avoided according to the requirements of Green Analytical Chemistry, in some GC applications they are essential. However, the combination of a derivatization reaction with a solvent-free microextraction method is advantageous and was studied in Chapter 5. The simultaneous analysis of fatty acids and fatty acid methyl esters is challenging. Overcoming this challenge, an isotope-labeling in-situ derivatization of a broad range of different fatty acids with subsequent SPME arrow headspace extraction was developed, which allowed the additional analysis of fatty acid methyl esters, by further developing the method from Chapter 4. The method was evaluated with surface water samples and samples from different bioreactor experiments. Many standard and research methods implement a derivatization so the feasibility of microextraction in combination with derivatization has to be investigated to facilitate the standardization.

The choice of the extraction material is a critical step in SPME. Especially covering analytes with large differences in polarity is challenging as the material must ensure chemical interaction with polar as well as non-polar structures. Newly developed hydrophilic-lipophilic balanced (HLB) SPME and SPME arrow prototypes developed by CTC Analytics were characterized in Chapter 6 by using analytes of different substance classes. The development of novel phase materials is driven by specific requirements that remain uncovered by the commercial phase materials. Therefore,

the characterization is intended to discover if the requirements are properly met and to evaluate the future potential of HLB SPME and SPME arrow material.

The novel HLB SPME material characterized in Chapter 6 was tested in a non-target GC time-of-flight mass spectrometry (TOFMS) approach with parallel electron ionization (EI) and chemical ionization (CI) in Chapter 7. Specific focus was placed on the compound identification workflow using electron and chemical ionization data. Further, the extracted substances were classified by their chemical composition, substance class, and polarity. The investigation of the covered polarity range of the analytes by the headspace HLB SPME extraction and subsequent GC-EI&CI-TOFMS evaluates the potential of the HLB SPME material in non-target approaches.

3 Improving greenness and sustainability of standard analytical methods by microextraction techniques

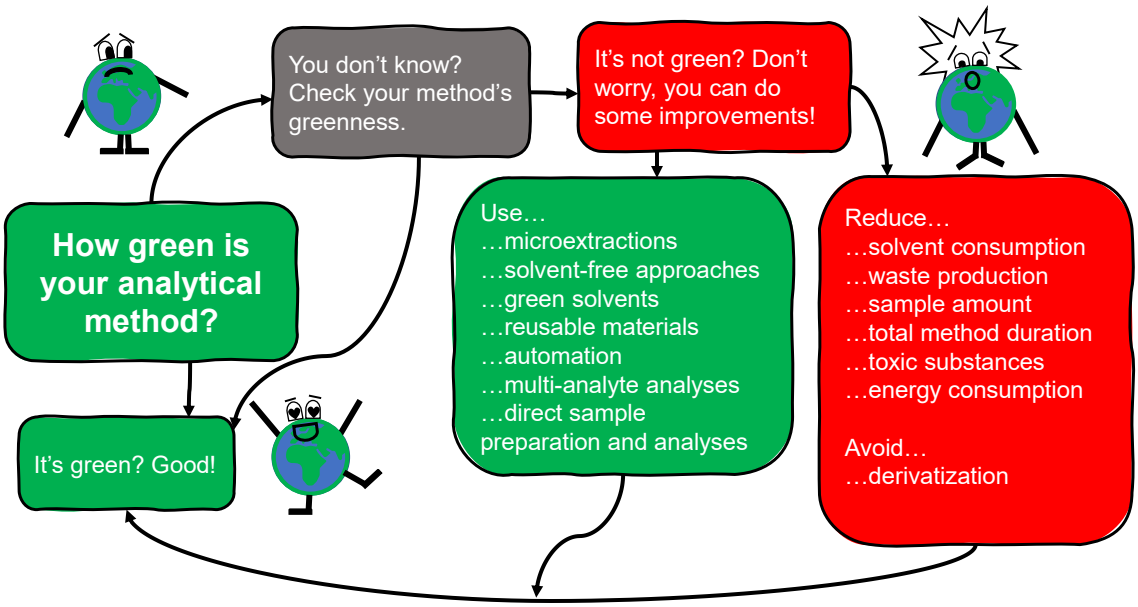

Adapted from: Lucie K. Tintrop, Amir Salemi, Maik A. Jochmann, Werner R. Engewald, Torsten C. Schmidt. Improving greenness and sustainability of standard analytical methods by microextraction techniques: A critical review, published in Analytica Chimica Acta (2023). © Elsevier 2023

3.1 Abstract

Since environmental awareness has increased in analytical chemistry, the demand for green sample preparation methods continues to grow. Microextractions such as solid-phase microextraction (SPME) and liquid-phase microextraction (LPME) miniaturize the pre-concentration step and are a more sustainable alternative to conventional large-scale extractions. However, the integration of microextractions in standard and routine analysis methods is rare, although these applications are used most frequently and have a role model function. Therefore, it is important to highlight that microextractions are capable of replacing large-scale extractions in standard and routine methods. This review discusses the greenness, benefits, and drawbacks of the most common LPME and SPME variants compatible with gas chromatography based on the following key evaluation principles: Automation, solvent consumption, hazards, reusability, energy consumption, time efficiency, and handling. Furthermore, the need

to integrate microextractions into standard and routine analytical methods is presented by using method greenness evaluation metrics AGREE, AGREEprep, and GAPI applied to USEPA methods and their replacements.

3.2 Introduction

Microextractions are green alternatives to large-scale extractions such as liquid extraction (LE), liquid-liquid extraction (LLE), and solid-phase extraction (SPE), due to their miniaturization associated with reduced use of resources, reusability, and enhanced user safety. For research laboratories, it is nowadays unpopular to use methods such as large-scale LE that require a high amount of solvent. Unfortunately, in routine analysis laboratories, LLE and SPE methods are still dominating, although greener replacement methods are increasingly available. This review aims to discuss the benefits and drawbacks of microextractions based on greenness parameters. Further, tools for greenness evaluation of analytical methods are presented and United States Environmental Protection Agency (USEPA) standard methods and published microextraction replacement methods are compared using the Analytical GREEnness metric approach (AGREE), AGREEprep and the Green Analytical Procedure Index (GAPI) to demonstrate the need for further miniaturization of standard and routine analysis methods. The main focus is on microextraction methods that are compatible with gas chromatography, adaptions for liquid chromatography are only exemplarily mentioned.

3.2.1 Method greenness evaluation

Analytical chemistry was aware early of its actions and the environmental impact of analytic processes. In 1999 Anastas and Warner first defined the principles of Green Chemistry [34] which since then have been evaluated and further defined for Green Analytical Chemistry (GAC) by various researchers [17, 35, 36]. In particular, chromatography [37] and microextractions [38, 39] were examined for their sustainability. The requirements for ideal green analytical methods originated from Green Chemistry and include but are not limited to [40, 41]:

- Direct, automatized, miniaturized, and multi-analyte approaches
- Minimal sample size, number of processed samples, and pre-treatment
- Reduction of chemical consumption and waste generation
- Reduction of hazards and risks
- Increased work safety and environmental friendliness.

For an overview of the evolution of green chemistry and green technical developments see Figure 3.1.

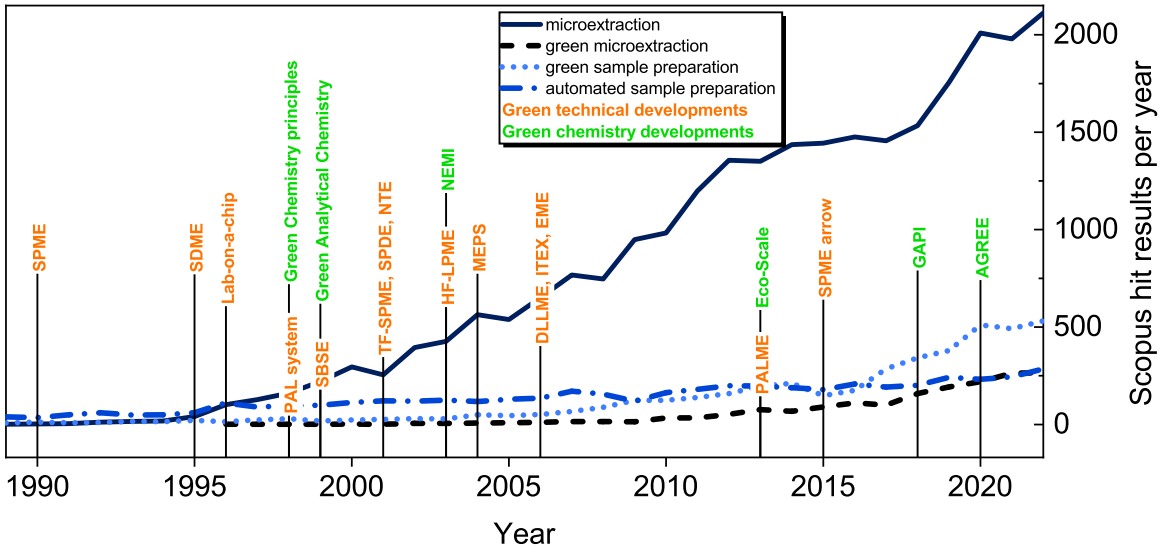

Figure 3.1 Evolution of Green Chemistry (green) and green technical developments (orange) over the past three decades. Lines display the Scopus hits per year for the terms “microextraction” (dark-blue line), “green microextraction” (black dashed line), “green sample preparation” (light-blue dotted line), and “automated sample preparation” (mid-blue dashed-dotted line). For abbreviations see Table 9.23 in the appendix.

The more resources, steps, and risks involved in an analytical procedure, the less green this method becomes. Therefore, the prevention of unnecessary or redundant procedures is an essential aspect of the way to more sustainable analytical chemistry. However, it seems to be difficult to find consensus on the question of what ‘green’ really means in practice. To improve this, evaluation metrics have been established to quantify the greenness of analytical methods, often with greenness scores. An ideal green method achieves the maximum score of the respective metric. One of the oldest metrics is the National Environmental Method Index (NEMI, 2002) by the United States Environmental Protection Agency (USEPA) and the United States Geological Survey (USGS), which includes a free website (www.nemi.gov) for informed green method selection from over 800 methods. The easy-to-understand greenness profile of NEMI shows four fields rating persistent, bioaccumulative, and toxic (PBT) chemicals, hazardous chemicals, corrosiveness, and waste as colored pictograms (Figure 3.2). [42] Another metric is the Analytical Eco-Scale (2012), which goes more into detail by subtraction of penalty points from a total of 100 points when parameters are not in agreement with an ideal green method [43]. The Green Analytical Procedure Index (GAPI, 2018) considers all steps of the analytical method covering sampling, sample

preparation, used reagents and compounds, instrumentation, and determination. By using multicriteria decision analysis, a symbol with five pentagrammes for each step of the analytical method is created (Figure 3.2) [44]. GAPI has been further improved and, under the name ComplexGAPI, additionally includes the greenness of the production of materials and chemicals for the subsequent analysis step. ComplexGAPI can be downloaded free of charge from the website www.mostwiedzy.pl/complexgapi. [45] The Analytical GREEnness Metric Approach (AGREE, 2020) includes an assessment of parameters from the 12 principles of GAC according to Galuszka et al. [40], unified into a 0-1 scale. The resulting pictograms show the final score of the analytical method and the score in each criterion as well (Figure 3.2). The software is freely downloadable on a website (www.mostwiedzy.pl/AGREE). [46] Another approach based on AGREE but modified specifically for sample preparation is AGREEprep (Figure 3.2), freely downloadable from mostwiedzy.pl/agreeprep. [47, 48] Figure 3.2 shows the pictograms of NEMI, GAPI, AGREE, and AGREEprep and also states the categories which are rated.

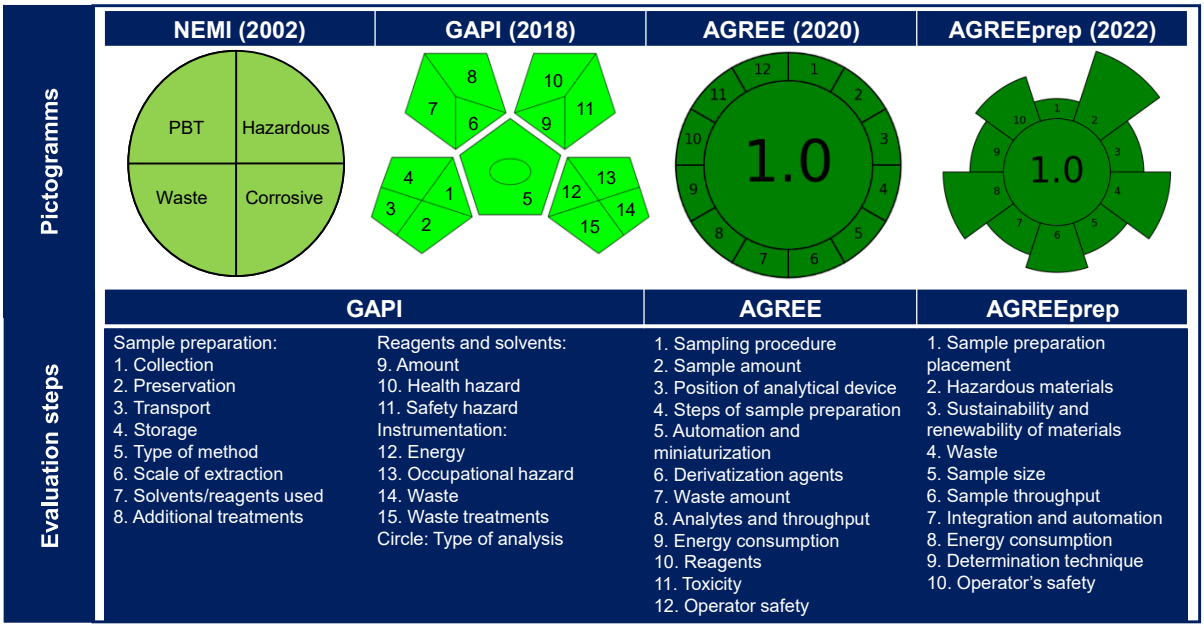

Figure 3.2 Example pictograms and detailed information about the evaluated steps of the National Environmental Method Index (NEMI), Green Analytical Procedure Index (GAPI), Analytical GREEnness Metric Approach (AGREE), and AGREEprep. PBT: Persistent, bioaccumulative, and toxic chemicals; Colors display the scoring of the different categories from green (good) to red (bad); AGREE/AGREEprep: the numbers in the ring display the different categories whereas the number in the middle displays the total method score.

Besides the many publications describing the need for green methods and green evaluations, there are also some that question the need for green analytical chemistry.

It is suggested that the methods should be primarily fit-for-purpose and have a high analytical performance and practicability. [49] The concept of white analytical chemistry combines all these factors of greenness, performance, and practicality of a method. Based on this, the red-green-blue (RGB) color model [50] was developed and a short time later the RGB 12 algorithm [51].

3.2.2 Microextraction

Extraction is a sample preparation step to enrich the analytes, separate them from their matrix, and hence, reduce interferences. In general, extraction can be considered the most prominent, time-consuming, and error-prone step preceding separation. Some extraction method variants allow on-line coupling with the separation or detection unit. Since the sensitivity and selectivity of mass spectrometry (MS), tandem mass spectrometry (MS/MS), and high-resolution mass spectrometry (HRMS) increased rapidly over the past decades, mass spectrometry coupled to chromatographic separations has become the gold standard for examining complex samples. That resulted in a decreased amount of sample required for analysis and enabled method miniaturization. The first publications using the term ‘microextraction’ appeared around 1940 dealing with the first downsized extraction apparatuses [52]. From then on, there have been sporadic studies on specific applications and developments of microextractions until the 1990s. A rethinking in sample preparation was initiated by the introduction of solid-phase microextraction (SPME) in 1990 by Arthur and Pawliszyn, as it offered a completely solvent-free, green, and miniaturized extraction method [16]. The relevance of the different LPME and SPME variants can be evaluated based on the number of publications as displayed in Figure 3.3. The terms SPME and LPME reached the highest number of publication hits in PubChem followed by dispersive liquid-liquid microextraction (DLLME) and stir bar sorptive extraction (SBSE).

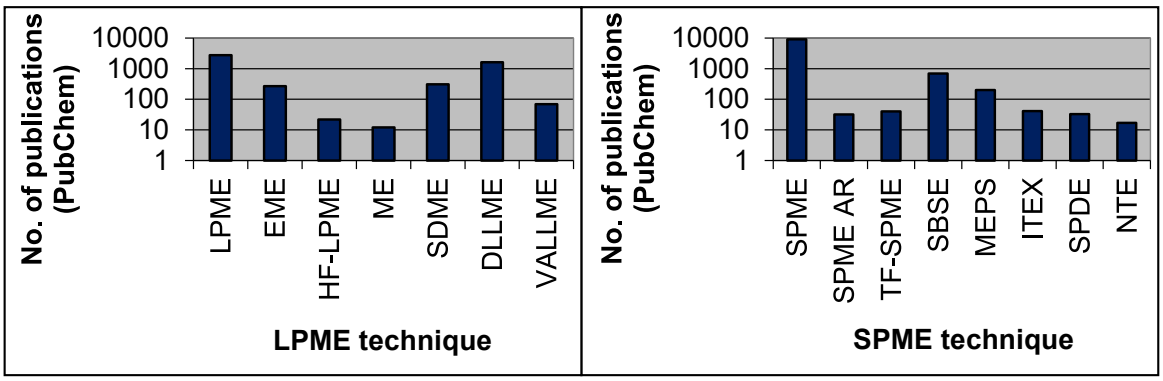

Figure 3.3 Number of publications for LPME (left) and SPME (right) variants taken from PubChem database (1992-2022) obtained with the keywords: “Liquid phase microextraction” (LPME), “Electromembrane extraction” (EME), “Hollow fiber liquid phase microextraction” (HF-LPME), “Microfluidic extraction” (ME), “Single drop microextraction” (SDME), “Dispersive liquid liquid microextraction” (DLLME), Vortex assisted liquid liquid microextraction (VALLME), “Solid phase microextraction” (SPME), “Solid phase microextraction arrow” (SPME AR), “Thin film solid phase microextraction” (TF-SPME), “Stir bar sorptive extraction” (SBSE), “Microextraction by packed sorbent” (MEPS), “In tube extraction” (ITEX), “Solid phase dynamic extraction” (SPDE), “Needle trap extraction” (NTE). Please note that the publication hits for the general terms LPME and SPME may include hits from their variants as well and can not be directly compared to their variant's hit number.

The extraction process is based on transporting one or more substances from a donor phase into an acceptor phase by sorption (for SPME variants) or solvation (for LPME variants). The success of the extraction process is strongly dependent on the molecular interactions of the analytes within the donor and the acceptor phase based on their chemical properties and the analytes’ state in the sample matrix (e.g. freely dissolved or particle-bound). Although there are different geometries, workflows, and modes of microextraction, they share fundamental principles. In general, the extraction phase is in direct or indirect contact with the sample phase and the system strives to reach thermodynamic equilibrium between all phases present in the system. In microextraction, these phases can be sample, acceptor phase(s), and air (air only if headspace extraction is used). The phase transition of analytes is described by equilibrium constants, which, when available, allow the calculation of analytes’ distribution between the phases at equilibrium conditions [53, 54].

The time that it takes to reach thermodynamic equilibrium is governed by extraction kinetics. Among others, temperature, ultrasound, electric field [55], vacuum for headspace extractions [56], solvent bubbles [57], multiple-cumulative trapping [58], and increasing the ionic strength by salting-out [59, 60] have been successfully used as ways to achieve faster extraction kinetics and thus faster equilibrium attainment. To

evaluate the efficiency of the extraction at specific experimental conditions, tools such as the depletion-curve method can be used [61]. Successful extraction is followed either by direct injection into the analytical system (liquid or gaseous acceptor phases) or by desorption (solid acceptor phases). The desorption can be performed thermally, by heating the extraction phase, or by partitioning of the analytes from the extraction phase into a suitable solvent. Some specific formats of extraction tools are not compatible with conventional injectors or liners, and therefore a thermal desorption unit (TDU) in gas chromatography (GC) or a modified multiple-port valve in high-performance liquid-chromatography (HPLC) needs to be implemented. Depending on the application and analytes, intermediate focusing may be necessary after injection or desorption.

3.2.2.1 Liquid-phase microextraction

Traditional processes such as LLE have been used for decades. In research, however, the trend is toward more miniaturized processes due to the high solvent consumption of LLE. This gave rise to liquid-phase microextraction (LPME), a generic term for all microextractions in which the acceptor phase is liquid. [55] A phase separation step (e.g. by centrifugation) can be necessary, to isolate the extractant from the sample. Efforts were made to find alternatives to the use of organic solvents, namely green solvents and surfactants: ionic liquids, deep eutectic solvents, natural deep eutectic solvents, supercritical fluids, bio-derived solvents, superheated water, and surface active agents [62, 63]. Nevertheless, most of the green solvents e.g. ionic liquids and DES, are only applicable for HPLC not for GC, due to their low vapor pressure [63]. Green solvents and surfactants are often not as environmentally friendly and user-safe as the word “green” may imply and for example, consume solvents in their production or are associated with health risks [64, 65]. The greenness of ionic liquids and deep eutectic solvents has been recently questioned as they were found to have high toxicity towards aqueous organisms. Additionally, supercritical fluids, such as carbon dioxide, consume relatively large amounts of energy. [63-65]

The classification and automation of various liquid-phase microextraction techniques have been reviewed [66-69]. An overview of different liquid-phase microextraction methods is shown in Figure 3.4. Single-drop microextraction, SDME, was introduced in 1995 as a miniaturized liquid phase extraction, in which a small droplet of an organic solvent is suspended on the tip of a syringe needle in the headspace or inside the bulk of the aqueous sample. [70, 71] SDME has been further developed and modified and

was performed inside a syringe [72], under vacuum [56], or used for a high throughput approach in a 96-well plate format [73]. Setups called lab-on-a-chip, microfluidic devices, or microfluidic-based LPME (MD-LPME), reduce the required amount of sample and are compatible with automation and online analytical methods [66, 74]. In membrane-based liquid-phase microextraction techniques, the donor and acceptor phases are separated by a membrane to increase the contact surface area between the two phases and protect the extraction phase against unwanted matrix constituents. [67, 75] Different modes have been successfully implemented in analyses, such as hollow-fiber liquid-phase microextraction (HF-LPME) [76] and parallel artificial liquid membrane extraction (PALME) [77]. In electromembrane extraction (EME), acidic or basic analytes are forced to migrate from the sample through the solvent-filled pores of a membrane into the acceptor phase, under an electric field. [78] DLLME uses the principle of solvent dispersion behavior in an aqueous sample for extraction by rapidly injecting a mixture of an extraction and dispersion solvent into the sample to form an emulsion of fine droplets. After that, the droplets have to be separated from the sample solution using centrifugation. Different modes of DLLME exist such as vortex-assisted DLLME (VALLME), and DLLME performed inside a syringe (lab-in-a-syringe) [79]. An alternative approach for the separation of the extraction phase from the sample mixture by cold-induced solidification is the solidified floating organic droplet microextraction (SFODME). [80]

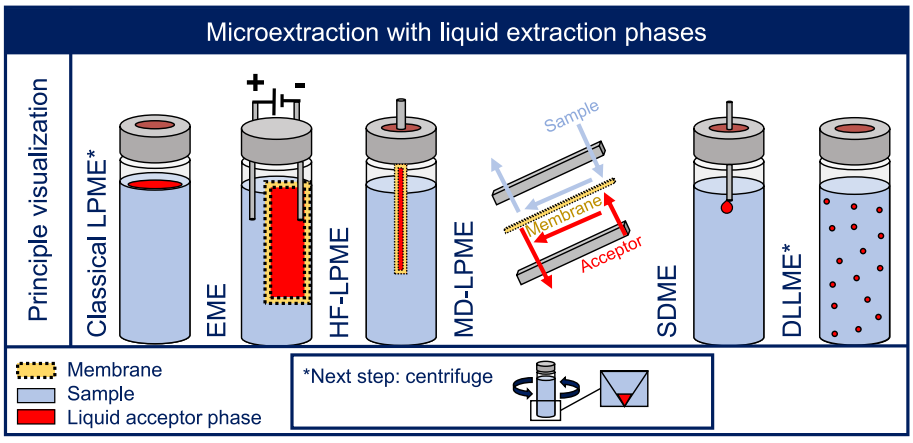

Figure 3.4 Overview of different microextraction methods with liquid extraction phases. HF-LPME and SDME can also be applied in headspace mode. Technical details of the microextractions are stated in Table 3.2. For abbreviations see Table 9.23 in the appendix.

3.2.2.2 Solid-phase microextraction (SPME)

SPME was introduced in 1990 by Arthur and Pawliszyn and was the first solvent-free, miniaturized extraction method. [16] This development was unique at the time and today SPME is still the most used microextraction method worldwide (see Figure 3.3). Numerous works and reviews dealing with SPME have been published covering for example general aspects [81], geometries and materials [23], and calibration strategies [82]. Different shapes and sizes of SPME variants are shown in Figure 3.5. A classical SPME device is a syringe-like holder with a retractable silica fiber coated with a sorbent film. In general, sampling of SPME is done by immersing the coated fiber either in the liquid sample (direct immersion) or in the gas phase above the sample (headspace) whereby the analytes are sorbed. [16] The extraction fiber is cleaned for reuse in the injector or an external heatable module. SPME has already been implemented in official analytical standard methods for the determination of PAHs in sediment-water (USEPA method 8272), pesticides in water (ISO method 27108), and volatile organic compounds in water (ISO 17943), among others. Next to the application in the lab, SPME can also be used as a portable passive- or on-site sampler [83] and for in vivo sampling in living systems (animals or plants) [30]. To overcome the fragility of the SPME fibers, an enhanced, more flexible form of memory nickel-titanium alloy called Nitinol was implemented for the needle and plunger. A further development of SPME, which is mechanically more stable, is SPME arrow, for which the extraction phase is coated onto an enlarged (in length and/or diameter) stainless steel rod with an arrow-shaped tip for septum penetration enclosed in an outer capillary for closing the device. [84] HiSorb shows a similar shape to SPME arrow, but has a thicker stainless steel rod and therefore a higher phase volume. [85] Thin-film SPME (TF-SPME) is a microextraction method with a higher phase volume achieved by the sheet-shaped geometry of the phase and the introduction of films or an impregnated mesh with bigger surface structures instead of the classical SPME phases [86]. An extraction tool with a larger extraction volume was developed by Baltussen et al. in 1999 [87] by using a stir bar coated with sorbent, called SBSE. Matrix-compatible or bio-compatible SPME is an over-coated SPME that protects the phase material from matrix components, particles, and biofouling and prevents the phase material from altering [88]. In addition, mixed extraction phase materials have been implemented to be able to extract a wide range of analytes with different chemical properties.

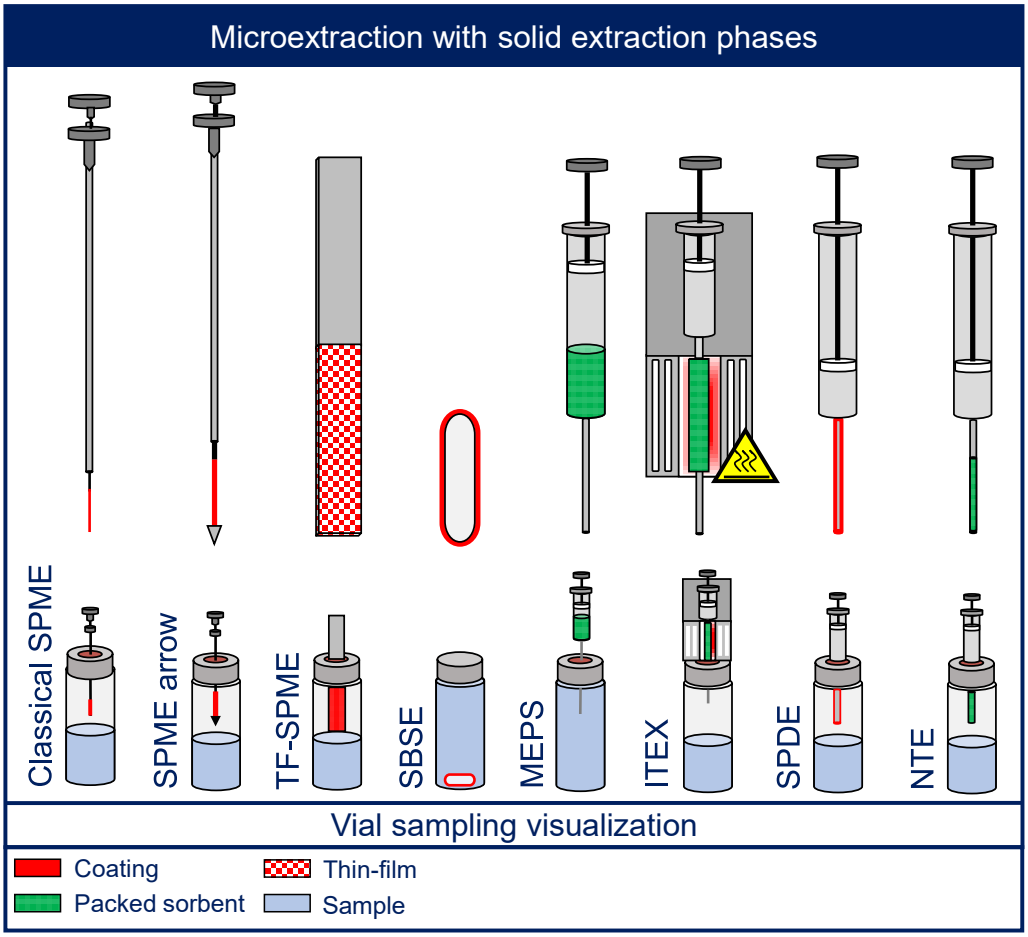

Figure 3.5 Overview of different microextraction methods with solid extraction phases. In general, headspace and direct immersion modes can be applied for all techniques, except ITEX (only HS). Visualization of sampling in the vials is done in headspace mode, except for SBSE and MEPS, where direct immersion mode is usually applied. Technical details of the microextractions are stated in Table 3.2. For abbreviations see Table 9.23 in the appendix.

3.2.2.3 Needle-trap and in-needle microextraction

To improve and simplify the automation of microextraction techniques, a variety of needle-based methods were developed that allow extraction and subsequent injection into GC systems [89]. Because of the syringe and needle device geometry and size, these techniques can easily be automated with xyz-autosampler systems. A distinction between these methods can be made based on the type of employed sorbent materials and geometries. Either the needle walls are coated internally with an immobilized extraction phase similar to a GC column such as in solid phase dynamic microextraction (SDME), or they are filled (or packed) with solid sorbent material. Is the sorbent material inside a syringe or a bin placed between the cannula and syringe body this technique is called microextraction by packed sorbent (MEPS) [90-92]. Another approach, needle-trap extraction (NTE), typically consists of a sorbent-packed

stainless steel needle of a glass syringe [93]. A further development of NTE is in-tube extraction (ITEX) and was introduced as a solvent-free dynamic headspace (DHS) approach in 2008 [94]. The ITEX setup consists of a packed trap material within a stainless-steel needle, which is connected to a gastight glass syringe and covered with an electrical heater (see Figure 3.5) [95].

3.2.2.4 Further developments of microextractions

A lot of further developments in microextraction methods originated from the optimization of several technical parameters to overcome drawbacks. In general five optimization strategies can be named: Increased extracted amount of analyte, enhanced stability, reduced solvent consumption, faster extraction kinetics, and enhanced accuracy. Table 3.1 compares the strategies, gives examples, and explains their implementation and effects.

Table 3.1 The four optimization parameters in microextraction method development, their technical implementation, and their effects. Examples are given for an original method and an enhanced method. For abbreviations see Table 9.23 in the appendix.

Goal	Implementation example	Example of original method → enhanced method	Effects
Increased extracted amount of analyte	-Bigger extraction device, higher volume, amount, or phase thickness -Higher surface area -Thin films -Sheet-shape -Vacuum	SPME → TF-SPME, SPME arrow, SBSE, Vacuum-HS-SPME LPME → DLLME	-Increased sensitivity -Higher solvent consumption -Slower extraction kinetic for solid phases
Enhanced stability	-Implementation of more robust materials or procedures	SPME → over-coated SPME, SPME arrow, bio-compatible SPME SDME → SFODME	-Eventually more steps in the procedure -Stability enhancement can lead to changes in method automation (e.g. non-fitting injector) but can also reduce automation errors
Reduced solvent consumption	-Reduction of extraction phase volume -Solvent-free approaches	LPME → SDME MEPS → ITEX, NTE, SPDE	-Lower phase volume decreases sensitivity
Acceleration of extraction kinetics	-Ultrasound -Electric field -Vacuum -Solvent bubbles -Reduce extraction phase thickness -Temperature	LPME → EME SPME → Vacuum-HS-SPME	-More steps in the procedure -Often higher energy consumption
Enhanced accuracy	-Implementation of materials that reduce matrix effects or act as a barrier	SPME → over-coated SPME, bio-compatible SPME LPME → EME	-More steps in the procedure -Materials can be more selective to reduce

Goal	Implementation example	Example of original method → enhanced method	Effects
			interferences with matrix components

3.3 Benefits and drawbacks of microextractions in terms of greenness

The choice of the fitting green microextraction method for a specific application is difficult, as many parameters have to be taken into account. In addition, some parameters act contrary to each other and the analyst has to decide which parameter is the more important one. Microextraction method selection guides have been published for example covering water analysis [20] and green sample preparation [19]. In addition, greenness evaluation tools can help to inform the analyst about critical steps in their method, already before the first operation, and guide the decision-making process. Table 3.2 summarizes technical details, the main benefits and drawbacks of the microextraction variants. This section focuses especially on the discussion of microextraction greenness parameters, which, based on the GAC principles, we here define to be:

- Automation and number of steps
- Solvent consumption
- Hazards
- Reusability
- Energy consumption

Two other discussed parameters that are not directly related to greenness but are nevertheless associated with extraction are time efficiency and sensitivity.

Table 3.2 Technical details, benefits and drawbacks of various liquid-phase and solid-phase microextractions. The methods are compared based on their automatability, solvent, waste and sample amount, acceptor phase amount/volume/dimension, hazards, reusability, and the number of steps. For abbreviations see Table 9.23. Autom.: Automation degree; So: Solvent; W: Waste; AP: Acceptor phase; Sa: Sample; TP: Transition phase; Liq: Liquid; Sd: Solid; G: Gaseous (all gaseous extractions can also be used for liquid and solid samples when operated in the headspace dependent on analyte volatility); SLM: Supported liquid membrane; DES: Deep eutectic solvent; Ref.: Reference(s).

Variant	Autom.	So, W, Sa amount AP amount/ volume/ dimension	AP/TP (examples)	Sample	Device reusable times	Steps	Pro and Con	Ref.
LE	Semi	So/W/AP: >10 mL Sa: >100 mL	cyclohexane, n-hexane, MTBE, toluene, butanol, chlorinated hydrocarbons	Liq, Sd	None	-Extraction -Separation -Concentration	Pro -High sensitivity due to large donor and acceptor phase volumes and concentrating of the analytes after extraction Con -Solvent/waste amount high -Steps are typically operated manually or semi-automated -Time-consuming	
LPME	Full	So/W/AP: <100 µL Sa: <10 mL	See LE	Lig, Sd, G	None	-Extraction -Separation	Pro -Reduced solvent consumption compared to LE -Automatable, not manual -Time-efficient -Cost-effective Con -Reproducibility of small volumes is important	[55, 62, 66-69]
Classical SDME	Full	So/W/AP: <7 µL Sa: <10 mL	chloroform, n-octane, cyclohexane, toluene, DES, chlorinated hydrocarbons	Liq, G	None	-Droplet formation -Extraction -Droplet withdrawal -Injection	Pro -Good extraction phase-to-sample ratio -Cost-effective -Simple device Con	[70, 96, 97]

Variant	Autom.	So, W, Sa amount AP amount/ volume/ dimension	AP/TP (examples)	Sample	Device reusable times	Steps	Pro and Con	Ref.
							-Instability of droplet in aqueous solution -Headspace droplet can fall into solution or get lost due to movements of the autosampler -Poor phase separation can cause problems with droplet collection (difficult to automate) -Small volume reproducibility is very important	
MD-LPME	Full	So/W/AP: <15 µL Sa: <15 µL	Acceptor phase: NADES, DES, alcohols Membrane: agarose, cellulose, polyproylen SLM: n-dodecane, polyproylen, tributyl phosphate	Liq, G	Chip: 10 x	-Extraction -Phase collection -Injection	Pro -Very miniaturized setup -Easy implementation in existing systems -Almost unlimited options to extend or modify MD, very good for specific approaches -Compatible with online-approaches -High analytical performance Con -Solvent consumption for cleaning device -Devices are often self-made or 3D printed and therefore not comparable between laboratories -Difficult to purchase	[66, 74, 98]
HF-LPME	Semi	So/W/AP: <5 µL Sa: <10 mL	Acceptor phase: acetonitrile, methanol Membrane: polypropylen SLM: n-dodecane	Liq, G	50 x	-Extraction -Injection -Membrane cleaning	Pro -Membrane separates matrix components and extraction solvent -Phase collection is simpler compared to other LPME approaches	[67, 75]

Variant	Autom.	So, W, Sa amount AP amount/ volume/ dimension	AP/TP (examples)	Sample	Device reusable times	Steps	Pro and Con	Ref.
							Con -Phase mixing is poorer than for other LPME approaches -Not fully automated -Lower sensitivity compared to other LPME approaches due to low sample amount	
PALME	Semi	So/W/AP: <5 µL Sa: <250 µL	Acceptor phase: formic acid Membrane: polypropylen SLM: n-dihexyl ether, dodecyl acetate	Liq, G	50 x	-Sample introduction -Clamping of acceptor and donor plate (manual) -Solvent introduction -Extraction -Removal of upper plates (manual) -Injection	Pro -High throughput in 96-well plate format possible -Could be automated in future -Could be useful for online approaches in future -See HF-LPME Con -See HF-LPME	[67, 75, 77]
EME	Full	So/W/AP: <5 µL Sa: <10 mL	Acceptor phase: formic acid Membrane: polypropylen SLM: heptanol, octanone, 2-nitrophenyl octyl ether	Liq	200 x	-Implementation of extraction device in the sample -Electric field -Extraction -Phase collection -Injection	Pro -High throughput with modified LC valves possible -Fast extraction due to electric field -Fully automated compared to the other membrane-based LPMEs -Works well for polar and ionizable substances -See HF-LPME Con -Electric field is necessary for extraction, difficult to use it as portable or passive sampler	[67, 75, 78]

Variant	Autom.	So, W, Sa amount AP amount/ volume/ dimension	AP/TP (examples)	Sample	Device reusable times	Steps	Pro and Con	Ref.
							-Phase mixing is poorer than for other LPME approaches -Only charged analytes can be extracted	
Classical DLLME	Semi	So/W/AP: <20 µL Sa: <10 mL	Acceptor phase: DES, chlorinated hydrocarbons, chlorobenzene, cyclohexane Dispersion solvent: acetone, acetonitrile, methanol	Liq	None	-Injection of dispersion and extraction solvent into sample -Mixing -Extraction -Centrifugation -Phase collection -Injection	Pro -High surface of emulsion allows fast and efficient extraction Con -Centrifugation makes automation complicated -Droplet formation is error-prone depending on the sample matrix -Collection of solvent phase is complicated to automate and error-prone	[68, 79, 99]
SFODME	Semi	So/W/AP: <20 µL Sa: <20 mL	Acceptor phase: 1-dodecanol, DES Dispersion solvent: acetone, acetonitrile, methanol	Liq	None	-Injection of dispersion and extraction solvent into sample -Mixing -Extraction -Cooling for solvent solidification -Phase collection and liquefication -Injection	Pro -Phase collection is easier due to solidified droplet compared to DLLME Con -Could only be fully automated for LC approaches with handmade or 3D-printed phase separator -Additional steps that have to be operated manually (cooling, phase collection)	[99]

Variant	Autom.	So, W, Sa amount AP amount/ volume/ dimension	AP/TP (examples)	Sample	Device reusable times	Steps	Pro and Con	Ref.
SPE	Semi	So/W: 10-2000 mL AP: 10-2000 mg Sa: 10-2000 mL	Silica, C18, C8, Cyano, Phenyl, Carbon, SAX, Florisil, Polymer	Liq, G	None	-Preconditioning -Extraction -Elution -Concentration -Injection	Pro -High concentration of analytes due to high sample volume: good sensitivity -Good sample clean-up potential Con -Solvent/waste amount high -Some steps may have to be operated manually -Time-consuming	
Classical SPME	Full	So/W: None AP: 10 mm x 7-100 µm; Volume: 0.6 µL Sa: <20 mL	PDMS, DVB-PDMS, Acrylate, Carbon	Lig, Sd, G	100 x (DI); 500 x (HS)	-Extraction -Desorption in the injector -Thermal cleaning	Pro -Can be implemented in existing xyz-autosamplers without much effort -low number of procedure steps -solvent-free -non-hazardous Con -Fragile construction of fiber and needle complicates automation -Instability and swelling in solvents (complicates HPLC use)	[16, 23, 81-83, 88]

Variant	Autom.	So, W, Sa amount AP amount/ volume/ dimension	AP/TP (examples)	Sample	Device reusable times	Steps	Pro and Con	Ref.
SPME arrow	Full	So/W: None AP: 20 mm x 1.1-1.5 mm x 250 µm; Volume: 3.8-12 µL Sa: <20 mL	See classical SPME	Lig, Sd, G	100 x (DI); 500 x (HS)	-Extraction -Desorption in injector -Thermal cleaning	Pro -Thicker phase than SPME results in a wider linear range and better sensitivity -Mechanically more stable than SPME due to arrow-shaped tip and stainless steel backbone -Phase can be closed which reduces sample loss Con -Thicker phase results in longer extraction and cleaning times -A wider injection port and liner are needed -Instability and swelling in solvents (complicates HPLC use)	[84]
TF-SPME	Semi	So/W: None AP: 10-20 mm x 4-10 mm x 90 µm; Volume: 3.6-18 µL Sa: <20 mL	PDMS, DVB-PDMS, PDMS-HLB	Lig, Sd, G	150 x (DI); 300 x (HS)	-Extraction -Desorption in injector or TDU -Thermal cleaning	Pro -Bigger surface than SPME -Fast extraction due to thin phase Con -Format complicates automation -A TDU or special injection strategy is needed for desorption	[86, 100, 101]
SBSE	Semi	So/W: < 15 µL AP: 10-40 mm x 4-10 mm x 0.5-1 mm; Volume: 20-400 µL Sa: <2 L	PDMS, ethylenglycol-silicone	Lig, Sd, G	100 x (DI) >500 x (HS)	-Introduction of SBSE in sample (manual) -Mixing -Extraction -Taking SBSE out of sample (manual) -Desorption in Injector	Pro -Thicker phase than SPME -Applies to rather large sample volumes -Sample can be mixed with the coated stir bar, no other mixing necessary Con -Eventually solvent consumption for cleaning device	[87, 102, 103]

Variant	Autom.	So, W, Sa amount AP amount/ volume/ dimension	AP/TP (examples)	Sample	Device reusable times	Steps	Pro and Con	Ref.
						-Thermal/Solvent cleaning	-TDU or similar is needed for desorption -Is not completely automated	
MEPS	Full	So/W: <10 µL AP: <10 mg Sa: <50 µL	C18, Silica, C2, C8, C2-SCX	Liq	100 x	-Extraction -Desorption in solvent -Injection	Pro: -Easy to automate as being performed in classical syringes -Wide variety of standard SPE sorbents can be used -Principle is similar to SPE but miniaturized and automated -Lower solvent consumption than SPE Con: -Solvent consumption for analyte desorption and extraction phase cleaning -Only applicable to liquid samples	[90-92]
ITEX	Full	So/W: None AP: <60 mg Sa: <10 mL	Carbopack, Carbosieve SIII, Carboxen 1000, Tenax GR, Tenax TA	G	200 x	-Extraction -Injection with external thermal desorption -Thermal cleaning	Pro -No solvent necessary for cleaning due to high-temperature cleaning with module -Large sorbent volume -Multiple extraction cycles lead to efficient enrichment Con -Only applicable for headspace extraction -Only applicable with autosamplers supporting ITEX -Special syringes have to be purchased	[94, 95]

Variant	Autom.	So, W, Sa amount AP amount/ volume/ dimension	AP/TP (examples)	Sample	Device reusable times	Steps	Pro and Con	Ref.
SPDE	Full	So/W: None AP: 56 mm x 0.5 mm x 100 µm; Volume: 5.6 µL Sa: <20 mL	PDMS, PDMS-carbon, ethylene glycol, Carbowax	Liq, G	100 x	-Extraction -Injection -Thermal cleaning	Pro -Solvent-free due to thermal desorption and cleaning -Easy implementation in automated systems -Mechanically more stable than SPME because of internally coated needle Con -Instability and swelling in solvents (complicates HPLC use)	[104, 105]
NTE	Full	So/W: None AP: <1 mg Sa: <20 mL	Carbopack X, Carboxen 1000, Tenax, DVB, HayeSep Q	Liq, G	100 x	-Extraction -Injection -Thermal cleaning	Pro -Solvent-free desorption in injector -Applicable to liquid and gaseous samples Con -Low sorbent amount reduces sensitivity -Packed needle can be clogged by sample particles	[93, 106]

3.3.1 Automation and number of steps

Nowadays automatability of a method is of great importance for its greenness and acceptance in the scientific community. xyz-automated systems are most suitable to integrate miniaturized methods and meet other criteria such as integration in analysis systems, high throughput, labor power-, time-, and cost-reduction. Additionally, autosamplers can reproducibly handle small volumes, reduce the contact of staff with chemicals and samples, and avoid the unwanted introduction of impurities. The number of operational steps should be as low as possible. Full automation of microextraction methods increased significantly in recent years, which is also evident in the increased number of publications on fully automated microextraction methods. However, some methods are not fully automated namely HF-LPME, PALME, DLLME, SFODME, TF-SPME, and SBSE because they have steps that have to be operated manually. These manual steps are for example plate clamping and removal in PALME, centrifugation in DLLME, and transport and/or handling of the extraction phase in SBSE, SFODME, and TF-SPME. Methods that have a low number of steps (<5, see Table 3.2) are preferred, as their operation in general is easier and better to automate. Examples of methods with a low number of steps are SDME, MD-LPME, HF-LPME, EME, all SPME variants, and all in-needle or needle-trap-based microextractions. Improvements in microextractions have been made to enhance the stability and thus integration into automated systems (see Table 3.1 and Table 3.2). This was implemented by using more robust extraction tool materials (e.g. stainless steel) to improve mechanical stability (SPME arrow), using innovative coatings to enhance phase stability and reduce phase altering (over-coated or bio-compatible SPME), or improving the stability of the organic droplet (SDME to SFODME). On the other side enhancing robustness and stability can lead to more steps in the procedure and difficulties with automation (SFODME) or injector size (SPME arrow).

3.3.2 Solvent consumption

High solvent consumption is not sustainable, causes harmful waste, and is a problem all laboratories have to deal with. As an example: a solvent consumption as in LE would typically add up to ~100 L of organic solvent waste for 1000 samples whereas in LPME this would only be ~100 mL/1000 samples, which makes a major difference, especially for laboratories with high sample throughput (e.g. routine analysis laboratories). Solvent waste is not only an ecological problem but is also economically non-profitable due to high costs for the required purity of solvents used plus high disposal costs of

the used solvents. High solvent-consuming methods such as LE, LLE, or SPE should be avoided and solvent-reduced microextractions with a solvent consumption below 100 µL per sample (the lower, the better) should be used, which applies to almost all LPME variants depending on their mode of operation (see Table 3.2). Solvent consumption of fabrication of materials or purification of solvents often is neglected in the greenness assessment but definitely has an impact on the greenness of the overall analytical procedure, however, it was included by the recently developed ComplexGAPI metric [45]. On the other side, solvent volume reduction accompanies phase capacity reduction, which reduces analytical sensitivity. Solvent-free microextraction methods such as all SPME variants and most of the in-needle and needle-trap microextractions, except MEPS, are the best way to make the extraction process greener and compensate for the reduced sensitivity due to miniaturization with increased enrichment factors of the sorption process.

3.3.3 Hazards

Hazards in extraction are mostly referring to the used solvents. Therefore solvent-free microextraction methods are in general non-hazardous. Hazards that can occur from solvents are explosivity, flammability, oxidation, toxicity, irritation, mutagenicity, and carcinogenicity. Solvents that are threats to human and environmental health are for example chlorinated solvents, methanol, and benzene. Especially chlorinated solvents are often used as extraction solvents in DLLME, which should be avoided. In recent years, a wide variety of environmentally friendly solvents and surfactants have been developed, but some green solvents have recently been questioned based on their greenness due to human or environmental health hazards and high energy consumption during their production. [62, 63]

3.3.4 Reusability

Reusability of chemicals and materials is important to reduce the waste amount. To be able to reuse materials and chemicals, cleaning is important to exclude contaminations or carry over from other measurements. For solvents, cleaning on a lab scale is not efficient when analytical purity is needed. Solid extraction materials or membranes can be reused after thermal or solvent cleaning. Thermal cleaning is preferred as it is solvent-free, but on the other side thermal cleaning is energy-consuming. In cleaning processes, there is no guarantee that analytes are eliminated so the testing of the effectiveness of cleaning should be done in any case. Solid extraction materials can be reused 100-500 times (see Table 3.2) depending on the operation mode

(headspace or direct immersion) and sample matrix. Direct contact of the sample and extraction material reduces the reusability time as it accelerates material altering. Alternative materials that are more stable at direct immersion conditions are, e.g., over-coated or bio-compatible SPME. A headspace application can be used for volatile and semi-volatile analytes and has the advantage of slower material altering by acting as a barrier for matrix components.

3.3.5 Energy consumption

With the use of renewable resources for energy generation the term energy consumption would become less important, unfortunately, nowadays energy consumption is still an important parameter to reduce CO_2 emissions. In general, energy-consuming steps are operating temperatures other than room temperature and high energy-consuming devices and steps such as Soxhlet-Extraction, heated solvent evaporation for longer than 150 min, LCs, GCs, and MSs, X-ray diffraction and nuclear magnetic resonance [46]. Direct analyses such as in-field and online analyses are preferred.

3.3.6 Time efficiency, accuracy and sensitivity

Method sensitivity, accuracy, and time efficiency are discussed together as they strongly influence each other. Sensitivity is dependent on the extracted amount that is dictated by the extraction efficiency and the phase geometries involving phase volume, phase thickness, and surface area. Therefore, small phase volumes are less suitable for trace analysis. Higher analytical method sensitivity has been gained by the expansion of the surface area (DLLME, TF-SPME) or extension of the phase thickness and volume (SPME arrow, SBSE), as shown in Table 3.1. In general, it can be said: the higher the phase volume, the higher the extraction capacity.

Accuracy is an important parameter of analytical methods. Factors affecting the accuracy can be, among others, the sample matrix, the stability of the analytes, the extraction efficiency, but also the accuracy of separation and detection [107]. Matrix effects are a problem in microextraction methods and negatively affect their accuracy, often limiting their use. To compensate for this effect, internal standards can be used, or membrane-protected, overcoated, or headspace mode techniques can be employed. The extraction time efficiency is dependent on the extraction kinetics. The thickness of an extraction phase influences the extraction kinetics: the bigger the phase thickness, the slower the kinetics. Thicker extraction phases as in SBSE or SPME arrow have slower extraction kinetics and are less time-efficient, whereas TF-

SPME, EME, solvent bubbles, multiple-cumulative trapping, salting-out, vacuum- and ultrasonic-assisted extractions show faster extraction kinetics (see Table 3.1 and Table 3.2).

3.4 Greenness evaluation of standard methods

Standard methods such as USEPA, International Organization for Standardization (ISO), and European Committee for Standardization (CEN) are used every day and worldwide by thousands of labs. This is why it is so important to re-evaluate these methods in terms of their greenness. Tons of resources and environmentally harmful waste could be saved if standard methods were further miniaturized. However, only a few of the standard methods employ microextraction methods, which is the step that would save the most resources. Furthermore, the miniaturization of the steps facilitates the automation of the full procedure. Proposals for the integration of microextraction methods into standard methods, such as those of the USEPA, are numerous. To demonstrate the need to re-evaluate existing non- or semi-miniaturized standard methods, three uniformed evaluation programs, AGREE [46], AGREEprep [47, 48], and GAPI [44] were applied exemplarily to four USEPA methods of different ages, using GC analysis and covering different analytes: phenols, carbonyl compounds, haloacetic acids, and polycyclic aromatics. Additionally, for three of the USEPA methods equivalent replacement methods applying microextractions were evaluated. The replacement methods were carefully selected based on the detailed description, evaluation, and optimization of the presented sample preparation method, which simplified the application of greenness evaluation tools. Further, only methods were considered as replacements methods that clearly stated to replace the according USEPA method e.g. in terms of analytical performance and choice of analytes. Information about the methods is shown in Table 3.3 and the pictograms of the greenness metric evaluations are shown in Figure 3.2. Greenness evaluation metrics primarily focus on the greenness and sustainability of the methods, however, often missing are the method performance and practicability, which also have to be taken into account as discussed e.g. in the concept of white chemistry [51]. If the method's performance and/or practicability are poor, this could limit the implementation of a method independent of its greenness.

USEPA method 604 [108] presents a derivatization-free phenol determination in aqueous samples by using LLE followed by GC-FID. The procedure uses methylene

chloride as an extraction solvent in a manual separatory funnel LLE with multiple solvent exchange steps and solvent evaporation before analysis.

The replacement method proposed by Buchholz et al. [109] uses DI-SPME followed by GC-FID or GC-MS to directly extract the phenols from the water sample at room temperature. Therefore, the replacement method is solvent-free and does not require additional sample treatment other than microextraction, which shortens and simplifies the overall procedure.

The USEPA method 556 [110] determines carbonyl compounds in drinking water followed by GC-ECD and uses the same LLE extraction procedure as USEPA method 604, but requires an additional derivatization step with PFBHA. Cancho et al. [111] published a replacement method with an in-situ PFBHA derivatization before HS-SPME at room temperature and followed by GC-ECD.

In USEPA method 552.3 [112], a more miniaturized LPME approach, is used with methanol derivatization for the determination of haloacetic acids in drinking water by GC-ECD. A replacement method presented by Casas Ferreira et al. [113] combines TFEA/EDC in-situ derivatization with MEPS, analyzed by GC-MS.

One of the few miniaturized USEPA methods with solvent-free SPME is method 8272 [14], where polycyclic aromatics are analyzed in sediment pore water with GC-MS in SRM mode. Depending on the type of sample additional sample treatment steps are necessary: centrifugation of sediment or flocculation and centrifugation of groundwater or tap water samples.

Table 3.3 Information about the USEPA and replacement methods, which have been evaluated by the greenness metric approaches. For abbreviations see Table 9.23.

Method	Sample preparation	Analysis	Analytes	Lit.
USEPA 604 (1984)	LLE	GC-FID	Phenols	[108]
Buchholz (1993)	DI-SPME	GC-FID, GC-MS	Phenols	[109]
USEPA 556 (1998)	LLE, derivatization (PFBHA)	GC-ECD	Carbonyl compounds	[110]
Cancho (2002)	HS-SPME, *in-situ* derivatization (PFBHA)	GC-ECD	Aldehydes	[111]
USEPA 552.3 (2003)	LPME, derivatization (methanol)	GC-ECD	Haloacetic acids	[112]
Casas Ferreira (2013)	MEPS, *in-situ* derivatization (TFEA, EDC)	GC-MS	Haloacetic acids	[113]
USEPA 8272 (2007)	DI-SPME	GC-MS	Polycyclic aromatics	[14]

The results of the greenness evaluations are shown in Figure 3.6. It can be seen that the replacement methods achieve better scores than the original USEPA methods in all cases. Original USEPA methods reach AGREE scores ranging from 0.34-0.38,

AGREEprep scores ranging from 0.10-0.15, and GAPI pictograms with G2 Y3-4 and R8-9. The replacement methods score in AGREE from 0.46-0.65, in AGREEprep from 0.27-0.75, and GAPI pictograms with G3-7, Y2-4, and R5-7. USEPA method 8272, which uses SPME, acts as an example for the implementation of solvent-free microextraction in standard methods and reaches scores in the range of the replacement methods (AGREE score 0.59; AGREEprep score 0.72; GAPI G5, Y4, R5). USEPA method 8272 represents a positive example of the implementation of microextraction in standard methods, therefore no replacement method was presented in this case. The lowest rated steps in USEPA method 604 were the high sample amount of 1 L, excessive use of solvents for LLE (up to 360 mL per sample), manual and non-miniaturized sample preparation steps, use of toxic solvents and reagents and high waste amounts (up to 350 mL per sample). The two more recent USEPA methods 556 and 552.3 reached better scores for semi-automatic and more miniaturized approaches. The replacement and USEPA method 8272 methods were positively rated for automated and miniaturized approaches, low waste amounts (None-15.4 mL), and low amounts of toxic solvents (None-250 µL). The method of Buchholz et al. for phenol determination and the USEPA method 8272 is rated with the best scores for being solvent-free, fully automated, and extremely miniaturized [14, 109].

All in all, this comparison shows the potential of microextraction for the implementation in standard methods and should further motivate analytical chemists to pursue corresponding updates in standardization processes.

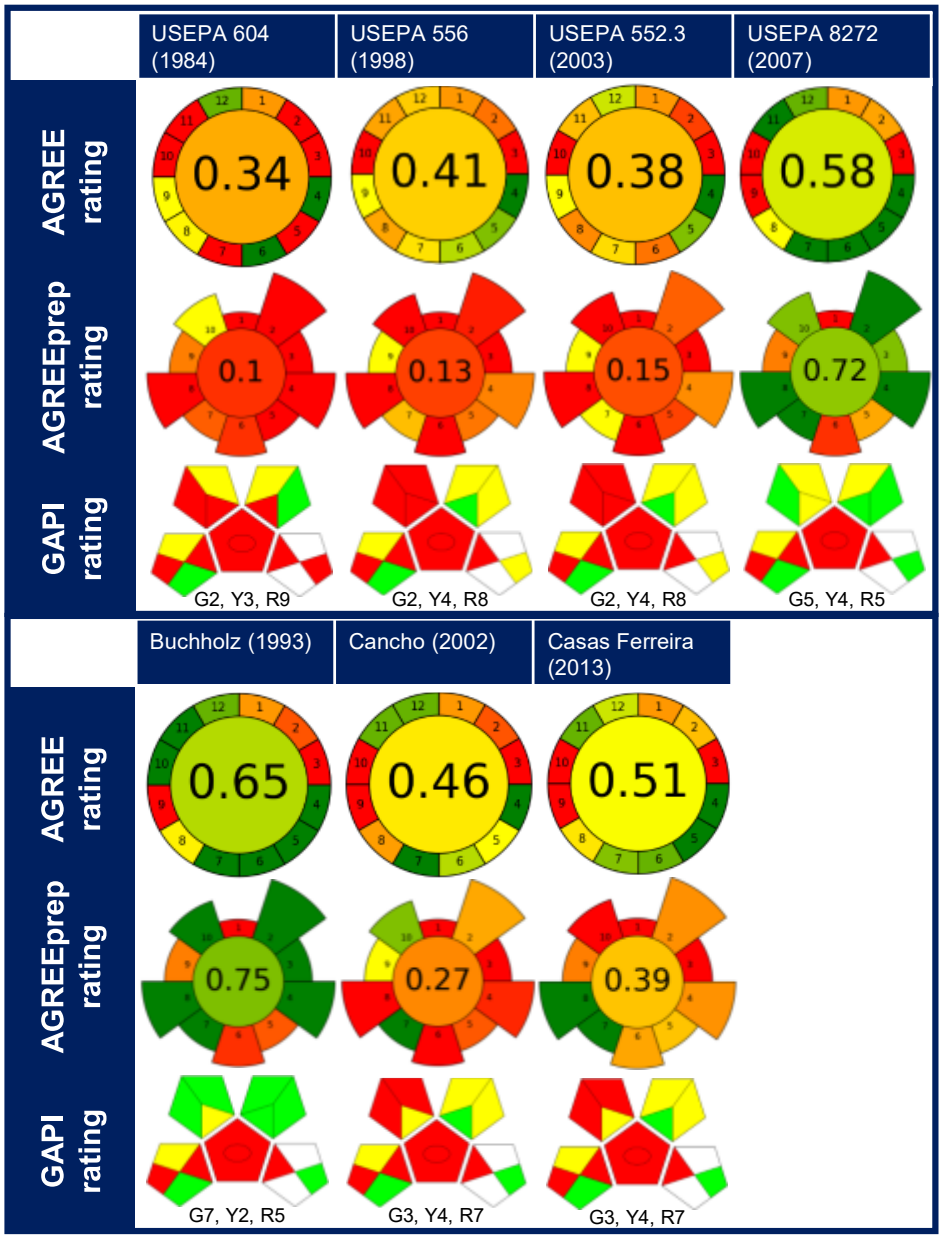

Figure 3.6 Analytical GREEnness metric approach (AGREE), AGREEprep and Green Analytical Procedure Index (GAPI) applied to standard methods of the United States Environmental Protection Agency (USEPA) and published replacement methods involving microextraction. White fields in GAPI are the steps “Occupational hazard” and “Waste treatments” which could not be rated based on the description of the methods. For USEPA method 8272, no replacement method is presented, as in this case a microextraction is already implemented. G: Green fields; Y: Yellow fields; R: Red fields.

3.5 Conclusion

This review summarizes the most common types of green microextractions. Furthermore, parameters that make the methods more sustainable are discussed and tools for optimizing methods and evaluating greenness are presented. We expect that

microextraction methods will be increasingly used in the future and advocate that standard methods must be miniaturized and at best solvent-free. The greenness evaluation with AGREE, AGREEprep, and GAPI showed, that microextraction methods are a valuable option for the implementation in standard methods. In addition, for most of the non-green standard methods replacement methods have been published over the past 20 years. Another important factor next to greenness is, that the replacement methods have to prove similar or better performance to ensure their future application. However, the adaptation of standard methods to greener methods is proceeding too slowly, in our opinion. This review intends to encourage analysts to evaluate and optimize their methods, to make them environmentally friendly, and to give an impulse that routine analysis should include method greenness evaluation as a standard parameter. By implementing green microextraction methods into their daily routines and research, analytical chemists contribute to their responsibility for a sustainable future.

4 Analysis of fatty acid methyl esters from aqueous samples by headspace SPME arrow extraction followed by GC-MS/MS analysis

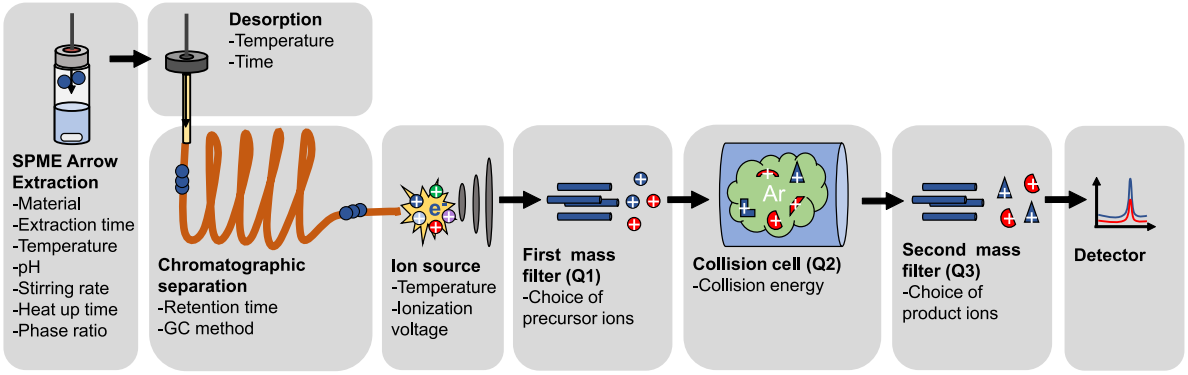

Adapted from: Lucie K. Tintrop, Maik A. Jochmann, Thomas Beesley, Marco Küppers, Ruth Brunstermann, Torsten C. Schmidt. Optimization and automation of rapid and selective analysis of fatty acid methyl esters from aqueous samples by headspace SPME arrow extraction followed by GC-MS/MS analysis, published in Analytical and Bioanalytical Chemistry (2022). © Springer Nature 2022

4.1 Abstract

The analysis of fatty acid methyl esters (FAMEs) is of high relevance for monitoring and control of various industrial processes and biological systems. In this study, a novel, green analytical approach for the determination of 24 FAMEs from aqueous samples is proposed, which is based on a headspace solid-phase microextraction (SPME) arrow followed by gas chromatography coupled to tandem mass spectrometry (GC-MS/MS). The method was substantially accelerated to a run time of 44 min per sample by thorough optimization and automation of the relevant parameters. The limiting parameters, mostly based on expediting equilibrium attainment, were found to be parameters of extraction: material, pH, time, and temperature, which were optimized to divinylbenzene polydimethylsiloxane (DVB-PDMS), pH 2, 20 min, and 70 °C, respectively. The optimization and automation of the method led to low method detection limits (9-437 ng L^{-1}) and high selectivity. Evaluation of the method on real samples was done by analyzing the aqueous phase of a bioreactor, whereby the matrix effect could be greatly reduced due to dilution and headspace sampling. The rapid, sensitive, selective, and matrix-reduced approach is found to be not only a novel

method for water analysis but is promising for further applications, e.g., with solid and gaseous samples containing FAMEs.

4.2 Introduction

Fatty acid methyl esters (FAMEs) are relevant substances in the food industry, microbiology, water analysis, and biodiesel production [114-117]. In these fields, they are mainly investigated for quality or process control and serve as major components in biodiesel [118], lipid metabolism products in plants and microorganisms [115], food ingredients [114], and as potential new antibiotics that could contribute to solving the problem of multi-drug resistance [11]. Furthermore, FAMEs serve as platform chemicals and are used for large-scale industrial production of surfactants, emulsifiers, or resins [10]. In industrial production, FAMEs are easier to handle in comparison to fatty acids, since they have the advantage of lower boiling points and are less corrosive [10]. The methyl esterification of fatty acids to FAMEs is a frequently used derivatization method in fatty acid analysis by GC. However, it is not possible to distinguish naturally occurring FAMEs from the derivatized fatty acids in the sample when esterification is applied. Therefore, it is important to determine the FAMEs in the sample prior to derivatization.

In Germany, the Renewable Energy Sources Act (EEG) stipulates that the percentage of renewable energy should be increased to 60% by 2035. Especially, carbon-rich wastewaters as feed for bioreactors have the potential of being reused as a basis for platform chemicals, whereby large amounts of carbon dioxide can be saved [7, 8]. Particularly, the direct extraction of FAMEs from such bioreactors is of interest as they can be utilized in biodiesel production.

The determination of FAMEs by gas chromatography (GC) has already been described using various detectors, including flame ionization detector (FID) [119], mass spectrometry (MS) [120], and tandem mass spectrometry (MS/MS) [118]. However, complex matrices require the extraction of FAMEs. Frequently used sample preparation methods to separate and enrich FAMEs from the matrix are solid-phase extraction (SPE) [121] and liquid-liquid extraction (LLE) [118] as well as microextraction methods such as SPME [122], hollow-fiber liquid-phase microextraction (HF-LPME) [123] and dispersive liquid-liquid microextraction (DLLME) [116]. In general, extensive solvent, time, and material-consuming LLE and SPE methods should be avoided for environmental reasons. This has been remedied by miniaturization of the extractions, which save solvents in the case of DLLME and HF-

LPME and even operate solvent-free in the case of SPME. The development of SPME to SPME arrow reduced problems concerning mechanical stability and increased the size of the sorption phase [124]. After the first study on SPME arrow sampling in 2015 [84], its use has been described in many studies covering different analytes and applications, including determination of polycyclic aromatic hydrocarbons in water [124], organic compounds in the atmosphere [125], volatiles in fish sauce [126], amines in wastewater and phosphorous flame retardants in water [127], among others.

Analytical chemistry has a major responsibility concerning the adaptation and development of green and sustainable methods. Green analytical chemistry does not clearly define the characteristics of a green method but increases awareness for miniaturization, automation, direct analysis, reagent replacement, multianalyte determinations, and operator safety, amongst others [18, 42, 128]. The demands for greener, faster, and more sensitive methods are ever-increasing. Automation, method optimization, solvent-free microextraction methods, and SPME arrow, in particular, offer a high potential to meet future demands and thus are worth further research and study [128, 129].

This work is the first to deal with SPME arrow extraction of 24 FAMEs from aqueous samples. SPME arrow is used as a green extraction method, which is solvent-free in contrast to conventional extraction methods and has a larger phase volume compared to SPME. Since the extraction parameters had a strong influence on the success of the method, this was intensively studied and discussed, which can provide the basis for future studies in this field. The novel combination of sensitive SPME arrow headspace extraction without matrix contact and selective determination by GC-MS/MS operating in MRM (multiple reaction monitoring) mode indicates an almost unlimited range of possible applications in target analysis.

4.3 Material and methods

4.3.1 Reagents and materials

Methyl heptanoate (C7:0Me, ≥ 99.8%), methyl nonanoate (C9:0Me, ≥ 99.8%), isotope-labeled methyl heptanoate d_{33} (C17:0dMe, ≥ 97.5%) and 37-component FAME mix with varying concentrations of 200-600 mg L^{-1} were purchased from Sigma Aldrich (Steinheim, Germany). The FAME mix with varying concentrations was containing the following compounds (used abbreviations are given in brackets): Methyl hexanoate (C6:0Me), methyl octanoate (C8:0Me), methyl decanoate (C10:0Me), methyl undecanoate (C11:0Me), methyl dodecanoate (C12:0Me), methyl tridecanoate

(C13:0Me), methyl tetradecanoate (C14:0Me), methyl pentadecanoate (C15:0Me), methyl hexadecanoate (C16:0Me), methyl heptadecanoate (C17:0Me), methyl octadecanoate (C18:0Me), methyl eicosanoate (C20:0Me), methyl heneicosanoate (C21:0Me), methyl docosanoate (C22:0Me), methyl cis-9-hexadecenoate (C16:1cMe), methyl trans-9-octadecenoate (C18:1tMe), methyl cis-9-octadecenoate (C18:1cMe), methyl all-cis-9,12-octadecadienoate (C18:2cMe), methyl all-cis-6,9,12-octadecatrienoate (C18:3c6Me), methyl all-cis-9,12,15-octadecatrienoate (C18:3c9Me), methyl all-cis-5,8,11,14,17-eicosapentaenoate (C20:5cMe). Sulfuric acid (H_2SO_4, ≥ 95%) was purchased from Fisher Scientific (Loughborough, United Kingdom). Stock solutions of single substances (1 g L^{-1}) were prepared in methanol (100.0%, VWR, Fontenay-sous-Bois, France) and stored at 4 °C. Samples for the optimization and method validation procedure were prepared in bi-distilled water (Bi-Distillation apparatus Bi 18E with quartz glass, Quarzglas QCS, Germany).

4.3.2 GC-MS/MS analysis

Separation and detection were performed by a Shimadzu GCMS-TQ-2010 (Shimadzu Deutschland GmbH, Duisburg, Germany) in MRM scan mode equipped with a Zebron ZB-FAME capillary column (30 m x 0.25 mm x 0.20 µm, Phenomenex, Torrance, USA) using helium (5.0, AirLiquide, Oberhausen, Germany) as carrier gas with a column flow of 1.8 mL min^{-1} and argon (5.0, AirLiquide, Oberhausen, Germany) as collision gas. The oven temperature program started at 40 °C, was held for 5 min, and was raised at a rate of 6 °C min^{-1} to 210 °C. The injector, transfer line, and ion source temperature were set to 250 °C, 180 °C, and 180 °C, respectively. Thermal desorption of the analytes from the SPME arrow fiber was conducted in the injector for 4 min with a solvent cut time of 5 min. The GC injection port was modified for the use of wider SPME arrow fibers and a splitless liner (1.8 mm x 5 mm x 95 mm, Topaz liner, Restek, Bad Homburg, Germany) was installed. The optimized MRM settings can be seen in the appendix in Table 9.2 and the ionization voltage and emission current were 70 eV and 60 µA, respectively. The method was used for SPME arrow injection as well as liquid injection with 0.5 µL injection volume. As response, the peak area determined by the TIC of MRM transitions was used. [130] Two transitions are sufficient to identify compounds according to the European Commission [131], but to increase the robustness of identification and to extend the applicability of the method in future works, multiple transitions were optimized which can be used for the determination of

FAMEs with GC-MS/MS operating in MRM mode. The geometric mean was used for averaging normalized data.

4.3.3 Sample preparation, extraction and automation

Since the analytes are extracted from the headspace, the ratio of headspace to liquid phase was 10 mL:10 mL. After heating the sample for 14 min (determined in pre-experiment), the SPME arrow fiber is inserted through the septum in the cap of the vial and the phase material is exposed. The FAMEs are sorbed to the phase material and after the extraction time has elapsed, the phase material is retracted into the cavity of the tool. The FAMEs are then immediately desorbed in the GC injector.

Full automation of the sample preparation, including the addition of standard solutions, pH adjustment, and extraction, was conducted with an RTC PAL autosampler and the following units: Agitator, DeCapper module, FiberConditioning module, Wash station, SPME arrow tool, 10 µL liquid tool, 100 µL liquid tool, Tool park station, all from CTC Analytics (Zwingen, Switzerland) and heating and stirring plate RTC basic (IKA, Staufen, Germany). SPME arrows were used with polydimethylsiloxane (PDMS), divinylbenzene polydimethylsiloxane (DVB-PDMS), carbon wide range divinylbenzene polydimethylsiloxane (CWR-DVB-PDMS), carbon wide range divinylbenzene (CWR-DVB) and polyacrylate (PA) as polymer sorption phases (BGB Analytik, Böckten, Switzerland).

The workflow for one sample was as follows: Sample is opened (DeCapper module) and standard solutions and H_2SO_4 for pH adjustment are added (liquid tools); tempering of MeOH-vial and chemical fiber cleaning in the headspace of MeOH (Heatex); thermal fiber cleaning (Fiber conditioning module); Tempering and stirring (heating and stirring plate); extraction (SPME arrow tool); Desorbing in GC injector (SPME arrow tool). The autosampler and automation software used was Chronos (version 5.1.20, Axel Semrau, Strockhoevel, Germany). The total method run time is 82 min. Due to an overlapping schedule, the next sample can already be prepared while the GC-MS/MS measurement is running. This saves 38 min per sample and results in a reduced run time of 44 min for one sample.

4.3.4 Optimization procedure

Selection of the optimal extraction parameters was done by one-factor-at-a-time (OFAT) and design of experiment (DOE) using the design of experiments application of OriginPro (Version 2020, OriginLab Corporation) [132]. The use of DOE reduces the sample number to a minimum, saves resources, and additionally observes factor

interactions. The DOE model used was a Box-Behnken model with the following settings: center points per block: 1, randomized design.

4.4 Method validation

4.4.1 Analytical performance

The calibration standards were prepared by spiking bi-distilled water, acidified to pH 2, with the FAME mix with varying concentrations. The internal standard (C17:0dMe) was spiked to each sample of method validation in a concentration of 2 µg L^{-1} and the peak areas of each analyte were normalized to the internal standard peak area. As the calibration ranged over two orders of magnitude, two concentration ranges were chosen for calibration. In the first calibration, the concentration of analytes ranged from 10-1,500 ng L^{-1} with five concentration levels, and in the second calibration, the concentration ranged from 500-10,500 ng L^{-1} (or 0.5-10.5 µg L^{-1}) with seven concentration levels. For each concentration level, 7 replicates were measured, leading to the relative standard deviation (RSD) values. To further evaluate the method, the method detection limit (MDL) was determined according to US Environmental Protection Agency's MDL procedure (Revision 2, 2016) [133]. The MDL was obtained at a concentration level with an S/N-ratio of 5 to 1 for all FAMEs in a spiked blank sample by using the single-tailed students' t-value with a confidence level of 99% ($t_{(6,\ 1-\alpha\,=\,0.99)} = 3.143$) and the standard deviation S_s of seven replicates ($MDL_s = t_{(n-1,1-\alpha\,=\,0.99)}S_s$).

4.4.2 Extraction efficiency

To evaluate the efficiency of extraction, the depletion-curve method according to Zimmermann *et al.* was used. [61] To that end, the sample is extracted 10 times to determine the depletion of the analyte's peak area, which in general follows a model function for exponential decay $\mathrm{f(x)} = \mathrm{ab}^x$. After that, the depletion curve is linearized by applying the natural logarithm (ln) to the peak area, consequently, the depletion follows the model function for linear equations $\mathrm{f(x)} = \mathrm{a} + \mathrm{bx}$. From the linear equation, the extraction efficiency E_E is obtained as the slope b of the linear equation by $1 - \mathrm{E}_E = \mathrm{e}^b$.

4.4.3 Real sample

The real sample was taken from the aqueous phase of a bioreactor fed by carbon-rich wastewater from a combustion plant. The quantification of the FAMEs was done by diluting the sample 1:4, 1:10, 1:100, and 1:1,000, and normalizing the peak area to the

internal standard. Relative recovery of the FAMEs in the real sample was obtained by dividing the 1:100 diluted sample into 10-mL aliquots to allow the measurement of triplicates of the spiked and non-spiked sample. The FAME mix with varying concentrations was spiked to the sample to achieve a dilution of 1:400,000 (corresponds to concentrations of 0.5-1.5 µg L^{-1}). Relative recovery was calculated by subtracting the spiked concentration from the non-spiked concentration and matching the result with the calibration.

4.5 Results and discussion

4.5.1 GC-MS/MS analysis

Since the electron ionization (EI) source strongly fragments the FAMEs, the molecular ion has a low abundance leading to lower sensitivity when exclusively used as a precursor ion in MRM. Therefore, in addition to the molecular ions specific EI fragments, previously selected by a product ion scan and according to Härtig et al. [134] (see appendix Table 9.1), were chosen for the MRM. These smaller fragments are generated in the EI source and can be assigned to a substance by chromatographic separation in combination with the previous product ion scan. The selection of precursor and product ions is shown in the appendix in Table 9.2. In this work, all 5-6 transitions were used as quantifiers and qualifiers. Using the here-stated MRM transitions and the TIC of MRM transitions for quantification may not apply to every sample matrix due to possible interfering compounds. Therefore its use has to be evaluated in method development by observing the ion ratios. Although the use of TIC of MRM transitions for quantification could lead to higher error proneness, on the other hand, it gains sensitivity so that the matrix can be diluted and dilution can reduce matrix effects. The deviation of the ion ratios was monitored throughout the measurements and was found to be always below ±10% (see appendix Figure 9.1) in ultrapure water and real sample and no errors and/or disturbing substances were found. The observed ion ratios for every analyte are shown in the appendix in Table 9.2. To increase the response, the collision energy (CE) was optimized in the range of 5-30 eV, which is specific for each transition. The optimization resulted in a response increase of 20-60% (Figure 4.1 a). An ion source temperature of 180 °C and standard

ionization voltage of 70 eV led to the highest response (Figure 4.1 b), as the abundance of the chosen fragments and molecular ions increased.

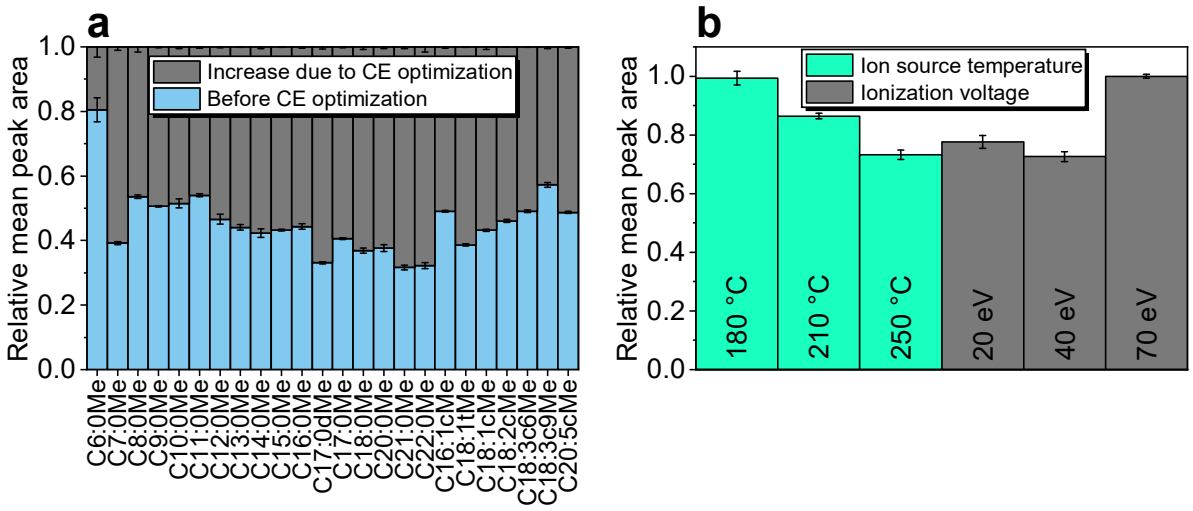

Figure 4.1 Results of GC-MS/MS FAMEs method optimization. (a) Relative peak areas before (blue) and increase after collision energy optimization (grey). (b) Optimization of ion source temperature (green) and ionization voltage (grey). Experimental conditions: n = 3; (a) CE before optimization: 5 eV, CEs for optimization: 5, 10, 15, 20, 25 and 30 eV; (b) ionization voltage at ion source temperature optimization: 70 eV, ion source temperature at ionization voltage optimization: 250 °C.

4.5.2 Optimization of the extraction procedure

4.5.2.1 Effect of extraction temperature

In order to optimize the extraction parameters, OFAT (time, material, cleaning, stirring rate) and DOE (temperature, pH) strategies were used. As a result of DOE, the normalized fitted response of temperature-dependent extraction yields for all FAMEs is shown in Figure 4.2 a (R^2 = 0.9231 and adjusted R^2 = 0.6922 of quadratic fit). At a higher temperature, the headspace concentration of the analytes increases (Figure 4.2 b, calculation shown in the appendix; literature data not available for unsaturated FAMEs) consequently the extracted amount increases. Considering the three-phase system (aqueous phase, headspace, and fiber) and total equilibrium, the fraction of analytes located on the fiber is high for the >C13:0Me FAMEs (Figure 4.2 c), whereas the fractions in water and headspace are lower. The equilibrium constants were obtained with pp-LFER calculations (shown in the appendix), but literature data were not available for all FAMEs and only for PDMS fiber material [135]. The relationship between high affinity to the phase material and the transfer of the analytes into the headspace leads to the effect that under equilibrium conditions almost 100% of the >C13:0Me FAMEs can be extracted (Figure 4.2 c, see appendix Table 9.3). Nevertheless, equilibrium is often not reached during sample preparation due to time

constraints, resulting in lower fractions in practice. A different effect is revealed by the short-chain FAMEs (< C10:0Me), where the highest response is between 40-65 °C. This effect can be explained by the low affinity to the phase material combined with an accelerated sorption/desorption equilibrium for the < C10:0Me FAMEs.

A higher extraction temperature leads to increased droplet formation due to the condensation of water on the SPME arrow material (see appendix Figure 9.4) and an increase of retention time, only determined for C6:0Me, averaged to 7.15 min at 40 °C, 7.18 min at 65 °C and 7.21 min at 90 °C. These retention time shifts are a sign of an increased amount of injected water since water expands a thousandfold in the injector and creates a thin layer inside the column [136]. The extraction temperature was lowered to 70 °C for the final method.

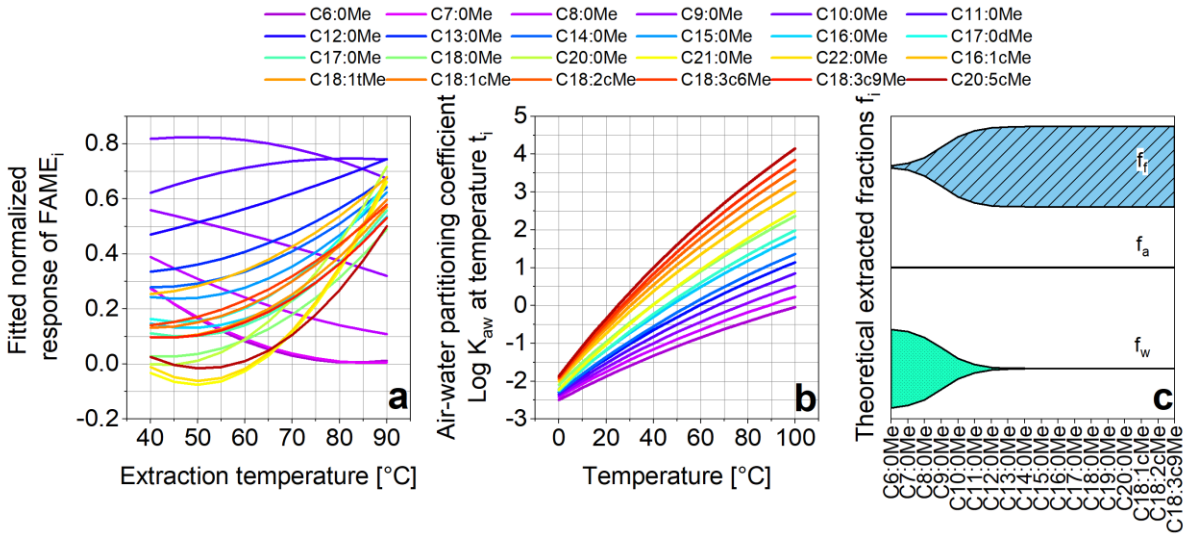

Figure 4.2 Results of extraction temperature optimization. (a) Fitted normalized response of extraction temperature dependency for single FAMEs obtained with DOE. (b) Temperature dependency of the Henrys law constant K_{aw} for saturated FAMEs. (c) Kite-plot of theoretical distributions of FAMEs in the three sample phases air f_a, water f_w and sorbed to the SPME arrow fiber f_f (PDMS) at 25 °C for saturated FAMEs and some unsaturated FAMEs. Experimental conditions for (a): n = 3; Sample: FAME mix with varying concentrations 1:400,000 diluted in bidistilled water. Extraction parameters: stirring rate: 1,500 rpm, 30 min, DVB-PDMS, varying temperature (40-90 °C), pH 2.

4.5.2.2 Effect of extraction pH

To evaluate the effect of pH on hydrolysis of the FAMEs the hydrolysis half-life is calculated with help of the pseudo-first-order rate constants at 25 °C for the acid, neutral and base-catalyzed hydrolysis of saturated FAMEs, taken from Rayne *et al.* [137] (calculation shown in the appendix). Results of Figure 4.3 a and b were obtained with DOE (R^2 = 0.9231 and adjusted R^2 = 0.6922 of quadratic fit). At 40 °C, the optimal pH value is between 3 and 6, which corresponds to a hydrolysis half-life above 100 d

(Figure 4.3 a and c). At 90 °C, however, the optimal range of pH value shifts to pH 2, indicating acid-catalyzed hydrolysis must have a negligible influence on response reduction. Literature data for Figure 4.3 c was not available for unsaturated FAMEs and literature data for temperature-dependent hydrolysis half-life was also not available. Figure 4.3 c shows the regular hydrolysis half-life shape with a maximum hydrolysis half-life at pH 5.5 and a minimum hydrolysis half-life at pH 14. Thus, the base-catalyzed hydrolysis is three orders of magnitude faster and more relevant than the acid-catalyzed hydrolysis. The stronger effect of base-catalyzed hydrolysis can be confirmed, resulting in a 50% response reduction from pH 6 to 12 (Figure 4.3 a and b). When the effect of pH on the individual FAMEs is considered (Figure 4.3 b), the optimal pH of 2 is confirmed in most cases but is almost constant between pH 2-5 for < C12:0Me FAMEs. To keep the effect of hydrolysis time as low as possible, the pH adjustment of every single sample was done by the autosampler directly before sample heat up, avoiding any storage time.

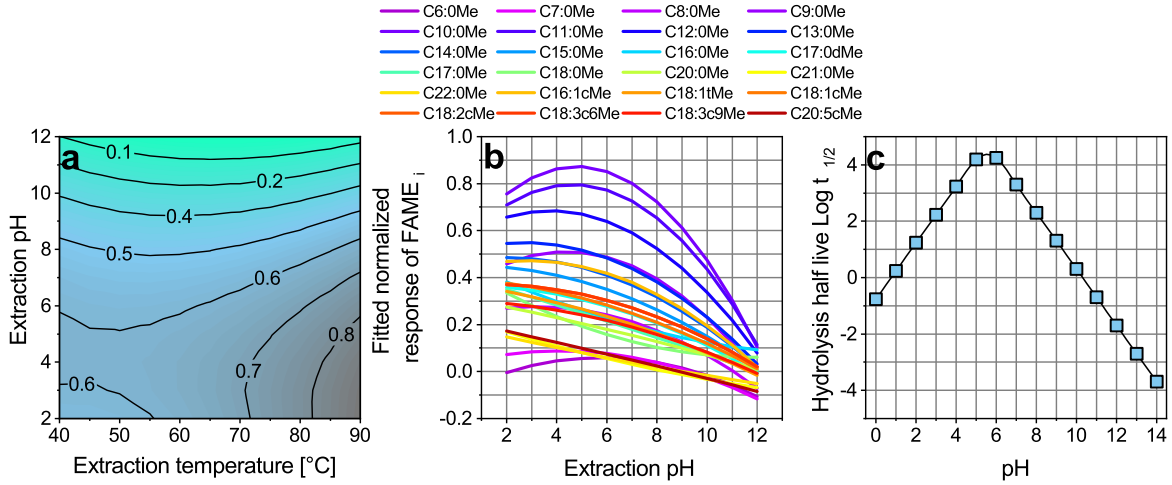

Figure 4.3 Results of extraction pH optimization. (a) Contour plot of extraction pH and extraction temperature optimization for all FAMEs. (b) Fitted normalized response of extraction pH dependency of single FAMEs. (c) Determined pH dependency of hydrolysis half-life $t_{1/2}$ in days representative for all saturated FAMEs. Experimental conditions for (a) and (b): n = 3; Sample: FAME mix with varying concentrations 1:400,000 diluted in bidistilled water; Extraction parameters: stirring rate: 1,500 rpm, 30 min, DVB-PDMS, varying temperature (40-90 °C) and pH (2-12).

4.5.2.3 Effect of extraction time

To determine an averaged optimal extraction time, experiments were performed with 30 s to 1,800 s extraction time, with the longest extraction time 1,800 s (30 min) achieving the best results (Figure 4.4). However, considering the benefit of a 10 min shorter method and a loss of only approximately 10% response, an extraction time of 1,200 s (20 min) was used in further experiments. Single extraction profiles can be

found in the appendix (Figure 9.2 and Figure 9.3). For C6:0Me, the response remains constant (± 15%) during all extraction times due to fast equilibrium attainment, which can also be seen in the extraction profile for C6:0Me (see appendix Figure 9.2).

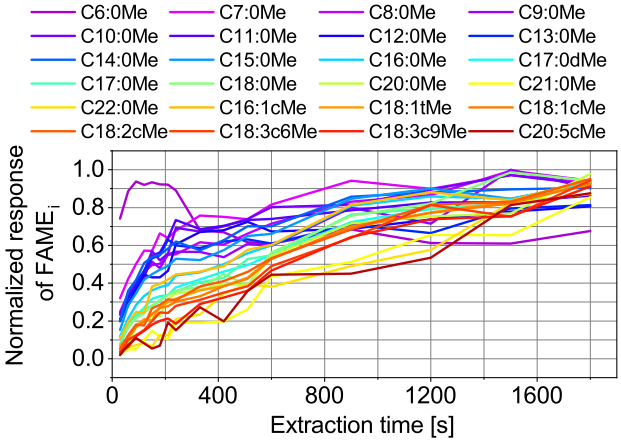

Figure 4.4 Results of extraction time optimization showing extraction profiles for single FAMEs. Experimental conditions: n = 3; Sample: FAME mix with varying concentrations 1:400,000 diluted in bidistilled water; Extraction parameters: stirring rate: 1,500 rpm, varying extraction time (30, 60, 90, 120, 150, 180, 210, 240, 330, 420, 510, 600, 900, 1,200, 1,500, 1,800 s), DVB-PDMS, 70 °C, pH 2.

4.5.2.4 Effect of extraction material

Five SPME arrow sorbents PA, DVB-CWR-PDMS, PDMS, CWR-PDMS, and DVB-PDMS were tested (Figure 4.5), with DVB-PDMS covering the broadest and CWR-PDMS the narrowest range of analytes. PDMS and PA are the best sorbents for unsaturated FAMEs, plus PA also covers long-chain FAMEs >C13:0Me. DVB-CWR-PDMS covers medium-chain C8:0Me-C12:0Me and CWR-PDMS only short-chain C6:0Me-C8:0Me FAMEs sufficiently well. To cover the broadest range of analytes DVB-PDMS was used in the final method.

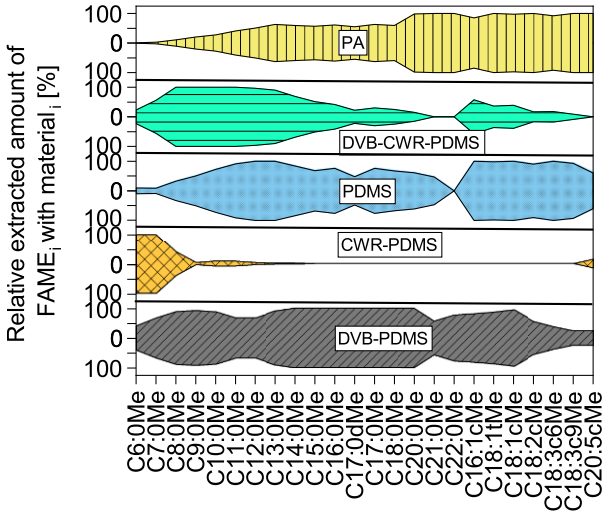

Figure 4.5 Results of SPME arrow material optimization presented as kite diagrams showing the distributions of the respective FAMEs on the different extraction phases. Experimental conditions: n = 3; Sample: FAME mix with varying concentrations 1:400,000 diluted in bidistilled water; Extraction parameters: stirring rate: 1,500 rpm, 30 min, varying SPME arrow material (PA, DVB-CWR-PDMS, PDMS, CWR-PDMS, DVB-PDMS), 70 °C, pH 2.

4.5.2.5 Effects of stirring rate, SPME arrow cleaning parameters and stir bar material

Testing stirring rates of 500, 1,000, and 1,500 rpm for the extraction, the response was increased by 28% from 500-1,500 rpm (data not shown) due to faster equilibrium attainment. Since the analytes have a high affinity for the phase material, the carryover of the analytes into the next measurement has to be monitored. The correlation between carry-over and cleaning process was determined by measuring blanks after each cleaning. The percentages for carry-over refer to the quantity found in the blank in relation to the quantity in the previously measured sample. Different SPME arrow cleaning methods were tested, but the best results were achieved by a chemical cleaning step prior to thermal cleaning, which to the best of our knowledge, has not yet been reported in literature. By adding a chemical cleaning step of the fiber in the headspace of MeOH (1 mL MeOH in 20 mL vial) for 2 min prior to the thermal cleaning step, the carryover could be reduced from >4% (thermal cleaning) to < 1% (chemical and thermal cleaning) and additionally the fiber cleaning parameters could be decreased from 15 min at 300 °C to 10 min at 280 °C. The vial for chemical cleaning can be reused several times (average 40 times in this study), depending on the used concentration. Without cleaning, 6% of the analytes remain on the fiber. Consequently, 94% of the analytes are desorbed in the injection. Longer chain FAMEs >C16:0Me had a higher occurrence in the carry-over because they have a higher affinity for the phase

material and thermal desorption is slower. Another source of 8% analyte loss was obtained when Teflon instead of glass was used as stir bar material (data not shown). Therefore, glass stir bars were used in the following experiments.

4.5.3 Validation of the analytical method

The FAMEs were calibrated in a range of 10-10,500 ng L^{-1}. As this wide range showed different linearities, it was divided into two calibrations for the quantification calculations of the real samples. The results for both calibrations 10-1,500 ng L^{-1} and 500-10,500 ng L^{-1} are listed in Table 4.1. The low calibration showed good linearity for most of the FAMEs ($R^2 \geq 0.9319$) however, was not linear for C20:0Me, C21:0Me, C22:0Me, and C20:5cMe ($R^2 \leq 0.8448$). The non-linearity of the longer-chain FAMEs at the low calibration indicates that a smaller amount is injected into the GC, which could be due to less optimal extraction parameters. In addition, the sorption/desorption equilibrium attainment is slower and the FAMEs would need longer to increase the amount sorbed to the fiber (see time-dependent extraction profiles in Figure 4.4). The high calibration showed good linearity for all FAMEs ($R^2 \geq 0.9657$). The MDLs ranged from 9-437 ng L^{-1} and were higher for long-chain FAMEs (≥ C18:0Me carbon atoms). Single calibration plots and linear regression functions of calibration are shown in the appendix (Figure 9.5, Figure 9.6, and Table 9.4). Extraction efficiencies ranged from 13-59% (n = 3, $R^2_E \geq 0.7581$), which are comparable with extraction efficiencies determined with SPME arrow extraction for PAHs by Kremser *et al.* [124]. Relative recovery of 69-127% was observed for spiked diluted (1:100) real samples in the dilution of 1:400,000 (corresponds to concentrations of 500-1,500 ng L^{-1}). Single depletion curves and linear regression functions of extraction efficiency are shown in the appendix (Figure 9.7, Figure 9.8 and Table 9.4).

Table 4.1 Analytical method validation results. R^2_1: linear regression coefficient of calibration (10-1,500 ng L^{-1}), R^2_2: linear regression coefficient of calibration (500-10,500 ng L^{-1}), MDL: method detection limit, RSD_1: relative standard deviation of calibration (10-1,500 ng L^{-1}) at second calibration point (n = 7, 100-300 ng L^{-1}), RSD_2: relative standard deviation of calibration (500-10,500 ng L^{-1}) at fifth calibration point (n = 7, 6,500-7,500 ng L^{-1}), E_E: extraction efficiency, R: relative recovery of analytes in 1:100 diluted real sample spiked with 500-1,500 ng L^{-1}, c: calculated concentration of analytes in real sample (diluted 1:4, 1:10, 1:100 and 1:1,000). Experimental conditions: Optimized parameters were used.

FAME	R^2_1	R^2_2	MDL [ng L^{-1}]	RSD_1 [%]	RSD_2 [%]	E_E [%]	R [%]	c [µg L^{-1}]
C6:0Me	0.9963	0.9761	23	31	27	13	75	27
C7:0Me	0.9606	0.9952	41	19	19	32	79	4
C8:0Me	0.9861	0.9992	16	11	15	59	76	0.3
C9:0Me	0.9883	0.9904	17	7	10	49	118	nd

FAME	R^2_1	R^2_2	MDL [ng L^{-1}]	RSD_1 [%]	RSD_2 [%]	E_E [%]	R [%]	c [µg L^{-1}]
C10:0Me	0.9962	0.9877	16	8	10	50	79	nd
C11:0Me	0.9999	0.9907	11	13	14	47	126	nd
C12:0Me	0.9966	0.9972	16	19	16	47	87	0.1
C13:0Me	0.9948	0.9953	13	23	16	48	127	nd
C14:0Me	0.9954	0.9875	26	19	9	47	88	1.3
C15:0Me	0.9933	0.9954	12	22	29	44	112	nd
C16:0Me	0.9862	0.9845	89	17	33	35	117	76
C17:0Me	0.9943	0.9793	10	24	36	20	117	11
C18:0Me	0.9829	0.9872	163	24	25	12	115	525
C20:0Me	nl	0.9818	119	nl	17	22	69	15
C21:0Me	nl	0.9657	124	nl	22	24	82	3
C22:0Me	nl	0.9928	290	nl	26	20	87	15
C16:1cMe	0.9878	0.9957	9	18	19	50	109	nd
C18:1tMe	0.9319	0.9755	14	37	36	22	109	nd
C18:1cMe	0.9664	0.9756	18	28	36	26	75	3490[a]
C18:2cMe	0.9758	0.9838	145	bm	32	42	100	402
C18:3c6Me	0.9622	0.9973	12	23	18	47	89	nd
C18:3c9Me	0.9503	0.9939	9	28	21	48	79	nd
C20:5cMe	nl	0.9817	437	bm	27	36	126	nd

[a]Was used as an extractant for the products in the bioreactor
nd: Substance is not determined
nl: Calibration curve is not linear
bm: Calibration point is below MDL

4.5.4 Real sample analysis

Analysis of the aqueous phase in a bioreactor showed the highest concentration for C18:1c (3.5 mg L^{-1}), which was added to the bioreactor for extraction of the produced substrates. Additionally detected FAMEs, listed in Table 4.1 were in the range of 0.1-525 µg L^{-1}. Figure 4.6 shows chromatograms of the optimized MRM (A) and a Q3 Scan (single quadrupole operation mode) of the sample (B). The baseline noise and interfering peaks could be eliminated using MRM. Additionally, more FAMEs, especially in low concentrations, could be detected by MRM.

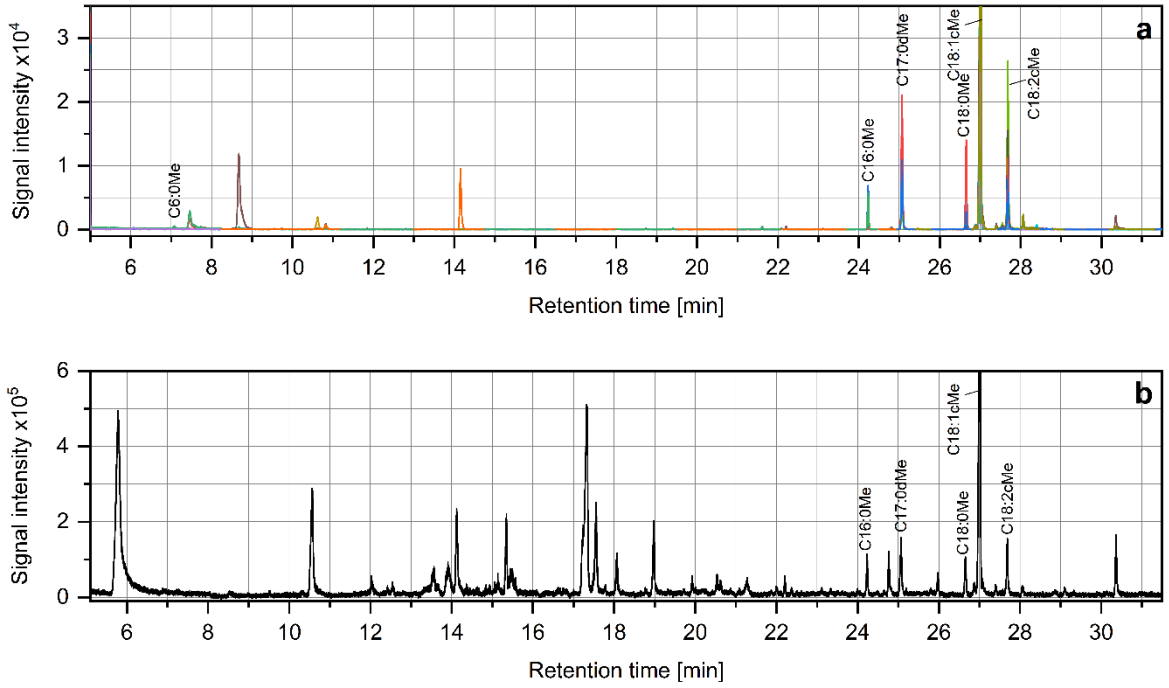

Figure 4.6 Chromatograms of real sample (1:100 diluted) from a bioreactor analyzed in MRM Mode (a) and Q3 Scan (b). Colors indicate specific transitions of MRM according to Table 9.2.

4.5.5 Comparison with other methods

To the best of our knowledge, there is no other study dealing with the extraction of FAMEs from aqueous samples via SPME arrow. Studies from the last ten years proposed the analysis of FAMEs from biodiesel, wastewater, bio-liquid, and bacterial cells (after fatty acid derivatization) with LLE [118], DLLME [116], HF-LPME [123], SPE [121] and SPME [122]. Since biodiesel matrices differ widely from aqueous matrices, only the method for FAME determination in wastewater by Yu *et al*. is comparable with the samples presented here. The method proposed by Yu *et al.* was applied only to C16:0Me and C18:0Me and calibrated in a higher concentration range (0.2-5 mg L^{-1}), exhibiting LODs of 0.05-0.3 mg L^{-1} and RSDs from 6-14%. The method proposed here covered 24 FAMEs and was calibrated in a lower concentration range to achieve matrix dilution of the samples. The LODs were lower and ranged from 0.01-1.9 mg L^{-1}, however, the RSDs had a broader range of 7-37%.

4.6 Conclusions

A fully automated and rapid green sample preparation and GC-MS/MS MRM method for the detection of FAMEs in aqueous samples was developed. Optimization and full automation greatly improved the analytical performance of the method. The optimal conditions depend on the structure of the FAME under consideration and can be

compared and explained using theoretically calculated and literature data. Due to full automation and an overlapping schedule, 32 samples can be analyzed in one day (method run time 44 min). The sensitivity of the application was improved significantly by using SPME arrow but shows a smaller linear range and higher RSD values compared to conventional extraction methods. However, the vast majority of studies have been conducted analyzing high concentrations of FAMEs in non-aqueous samples (e.g., biodiesel), methods dealing with the analysis of FAMEs in aqueous samples are still lacking. The results found in this study, suggest that the method can be used for the analysis of FAMEs in samples even with high matrix load, with the advantages of MRM scanning, sample dilution, and headspace extraction. After this, further sample types (solid, gaseous, biological, etc.) for FAMEs analysis could be tested, wherein the method parameters of this study can be subsequently utilized.

5 Isotope-labeling *in-situ* derivatization and HS-SPME arrow GC-MS/MS for the simultaneous analysis of fatty acids and fatty acid methyl esters in aqueous samples

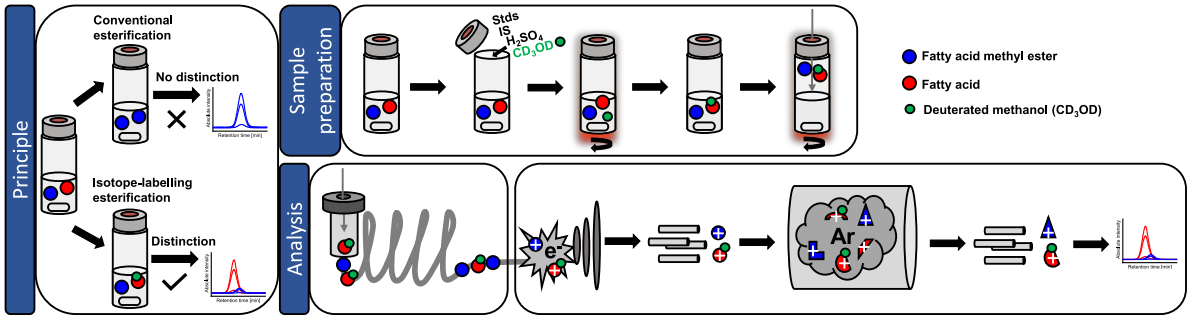

Adapted from: Lucie K. Tintrop, Jana R. Lieske-Overgrand, Kaliyani Wickneswaran, Rukiyye Abis, Ruth Brunstermann, Maik A. Jochmann, Torsten C. Schmidt. Isotope-labeling in situ derivatization and HS-SPME arrow GC-MS/MS for simultaneous determination of fatty acids and fatty acid methyl esters in aqueous matrices, published in Analytical and Bioanalytical Chemistry (2023). © Springer Nature 2023

5.1 Abstract

Fatty acids (FAs) and fatty acid methyl esters (FAMEs) co-occur in many samples, and analysis of both substance classes is frequently of high interest. To this end, this study introduces the first method for simultaneous determination of FAs and FAMEs including fully automated solvent-free solid-phase microextraction (SPME) arrow headspace extraction combined with isotope-labeling *in situ* FA derivatization with deuterated methanol (CD_3OD). By using the chromatographic isotope effect (ΔR_t = 0.03 min) and the +3 *m/z* mass shift, FAs can be selectively differentiated from the FAMEs during gas chromatography tandem-mass spectrometry (GC-MS/MS) operated in the multiple reaction monitoring (MRM) acquisition mode. Additionally, an approach is presented to predict the retention times of deuterated compounds. Optimization of the derivatization conditions was accomplished by design of experiments and found to be 20 min, 50 °C, 4 v/v% CD_3OD, and pH 2.1. During method validation, FAs and FAMEs were calibrated in different concentration ranges by standard addition in five real matrices and ultrapure water leading to good linearities and method detection limits for FAs ranging from 1-30 µg L^{-1} and for FAMEs from

0.003-0.72 µg L^{-1}. FAs and FAMEs were detected in real samples from surface water, wastewater treatment plant effluent, and three different bioreactor samples and could be quantified in concentrations ranging from 2-1056 µg L^{-1} for FAs and 0.01-14 µg L^{-1} for FAMEs.

5.2 Introduction

5.2.1 Relevance of simultaneous determination of FAs and FAMEs

Fatty acids (FAs) and fatty acid methyl esters (FAMEs) are important substance classes in science and technology including the fields of medicine [138-140], microbiology [141, 142], geochemistry [143], energy [118, 144, 145], industrial production [146], and wastewater treatment [119, 147, 148]. In general, FAs occur more frequently and in higher concentrations and are therefore the more intensively studied substance class compared with FAMEs. The simultaneous analysis of FAs and FAMEs is advantageous for various applications, as they are related, can be converted into each other, and often appear together. Some examples of application fields for the simultaneous determination of FAs and FAMEs are briefly mentioned below.

FAs are present in healthy organ tissues, however, metabolic pathways have been discovered in which tissue FAs are partly transformed into FAMEs after methanol intoxication. [149] In humans, drastically increased FAME levels can be found in tissues in case of long-term alcohol abuse. [140] A similar phenomenon can be observed in insects such as *O. furnacalis*, which can be a target of this process after plant-defense-based methanol intoxication. [150] Some defense mechanisms of microorganisms and plants are based on the production of antimicrobial FAMEs or FAs, which show an inhibitory effect. [11, 151] FAs are known to interfere with relevant biological processes, especially anaerobic digestions as in wastewater and digested sludge treatment, biodiesel, and biogas production. [11-13] For example, long-chain FAs were found to promote the growth of specific microorganisms such as *M. parvicella* which causes serious problems such as bulking and filamentous foaming in activated sludge systems. [148] In biodiesel or biogas production, lipids are often used as a source to establish the formation of desired products or as feed for microorganisms. [7, 8] In biodiesel production processes, the lipids produced in the bioreactor are converted to methyl esters after extraction by the addition of methanol for methyl esterification. [152] In another study, *E. coli* was modified to be able to directly

synthesize FAMEs for biodiesel from free FAs by utilizing a bacterial fatty acid methyltransferase. [144]

In all of the above-mentioned applications, it is an advantage to be able to use a simultaneous FA and FAME method to determine actual values and/or to monitor the effectiveness of the conversion processes over time. Further advantages result from the time, resources, and cost savings of the simultaneous analysis compared to two individual analyses.

5.2.2 Analysis of FAs and FAMEs

Gas chromatography is a common procedure to investigate FAs, their derivatives, and FAMEs, which has been described in many studies. [138, 143, 145, 148, 153]. When analyzing FAs a derivatization is recommended due to several problems that occur in the analysis of underivatized fatty acids such as low sensitivity, reproducibility, and recovery [154]. In addition, long-chain FAs tend to decompose at high temperatures. In general, derivatization reactions are performed in a solvent, but for aqueous samples, this would require sample preparation with an extra solvent-consuming extraction step such as solid-phase extraction (SPE) or liquid-liquid extraction (LLE) and additional steps such as solvent evaporation and reconstitution. Although SPE and LLE are still used to a large extent, their environmental impact and greenness evaluations are poor and they should be avoided as equal or even better-performing alternatives already exist. To be able to apply the derivatization to aqueous samples, it should be possible to integrate the derivatization reaction into the sample preparation process without much additional effort. This can be utilized by *in situ* derivatization, which has the advantage that it does not require additional time-consuming steps leading to analyte loss and it can be performed directly in the sample, being compatible with various matrices. Additionally, *in situ* derivatization can be combined with solvent-free and miniaturized microextraction techniques such as solid-phase microextraction, and both processes can be integrated into automated systems. Alkylation, esterification, and amide formation can be used for *in situ* derivatization of fatty acids, with esterification being the method with the least changes to the molecule [154]. Formation of methyl or ethyl ester derivatives of carboxylic acids in aqueous samples can be achieved with dimethyl sulfate [155, 156], diethyl sulfate [157], or alcohols in combination with a mineral acid [141]. In recent years, the use of highly toxic reagents, including dimethyl sulfate and diethyl sulfate, has become increasingly unpopular, as

it is a risk to health (mutagenic and cancerogenic) and the environment. As a result, the demand for environmentally friendly, green procedures has become higher. Moreover, alcohols and mineral acids are easy to handle and available in almost every laboratory.

However, so far no method capable of analyzing FAs and FAMEs in one run has been described in the literature. One reason for this may be the classically utilized derivatization technique for FAs in GC analysis: methyl esterification, which makes it impossible to distinguish the FAs and FAMEs. Here, a method is presented which allows the simultaneous detection of derivatized fatty acids and their methyl esters. The novel approach presented in this study uses deuterated methanol (CD_3OD) and H_2SO_4 to transform the FAs *in situ* directly in the aqueous sample resulting in a consecutive mass shift of 3 m/z and an inverse chromatographic isotope effect, which was determined by GC-MS/MS. The chromatographic isotope effect was observed and used for more reliable compound identification, therefore its characteristics are briefly mentioned in the following. [158-160] Many conventional columns are not able to separate isotopologues, mostly due to unsuitable polarity. Moreover, for nonpolar columns usually an inverse isotope effect, where the heavier isotopologue is eluted before its counterpart, and for polar columns a normal isotope effect, where the heavier isotopologue is eluted after its counterpart, is observed. [160] Meier-Augenstein suggested that the lower retention time of the heavier isotopologues can not be assigned to differences in vapor pressure because the lighter molecule would have an earlier elution due to higher vapor pressure. Since the opposite is observed, the earlier elution of the isotopologues has to be the result of weaker solute-stationary phase interactions, mainly induced by Van-der-Waals dispersion forces and caused by a lower molecular volume of the deuterated molecule. The lower molecular volume is a result of higher C-D bond strength reducing the bond length and zero-point vibrational energy. [161, 162]

The derivatization conditions were optimized using a design of experiment Box-Behnken model. With the application of headspace solid-phase microextraction (SPME) arrow in this study, the extraction step could be simplified, shortened, and solvent-free. SPME arrow, a further developed SPME, enhances mechanical stability and phase volume resulting in higher sensitivity. Compared to solvent-consuming extraction methods, such as LLE and SPE, SPME is easier to automate, applicable to aqueous samples, and follows terms of green sample preparation. [124, 129]

5.3 Material and methods

5.3.1 Reagents and materials

Hexanoic acid (C6:0, ≥ 98%), octanoic acid (C8:0, ≥ 98%), nonanoic acid (C9:0, ≥ 99.5%), decanoic acid (C10:0, ≥ 99.5%), undecanoic acid (C11:0, ≥ 98%), dodecanoic acid (C12:0, ≥ 99.5%), tridecanoic acid (C13:0, ≥ 98%), tetradecanoic acid (C14:0, ≥ 99.5%), pentadecanoic acid (C15:0, ≥ 99%), hexadecenoic acid (C16:0, ≥ 99%), isotope-labelled hexadecenoic acid d_{31} (d_{31}-C16:0, ≥ 99%), heptadecanoic acid (C17:0, ≥ 98%), octadecanoic acid (C18:0, ≥ 98.5%), nonadecanoic acid (C19:0, ≥ 98%), eicosanoic acid (C20:0, ≥ 99%), heneicosanoic acid (C21:0, ≥ 99%), doeicosanoic acid (C22:0, ≥ 99%), *cis*-9-hexadecenoic acid (C16:1-c9, ≥ 98.5%), *cis*-9-octadecenoic acid (C18:1-c9, ≥ 99%), *trans*-9-octadecenoic acid (C18:1-t9, ≥ 99.0%), *cis*-9, 12-octadecadienoic acid (C18:2-c9-12, ≥ 99%), *cis*-9,12,15-octadecatrienoic acid (C18:3-c9-12-15, ≥ 99%), *cis*-6,12,15-octadecatrienoic acid (C18:3-c6-9-12, ≥ 99%), *cis*-5,8,11,15,17-eicosapentanoic acid (C20:5-c5-8-11-15-17, ≥ 98.5%), heptanoic acid methyl ester (C7:0Me), nonanoic acid methyl ester (C9:0Me, ≥ 99.8%), isotope-labelled heptadecenoic acid methyl ester d_{33} (d_{33}-C17:0Me, ≥ 97.5%) and 37-component FAME mix in dichloromethane with varying concentrations of 200-600 mg L^{-1} were purchased from Sigma Aldrich (Steinheim, Germany), and heptanoic acid (C7:0, ≥ 98%) from Fisher Scientific (Loughborough, United Kingdom). The derivatization reagents istotope-labelled methanol (CD_3OD, ≥ 99.8 %) and sulfuric acid (H_2SO_4, ≥ 95%) were purchased from Deutero (Kastellaun, Germany) and Fisher Scientific (Loughborough, United Kingdom), respectively. Stock solutions (1 g L^{-1}) were prepared in chloroform (≥ 99.8%, Sigma Aldrich, Steinheim, Germany) and stored in the fridge at 4 °C. Ultrapure water was purchased from Bi-Distillation apparatus (Bi 18E with quarz glass, Quarzglas QCS, Germany). With the FA stock solutions a FA mix was prepared in chloroform with a concentration of 40 mg L^{-1} for each FA. The 37-component FAME mix with varying concentrations of 200-600 mg L^{-1} for each FAME was diluted 1:100 in chloroform to 2-6 mg L^{-1}. Another FAME mix was prepared in a concentration of 2 mg L^{-1}, withC7:0Me and C9:0Me, because they were missing in the 37-component FAME mix. FAs are transformed to isotope-labeled FAMEs during derivatization and are referred to as d_3-FAMEs throughout this work, therefore the suffix "d_3" is added to the abbreviations, e.g. C6:0Me-d_3.

5.3.2 GC MS/MS analysis

The simultaneous analysis of FAMEs and FAs was done by using a GC 2010 with a MS/MS TQ8040 (Shimadzu Deutschland GmbH, Duisburg, Germany) operating in MRM mode. The MRM settings are shown in Table 9.5 in the appendix. Separation of the analytes was performed by a Zebron ZB-FAME capillary column (30 m x 0.25 mm x 0.20 µm, Phenomenex, Torrance, USA) for which the oven temperature program started at 40 °C, held for 5 min, and was raised with a rate of 5 °C min^{-1} to 210 °C, held for 5 min. Helium (5.0, AirLiquide, Oberhausen, Germany) was used as carrier gas with a column flow of 1.8 mL min^{-1}, and argon (5.0, AirLiquide, Oberhausen, Germany) as collision gas. Injection of the analytes was done by splitless thermal desorption from the SPME arrow fiber by 250 °C for 4 min using a SPME arrow liner (1.8 mm x 5 mm x 95 mm, Topaz liner, Restek, Bad Homburg, Germany) and a wider injector needle guide for SPME arrows (Shimadzu Deutschland GmbH, Duisburg, Germany). The transfer line and ion source temperature were set to 180 °C and a solvent cut of 5 min was applied. Electron ionization (EI) was conducted at standard 70 eV. The analytical signal was integrated and the peak area was used as response in data evaluation. One quantifier ion was used for each analyte, which is stated in Table 9.5 in the appendix.

5.3.3 Automation of sample preparation

The sample preparation was fully automated with a robotic tool change prep and load (RTC PAL) autosampler (CTC Analytics, Zwingen, Switzerland) including the following steps: addition of standards, internal standards, and derivatization reagents; sample derivatization; analyte extraction by SPME arrow, sample injection, and SPME arrow fiber cleaning. All modules, units, and tools are shown in Table 9.6 in the appendix. Due to the robotic tool change option, the autosampler was able to change the tools during the procedure. The whole automation procedure is shown in the appendix in Table 9.7. The overall method time was 123 min, but the sample preparation overlaps with the GC runtime, therefore 39 min per run can be saved resulting in a reduced run time of 84 min per sample and a sample throughput of 17 samples per day.

5.3.4 Extraction procedure

The SPME arrow headspace extraction procedure for FAMEs was optimized in previous work [163] to be an extraction time of 20 min, divinylbenzene polydimethylsiloxane (DVB-PDMS) extraction material, temperature of 70 °C, pH 2 (here: 2.1), stirring with glass stir bars at 1500 rpm and fiber cleaning by chemical

cleaning in the headspace of 1 mL of Methanol (here: CD_3OD) at 70 °C followed by thermal cleaning at 280 °C. The SPME arrow extraction was performed in the headspace of a 20-mL vial with 10 mL of sample.

5.3.5 Optimization of derivatization parameters

Selection of the optimal derivatization temperature (40-90 °C), time (1-60 min), pH (2-4), and CD_3OD content (1-5 v/v%) was done by using the Design of Experiments (DOE) application of OriginPro (Version 2022, OriginLab Corporation). A Box-Behnken model was used for optimization with four continuous factors, one center point per block, and 25 runs. The final parameters were selected by averaging the optimal parameters of all FAs. The DOE was conducted in ultrapure water spiked with a FA concentration of 40 µg L^{-1}.

5.3.6 Method validation

Calibration of FAs and FAMEs was performed directly in the samples' matrix by spiking the required amount of FA mix and FAME mixes to the matrix solution. In ultrapure water, FAs were calibrated in the range of 4-120 µg L^{-1}, and FAMEs were calibrated in the range of 0.2-2.8 µg L^{-1} with five concentration levels and seven replicates per concentration level. In the real samples (SW, WWTP, BR1-BR3), the quantification was performed by standard addition with four concentration levels plus the non-spiked sample (FAs: 0-80 µg L^{-1}; FAMEs: 0-2.2 µg L^{-1}) in triplicates per concentration level. The internal standards d_{31}-C16:0Me-d_3 and d_{33}-C17:0Me were spiked to the solution in a concentration of 40 µg L^{-1} prior to extraction and derivatization. Peak area normalization using internal standards was not performed, as it was worsening the linearity, especially in the real sample. However, the internal standards were used to monitor fluctuations during the measurements and for retention time prediction. Assessment of the method detection limit (MDL) was done according to the MDL procedure for a spiked blank sample released by the US Environmental Protection Agency (Revision 2, 2016). [133] Recovery measurements were conducted in triplicates by spiking the real samples with 80 µg L^{-1} with the FA mix and with 1.8-2.2 µg L^{-1} of the FAME mixes and matching the found concentrations to the calibration curve. The RSDs were calculated for the spiked real samples of the recovery measurements.

5.3.7 Real samples

All of the real matrices were filtered with a polypropylene syringe filter with 0.45 µm pore size (BGB Analytik, Boeckten, Switzerland) to avoid the growth of microorganisms during the measurement and storage time. The abbreviations and measured dilutions are shown in Table 5.1. All real matrices were stored in the freezer (-18 °C). The conditions for BR1-BR3 indicate different settings of thermal aqueous digestion experiments of biowaste. The bioreactors were large-scale aqueous systems (>500 L) operated at room temperature and tested for the reusability of biowaste in terms of fatty acid production by microorganisms. Different biowaste pre-treatment conditions were applied to test the influence on FA production. After digestion, the remaining aqueous phase was separated from solid biowaste parts by pressurized filtration. Analysis of the real samples was similar to the analysis of the calibration standards. SW and WWTP samples were measured non-diluted whereas BR1-BR3 were measured in 1:10 dilution.

Table 5.1 General information about the real samples including the used abbreviations and measured dilutions.

Source	Abbr.	Dilution
Surface water, lake	SW	None
Surface water, wastewater treatment plant effluent	WWTP	None
Bioreactor sample, (22 °C, 24 h)	BR 1	1:2
Bioreactor, (70 °C, 60 min)	BR 2	1:2
Bioreactor, (132 °C, 20 min)	BR 3	1:2

5.4 Results and discussion

5.4.1 GC-MS/MS analysis

5.4.1.1 Chromatographic isotope effect

When using MS/MS as in this work, there is no need for complete separation, since specific transitions can be selected in the MRM scan and full separation would require a longer GC run time. The average resolution of FAMEs and d_3-FAMEs was found to be Rs = 0.14, which indicates that the peaks could not be fully separated by gas chromatography. Even lower temperature gradients could not achieve full separation. This may be due to the close structural similarity of FAMEs and d_3-FAMEs and their small mass difference of 3 m/z. Figure 5.1 exemplarily shows the inverse chromatographic isotope effect, which is reflected by the shorter retention time of ΔR_t = 0.03 min (1.8 s) for d_3-FAMEs compared to FAMEs. The chromatographic

isotope effect facilitates distinguishing between FAMEs and d_3-FAMEs in combination with different transitions in the MRM scan.

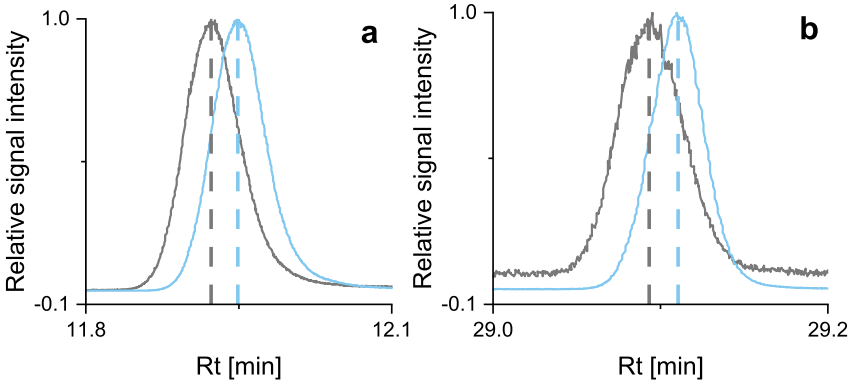

Figure 5.1 MRM chromatograms with relative signal intensity displaying the inverse chromatographic isotope effect of FAMEs (grey) and d_3-FAMEs (blue). Exemplarily shown for a: C8:0Me and C8:0Me-d_3, b: C20:0Me and C20:0Me-d_3; Quantifier transitions were chosen for the visualization. Sample: UW spiked with 40 µg L^{-1} FAs and 1.1-1.6 µg L^{-1} FAMEs.

5.4.1.2 Retention time prediction of deuterated molecules

When a linear temperature gradient is used, the retention time of deuterated molecules can be predicted based on the number of deuterium atoms in the molecule. This approach is helpful not only for deuterated FAMEs but generally for deuterated internal standard identification because they often have no registered mass spectra. It takes time to find them in the chromatogram, especially when the molecular ion is not the base peak. In contrast, with the described retention time prediction approach, the identification of deuterated internal standards can be simplified. First of all, a fitting chromatographic linear temperature gradient has to be chosen for the separation of all desired FAMEs. After that, the retention time shift for the gradient has to be observed by measuring one FAME and d_3-FAME solely. Thus, the retention time shift per deuterium atom (Rt_{shift}) can then be calculated by subtracting the retention time of the d_3-FAME (Rt_{d_3-FAME}) from the retention time of the FAME (Rt_{FAME}) and dividing this by the number of deuterium atoms of the d_3-FAME (n_d):

$$Rt_{shift} = \frac{Rt_{FAME} - Rt_{d_3-FAME}}{n_d}$$

In this study, the retention time shift per deuterium atom resulted in average 0.009 min (0.55 s). The retention times of d_3-FAMEs could be predicted with average 99.98% conformity (see appendix Table 9.8). A constant retention time shift was not expected

in this manner because the relative mass difference of the molecules differs significantly with the length of the alkane chain.

5.4.1.3 Development of the MRM method

As the FAMEs and d_3-FAMEs fragment strongly in the EI source and the molecular ions show a low abundance, specific EI fragments were chosen as precursors. There were two exceptions for this: for the internal standards d_{31}-C16:0Me-d_3 and d_{33}-C17:0Me a higher abundance of their molecular ions was observed, consequently, their molecular ions were selected as precursors, among others. d_3-FAME fragmentation was theoretically considered before MRM method development by calculating the d_3-FAME fragment equivalents based on the known fragments for the FAMEs. To be able to distinguish between d_3-FAME and FAMEs, only d_3-FAME fragments incorporating the ester group with the observable mass shift of +3 m/z can be taken into account. Equivalent fragment formation of +3 m/z could be confirmed for many transitions and was helpful for the development of the MRM method. The precursors of the FAMEs were chosen based on the known fragmentations shown in Table 9.9 in the appendix, according to Haertig et al. [134]. In all cases, the chosen d_3-FAME and FAME precursors have two or more of the following structures: McLafferty rearrangement ion, shorter-chain methyl ester ion, and molecular ion. The McLafferty rearrangement ion was found to be 74 m/z for the FAMEs, 77 m/z for d_3-FAMEs and the internal standard d_{33}-C17:0Me, and 80 m/z for the internal standard d_{31}-C16:0Me-d_3. Collision-induced dissociation (CID) product ions of the precursors were observed and selected with help of a product ion scan. The structure of product ions could be assigned to alkyl ions, alkenyl ions, and methyl ester ions or fragment losses subtracted from the precursor ion such as methanol-, methoxy-, methoxycarbonyl losses and the losses of the before mentioned carbon alkyl- and alkenyl fragments. A detailed list of the known fragments of FAMEs and the observed fragments of d_3-FAMEs is shown in the appendix in Table 9.9. In the MRM method, six specific transitions can be set per time frame, consequently, this results in three transitions, one for quantification and two for identification, for each compound. Optimal collision energies were determined by testing the CEs 5, 10, 15, 20, 25, and 30 eV and choosing the CE generating the highest peak area of the analyte. The MRM parameters are shown in Table 9.5 in the appendix.

5.4.2 Optimization of the derivatization procedure

The best DOE model for fitting the sum of all optimized FA responses was the full quadratic model with a correlation coefficient of 0.75, equations of all models are shown in the appendix. For the single FA responses, the R^2 value of the quadratic fit ranged from 0.54-0.86. No effect of chain length nor double bonds was observed for the goodness of fit, rather the values scattered slightly over the whole range. One of the most powerful benefits of process optimization by DOE is that term combinations and significant terms can be observed, significant terms will give a p-value <0.05. All p-values are shown in the appendix in Table 9.10, whereas significant values are marked green. No term has been significant for all FAs, but the pH was the most influential parameter on the FA derivatization reaction, followed by time and temperature.

The optimal derivatization parameters were determined by DOE for every single FA. Furthermore, these values have been averaged to get optimal values for the whole method (see in the appendix). The final optimal derivatization conditions were found to be pH 2.1, a temperature of 50 °C, 20 min, and a CD_3OD content of 4 v/v%. In Figure 5.2 the surface plots for the significant (a-c) and non-significant (d-f) factor combinations of all FAs are shown for which the response was cumulated. The optimal regions are displayed by red to orange color and a surface direction of 1. A preferred reaction temperature of 50 °C was unexpected as in most non-in situ derivatization reactions a higher temperature (of 60-100°C) is chosen. [148, 164] Furthermore, a CD_3OD content of 4 v/v% was unexpected, as one may assume that a higher CD_3OD content would lead to higher esterification yields. However, the optimal factors for both, temperature and CD_3OD, are assumed to have the same origin, when the whole system is considered. The SPME arrow extraction yield is substantially worsened by high solvent concentrations. During the chemical cleaning step, this behavior is utilized to remove the remaining compounds from the extraction material. However, two processes compete: 1. the increased conversion of FAs to d_3-FAMEs at higher CD_3OD concentrations and 2. the desorption of analytes from the fiber at higher CD_3OD concentrations. A similar competition applies for the temperature where: 1. the higher temperature increases the concentration of CD_3OD in the headspace of the vial and 2. the conversion of FAs to d_3-FAMEs increases at higher temperatures.

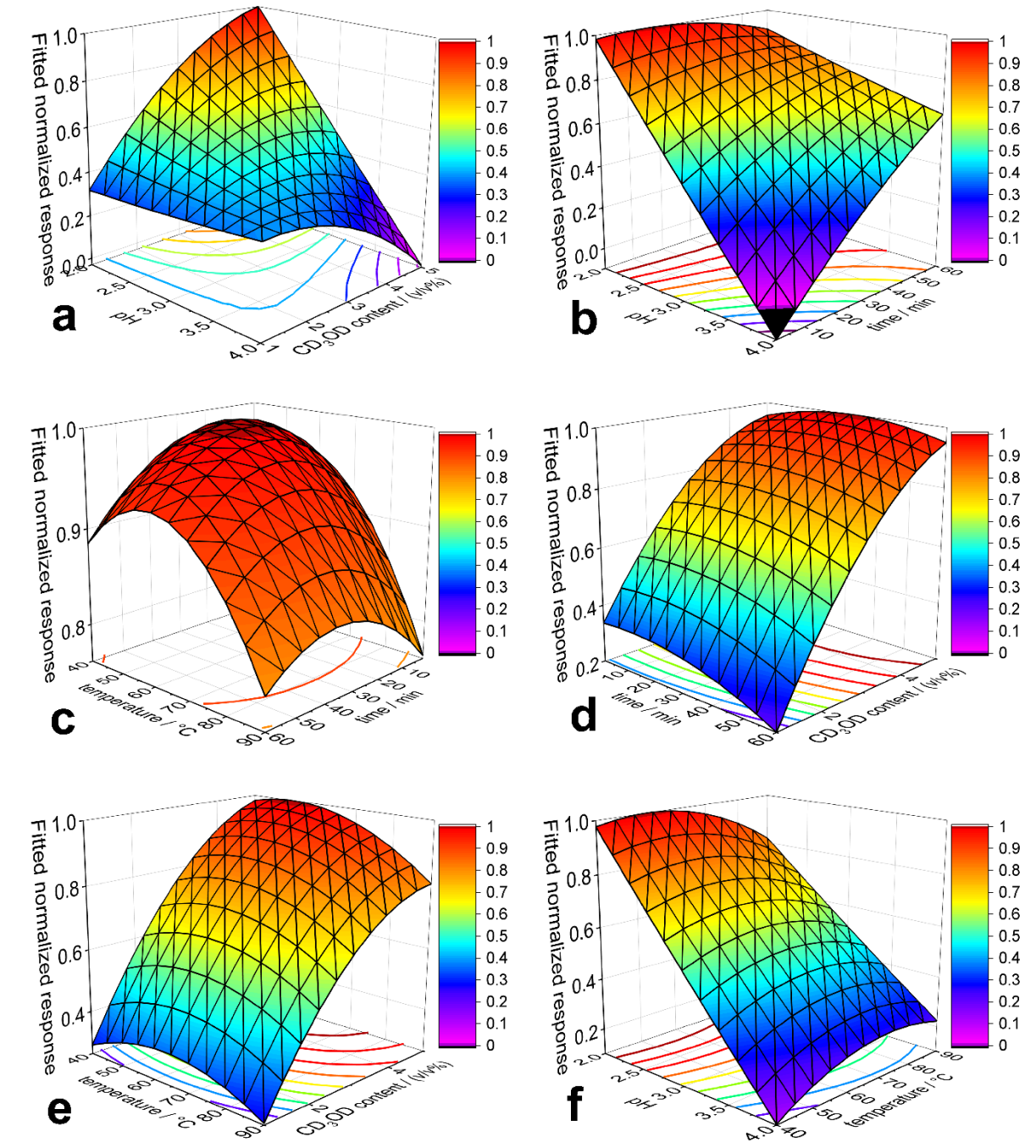

Figure 5.2 Response surface plots of the significant (a-c) and non-significant (d-f) factor combinations for derivatization parameter optimization by design of experiment. a: pH vs. CD_3OD content; b: pH vs. time; c: Temperature vs. time; d: Time vs. CD_3OD content; e: Temperature vs. CD_3OD content; f: pH vs. temperature. For experimental conditions see the respective sections.

5.4.3 Evaluation of the derivatization reaction

To evaluate the conversion ratio of FAs transformed into their d_3-FAME derivatives, the peak area of the internal standard which is transformed during esterification d_{31}-C16:0Me-d_3 is divided with the internal standard which is not transformed during

esterification d_{33}-C17:0Me. This approach is intended to give an overview of the general conversion yield in an aqueous solution. In ultrapure water, an esterification conversion of only 3% was observed for the internal standards. As often discussed in the literature, the esterification conversion in aqueous solution is very low as water is inhibiting the esterification. [164] The first impression is that this low conversion yield seems to be a disadvantage, but in the simultaneous method, it is an advantage since this difference allows calibration of FAs and FAMEs at different concentration ranges. Different concentration ranges are required since in most samples of natural or biological systems FAs are present in a large excess in contrast to FAMEs, which could also be confirmed by measuring different real samples. Exceptions to this are, for example, biodiesel samples, which contain predominantly FAMEs [165].

Another process that needs to be observed during the derivatization reaction is transesterification. Transesterification means that an ester group is replaced in presence of another alcohol. This process could happen for the FAMEs in the presence of CD_3OD and could interfere with the *in situ* derivatization as it would produce d_3-FAMEs. To test the derivatization for transesterification, the whole sample preparation was processed normally, with the difference that only the FAMEs were added to the solution. Transesterification seemed a likely, natural process, which cannot be avoided during this approach. However, no signal of d_3-FAMEs was observed, therefore it can be assumed that the quantity is below the MDL. Additionally, another test was done by processing the whole sample preparation normally but adding only FAs to the solution, which showed no difference in the signals compared to a solution where FAs and FAMEs were added. Hydrogen-deuterium exchange again is a natural process that occurs to some extent, however, no reduction in the signal of FAMEs was observed when adding FAMEs and CD_3OD, so the extent of exchange must be very low. This shows, that the method is reliably working in the targeted concentration ranges without an observed transesterification or other interferences between FAs and FAMEs.

The success of esterification strongly depends on the amounts in which the derivatization reagents are added. To estimate the required amounts, the molar excess of the derivatization reagents was calculated in Table 9.12 in the appendix for all concentrations used in the calibration. Even at the highest concentration of 200 µg L^{-1} and the optimal pH of 2.1, an 800-fold molar excess of the H^+ concentration over the total FA concentration is obtained. For CD_3OD at this concentration, a 50,000-fold molar excess is present.

5.4.4 Validation of the analytical method

The method detection limit (MDL) and recovery (R) are shown in Figure 5.3, the linear regression functions of the calibration are shown in Table 9.13 in the appendix, and the original values are shown in Table 9.14 in the appendix, respectively. The averaged R^2 values for calibration in the different samples ranged from 0.9442-0.9709, which is satisfactory for a multi-component analysis in very complex matrices. It was found that the matrices of the real samples were not interfering with the esterification reaction or SPME arrow extraction as the FAs and FAMEs could be calibrated in all matrices. In addition, no strong deviation of the slopes nor a trend that could be assigned to a specific matrix was observed. The averaged MDLs for the FAs ranged from 5-9 µg L^{-1} and for the FAMEs they ranged from 0.17-0.20 µg L^{-1}. The MDL ranges are comparable throughout the different matrices, however, it can be noticed that the saturated FAs and FAMEs >C16:0 tended to have higher MDLs and lower R^2 values. Lower R^2 values and poorer MDLs for longer chain FAMEs were already found in our previous study. [163] One reason may be that the equilibrium attainment during extraction for these analytes takes longer resulting in a lower response. The recoveries show good results, ranging from 70-135% for the FAs and 56-123% for the FAMEs, with averaged values ranging from 83-104%.

It can be noticed, that the results for both, the FAs and FAMEs, were good, although the FAs are additionally going through the derivatization step. This shows that the derivatization works reliably and does not cause strong fluctuations. Compared to our the previous study [163], the MDLs and calibration ranges for FAMEs in this study have been higher because one quantification ion was used whereas in the previous study, the total ion current of MRM transitions was used for quantification. In addition, in this study three of the six MRM channels have been used for each FA and FAME.

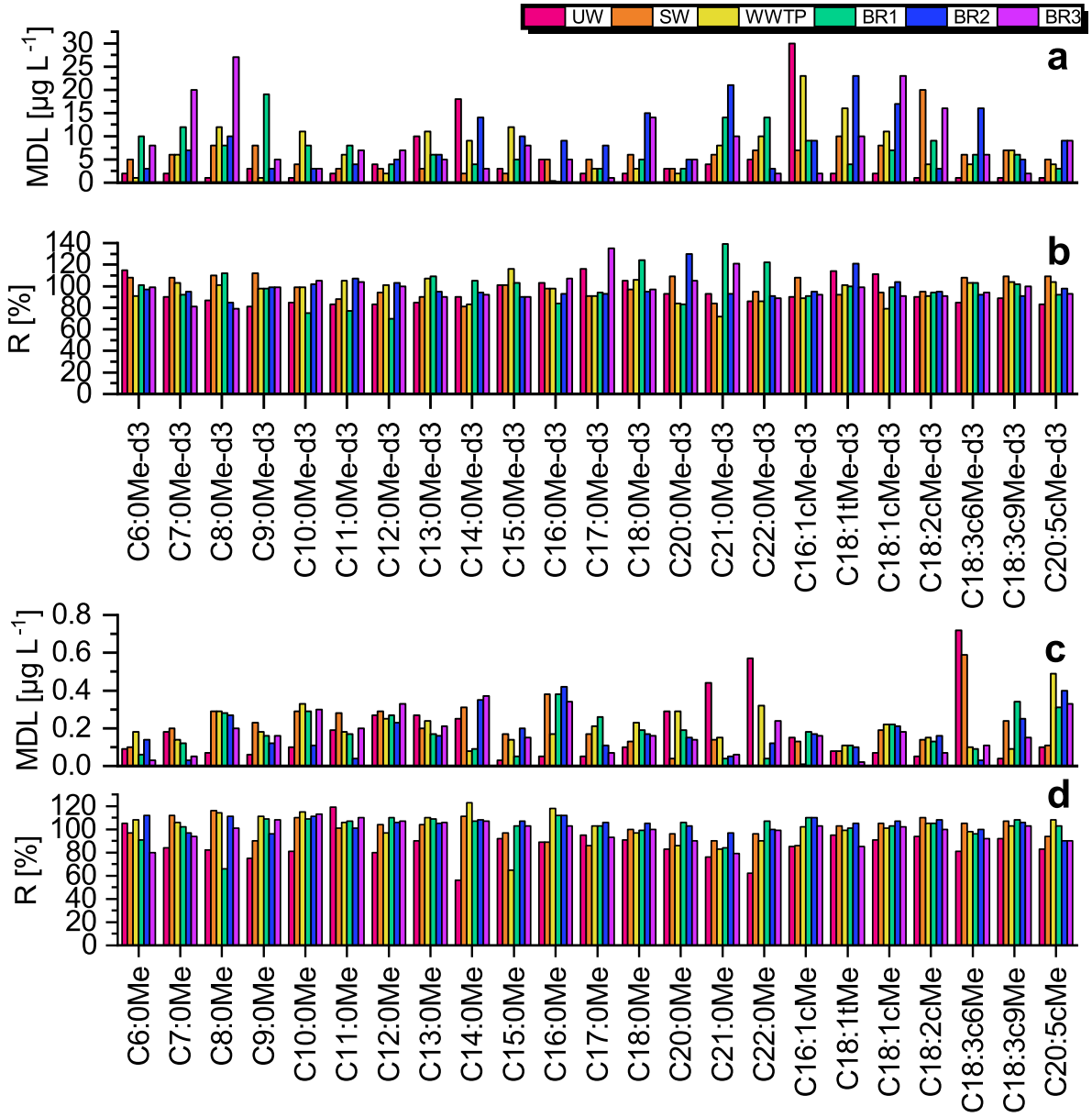

Figure 5.3 Results of method validation in different matrices with the method detection limit (MDL) and recovery (R) visualized as bar plots. Original values are shown in the appendix in Table 9.14.

5.4.5 Quantification of FAs and FAMEs in real samples

Different real samples, two surface water samples, and three bioreactor samples (see Table 5.1) were analyzed with the developed method to test the method's applicability in real matrices and to quantify the FAs and FAMEs in these samples. Figure 5.4 demonstrates the percentual FA and FAME distribution in the different real samples as segmented cake plots and Table 9.15 in the appendix displays the determined concentrations in µg L^{-1}. It can be seen, that the FAs show a higher variety in the number of detected compounds than the FAMEs. The highest concentrations of FAs

were found for C18:1tMe-d_3 in SW (105 µg L^{-1}), WWTP (83 µg L^{-1}), BR2 (674 µg L^{-1}), for C18:2cMe-d_3 in BR1 (653 µg L^{-1}) and C18:1cMe-d_3 in BR3 (1060 µg L^{-1}). Overall, the highest total FA concentration was found for BR3 (4940 µg L^{-1}) demonstrating that thermal digested pre-treated biowaste at 132 °C for 20 min produces more FAs than at 22°C for 24h or 70 °C for 60 min. Thus, it can be concluded that the FA concentration in the bioreactor increases with increasing pre-treatment digestion temperature, although shorter digestion times have been applied. Nevertheless, at 132 °C digestion temperature a higher variation was found, in particular, more saturated FAs were detected. The cumulated concentrations of FAs in the real samples were in the following order: WWTP<SW<BR1<BR2<BR3, whereas the cumulated concentrations of the surface water and wastewater treatment plant effluent (263-404 µg L^{-1}) and the three bioreactor samples (2110-4940 µg L^{-1}) were in the same order of magnitude, respectively.

The overall variation and concentration range of FAMEs in the samples was lower than that of the FAs. The reason may be that the FAMEs are less common and lower concentrated because they are less involved in biological processes than FAs. Additionally, the bioreactor was designed to produce FAs. The highest concentrations of FAMEs were found for C18:3c6Me in all samples ranging from 0.85-14 µg L^{-1}, with the highest concentration for BR2. The cumulated concentration of FAMEs in the real samples can be arranged as follows: WWTP<SW<BR1<BR3<BR2. Figure 5.5 presents exemplarily MRM chromatograms of spiked UW, SW, WWTP, and BR1-BR3.

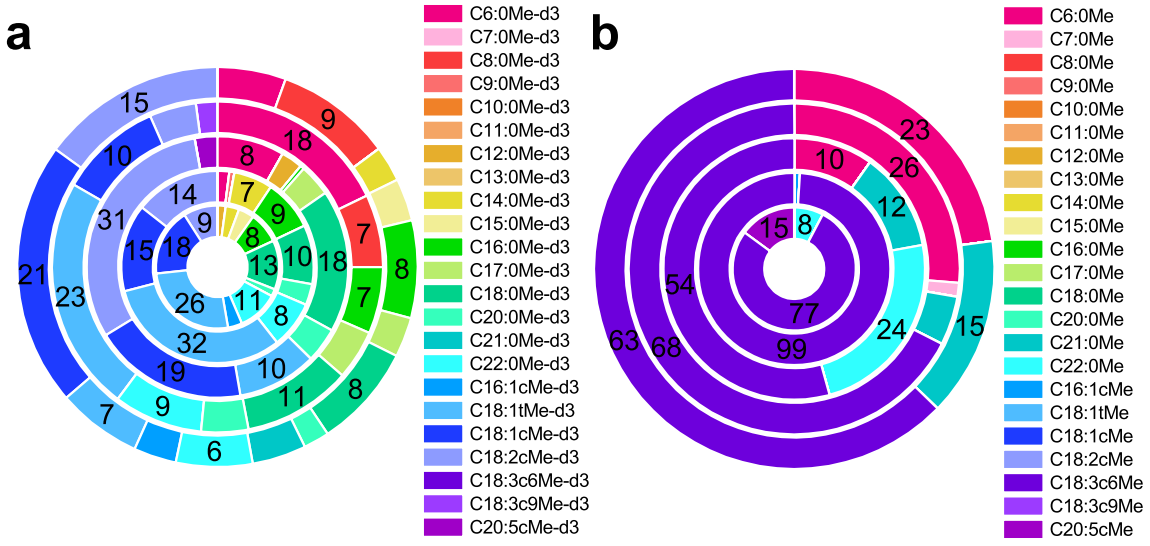

Figure 5.4 Percentual distribution of FAs (a) and FAMEs (b) in the real samples. Real samples are displayed from inside to outside: SW, WWTP, BR1, BR2, BR3. SW: Surface water; WWTP: Wastewater treatment plant effluent; BR1-BR3: Bioreactor

samples 1-3. Only percentual values above 3% are displayed as numbers. For experimental conditions see the respective sections.

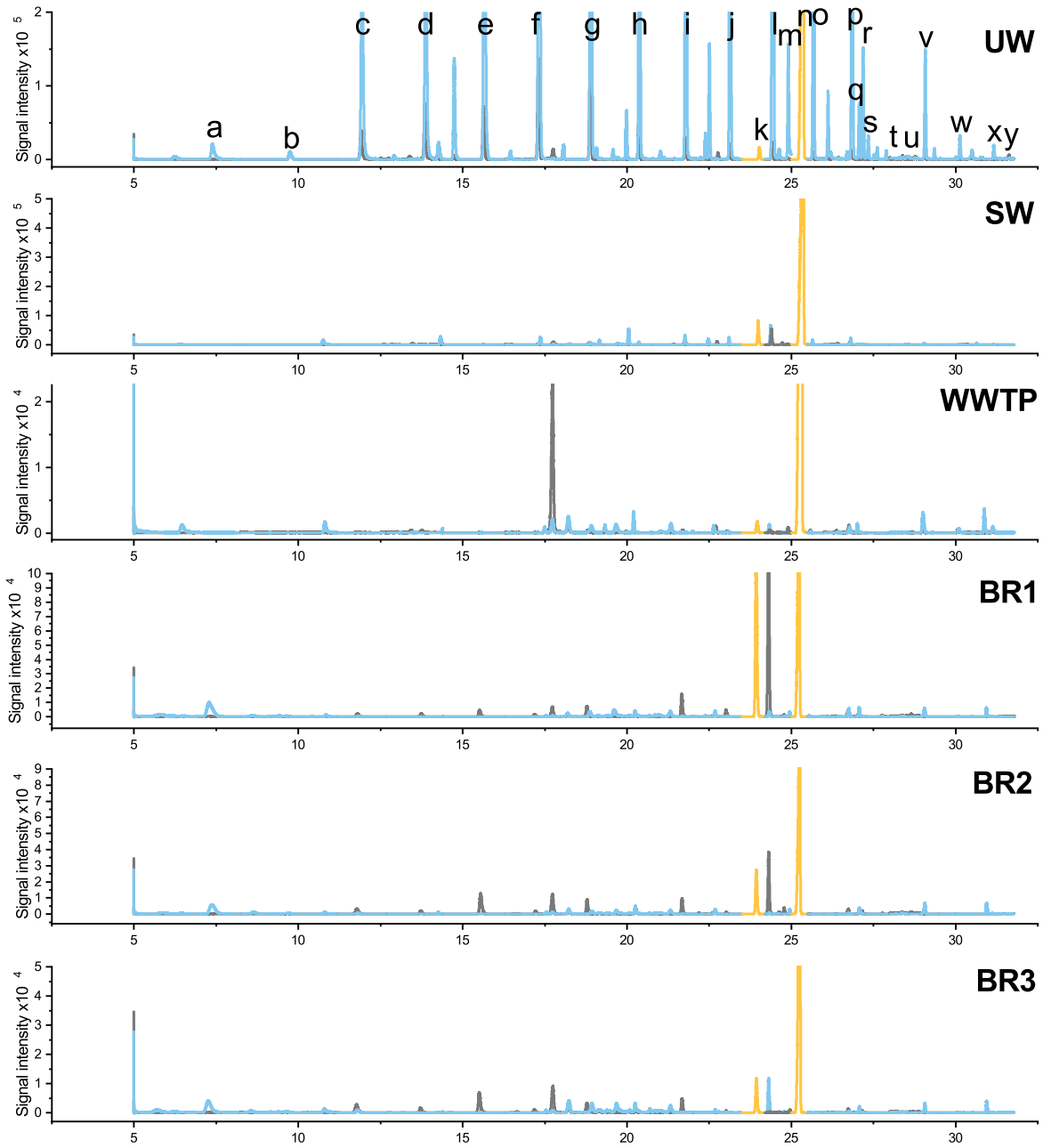

Figure 5.5 Multiple reaction monitoring (MRM) chromatograms of the d_3-FAMEs (grey), FAMEs (blue), and internal standards (yellow) in spiked ultra pure water (UW), and non-spiked real samples from surface water (SW), wastewater treatment plant effluent (WWTP) and bioreactor 1-3 (BR1-BR3). The components are marked as follows: a: C6:0Me-d_3/C6:0Me; b: C7:0Me-d_3/C7:0Me; c: C8:0Me-d_3/C8:0Me; d: C9:0Me-d_3/C9:0Me; e: C10:0Me-d_3/C10:0Me; f: C11:0Me-d_3/C11:0Me; g: C12:0Me-d_3/C12:0Me; h: C13:0Me-d_3/C13:0Me; i: C14:0Me-d_3/C14:0Me; j: C15:0Me-d_3/C15:0Me; k: d_{31}-C16:0Me-d_3; l: C16:0Me-d_3/C16:0Me; m: C16:1Me-d_3/C16:1Me; n: d_{33}-C17:0Me; o: C17:0Me-d_3/C17:0Me; p: C18:0Me-d_3/C18:0Me; q: C18:1tMe-d_3/C18:1tMe; r: C18:1cMe-d_3/C18:1cMe; s: C18:2cMe-d_3/C18:2cMe; t: C18:3c6Me-

d_3/C18:3c6Me; u: C18:3c9Me-d_3/C18:3c9Me; v: C20:0Me-d_3/C20:0Me; w: C21:0Me-d_3/C21:0Me; x: C22:0Me-d_3/C22:0Me; y: C20:5cMe-d_3/C20:5cMe.

5.4.6 Analytical Greenness Metric Approach (AGREE)

Every analytical method uses resources and energy and produces waste, but some methods have a lower environmental impact and are greener than others. For the evaluation of the method's greenness, the Analytical GREEnness Metric approach (AGREE) open-source software [46] was applied to the method's parameters. With an aspired optimal value of 1.0, the AGREE score of this method is 0.47 (see Figure 5.6). This result means that the method has some parameters that should be further optimized for a lower environmental impact but also has parameters that already have a low impact. The worst scores were obtained for the analysis being off-line, the high energy consumption of GC-MS/MS, and the type and amount of used derivatization reagents. The best scores were obtained for few steps of sample preparation, automation, and miniaturization degree, waste amount, and a high number of determined analytes per run. The utilization of solvents and reagents, mostly chloroform and CD_3OD, negatively influenced the rating in several categories. In addition, the relatively large sample amount of 10 mL increases the amount of required reagents and solvents.

It has to be taken into account that the perfect green method does not exist, but it is important to increase awareness of the environmental impact and it is also helpful for other works, which can make decisions based on the greenness scores of existing methods.

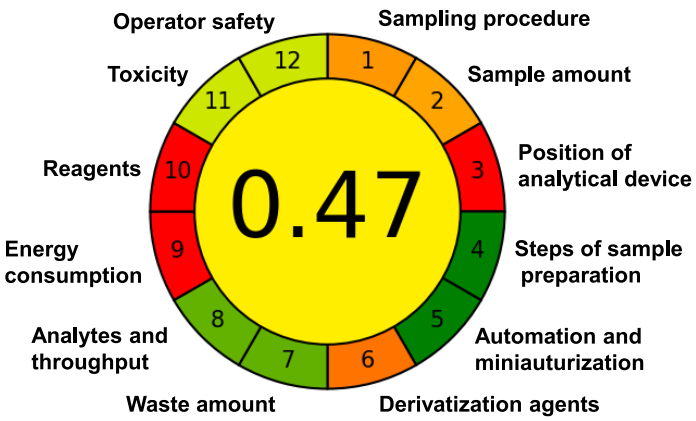

Figure 5.6 Analytical greenness metric approach (AGREE) pictogram with labeled steps for the developed method.

5.5 Conclusions

The introduced method allowed simultaneous qualification and quantification of FAs and FAMEs in several aqueous matrices ranging in complexity. Due to the isotope-labeling derivatization of the FAs and the resulting mass and retention time shift the method run time is fast compared to two single analyses. The *in situ* derivatization and SPME arrow headspace extraction allowed full automation of the whole sample preparation with an overlapping scheduled run time (including analysis) of 84 min. Consequently, 17 samples with 46 target analytes each can be analyzed in one day. The method is suitable for all samples in which FAMEs are suspected in addition to FAs. The samples analyzed here have been from natural as well as industrial systems and always contained FAs and FAMEs. Certainly, the concentration of FAMEs was mostly lower but occurred in concentration ranges that cannot a priori be ignored and could lead to false-high values during classical esterification with MeOH. *In situ* derivatization was used here as an example of an advanced automated derivatization mode, however, isotope-labeling derivatization can be used as a non-*in situ* derivatization as well and can easily be integrated into already existing derivatization methods, since only MeOH has to be replaced by CD_3OD. Due to the findings of this study, it is recommended to replace MeOH with CD_3OD in future esterifications as it gains more reliable results when FAMEs are present next to FAs. In the real samples FAs have been found in much higher concentrations (2-1056 µg L^{-1}) and broader variety than FAMEs (0.01-14 µg L^{-1}). The bioreactor samples contained the highest concentrations of both. The bioreactors fed with biowaste pre-treated at 132 °C contained the highest cumulated FA concentration.

6 Characterization of a hydrophilic-lipophilic balanced SPME material for enrichment of analytes with different polarities from aqueous samples

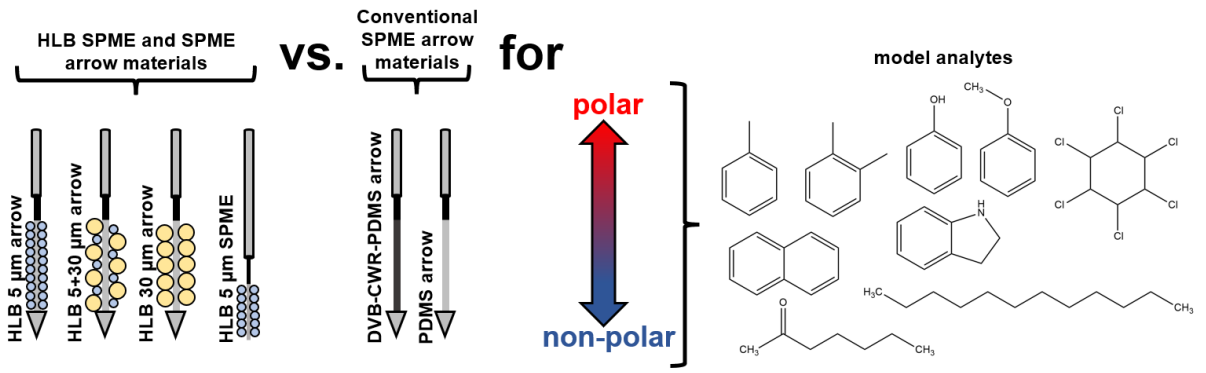

Adapted from: Lucie K. Tintrop, Leonardo Solazzo, Amir Salemi, Maik A. Jochmann, Torsten C. Schmidt. Characterization of a hydrophilic-lipophilic balanced SPME material for enrichment of analytes with different polarities from aqueous samples, published in Advances in Sample Preparation (2023). © Elsevier 2023

6.1 Abstract

The choice of the extraction material is a critical step in solid-phase microextraction (SPME), especially the extraction of analytes which strongly differ in their polarity is challenging. This study is intended to give first insights into the headspace extraction of analytes with large differences in polarity by using a novel hydrophilic-lipophilic-balanced (HLB) SPME material with different particle sizes (5 µm, 5+30 µm, and 30 µm) in classical SPME as well as SPME arrow format. The obtained results were compared to conventional and already established divinylbenzene carbon wide-range polydimethylsiloxane (DVB-CWR-PDMS) and PDMS SPME arrow fibers. The chosen model analytes toluene, indole, phenol, anisole, *o*-xylene, naphthalene, 2-heptanone, n-dodecane, and lindane are assigned to different substance classes with K_{aw} values ranging from -5.0-2.5 and K_{ow} values from 1.5-7.5. The highest amount of the analytes was extracted by the HLB 5+30 µm arrow and the HLB 5 µm arrow, whereas the HLB SPME with a six times smaller phase volume compared to an SPME arrow, performed almost as well as the DVB-CWR-PDMS arrow. The 8-point calibration with the 5+30 µm HLB SPME arrow in the range of 5-70 µg L^{-1} of the analytes showed good linearity with R^2 values ranging from 0.9765-0.9982, method detection limits from 0.9-

6.2 µg L^{-1} and relative standard deviations from 2-31%. For all of the observed analytes, the HLB material performed better than the conventional extraction materials and has great potential to replace the conventional extraction materials in many applications.

6.2 Introduction

Since its introduction by Arthur and Pawliszyn until today solid-phase microextraction (SPME) has been the most used microextraction method worldwide. [16] One of the advantages of SPME is the simplicity in application since the fiber is introduced in a syringe-like holder, which makes the implementation into autosampler systems easy. Further, SPME is completely solvent-free and therefore considered a green approach that replaces and miniaturizes extractions that consume solvents such as liquid-liquid extraction (LLE) and solid-phase extraction (SPE) [166, 167]. The application range of SPME is almost limitless, as it can be used in headspace or direct immersion mode proposed for example for environmental samples [168], food [169], medical samples [170], on-site measurements [171], passive sampling and in-situ sampling in living organisms [30]. A further developed SPME is the SPME arrow, which has a larger phase volume (3.8 µL compared to 0.6 µL for classical SPME), a stainless steel core, and an arrow-shaped tip [84, 124]. The stainless-steel core and arrow-shaped tip enhance the mechanical stability and septum penetration of the SPME arrow, compared to classical SPME fibers, which can be bent easily due to errors e.g. misalignment of the autosampler.

In general, the extraction of polar as well as non-polar analytes is challenging using one extraction material. The polarity of organic substances has often been described using different concepts, but unfortunately, until today no unified agreement has been found. Polarity is easily described qualitatively, but a precise definition and quantitative determination raise significant problems. Basically, polarity describes the charge dislocation and charge of atoms in a molecule. Reichardt et al. described polarity as the solvation capability of a solvent against solute molecules driven by intermolecular forces of any kind. [172] These definitions indicate already how complex the description of polarity is and that it cannot be described by a single physical constant. Concepts to describe the polarity of a molecule are for example the electronegativity, μ_m-scale, $E_T(30)$-Scale, basicity, polarizability, molecular dipole moment, and the Linear-Solvation-Energy-Relationship (LSER). [173] For the latter, an online tool has been created that allows the prediction of partitioning constants based on various substance

descriptors. [135] The partitioning constants describe the distribution of a substance between two phases, which provides information about the behavior of a compound, and in particular about the polarity. Two important equilibria are the Henry's law (or air-water partitioning) constant and the octanol-water partitioning constant.

The choice of the extraction material is a critical step in SPME. Polydimethylsiloxane (PDMS) and carbon wide range (CWR) are used to extract non-polar compounds, whereas, in combination with divinyl benzene (DVB) as DVB-PDMS or DVB-CWR-PDMS, these fibers are used to extract polar to non-polar compounds. However, these materials show a high affinity for volatile compounds and lack affinity for low-boiling compounds. [174] A hydrophilic-lipophilic balanced (HLB) extraction material was recently introduced for this purpose containing lipophilic divinylbenzene for the extraction of non-polar compounds and hydrophilic n-vinylpyrrolidone for the extraction of polar compounds. [174] The HLB material for SPME arrows was introduced for the first time by Yu *et al.* for the extraction of microbial metabolites and fatty acids from salmon filets [31]. The HLB SPME arrow used by Yu et al. was prepared manually by the authors. In this study, prototypes for commercial HLB SPME and HLB SPME arrows were characterized and compared to PDMS and DVB-CWR-PDMS according to their covered polarity range, particle size, optimal extraction parameters, extraction efficiency, and carry-over effect.

6.3 Material and methods

6.3.1 Chemicals and materials

Heptanoic acid methyl ester (≥ 99.8%), toluene (≥ 99.8%), indole (≥ 99%), phenol (≥ 99%), naphthalene (≥ 99%), 2-heptanone (≥ 99%), n-dodecane (≥ 99%), γ-hexachlorocyclohexane (Lindan, ≥ 99%), and methanol (≥ 99%) were purchased from Sigma Aldrich (Steinheim, Germany). Anisole (≥ 99%), o-xylene (≥ 99%), and chloroform (≥ 99%) were purchased from Fisher Scientific (Loughborough, United Kingdom). Standard and mix solutions were prepared in chloroform in a concentration of 1 g L^{-1} and 100 mg L^{-1}, respectively, and were stored in the fridge at 5 °C. For the preparation of aqueous samples, ultrapure water was withdrawn from a bi-distillation apparatus (Bi 18E with quartz glass, Quarzglas QCS, Germany).

6.3.2 GC-MS/MS analysis

Gas chromatographic separation prior to tandem-mass spectrometry was conducted by using a GC 2010 with a MS/MS TQ8040 (Shimadzu Deutschland GmbH, Duisburg, Germany) equipped with a Zebron ZB-35 capillary column (30 m x 0.25 mm x 0.25 µm,

Phenomenex, Torrance, USA), a SPME arrow liner (1.8 mm x 5 mm x 95 mm, Topaz liner, Restek, Bad Homburg, Germany) and a wider injector needle guide for SPME arrows (Shimadzu Deutschland GmbH, Duisburg, Germany). The column oven program started at 40 °C and was raised at a rate of 30 °C min^{-1} to 65 °C, then raised at a rate of 2 °C min^{-1} to 80 °C, then raised at a rate of 20 °C min^{-1} to 180 °C and finally raised with a rate of 40 °C min^{-1} to 300 °C. The column flow was 1.5 mL min^{-1} and helium (5.0, AirLiquide, Oberhausen, Germany) was used as carrier gas. The analytes were thermally desorbed at a sampling time of 1 min and splitless injection mode was applied. The injector, ion source, and transfer line were heated at 280 °C. The MS/MS was operated in MRM mode with a solvent cut time of 4 min and argon (5.0, AirLiquide, Oberhausen, Germany) was used as collision gas. The MRM transitions and collision energies are shown in Table 9.16 in the appendix. Standard 70 eV was applied for electron ionization (EI) of the analytes. The chromatographic peak of one quantifier ion (see Table 9.16 in the appendix) for each analyte was integrated and the peak area was used as a response for further data evaluation.

6.3.3 Sample preparation and extraction

The sample preparation procedure was fully automated including the following steps: addition of internal standards, addition of analyte mix, sample heating, SPME arrow extraction, injection, and SPME arrow fiber cleaning. A robotic tool change prep and load (RTC PAL) autosampler (CTC Analytics, Zwingen, Switzerland) was used to conduct the tasks. For SPME and SPME arrow extraction, prototype HLB SPME (10 mm x 110 µm with 5 µm particle size) and three different particle sizes 5 µm, 30 µm and 5+30 µm for HLB SPME arrow (20 mm x 120 µm x 1.1 mm) were provided by CTC Analytics (Zwingen, Switzerland) with PDMS as binder. Additionally, conventional PDMS (20 mm x 100 µm x 1.1 mm), CWR-DVB-PDMS (20 mm x 120 µm x 1.1 mm), and PA SPME arrow (20 mm x 120 µm x 1.1 mm) fibers were used (CTC Analytics, Zwingen, Switzerland).

6.3.4 Material characterization

For the HLB material characterization, the extraction time and temperature were optimized using the HLB SPME, HLB SPME arrows with 5 µm, 30 µm, and 5+30 µm particle size, PDMS SPME arrow, and CWR-DVB-PDMS SPME arrow. For this purpose, a central composite response surface design of experiment (DOE) was developed using OriginPro software (Version 2022, OriginLab Corporation) with 2 continuous factors (temperature 40-70 °C, time 1-30 min) and one categorical factor

(extraction material) leading to 96 runs of parameter combination. To evaluate the extraction efficiency of the different materials, the depletion curve method [61] was applied by extracting nine times from the same sample in duplicates. The percentual extraction efficiency E_E is then calculated from slope b of the linear equation resulting from the logarithmic peak area plotted against the number of extractions by using the formula $E_E = -(10^b - 1) \cdot 100$. The carry-over of analytes into the next measurement was determined with the optimal extraction material by extracting and injecting one sample and after cleaning of the fiber injecting again to evaluate the amount of remaining analytes on the fiber material after one sample preparation, measurement, and cleaning cycle.

6.3.5 Method validation

The optimal fiber material was used for calibration of the analytes in concentrations of 5, 10, 20, 30, 40, 50, 60, and 70 µg L^{-1} in quadruplicates, and the internal standard (Heptanoic acid methyl ester) was spiked in a concentration of 50 µg L^{-1}. The method detection limit (MDL) was calculated according to the MDL procedure (Revision 2, 2016) released by the United States Environmental Protection Agency [133].

6.4 Results and discussion

6.4.1 Selection of analytes

To be able to characterize the fiber material in terms of the covered polarity range, analytes from different substance classes with different polarities were chosen for this study. Among the many concepts and scales to state the polarity of a molecule, plotting the logarithmized air-water partitioning constant log K_{aw} against the logarithmized octanol-water partitioning constant log K_{ow} as presented by Lorenzo-Parodi et al. [20] was found most suitable in this approach as it combines the volatility and hydrophobicity/lipophilicity of the analytes in one graphic. The plot of the investigated analytes is shown in Figure 6.1. The selected substance classes were aromatic hydrocarbons, amines, ketones, anisoles, alkanes, pesticides, phenols, esters, and polycyclic aromatic hydrocarbons (PAHs). With the selected analytes a wide polarity range from log K_{ow} values of 1.5-7.5 and different volatilities ranging from log K_{aw} values of -5.0-2.5 were covered. n-dodecane was the most lipophilic substance and phenol was the most hydrophilic substance.

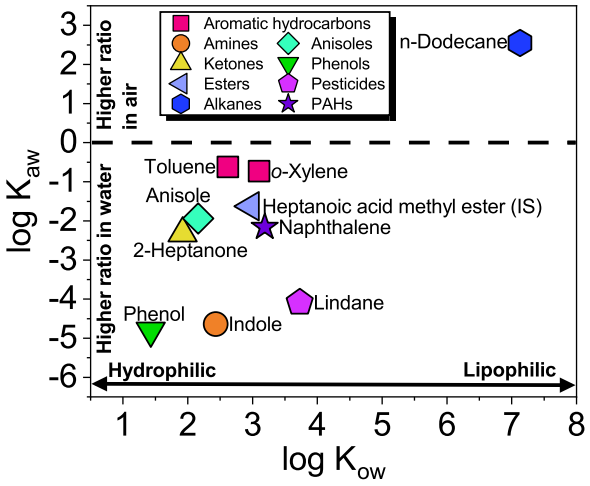

Figure 6.1 Volatility and polarity of the investigated analytes affiliated to their substance classes presented by logarithmic octanol-water K_{ow} and air-water K_{aw} partitioning constants. Partitioning constants were calculated using the UFZ Helmholtz Centre LSER online database [135] and are shown in the appendix in Table 9.17. IS: Internal standard; PAHs: Polycyclic aromatic hydrocarbons.

6.4.2 Extraction material characterization

6.4.2.1 Influence of extraction material and HLB-particle size

The optimal extraction material for the enrichment of the chosen analytes was determined with the DOE. The results of the relative extracted peak area with the varying extraction materials are presented in Figure 6.2. It shows that the distribution pattern of relative extracted peak area is very similar for all of the analytes, except for lindane. The HLB arrow materials reached the highest extracted amounts for all of the analytes following the pattern: HLB 5+30 µm > HLB 30 µm > HLB 5 µm.

Lindane, however, behaves differently from the other analytes, as the HLB 5 µm arrow extracted the highest amount with significantly lower extracted amounts for HLB 30 µm arrow and HLB 5+30 µm arrow. For lindane, the DVB-CWR-PDMS material reached the second-best results followed by the HLB 5 µm SPME. The 5 µm particle size may perform better than the 30 µm, as smaller particles reach a higher surface area, and therefore the chances to bind via adsorption increase. In addition, absorption is not the dominant extraction mechanism for any of the analytes, as the PDMS arrow, which extracts the analytes by absorption only, led to the lowest extracted amounts. So for the extraction of the selected analytes with a broad polarity range a material that combines adsorbing and absorbing materials, such as HLB and DVB-CWR-PDMS, is favored. However, the influence of the PDMS binder on the HLB particles, and therefore on the extraction of analytes, is negligible, as recently discovered by Murtada et al. [175]

The HLB SPME fiber often reached comparable extracted amounts to the DVB-CWR-PDMS arrow fiber, although the phase volume of the SPME arrow fiber is ~6 times higher (3.8 µL) than the classical SPME's phase volume (0.6 µL). The PDMS arrow fiber material reached the lowest extracted amounts for all analytes and in some cases extracted no analyte at all. This shows the excellent enrichment ability of the HLB material compared to the more common fiber materials.

The extraction of phenol from the headspace of the water samples was challenging, as it was only extracted in very small amounts for all of the observed fiber materials. Phenol is therefore not included in any of the shown results of this study. In other studies of headspace phenol extraction, polyacrylate (PA) [109, 176], carboxen-PDMS, and PDMS SPME (the last two for derivatized phenols) [177] were successfully applied. Due to this an additional test measurement was done by using a polyacrylate (PA) SPME arrow fiber, but the outcome was still not satisfying as the peak height was ~110,000, 4,000, and 8,000 counts for liquid injection in full scan, HLB 5+30 µm arrow, and PA arrow, respectively. As displayed in Figure 6.1, phenol was the most hydrophilic substance with the lowest K_{ow} and K_{aw} values of the observed analytes. Consequently, the amount of phenol in the headspace is low, which causes the low extracted amounts with all of the fiber materials.

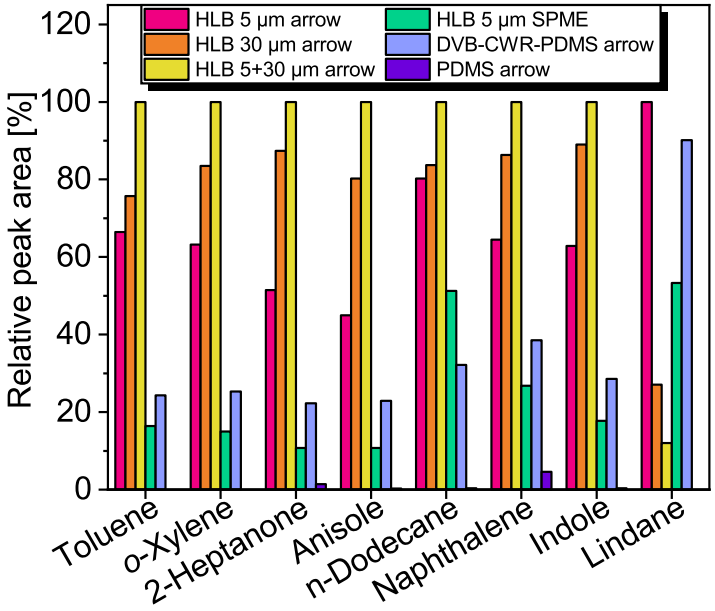

Figure 6.2 Relative peak areas obtained with different SPME and SPME arrow materials in headspace mode. Tested arrow materials were HLB 5 µm, HLB 30 µm, HLB 5+30 µm, DVB-CWR-PDMS, and PDMS. The tested classical SPME material was HLB 5 µm.

6.4.2.2 Optimal extraction temperature and time

Two other extraction parameters, time and temperature, have been optimized with DOE. Figure 6.3 shows the resulting contour plots of the different analytes with normalized peak area as the response and the optimal fiber materials as the hold value. The optimal regions are displayed in pink. For indole and lindane (see Figure 6.3 B and H) the extraction time and temperature had a clear optimal region at 30 min and 70 °C with a response ranging from 0-1. Toluene and *o*-xylene show an optimal region at 1 min and 40 °C (response range 0.3-1 and 0.7-1, Figure 6.3 A and D), whereas for naphthalene the highest response was achieved at 70 °C and 27 min (response range 0.5-1, Figure 6.3 E). For anisole, 2-heptanone, and n-dodecane (Figure 6.3 C, F, and G) almost the whole experimental range was optimal, elucidated by only slight differences in the response (0.8-1). The results show that the optimal extraction time and temperature are very much analyte-dependent. At a high extraction temperature, the amount of analyte in the headspace increases, but the fiber-air partitioning decreases with higher temperature. The differences in optimal extraction time and temperature result from different fiber material affinities and the complexity of a multianalyte system. The optimal extraction parameters determined with DOE (calculation shown in the appendix in Table 9.18) were found to be the HLB 5+30 µm arrow, temperature 61 °C and 17 min.

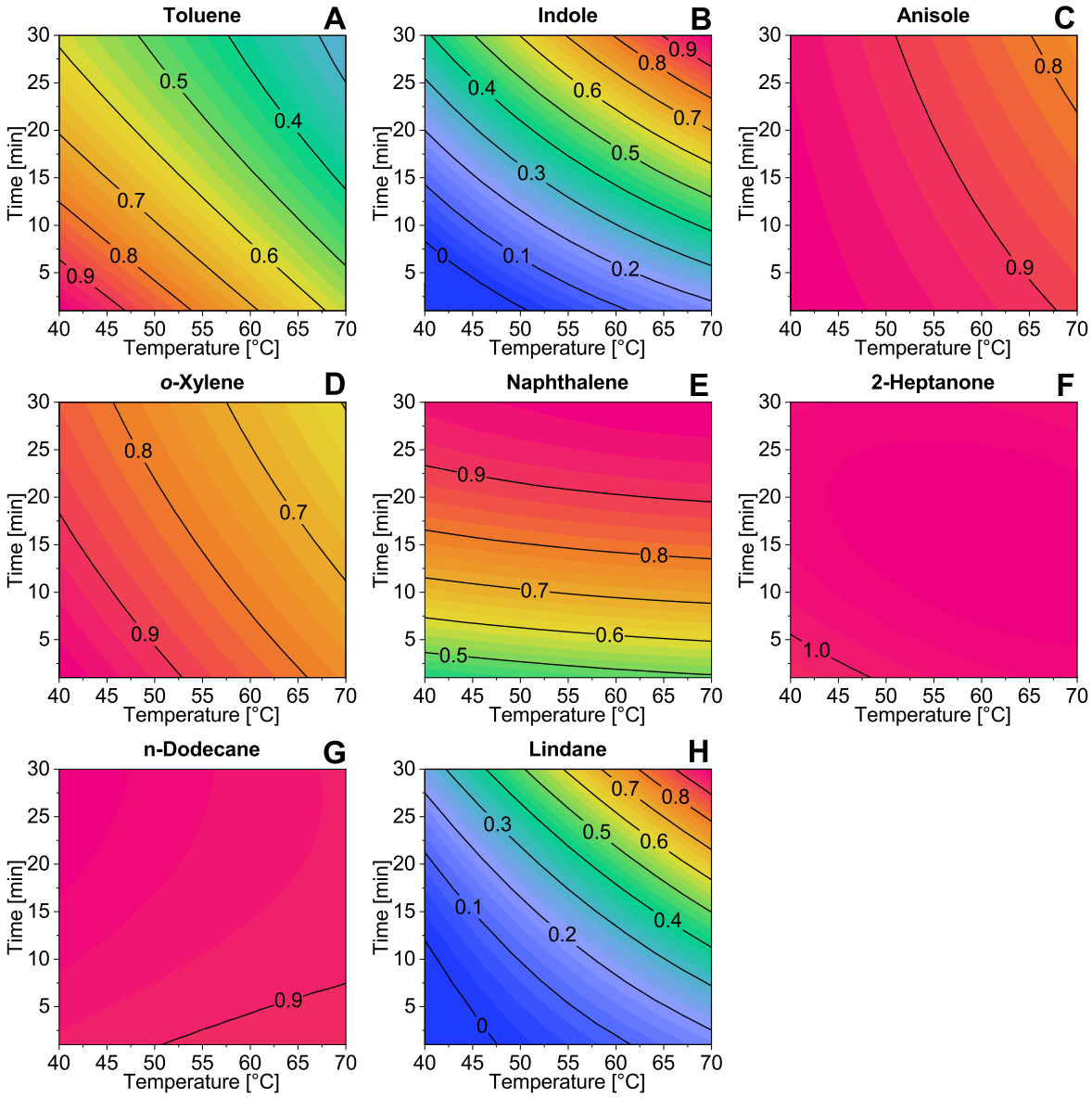

Figure 6.3 Contour plots of toluene (A), indole (B), anisole (C), *o*-xylene (D), naphthalene (E), 2-heptanone (F), n-dodecane (G) and lindane (H) for the optimization of extraction temperature and time. The hold value for the extraction material was 5+30 µm arrow for analytes A-G and HLB 5 µm arrow for lindane (H). The peak area of all analytes has been normalized to the maximum and the colors indicate the value from blue (low) to pink (high).

6.4.2.3 Extraction efficiency

The extraction efficiency is important for the fiber material characterization, as it determines the relative amount of extracted analyte. As optimal extraction time and temperature, 17 min and 61 °C were chosen according to the results of the DOE. In Figure 6.4, three exemplary depletion curves and linearized depletion curves for naphthalene, n-dodecane, and 2-heptanone are shown. For most of the analytes, the peak area decreased for example for naphthalene and n-dodecane, and the extraction efficiency was properly determined. For 2-heptanone, anisole, and indole, however,

the peak area was not or only slightly decreasing during the nine extractions. Normally a decreasing peak area could be determined after nine extractions [61]. 2-heptanone, anisole, and indole are rather hydrophilic substances with a low K_{ow} value (see Figure 6.1) so the observed effect could be explained by the recurring equilibrium attainment for each extraction. The extracted fraction in each extraction is small, thus the overall depletion can not be observed during nine extractions. The determined extraction efficiencies of each material for each analyte are listed in Table 6.1.

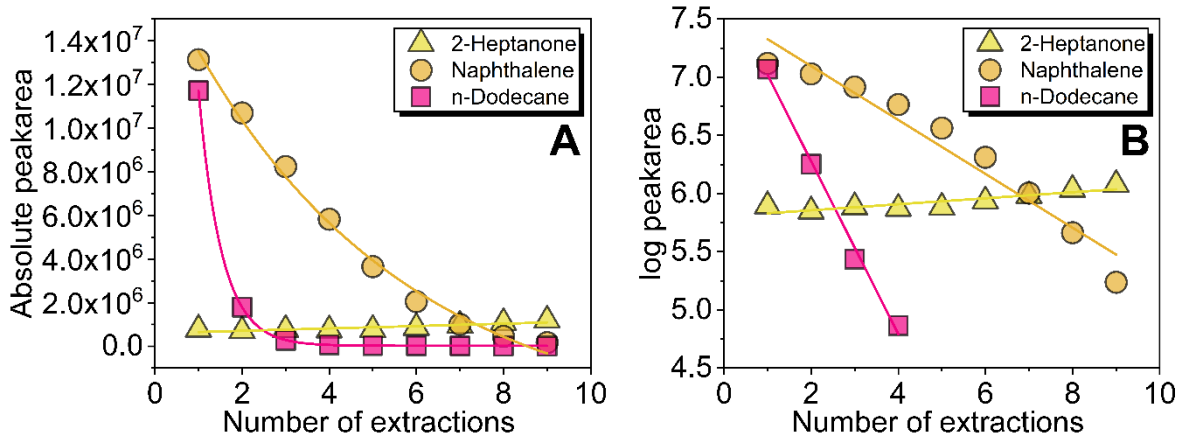

Figure 6.4 Depletion curves resulting from the determination of the extraction efficiency by using the depletion curve method. Depletion curves with the absolute peak area (A), and linearized curves with logarithmic peak area (B).

6.4.2.4 Carry-over evaluation

Next to the efficiency of the extraction, it is also important to determine the carry-over of the observed analytes into the next measurement as it gives information about the effectivity of the fiber cleaning process. A carry-over into the next measurements can cause false-positive analyte detection and is important for quality control of an analytical method utilizing reusable extraction materials. An advanced cleaning strategy, developed in another study [163], was used which is a combination of chemical cleaning of the fiber in the headspace of 1 mL methanol in a 20 mL vial at 60 °C for 5 min and subsequent thermal fiber cleaning at 280 °C for 10 min. The introduction of the fiber into a solvent gas phase allows the analytes to desorb, whereas in thermal cleaning the remaining solvent and analytes are further desorbed. The carry-over was determined for the optimal fiber material HLB 5+30 µm arrow and the results are listed in Table 6.1. The relative carry-over was 0.94% for lindane and below 0.16% for all of the other analytes, which indicates sufficient cleaning. Lindane has a high solubility in methanol (25-40 g L^{-1} [178]) and thus should be removed by the chemical cleaning step. The higher relative carry-over of lindane compared to the other analytes

can result from a high affinity to the phase material. A high carry-over for lindane of ~80% and ~50% for DVB-CWR-PDMS and DVB-PDMS fibers, respectively, was observed by McManus et al [179]. However, the value of carry-over observed in this study <1% is much lower than observed by McManus et al., which indicates a higher effectiveness of the applied cleaning process.

6.4.3 Method validation

To test the linearity and sensitivity of the optimal HLB 5+30 µm arrow fiber material, a calibration from 5 to 70 µg L^{-1} with eight calibration points was conducted. Table 9.19 in the appendix lists the linear regression functions and correlation coefficients R^2 and Table 6.1 lists the MDLs and relative standard deviation (RSD) at a concentration of 10 and 60 µg L^{-1}. The calibration was linear for all of the analytes and achieved acceptable MDLs and RSDs. It was observed that the RSD value for toluene was increasing with higher concentration which results from higher fluctuations in the multi-analyte system at higher concentrations (e.g. saturation of the phase material), but for all of the other analytes, it remains constant. The internal standard was not used for peak area normalization as the behavior of the analytes differed too much and the internal standard normalization did not improve repeatability.

Table 6.1 Results of extraction efficiency determination, carry-over evaluation, and method validation for each analyte. HLB: Hydrophilic-lipophilic balanced; SPME: Solid-phase microextraction; DVB: Divinylbenzene; CWR: Carbon wide range; PDMS: Polydimethylsiloxane; E_E: Extraction efficiency; MDL: Method detection limit; RSD_1: Relative standard deviation at a concentration of 10 µg L^{-1}; RSD_2: relative standard deviation at a concentration of 60 µg L^{-1}.

Analyte	E_E HLB 5 µm arrow [%]	E_E HLB 30 µm arrow [%]	E_E HLB 5+30 µm arrow [%]	E_E HLB 5 µm SPME [%]	E_E DVB-CWR-PDMS arrow [%]	E_E PDMS arrow [%]	Carry-over [%]	MDL [µg L^{-1}]	RSD_1 [%]	RSD_2 [%]
Toluene	29	25	24	29	23	-	0.14	6.2	3	25
o-Xylene	33	35	35	27	30	-	0.04	1.4	9	4
2-Heptanone	-	-	-	-	-	-	nd	2.9	16	7
Anisole	2	-	-	-	-	-	nd	2.7	9	11
Heptanoic acid methyl ester	19	34	30	14	19	-	nd	-	-	-
n-Dodecane	70	54	82	51	82	52	0.02	1.9	8	9
Naphthalene	16	41	41	-	46	9	0.03	0.9	5	2
Indole	-	-	1	-	-	-	0.16	4.1	19	21
Lindane	-	6	3	-	-	-	0.94	1.3	28	31

6.5 Conclusions

The HLB fiber material is well suited for the extraction of analytes with different polarities. Compared to the conventional extraction materials PDMS and DVB-CWR-PDMS, the HLB arrow fibers perform much better and even the HLB SPME with a six times lower phase volume reaches comparable results to the DVB-CWR-PDMS arrow fiber. Still, there are further investigations needed covering more analytes, and testing different extraction approaches such as direct immersion or compatibility with on-fiber derivatization. Based on the results obtained here we see potential of the HLB fiber material to become the new use-one-for-all extraction device, which could perfectly be integrated into non-target analysis approaches, where a fiber material is needed that covers a broad polarity range.

7 Evaluation of GC-EI&CI-TOFMS for non-target analysis of wastewater using hydrophilic-lipophilic balanced SPME

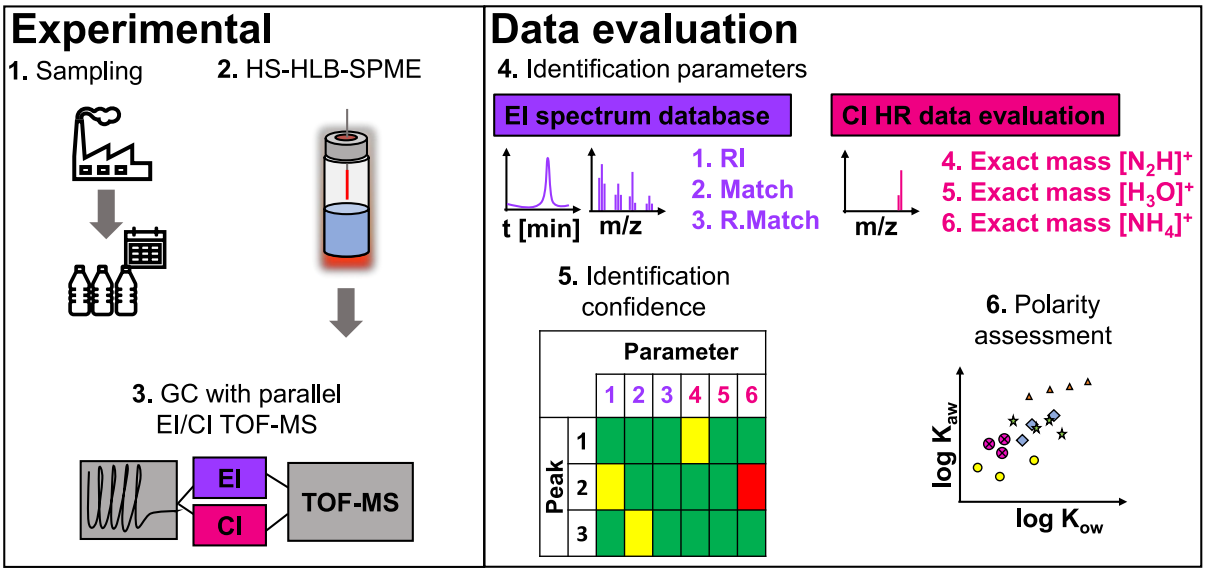

Adapted from: Lucie K. Tintrop, Steffen Bräkling, Marleen Vetter, Willi Eßer, Felix Drees, Amir Salemi, Maik A. Jochmann, Sonja Klee, Torsten C. Schmidt. Evaluation of GC-EI&CI-TOFMS for non-target analysis of wastewater using hydrophilic-lipophilic balanced SPME, submitted to Analytical Chemistry (2023).

7.1 Abstract

The evaluation of non-target analysis (NTA) techniques for the monitoring of wastewater is important as wastewater is an anthropogenic pollution source for aquatic ecosystems and a threat to human and environmental health. This study presents the proof-of-concept NTA of industrial wastewater samples. A prototype hydrophilic-lipophilic balanced (HLB) SPME and gas chromatography interfaced with time-of-flight high-resolution mass spectrometry (GC-TOF-HRMS) with electron ionization (EI) and chemical ionization (CI) in parallel are employed. The HLB-SPME was tested as a solvent-free headspace extraction. As the combination of parallel CI and EI data provides a comprehensive dataset as a unique feature, this study is strongly focused on the compound identification procedure and confidence reporting of exemplary substances. Furthermore, the use of three different CI reagent ions including $[N_2H]^+/[N_4H]^+$, $[H_3O]^+$, and $[NH_4]^+$ enables a broad range of analytes to be ionized in terms of selectivity and softness. The complementary information provided by EI and

CI data allows the determination of a sum formula in 97% of cases. The polarity coverage based on the physico-chemical properties of the analytes (such as volatility, water solubility, hydrophilicity, and lipophilicity) was visualized by using Henry's law and octanol-water partitioning constants. In conclusion, the presented approach is shown to be valuable for water analysis, can be seen as complementary to liquid-chromatography (LC) based methods in terms of polarity coverage, and allows enhanced and accelerated compound identification compared to utilizing only one type of ionization.

7.2 Introduction

The release of organic pollutants into the aquatic environment is mainly caused by anthropogenic activities such as agriculture, waste management, or industrial production. Known environmental pollutants are regulated nationally or internationally e.g. by the EU Water Framework Directive 2013/39/EU [180] and the United States Environmental Protection Agency Clean Water Act [181]. In addition, the so-called "priority substances" listed in directive 2013/39/EU and "toxic pollutants list" [182] referenced by the Clean Water Act only represent a small fraction of the extremely broad variety of anthropogenic pollutants. [183] To identify novel pollutants in e.g. lakes [1], rivers [2], wastewater [4], and drinking water [184] or to monitor the removal of pollutants and possible formation of transformation products during wastewater treatment [185], non-target analysis (NTA) is an essential tool. Harmful substances that enter the aquatic environment can have severe adverse effects on both, the ecosystem and human health. [186, 187] Hence, it is important to closely monitor the ever-changing composition of inflows in the aquatic environment. [188]

Due to the nature of aquatic samples, high-performance liquid-chromatography (HPLC) is the most commonly used separation method for NTA of water samples, often coupled to electrospray ionization (ESI) interfaced with high-resolution mass spectrometry (HRMS) [189] enabling the determination of exact masses. In addition, fragment spectra generated subsequently by e.g., collision-induced dissociation (CID), can give insight into the analytes' structure.

GC represents an alternative to HPLC-based methods and covers a very complementary polarity range to HPLC. Indeed, approaches using GC-HRMS for water analysis such as the detection of contaminants in the arctic environment [190], surface water [191], and determination of pollutants in wastewater [192] have previously been reported. Electron ionization (EI) is the gold-standard ionization

method for GC-MS. Especially for non-polar analytes, which show poor ionization efficiencies with ESI, using GC-EI-HRMS may be advantageous. [193] In contrast to HPLC-based ionization methods such as ESI and atmospheric pressure chemical ionization (APCI), EI shows strong in-source fragmentation. Although EI fragmentation is very reproducible and thus facilitates compound library comparisons with e.g., the NIST/EPA/NIR library [194], the molecular ion is often lost rendering unknown compound identification difficult [195]. In contrast, soft ionization methods compatible with GC, e.g., chemical ionization (CI), show less to no fragmentation and can therefore provide complementary information to EI. An instrument combining both EI and CI using a single time-of-flight (TOF) mass analyzer, also referred to as the ecTOF (TOFWERK, Thun, Switzerland), was introduced recently [196, 197] offering improved compound identification of known and unknown compounds.

GC, compared to HPLC, often requires more sophisticated sample preparation methods. [198] For the analysis of water, the transfer of analytes from the aqueous phase to a GC-suitable solvent or solid phase material and subsequent evaporation or desorption in the GC injector represents the main challenge. [20] However, sample preparation can also result in a favorable preconcentration of analytes of interest, a potential pre-selection of analytes, and a decrease in sample matrix effects. In recent years, microextraction methods have been increasingly used as they can be integrated into automated systems and meet several criteria of Green Analytical Chemistry (GAC). In combination with GC, solid-phase microextraction (SPME) [199] and stir bar sorptive extraction (SBSE) [200] have been used for NTA of water samples. Here, a SPME extraction material that is able to cover a broad range of different polarity analytes is required. With this in mind, a novel hydrophilic-lipophilic balanced (HLB) SPME material has recently been presented. [31] The HLB particles consist of a poly(divinylbenzene-*co*-N-vinyl-pyrrolidone) structure and allow hydrophobic interactions with the aromatic rings of divinylbenzene as well as hydrophilic interactions with the lactam ring of N-vinylpyrrolidone. [201]

In this proof-of-concept study, a NTA of wastewater samples was performed. The study aims to evaluate the polarity range covered by the novel extraction method in combination with the newly developed GC-EI&CI-TOFMS. Examples of compound identification are presented using the complimentary dataset providing high identification confidence. It should be noted that the presented workflow can be applied

to a broad range of samples consisting of volatile or semi-volatile analytes, and is not restricted to wastewater analysis.

7.3 Material and methods

7.3.1 GC-EI&CI-TOFMS analysis

The chromatographic separation was performed using a GC (7890A, Agilent Technologies, Santa Clara, USA) equipped with a Rxi-5ms capillary column (30 m x 0.25 mm x 0.25 µm, Restek, Bellefonte, USA). Helium (99.9999 mol%, Carbagas, Gümligen, Switzerland) was used as carrier gas with a flow of 1.2 mL min^{-1}. The GC injector was equipped with a Topaz SPME liner (0.75 mm ID, Restek, Bellefonte, USA) and set to 250 °C. The fiber was desorbed and cleaned for subsequent measurement for 15 min each in the injector. The injector was purged with 20 ml min^{-1} after 2 min. The GC oven program was as follows: 40 °C held for 5 min, raised to 170 °C with a rate of 5 °C min^{-1}, raised to 200 °C with a rate of 15 °C min^{-1}, raised to 260 °C with a rate of 10 °C min and raised to 325 °C with a rate of 20 °C min^{-1} held for 5 min. As detector, a parallel EI and CI TOF-HRMS (ecTOF; TOFWERK, Thun, Switzerland) was used. After GC separation, the column flow is split into equal parts and guided to the EI source operated at 70 eV and to the CI source [196] (both TOFWERK, Thun, Switzerland) The transfer lines, EI and CI sources were set to 280 °C, 280 °C and 300 °C, respectively. A solvent cut time of 350 s was used for EI. For CI, H_2, produced by a hydrogen generator (Precision Hydrogen Trace, Peak Scientific Instruments, London, United Kingdom), N_2 (99.9999 mol%, Carbagas, Gümligen, Switzerland), water, and a 30% ammonia in water mixture using a permeation tube setup were used for the generation of reagent ions $[N_2H]^+$/$[N_4H]^+$, $[H_3O]^+$ and $[NH_4]^+$ (more details in S and reference [197]). By using a reagent gas supply unit [197], the CI reagents could be switched between two GC runs without hardware changes. Each sample was measured three times while changing the CI reagents for each measurement, resulting in a dataset of EI triplicates with each having a different CI reagent. EI mass calibration was performed by pulsing perfluoroperhydrophenanthrene at the start of the measurement into the ion source background. For CI, traces of perfluorotributylamine (both ≥ 99.9%, Sigma Aldrich, Steinheim, Germany) were added continuously to the source background. AnalyzerPro XD® (SpectralWorks, Runcorn, United Kingdom) was used for chromatographic deconvolution and post-processing (parameters in the appendix in Table 9.20).

7.3.2 Sample preparation and chemicals

Cyclohexane (≥ 99%) was purchased from VWR (Darmstadt, Germany). An EPA 8270 mix, EPA semi-volatiles surrogate mix, and Alkane C7-C40 mix for retention index determination were purchased from Merck (Buchs, Switzerland). Dilutions (0.5 mg L^{-1} and 10 mg L^{-1}) of the EPA mixes were prepared in cyclohexane. The mixes were measured in a concentration of 0.5 mg L^{-1} and 2.5 mg L^{-1} for liquid injection and water samples for SPME measurements were spiked to a concentration of 5 µg L^{-1}. MilliQ water was produced by a Simplicity UV Water Purification System with 18.2 Ω (Merck, Darmstadt, Germany). Novel HLB-SPME fiber prototypes (10 mm x 110 µm, 5 µm particle size) with polydimethylsiloxane (PDMS) as support were provided by CTC Analytics (Zwingen, Switzerland). Headspace vials (20 mL) were filled with 4 mL of sample and the EPA semi-volatiles surrogate mix was added to produce a concentration of 5 µg L^{-1}. The vials were equilibrated for 15 min at 85 °C in a static headspace sampler (Ellutia, Ely, United Kingdom) and HLB-SPME enrichment of the analytes was performed in the headspace of the vials for 15 min at 85 °C. The workflow from sample collection, sample preparation by HS-HLB-SPME, and analysis using GC-EI&CI-TOFMS is presented in the appendix in Figure 9.9.

7.3.3 Industrial wastewater samples

Wastewater samples were collected from an industrial production plant as 24-hour representative samples for which an aliquot was sampled every hour and collected in the same container. The samples were taken over two time periods (abbreviated as Px) for several days (abbreviated as Dx) and stored at 4 °C.

7.4 Results and discussion

7.4.1 Inter-day variability of samples

The chemical composition of industrial wastewater can change and alternate considerably. Indeed, the high daily variation is displayed between Sample P1 D1 and P1 D4 using a volcano plot in Figure 7.1 A. The strong variation, even between consecutive days, and the regular occurrence of new compounds is comparable to other studies [202], justifying a NTA rather than a targeted approach for these wastewater samples. Although samples were taken from the same industrial plant, many compounds appear just for a single day and compounds found in both days can have very different relative intensities. The high variability between samples was also seen between other days.

However, as stated before, NTA using GC is still an emerging field compared to LC-based methods. Although GC-EI/MS is extremely powerful for targeted and suspect screening due to the high reproducibility and very comprehensive mass spectral libraries, identification of unknown compounds (not available in fragment spectra libraries) is relatively difficult using EI only due to the likely loss of molecular ion information. Figure 7.1 B shows the chromatogram for P1 D4. Two precisely aligned chromatograms for both ionization methods are obtained by the GC-EI&CI-TOFMS, allowing for improved compound identification. Examples of compounds identified with higher confidence due to the complementary dataset are shown in the next sections.

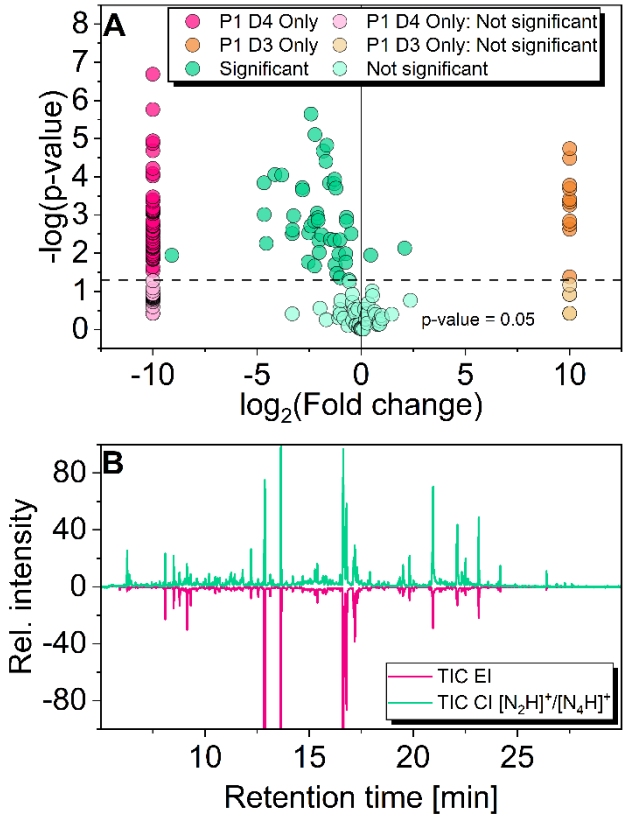

Figure 7.1 Exemplary volcano plot of EI data with the highest observed variation for triplicate measurements of samples P1 D3 and P1 D4 (A) and head-to-tail total ion current (TIC) chromatograms of CI $[N_2H]^+/[N_4H]^+$ (green, top) and EI (pink, bottom) from sample P1 D4 (B). For (A): On the x-axis the peak area change between the two samples is displayed by the $\log_2$ fold change. The y-axis shows the significance of the specific fold change for each compound displayed by the -log(p-value) of the one-way ANOVA. Compounds below a p-value of 0.05 were non-significant.

7.4.2 Compound identification using EI and CI data

As stated before, wastewater can contain a variety of different known and unknown substances. However, the identification of substances can be challenging in some cases. In the following examples, different approaches for compound identification using the combined CI and EI data set are shown. The presented example cases and

all other measured substances are listed in Table 9.21 in the appendix. Obviously, the compound identification confidence varies strongly from case to case depending on the evidence extractable from the dataset. A workflow to report the confidence of identification was published by Schymanski et al. [203] for LC-based detection methods. Although the overall data structure and therefore the data analysis using GC-HRMS is different from LC-HRMS/MS-based methods, the approaches described in references [203, 204] were predominately adapted (see SI) to report the identification confidence as shown in Table 9.21 in the appendix. The dataset recorded using the GC-EI&CITOFMS revealed a comprehensive number of complementary information. Parameters extracted from the data set as well as used software tools are listed below.
Compound identification using chromatographic data:

- Retention index (RI)

Compound identification using EI data:

- NIST similarity search (match factor (MF), reversed match factor (RMF), probability
- Structural investigation by fragmentation using “NIST MS Interpreter”
- Structural investigation by comparing fragmentations of structurally related compounds using “NIST hybrid similarity search” (HSS) (HSS MF, HSS RMF, original MF)
- Fragment and molecular ion (if existent)

Compound identification using CI data:

- Protonated/deprotonated molecule or adduct obtained with reagent ions $[N_2H]^+$/$[N_4H]^+$, and/or $[H_3O]^+$ and/or $[NH_4]^+$
- Exact mass
- Sum formula
- Structural investigation of fragmentation (if existent)

The values for acceptance of when a single parameter was considered reasonable are:

- A RI deviation of ± 20 for the obtained value to database value (if available)
- An EI MF and/or RMF of >800 (similarity and HSS)
- A mass error of ± 5 ppm for the calculation of the molecular ion sum formula (mainly from the CI data set)
- In addition to an obtained sum formula a fitting isotopic pattern must be present

In many cases the compound identification is straightforward. Here, a good EI fragment spectra library match in addition to a fitting RI and CI mass spectrum allows for a relatively confident identification. However, not every compound is listed in the EI libraries leading to low MFs. In addition, unspecific fragmentation and incomplete RI data can lead to misidentification and false positives.

In the following three examples, the data did not result in a straightforward identification. For these, the determination of the sum formula or tentative structure is shown in more detail.

7.4.2.1 Example 1: Identification of the sum formula

The molecular ion can give information about the sum formula of an analyte, which is especially important when EI mass spectra do not lead to a sufficient match. An analyte eluting at a retention time of 22.51 min (measured RI = 1818) resulted in MFs <703 and RMFs <713. Additionally, there was no M^+ in the EI mass spectrum (Figure 7.2), rendering the identification based only on EI difficult. In contrast, an intensive precursor ion could be identified as $C_{15}H_{28}O_2$ (exact molar mass 240.2089 Da) using all three CI reagents (the $[M+H]^+$ with *m/z* 241.2162 +0.1 ppm and the $[M+NH_4^+]$ with *m/z* 258.2428 +5.0 ppm). With no further structural information assessable, an identification level of 4 according to Schymanski et al. [203] could be achieved.

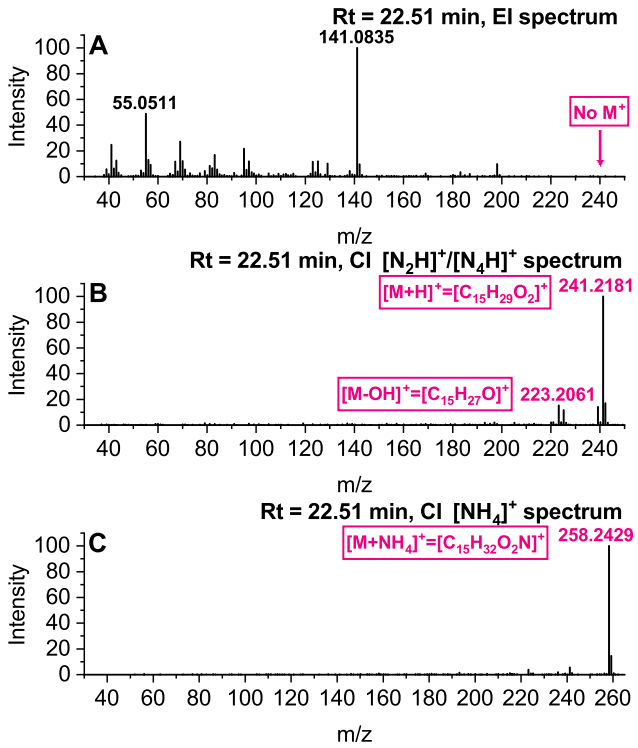

Figure 7.2 EI (A), CI $[N_2H]^+/[N_4H]^+$ reagent (B), and CI $[NH_4]^+$ reagent (C) mass spectra for a compound detected at a retention time of 22.51 min.

7.4.2.2 Example 2: Tentative structure identification of unknowns using EI and CI data

As stated before, the chemical diversity is too high for fragment spectra libraries to cover every molecule possible. However, an unsatisfying EI match can still contain important structural information that can be used for structure elucidation. Moorthy et al. [26] introduced the HSS to elucidate chemical structures by finding compounds sharing common structural features. Knowledge about the molecular mass is essential to the HSS to determine an accurate neutral loss spectrum. Fragments that match in the neutral loss spectrum but are shifted by a certain Δ mass in the similarity match indicate structural modifications of the analyte in these positions. This approach was executed for a compound detected at a retention time of 11.70 min (measured RI 1271). The M^+ shows a very low abundance in the EI mass spectrum, however, an intense $[M+H]^+$ was detected, concluding in a sum formula of $C_9H_{16}O_2$ (molar mass of 156.1150 Da; $[M+H]^+$ with CI reagent $[N_2H]^+/[N_4H]^+$ and $[H_3O]^+$ *m/z* 157.1223 +1.0 ppm; $[M+NH_4]^+$ with CI reagent $[NH_4]^+$ *m/z* 174.1489 +3.8 ppm). The EI fragment library search showed very poor match statistics for compounds sharing the same sum formula, with MFs <607 and RMFs <692. Experimental database RIs were not available for this compound and estimated database RIs were 1067-1223 ±69 (95% confidence interval). The target mass spectrum was then used for HSS by adding the nominal molar mass of 156, as NIST20 only allows for nominal mass information. Two entries showed reasonable HSS MFs for a Δ mass of *m/z* +14 and *m/z* +28 as shown in Figure 7.3 A and B. Respective mass spectra of the target compound are presented in Figure 9.10 in the appendix. These Δ mass values indicate an additional $-CH_2$ and $-C_2H_4$ group to the target, respectively. The HSS with a Δ mass of *m/z* +14 elucidates the compound dihydro-4,4,5,5-tetramethyl-2(3H)-furanone with a HSS MF of 809 (879 HSS RMF) compared to 518 of the original MF and a sum formula of $C_8H_{14}O_2$. Figure 7.3 C.1 shows the result of the HSS for this match. Fragments of the analyte mass spectrum that have the same neutral loss but are shifted by the Δ mass are indicated in grey (database spectrum) and pink (target spectrum). Here, the fragment at *m/z* 59 (grey) of the database spectrum is not present in the measured spectrum, but a fragment at *m/z* 73 (pink) appears in the target spectrum. The *m/z* 59 fragment was identified using the NIST MS interpreter to be $[C_3H_7O]^+$ (Figure 7.3 C.1, marked green) resulting in two possible structures for the fragment at *m/z* 73, $[C_4H_9O]^+$ and $[C_3H_5O_2]^+$ (Figure 7.3 C.2 and C.3, marked orange). Using the high-resolution EI data, fragment

m/z 73 could be identified as $[C_4H_9O]^+$ (Figure 7.3 C.2, marked orange), leading to the tentative structure C.6.

This tentative structure can further be confirmed using the second reasonable match of the HSS, 5-ethyl-4,4,5-trimethyloxolan-2-one with a HSS MF of 784 (913 HSS RMF, 447 original MF) and a Δ mass of *m/z* +28. As shown in Figure 7.3 B, a fragment of *m/z* 99 $[C_5H_7O_2]^+$ in the database spectrum (Figure 7.3 C.4, marked green) is shifted by *m/z* +28, resulting in a fragment of *m/z* 127 $[C_7H_{11}O_2]^+$ (Figure 7.3 C.5, marked orange) in the target spectrum. The structural elucidation of fragments allows specification of the tentative structure C.6 of the target compound.

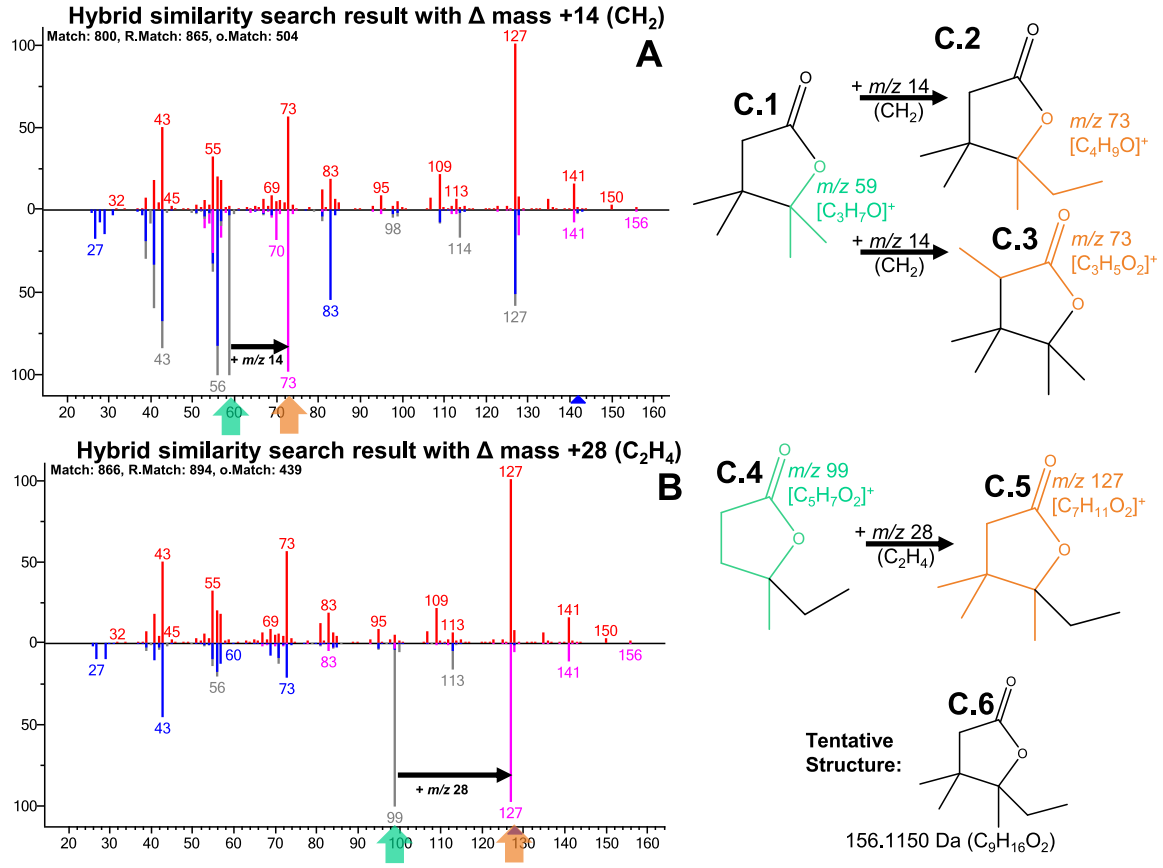

Figure 7.3 Hybrid similarity search results with Δ mass of *m/z* +14 (A) and *m/z* +28 (B) and respective fragment interpretation for the compound detected at a retention time of 11.70 min. The head-to-tail spectra show the spectrum of the target compound in red and the database spectrum in blue. Fragments of the library spectrum that are not found in the target spectrum (grey) but shifted by the corresponding Δ mass (due to structural difference) are indicated in pink. C.1 and C.4 represent the structures for the original database spectra A and B with the fragments indicated in green. The suggested structures of the target compound with a Δ mass of *m/z* +14 are represented by C.2 and C.3 and spectrum B with a Δ mass of *m/z* +28 by C.5 (Δ-mass-shifted fragments are indicated in orange). C.6 shows the tentatively identified structure of the compound of interest.

7.4.2.3 Example 3: Identification of the tentative structure using CI data

Commonly, CI shows less fragmentation than EI and is therefore conventionally used to identify the precursor ion. As shown in the experimental section, all samples were measured using three different CI reagents, showing different proton affinities and CI mechanisms. This results in different excess energies transferred to the analyte during the ionization step. Therefore, the ionization via $[N_2H]^+/[N_4H]^+$ commonly shows the strongest fragmentation followed by $[H_3O]^+$ and $[NH_4]^+$. Although fragmentation is normally not wanted using CI, it can still provide valuable structural information where EI fragmentation is too unspecific. A compound at a retention time of 17.31 min (measured RI 1541) was investigated. The EI chromatogram clearly indicates a M^+ with *m/z* 182.0985, and the database search states methyl-3-(phenylmethyl)-benzene as the tentative structure with a MF of 916, a RMF of 917, and a database RI of 1571. The M^+ is supported by the CI $[H_3O]^+$ reagent data which suggests a sum formula of $C_{14}H_{14}$ (182.1096 Da; $[M-H]^+$ *m/z* 181.1012 -0.4 ppm). Although this compound shows an excellent match of >900 the probability of 18.5% is rather low. This is due to the spectral similarity of phenylmethyl-benzene derivates and biphenyls. Indeed, 2,4'-dimethyl-1,1'-biphenyl with a database RI of 1531, for example, shows a MF of 897, a RMF of 897, and a probability of 9.5%. Due to the better fitting RI, 2,4'-dimethyl-1,1'-biphenyl may have an even higher identification confidence. However, the fragmentation in the CI $[N_2H]^+/[N_4H]^+$ mass spectrum reveals two intense and very specific fragments of *m/z* 91.0548 and *m/z* 105.0704, which are identified to be $[C_7H_7]^+$ and $[C_8H_9]^+$, respectively (see Figure 7.4 B). These two fragments unequivocally exclude a biphenyl as a possible structure, as the fragments are a result of the cleavage at the phenylmethyl-benzene position (see Figure 7.4 B). Since phenylmethyl-benzenes show significantly different toxicity to biphenyls [205], the correct identification of these compounds is of importance.

Interestingly, the CI $[NH_4]^+$ reagent mass spectrum acts peculiar as it shows a $[M+NH_4]^+$ adduct at *m/z* 200, but also a M^+ at *m/z* 182, and further fragments with high abundance, which is unusual. In general, the ionization of a non-polar compound such as 2,4'-dimethyl-1,1'-biphenyl with the $[NH_4]^+$ reagent ion is expected to be less efficient and with low to no signal in CI $[NH_4]^+$. The appearance of $[M+NH_4]+$ as well as M^+ at the same time indicates that the $[M+NH_4]^+$ adduct is very weakly bound and declustering occurs within the transfer stage of the mass analyzer resulting in a M^+ signal. [206]

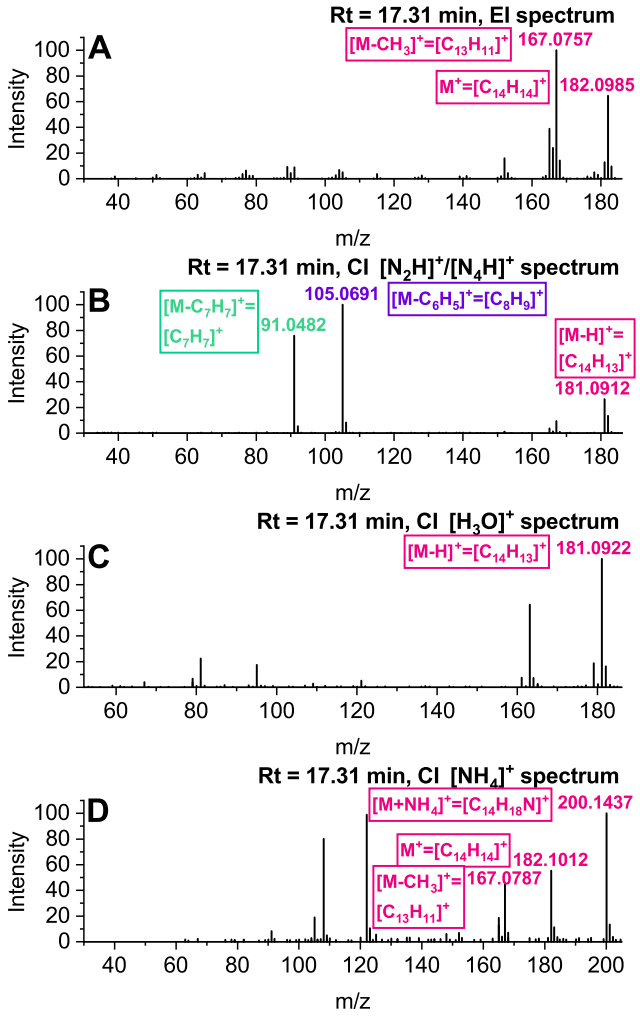

Figure 7.4 EI (A), $[N_2H]^+/[N_4H]^+$ (B), $[H_3O]^+$ (C) and $[NH_4]^+$ reagent ion (D) CI mass spectra for a compound detected at a retention time of 17.31 min.

7.4.3 Evaluation of compound identification parameters

Figure 7.5 summarizes the availability of information for different parameters used for compound identification. Figure 9.11 in the appendix presents the percentual distribution of the identification parameter quality as cake plots. Each bar in Figure 7.5 A-G represents a single measured compound (listed in Table 9.21 in the appendix) whereby the bar color indicates the quality of the specific identification parameter, while the bar length designates the normalized intensity of the chromatographic peak on a logarithmic scale.

The data set generated by EI was evaluated using the database MF, RMF, and RI. The MF states the similarity of the target versus the database spectrum and the RMF gives the similarity of the target spectrum reduced by the peaks that do not occur in the database spectrum versus the database spectrum and therefore, indicates potential distortion of the EI mass spectrum by coelution. Lower MFs, in general, occur

when the exact compound is not listed within the library and the match only shares structural similarities. MFs >800 were only found for 48% and RMFs >800 were found for 60% of all detected compounds (Figure 7.5 A and B). Figure 7.5 A and B also depict that intensity can partly influence the quality of the MFs and RMFs.

The RI is mainly used as complementary chromatographic information in addition to the mass spectrum and to differentiate isomers. As shown in Figure 7.5, compounds with high EI MFs but no matching RI are lowered from identification levels 2 to 3. The measured RI matches the database RI in 63% of cases (Figure 7.5 C).

The main advantage of CI is the relatively certain determination of the sum formula of an unknown analyte. With better mass accuracy, a higher certainty in the sum formula can generally be achieved. In this case, the mass accuracy of <5 ppm is given by the resolving power of the used TOF mass analyzer (R~5000) and is dependent on the quality of the mass calibration. Mass accuracy errors of <5 ppm were determined for 54-76% of compounds (Figure 7.5 D-F) among the three reagent ions. No precursor ion in $[N_2H]^+$/$[N_4H]^+$, $[H_3O]^+$, and $[NH_4]^+$ could be determined in 11%, 16%, and 36%, respectively. This value is the result of an increasing proton affinity of corresponding brønsted bases (494, 691, and 854 kJ mol^{-1} [207]). The highest value of non-available data is found for $[NH_4]^+$. Especially at high retention time, many alkylbenzenes eluted (see appendix Table 9.21), which are not ionizable by $[NH_4]^+$. However, $[NH_4]^+$ may improve the precursor ion yield for very fragile compounds as previously presented by Bräkling et al. [197]. The overall coverage of accurate mass precursor ion information is at ~86%, which highlights the advantage of using three different CI reagents. Especially the high coverage of the CI data for compounds with insufficient EI information is advantageous, as shown in Figure 7.5.

Applying the identification confidence levels by Schymanski et al. [203], 6% of the compound identities were confirmed with a reference standard (level 1), for 41% a structure was proposed (level 2a and b), for 24% a tentative structure was proposed (level 3), for 29% a molecular formula was stated (level 4) and for 4% only the accurate mass could be gained (level 5) (see Figure 7.5 G). However, for level 2 an identification confirmation by RI was necessary, which originally was not included by Schymanski et al. as the workflow was developed for LC-based methods.

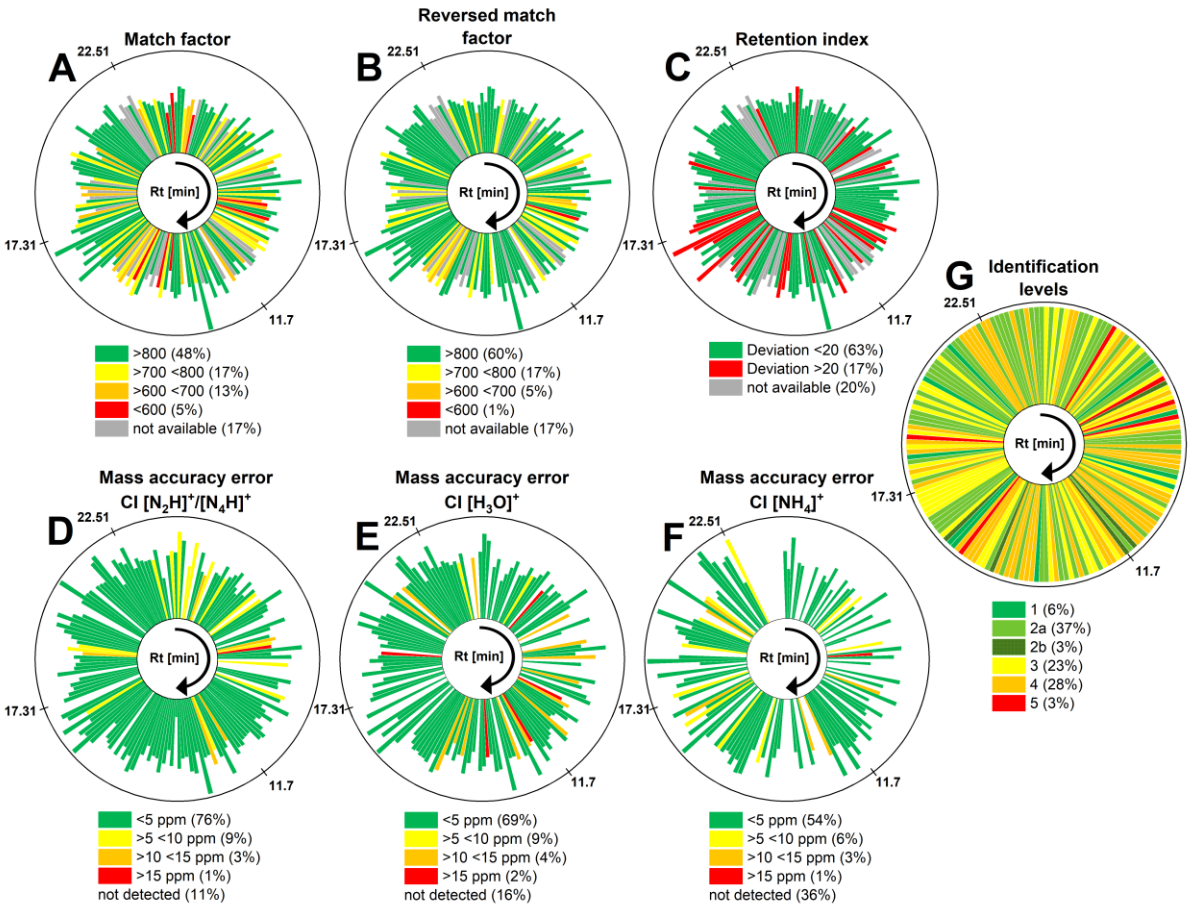

Figure 7.5 Identification parameters displayed as radial bar plots with logarithmic peak areas for match factor (A), reversed match factor (B), retention index (C), mass accuracy error for CI $[N_2H]^+/[N_4H]^+$ (D), CI $[H_3O]^+$ (E), CI $[NH_4]^+$ (F) reagent ions and identification levels of the found compounds (G) [203]. Each bar represents one compound from Table 9.21 in the appendix sorted by their retention time starting at 90° in clockwise circulation. The colors display the quality of the identification parameter. For A-C grey bars represent data that was not available from the database and for A-F missing bars represent compounds that were not detected for this ionization type. The retention time of the three discussed examples is stated on the circular axis.

7.4.4 Evaluation of polarity and compound classes

With little to no prior knowledge of a sample's constituents, a broad extraction method is paramount in NTA. The HLB-SPME material was developed to extract a broad variety of different polarity analytes. [31, 174] In this study, the identified compounds were used to investigate the material performance for different polarities and compound classes. A plot of octanol-water K_{ow} and air-water K_{aw} partitioning constants as presented by Lorenzo-Parodi et al. [20] was found most suitable to characterize the polarities of extracted analyte substance classes with the HLB-SPME (see Figure 7.6). When available, the partitioning constants (for 25 °C) for found substances were taken from the Linear Solvation Energy Relationship (LSER) database of the UFZ Helmholtz Centre [135] (see Table 9.22 in the appendix). In Figure 7.6 A, substance classes

cluster due to their similar physico-chemical behavior and indeed, the HLB material was able to extract a broad range of analytes with hydrophilic as well as lipophilic properties (log K_{ow} values from 0.76 to 9.64 and log K_{aw} ranges from -8.5 to 3). Alkanes were the most lipophilic substance class with the highest air-water ratio, whereas sulfones and phthalides were the most hydrophilic substances with the lowest air-water ratio. Figure 7.6 B displays the molecular composition, retention time, and molecular mass of the found substances. Most of the substances can be assigned to C_xH_y or $C_xH_yO_z$ compounds. Moreover, molecules containing nitrogen, sulfur, or chlorine could be identified. The molar weight of identified substances ranged from ~90-280 Da within a retention time of 6-27 min. These results show that the HLB-SPME material is well suited for application in NTA approaches. The range of detected analytes may be extended further when a direct immersion approach is applied in combination with a headspace extraction. [20] However, headspace extraction is preferred in most approaches for interaction prevention of non-volatile matrix components with the fiber material, which could lead to interferences and fiber material altering.

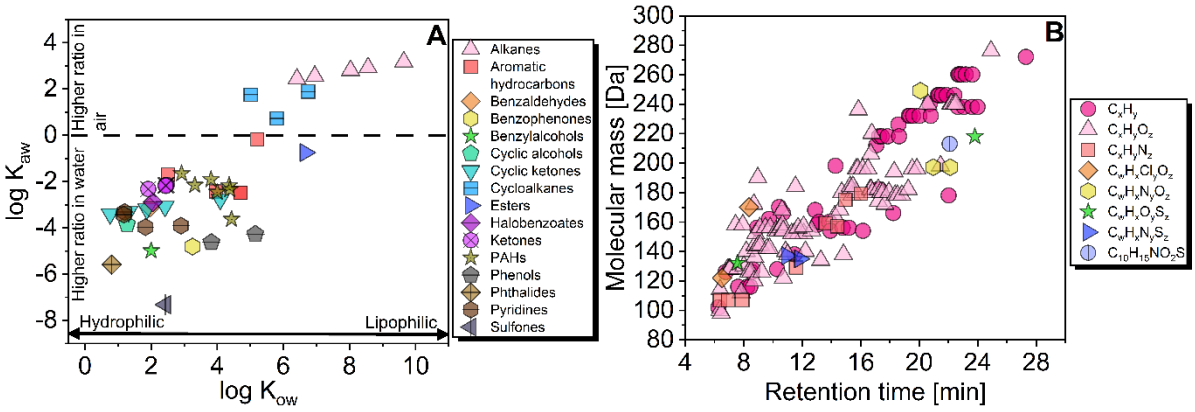

Figure 7.6 Double logarithmic correlation of air-water (K_{aw}) and octanol-water (K_{ow}) partitioning constants (A) and molecular composition (B) of the identified substances. Partitioning constants were taken from the LSER database of the UFZ Helmholz Center. [135]

7.5 Conclusions

For a proof-of-concept NTA study of wastewater, a novel HLB-SPME fiber material combined with the GC-EI&CI-TOF-HRMS was used for extraction, detection, and identification of unknown compounds. The broad polarity range and the many compound classes covered by the HLB-SMPE fiber material render it well-suited for use in NTA. The GC-EI&CI-TOFMS approach considerably improves identification confidence for unknown compounds compared to classical GC-(EI)MS, especially when employing different CI reagents during triplicate measurements. Due to the

solvent-free, miniaturized, and fast microextraction approach and the large amount of information gained during single GC-EI&CI-TOFMS measurements, this approach is consistent with GAC requirements.

8 General conclusion and outlook

Analytical Chemistry is constantly evolving and must adapt to new challenges such as the demand for greener analytical methods. Sample preparation is often described as the bottleneck and error-prone step in the analytical procedure – errors made in this step can hardly be corrected in subsequent analysis. It should also be noted that sample preparation is the bottleneck in terms of greenness, as most standard analytical techniques such as gas chromatography (GC) or high-performance liquid chromatography (HPLC) can hardly be optimized based on greenness. Nevertheless, some efforts such as miniaturization of HPLC systems have already been made [208], but for GCs and mass spectrometers (MSs), this is still lacking.

Developing new analytical methods involving microextractions helps to gain more knowledge about the feasibility of microextractions for standardization. The exemplary evaluation of United States Environmental Protection Agency (USEPA) standard methods using greenness evaluation tools showed that many old standard methods [108, 110, 112] are not green. In contrast, a more recent USEPA method, which was one of the few USEPA methods using microextraction [14], resulted in much better greenness scores. Replacing large-scale extraction with microextraction techniques vigorously enhances the method's greenness. Equally or better performing, greener replacement methods are already available for several years [109, 111, 113], so this is not the reason for the lack of application of microextractions in standard methods. Rather, the implementation process of the standard methods seems to be a problem. Greenness evaluation tools such as AGREE [46], AGREEprep [47], and GAPI [45] contribute to the evaluation and comparison of method greenness and give impetus to the steps in the analytical procedure that could be further improved. It is proposed that greenness evaluation should be implemented not only in research but particularly in routine analysis, as routine analysis has the highest sample throughput and therefore the highest potential to save resources. However, the systematic evaluation of standard methods requires governmental as well as scientific community action to contribute to a sustainable future.

The quality of analytical performance and applicability (e.g. automation) is an important point, that often finds less attention in greenness evaluation tools, but is important for the acceptance of the method in the scientific community. The concept of white analytical chemistry combines both: method greenness and analytical performance.

[51] Future method developments should include a detailed evaluation of method performance and comparison with already existing methods, preferably standard analytical methods, to forward standardization. The developed methods including SPME and SPME arrow exhibited good analytical method performance with low method detection limits, linear calibration ranges, and applicability to complex real water matrices. Nevertheless, the repeatability expressed by relative standard deviation values (RSD) of SPME and SPME arrow in some cases are higher (> 20%) than for liquid injections and methods with large-scale extractions, resulting from higher fluctuations during extraction and desorption steps. In addition, lower phase volumes are used which are more affected by small changes compared with large-scale extractions. Future investigations could address the higher RSDs in microextraction rendering suggestions for solving this problem. Some studies have already been published where repeatability was enhanced for example by novel phase materials [209, 210] or vacuum-assisted headspace SPME [211].

The automation of SPME as well as SPME arrow is simple as both have a classical syringe format, whereas for SPME arrow the injector of older GC models needs to be widened whereas for newer models this is not necessary. SPME arrow shows enhanced stability through the thicker stainless steel rod and arrow-shaped tip, which simplifies the automated handling and especially vial penetration. Not a single SPME arrow was bent during the whole experimental phase of this work, but in some cases, the coating was lost due to improper autosampler or operator actions. Next to the extraction, all of the other steps were automated including the addition of standards and internal standards, pH adjustment, and fiber cleaning, among others. In Chapter 7 SPME was used without an autosampler, which cost much more time and additionally could not run beyond the working hours of the operator. Automation already finds broad application in analytical chemistry, whereby in combination with microextraction, it poses a green, time- and cost-efficient way for sample processing. Automation should be applied to all newly proposed methods to the highest automation degree possible.

In all of the applications, a headspace extraction was used as it boasts several advantages. The headspace protects the fiber material from unwanted and/or solid matrix constituents in the sample that can degrade the fiber material and additionally has faster kinetics. [20] In addition, the fiber lifetime is known to be at least ~5 times longer in headspace than for direct immersion approaches. A disadvantage of

headspace extraction is, that it is limited to analytes that have a sufficiently high fraction in the air phase (~log K_{aw} > -6.0). [20]

The optimization of extraction and derivatization parameters (Chapters 4-6) was conducted by using design of experiment (DOE) approaches. A DOE approach is greener than a one-factor-at-a-time optimization as it reduces the number of measurement runs and additionally provides information about the influence of factor combinations. In terms of Green Analytical Chemistry (GAC), the necessity of every measurement has to be carefully considered. Optimal temperature, time, and extraction material were found to be critical parameters in SPME and SPME arrow extraction as they are strongly dependent on the analyte structure and can differ drastically even in the same substance class. The pH of the aqueous solution can additionally play an important role, when the analytes include dissociating groups, whereas the neutral form of the analyte is preferably passing over to the headspace and sorbing to the fiber material. Partitioning constants for air-water and air-fiber can help to partly understand the complexity of the multiphase system of a headspace extraction and are available in online databases [135]. Proper fiber cleaning is important to avoid carry-over of the analytes into the next measurement and consequently false-positive determination. During this work, an enhanced fiber cleaning approach was developed combining chemical cleaning of the fiber with gaseous methanol and subsequent thermal fiber cleaning at high temperature, which drastically reduced the carry-over effect.

SPME arrow can be combined with in-situ derivatization. In Chapter 5 the derivatization led to an additional substance class and twice the amount of substances being analyzed at the same time, saving considerable time and preventing false-positive determinations. Derivatizations are an unwanted step in terms of greenness. Therefore in applications where derivatizations are essential, novel derivatization approaches should be developed, which can be combined with microextraction methods and use fewer solvent amounts. Promising approaches could be on-fiber derivatization in combination with gas-generating vials for a reusable source of the derivatization agent and simple integration in an automated SPME process. [212] Next to the combination of a derivatization reaction with microextraction techniques, the application of green solvents/reagents, microwaves, ultrasound, derivatization directly in the GC injector (in-injector), or on the chromatographic column (on-column) was found to be a green way of operation. [213]

The challenge of covering a broad range of polarity was overcome by applying a novel hydrophilic-lipophilic balanced (HLB) SPME and SPME arrow material which contains hydrophilic as well as lipophilic groups. The characterization and application in a non-target analysis (NTA) approach of the HLB material showed that a broad range of different analyte polarities could be successfully extracted from the headspace. The HLB material may be the novel use-one-for-all material in SPME and related techniques in the future and should be investigated further for various applications. Especially, direct immersion approaches should be investigated to extend the range of covered air-water partitioning constants (K_{aw}), as this study only dealt with headspace extraction. In Chapter 7, the HLB SPME was combined with a novel GC time-of-flight mass spectrometer (TOFMS) NTA approach using electron ionization (EI) and chemical ionization (CI) in parallel for the analysis of industrial wastewater. The quality of compound identification was enhanced resulting from the generation of complementary EI and CI data. A parallel ionization data generation during one run is in agreement with GAC requirements, as the doubled information can be gained during one run compared to a single ionization data generation. The investigation of the feasibility of microextraction in GC-based NTA approaches is so far lacking and gives perspectives for future research.

This thesis contributes to the question if microextractions are capable of replacing large-scale extractions in research and standard analytical methods. The results show that SPME and SPME arrow offer in fact a simple and green alternative, but some challenges, as discussed before are still not fully overcome. At the moment it is in particular important to initiate the active standardization process of microextractions so future research in the field of miniaturized and automated sample preparation is required.

9 Appendix

9.1 Supporting material

9.1.1 Supporting material for Chapter 4

9.1.1.1 Mass spectral fragmentation patterns

Table 9.1 General mass spectral fragmentation patterns for identification of FAMEs adapted from Härtig et al. [134]. Precursors and product ions were selected based on known fragmentations. M: Molecular ion

Fragments [m/z]	Identification
43/57/71/85	Alkyl series
41/55/69/83	Alkenyl series
59	Methoxy carbonyl
74	McLafferty rearrangement ion
75	Dimethoxy methyl radical ion
87	C3:0 Methyl ester
90	Cleavage at OH, H-rearrangement
103	Cleavage at OH
143	C7:0 methyl ester
199	Cleavage at C10 methyl branching site
M-15	Loss of methyl
M-18	Loss of water
M-29	Loss of ethyl
M-31	Loss of methoxy
M-32	Loss of methanol
M-43	Loss of propyl
M-46	Loss of ethyl + water
M-59	Loss of methoxy carbonyl
M-74	Loss of Mc Lafferty fragment

9.1.1.2 Optimized MRM parameters

Table 9.2 MRM transitions from precursor to product ions with optimized collision energy and ion ratios for the determination of FAMEs. Experimental conditions: Sample: FAME mix with varying concentrations (diluted 1:100 in acetone); n = 3; Chosen CEs for optimization were 5, 10, 15, 20, 25 and 30 eV. CE before optimization was 5 eV for all transitions. All transitions were used for quantification (TIC of MRM transitions) and qualification. Time frame: chosen time frame for the given transitions; *Molecular ions; CE: Collision energy

FAME	Abbr.	CAS No.	Retention time (time frame) [min]	MRM Transitions Precursor ions>Product ions [*m/z*]	Optim. CE [eV]	Ion ratios [%]
Methyl hexanoate	C6:0Me	106-70-7	7.160 (5.00-8.25)	130*>74	10	2
				130*>55	15	1
				99>43	20	51
				99>71	5	100
				99>59	10	5
Methyl heptanoate	C7:0Me	106-73-0	9.572 (8.25-11.20)	144*>115	10	0.1
				112>85	5	66
				112>43	10	100

FAME	Abbr.	CAS No.	Retention time (time frame) [min]	MRM Transitions Precursor ions>Product ions [*m/z*]	Optim. CE [eV]	Ion ratios [%]
Methyl octanoate	C8:0Me	111-11-5	11.751(11.20-13.00)	102>59	10	45
				102>74	10	65
				158*>74	15	2
				158*>101	5	6
Methyl nonanoate	C9:0Me	1731-84-6	13.700 (13.00-14.75)	126>57	10	100
				126>109	5	10
				116>59	10	80
				116>83	10	8
				172*>101	10	14
				172*>143	5	10
Methyl decanoate	C10:0Me	110-42-9	15.492 (14.75-16.5)	140>71	5	45
				140>57	10	79
				130>69	10	100
				130>73	10	62
				186*>101	5	8
				186*>129	10	8
Methyl undecanoate	C11:0Me	1731-86-8	17.176 (16.50-18.00)	155>71	5	27
				155>57	15	29
				143>83	10	100
				143>87	10	21
				200*>143	5	36
				200*>101	10	47
Methyl dodecanoate	C12:0Me	111-82-0	18.734 (18.00-19.50)	169>95	5	72
				169>71	10	62
				157>97	10	100
				157>69	15	53
				214*>143	5	20
				214*>157	5	20
Methyl tridecanoate	C13:0Me	1731-88-0	20.209 (19.50-21.00)	171>101	10	100
				171>69	10	69
				183>95	5	22
				183>109	5	21
				228*>143	10	21
				228*>157	5	16
Methyl tetradecanoate	C14:0Me	124-10-7	21.615 (21.00-22.10)	197>95	5	14
				197>71	10	22
				185>101	10	100
				185>69	15	46
				242*>157	5	15
				242*>171	5	13
Methyl pentadecanoate	C15:0Me	7132-64-1	22.947 (22.10-23.70)	199>97	10	11
				199>101	10	93
				143>87	10	20
				143>83	10	100
				256*>171	5	36
				256*>199	5	36
Methyl hexadecanoate	C16:0Me	112-39-0	24.238 (23.70-24.50)	213>107	10	6
				213>69	15	49
				157>101	10	100
				157>97	10	57
				270*>199	5	45
				270*>185	5	41
				238>109	5	9
				238>137	5	6
				171>101	10	100
				171>69	15	77

FAME	Abbr.	CAS No.	Retention time (time frame) [min]	MRM Transitions Precursor ions>Product ions [*m/z*]	Optim. CE [eV]	Ion ratios [%]
Isotope-labeled methyl heptadecanoate-d_{33}	C17:0dMe	1219804-81-5	25.066 (24.95-25.40)	317*>219	10	69
				317*>171	10	32
				203>107	10	94
				155>94	10	100
				155>78	15	53
Methyl heptadecanoate	C17:0Me	1731-92-6	25.454 (25.40-25.80)	284*>199	10	43
				284*>143	10	43
				185>101	10	100
				185>83	10	18
				241>129	10	5
				241>97	10	13
Methyl octadecanoate	C18:0Me	112-61-8	26.657 (25.80-26.80)	298*>143	10	41
				298*>185	10	29
				255>109	10	6
				255>129	10	4
				199>101	10	100
				199>83	10	21
Methyl eicosanoate	C20:0Me	1120-28-1	28.855 (28.80-29.10)	326*>171	10	57
				326*>185	10	50
				283>101	10	100
				283>115	10	6
				227>111	10	7
				227>97	10	11
Methyl heneicosanoate	C21:0Me	6064-90-0	29.914 (29.10-30.20)	340*>185	10	78
				340*>143	10	70
				297>109	10	11
				297>83	15	19
				241>101	10	100
				241>85	10	6
Methyl docosanoate	C22:0Me	929-77-1	30.924 (30.20-31.35)	354*>199	10	73
				354*>143	15	63
				311>101	15	100
				311>97	15	13
				255>87	15	5
				255>129	10	3
Methyl cis-9-hexadecenoate	C16:1cMe	1120-25-8	24.710 (24.50-24.95)	268*>155	10	8
				268*>185	10	7
				194>96	10	77
				194>82	10	100
				141>109	10	20
				141>57	10	17
Methyl trans-9-octadecenoate	C18:1tMe	112-62-9	26.878 (26.80-27.45)	296*>213	10	8
				296*>141	10	37
				264>98	10	100
				264>111	10	69
				222>96	10	77
				222>82	15	99
Methyl cis-9-octadecenoate	C18:1cMe	2777-58-4	27.018 (26.80-27.45)	296*>213	10	8
				296*>141	10	34
				264>98	10	100
				264>111	10	70
				222>96	10	76
				222>82	15	98
Methyl cis,cis-9,12-octadecadienoate	C18:2cMe	112-63-0	27.684 (27.45-28.00)	294*>96	15	17
				294*>178	5	5
				123>81	10	100
				123>67	15	62

FAME	Abbr.	CAS No.	Retention time (time frame) [min]	MRM Transitions Precursor ions>Product ions [*m/z*]	Optim. CE [eV]	Ion ratios [%]
Methyl cis,cis,cis-6,9,12-octadecatrienoate	C18:3c6Me	16326-32-2	28.167 (28.00-28.50)	150>107	10	44
				150>121	10	28
				292*>94	10	5
				292*>108	20	3
				121>106	10	51
				121>92	10	86
				108>79	10	100
				108>67	15	23
Methyl cis,cis,cis Methyl cis,cis,cis-9,12,15-octadecatrienoate	C18:3c9Me	301-00-8	28.556 (28.50-28.80)	292*>94	20	3
				292*>108	15	1
				136>81	15	7
				136>121	10	7
				108>79	5	100
				108>67	10	18
Methyl cis,cis,cis,cis,cis-5,8,11,14,17-eicosapentaenoate	C20:5cMe	2734-47-6	31.389 (31.35-31.78)	316*>135	15	1
				316*>94	30	1
				133>91	15	43
				133>105	10	47
				108>79	5	100
				108>67	15	12

9.1.1.3 Ion ratio stability

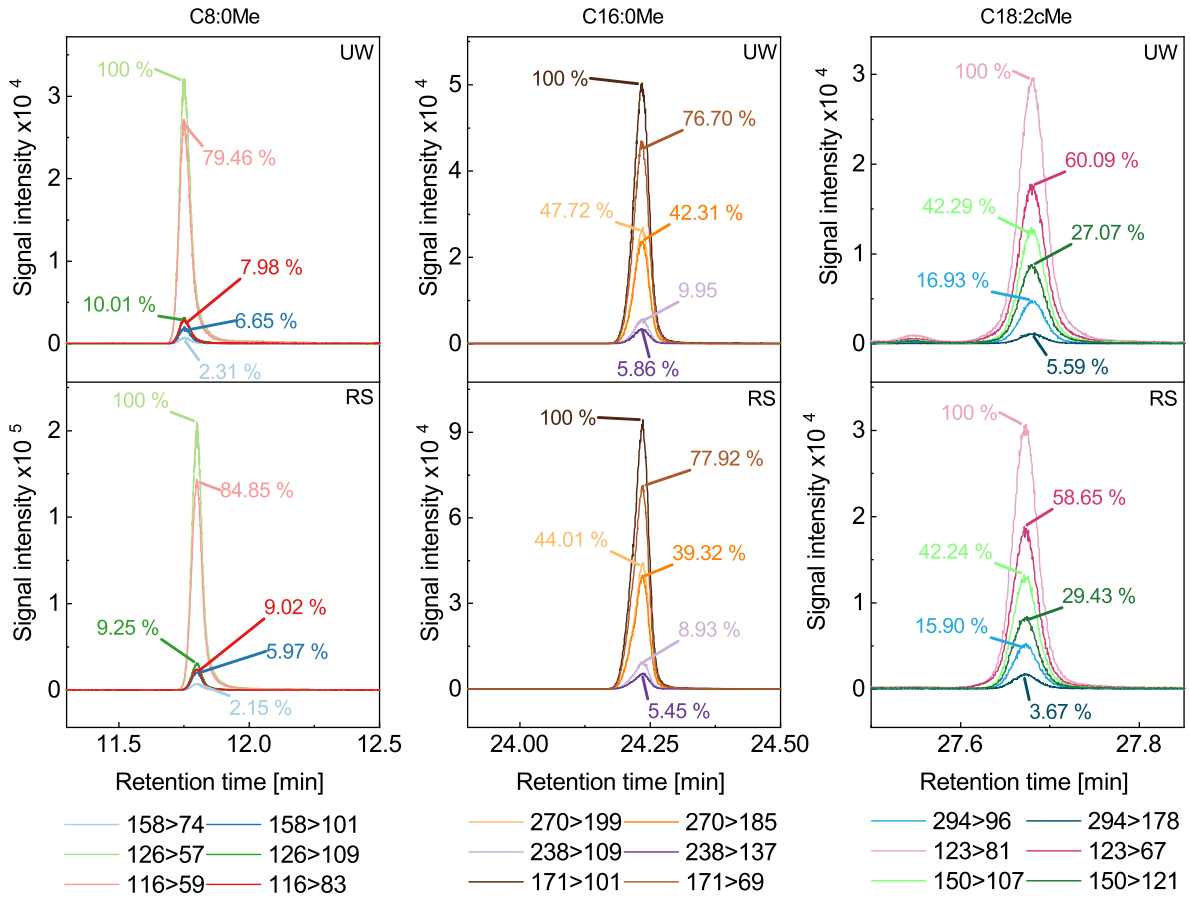

Figure 9.1 Ion ratio stability in ultrapure water (UW) spiked in 2-3 µg L^{-1} and spiked real sample (RS) in 0.5-1.5 µg L^{-1} exemplarily shown for C8:0Me, C16:0Me and C18:2cMe. Spiking solution: varied concentration FAME Mix

9.1.1.4 Theoretical extracted fractions

The partitioning of analytes in the three phases (headspace, sample, and polymer sorption phase of SPME arrow) under equilibrium conditions is described through the mass balance with the initial mass of the sample m_0, the mass in the aqueous phase m_w, the mass in the gaseous phase m_a and the mass extracted by the fiber m_f (Equation 1).

$$m_0 = m_w + m_a + m_f \qquad 1$$

First, the two equilibria describing the distribution of analytes between the water phase, gas phase, and fiber material are established (Equations 2 and 3). From this, the distribution coefficients between the water phase to gas phase K_{aw} and gas phase to fiber K_{fa} can be established.

$$Analyte\ (aq) \rightleftharpoons Analyte\ (g) \qquad K_{aw} = \frac{[Analyte\ (a)]}{[Analyte\ (w)]} \qquad 2$$

$$Analyte\ (g) \rightleftharpoons Analyte\ (f) \qquad K_{fa} = \frac{[Analyte\ (f)]}{[Analyte\ (a)]} \qquad 3$$

If the equilibria are combined and balanced, the equilibrium for the distribution between water phase to fiber is obtained and the corresponding distribution coefficient K_{fw} can be calculated as follows:

$$Analyte\ (aq) \rightleftharpoons Analyte\ (f) \qquad K_{fw} = \frac{[Analyte\ (f)]}{[Analyte\ (w)]} = K_{aw} \cdot K_{fa} \qquad 4$$

The volume ratio r_{fw} of SPME arrow fiber volume (3.8 µL) to water phase (10 mL) gives:

$$r_{fw} = \frac{V_f}{V_w} = \frac{3.8 \cdot 10^{-6} L}{0.01\ L} = 3.8 \cdot 10^{-4} \qquad 5$$

Theoretical extracted analyte fractions with an SPME arrow fiber (PDMS polymer sorption phase) f_f were determined by Equation 6.

$$f_f = \frac{1}{1 + K_{wf} \cdot r_{wf} + K_{af} \cdot r_{af}} \qquad 6$$

The partitioning constants between air and water K_{aw} and PDMS and air K_{fa} were calculated using the online database for polyparameter linear free energy relationships (pp-LFERs) from the UFZ Helmholz Center for environmental research [135] by using equation 7 [214] and equation 8 [215] with experimentally determined pp-LFER descriptors for polarizability/dipolarity S, solute hydrogen bond acidity A, solute hydrogen bond basicity B; McGowan's molar volume V, logarithmic gas-hexane partition coefficient L, and the excess molar refraction E. [216]

$$\log K_{wa} = -0.59 + 2.07\ S + 3.67\ A + 4.87\ B - 2.55\ V + 0.48\ L \qquad 7$$

$$\log K_{fa} = -0.04 + 0.54\ S + 1.14\ A + 0.58\ B + 0.79\ L + 0.01\ E \qquad 8$$

For the reversed equilibrium, the following applies:

$$\log K_{1,2} = -\log\ (K_{2,1}) \qquad 9$$

The temperature-dependent distribution constants for saturated FAMEs were determined using van't Hoffs equation

$$\log \frac{K_1}{K_2} = -\frac{\Delta H_r^0}{2.3\ R} \cdot \left(\frac{1}{T_1} - \frac{1}{T_2}\right) \qquad 10$$

Standard enthalpies of reaction ΔH_r^0 were calculated with standard formation enthalpies for the liquid $\Delta H_f^0(l)$ and gaseous $\Delta H_f^0(g)$ states were taken from CRC Lide [217].

Table 9.3 Calculated theoretical extracted equilibrium fractions f_f and distribution constants $log\ K_{wa}$, $log\ K_{fw}$ and $log\ K_{fa}$ from literature data. LSER descriptors were

taken from the database from the UFZ Helmholz center for environmental research [135]. S: polarizability/dipolarity; A: solute hydrogen bond acidity; B: solute hydrogen bond basicity; V: McGowan's molar volume; L: logarithmic gas-hexane partition coefficient; E: excess molar refraction

FAME	S	A	B	V	L	E	$\log K_{wa}$ (25 °C)	$\log K_{fw}$ (25 °C, PDMS)	$\log K_{fa}$ (25 °C, PDMS)	f_f [%]
C6:0Me	0.6	0	0.45	1.1693	3.874	0.08	1.73	1.88	3.61	2.8
C7:0Me	0.6	0	0.45	1.3102	4.356	0.08	1.59	2.39	3.99	8.5
C8:0Me	0.6	0	0.45	1.4511	4.838	0.07	1.47	2.91	4.37	22.6
C9:0Me	0.6	0	0.45	1.592	5.321	0.06	1.34	3.41	4.75	48.3
C10:0Me	0.6	0	0.45	1.7329	5.803	0.05	1.21	3.93	5.13	74.9
C11:0Me	0.63	0	0.45	1.8738	6.296	0.05	1.15	4.38	5.54	89.7
C12:0Me	0.6	0	0.45	2.0147	6.767	0.04	0.95	4.93	5.89	96.7
C13:0Me	0.64	0	0.45	2.1556	7.271	0.04	0.92	5.39	6.31	98.8
C14:0Me	0.6	0	0.45	2.2965	7.731	0.03	0.7	5.95	6.65	99.6
C15:0Me	0.68	0	0.45	2.4374	8.242	0.04	0.75	6.36	7.1	99.9
C16:0Me	0.6	0	0.45	2.5783	8.695	0.02	0.44	6.97	7.41	100.0
C17:0Me	0.6	0	0.45	2.7192	9.177	0.01	0.31	7.48	7.79	100.0
C18:0Me	0.6	0	0.45	2.8601	9.659	0.01	0.19	7.99	8.18	100.0
C19:0Me	0.6	0	0.45	3.001	10.238	0.01	0.11	8.50	8.63	100.0
C20:0Me	0.6	0	0.45	3.1419	10.75	0.00	-0.01	9.01	9.04	100.0
C18:1cMe	0.6	0	0.62	2.8171	9.76	0.15	1.17	7.22	8.36	100.0
C18:2cMe	0.64	0	0.73	2.7741	9.83	0.30	1.93	6.65	8.5	99.9
C18:3c9Me	0.75	0	0.83	2.7311	9.93	0.41	2.81	5.99	8.7	99.7

9.1.1.5 Single extraction profiles obtained by extraction time optimization

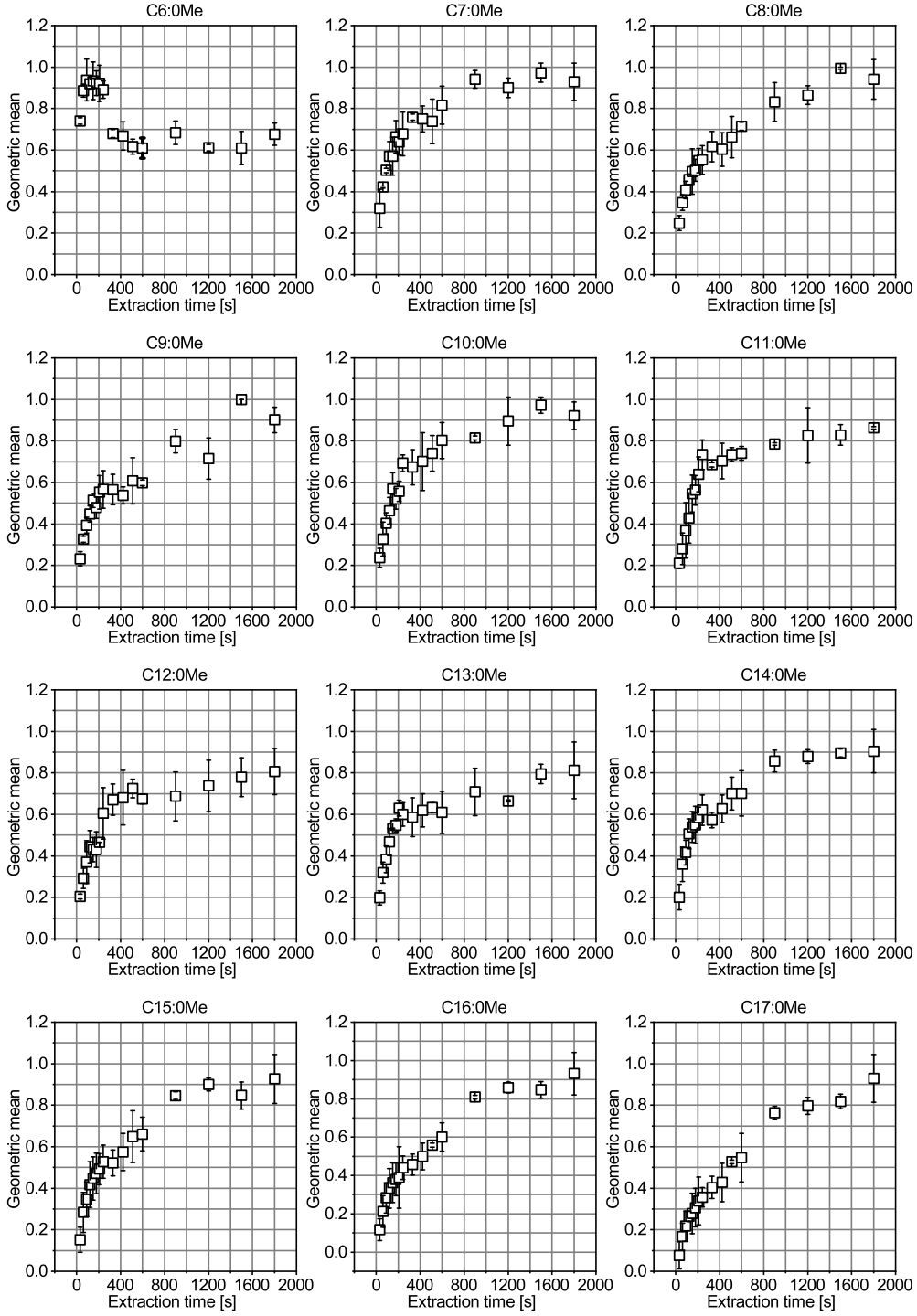

Figure 9.2 Optimization of extraction time for C6:0Me, C7:0Me, C8:0Me, C9:0Me, C10:0Me, C11:0Me, C12:0Me, C13:0Me, C14:0Me, C15:0Me, C16:0Me and C17:0Me. Experimental conditions: n = 3; Sample: FAME mix with varying concentrations 1:400,000 diluted in bidistilled water; Extraction parameters: stirring rate: 1500 rpm; DVB-PDMS, 70 °C, pH 2, varying extraction time: 30, 60, 90, 120, 150, 180, 210, 240, 330, 420, 510, 600, 900, 1200, 1500, 1800 s.

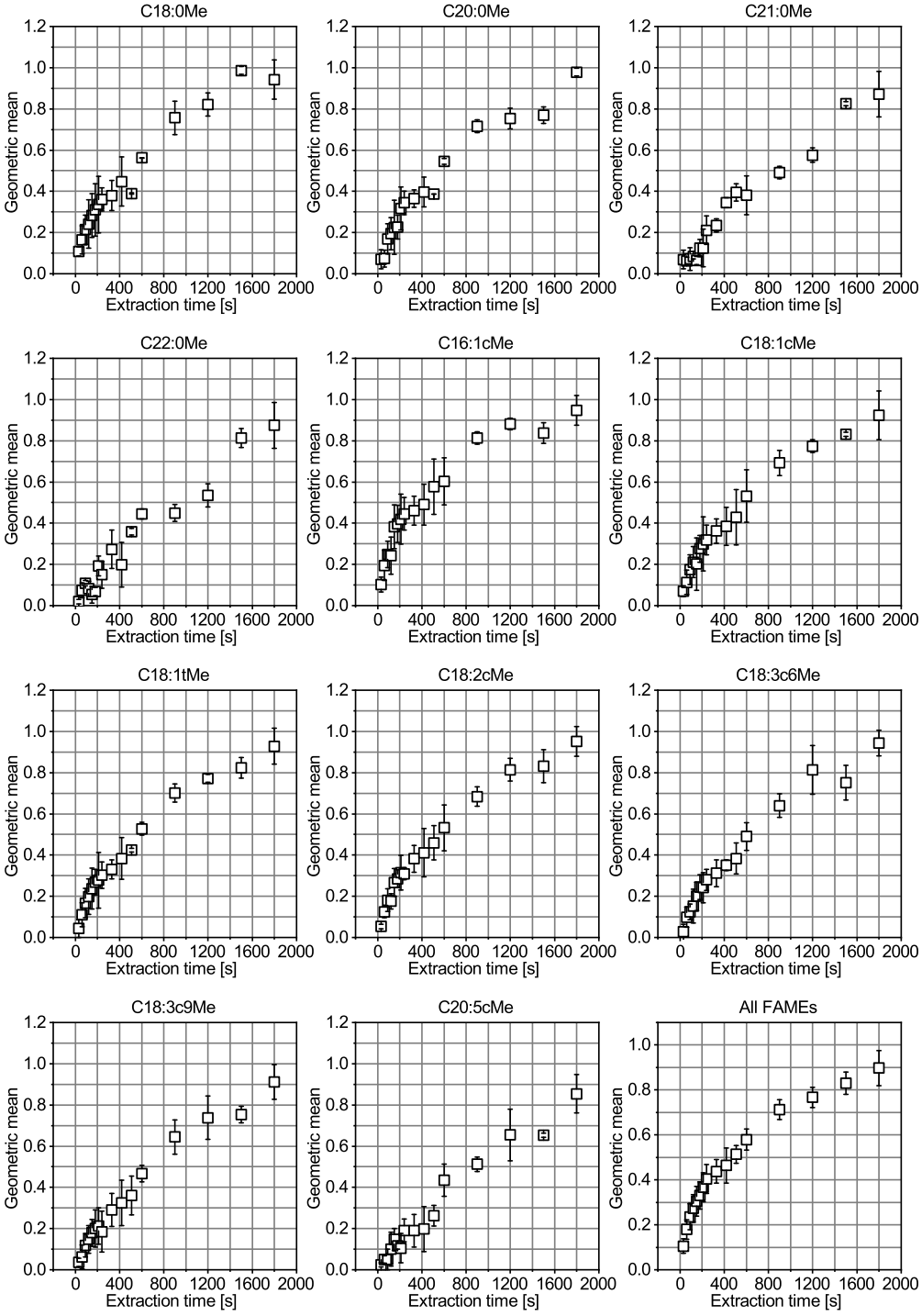

Figure 9.3 Optimization of extraction time for C18:0Me, C20:0Me, C21:0Me, C22:0Me, C16:1cMe, C18:1tMe, C18:1cMe, C18:2cMe, C18:3c6Me, C18:3c9Me, C20:5cMe and for all FAMEs. Experimental conditions: n = 3; Sample: FAME mix with varying concentrations 1:400,000 diluted in bidistilled water; Extraction parameters: stirring rate: 1500 rpm; DVB-PDMS, 70 °C, pH 2, varying extraction time: 30, 60, 90, 120, 150, 180, 210, 240, 330, 420, 510, 600, 900, 1200, 1500, 1800 s.

9.1.1.6 Calculation of hydrolysis half-life

To explain the shape of the curve for the fit of the extraction pH optimization, pH-dependent FAME hydrolysis has to be taken into account. Therefore the hydrolysis rate constant k_h and the hydrolysis half-live $t_{0.5}$, where 50% of FAMEs are hydrolyzed, were calculated. Pseudo-first order rate constants at 25 °C for the acid, neutral, and base-catalyzed hydrolysis of saturated FAMEs were taken from Rayne *et al.* [137].

$$k_h = k_A \cdot [H^+] + k_N + k_B \cdot [OH^-] \quad 11$$

$$t_{0.5} = \frac{\ln\left(\frac{1}{0.5}\right)}{k_h} \quad 12$$

As the pseudo-first-order rate constants were the same for C6:0Me-C18:0Me, they are independent of chain length and here only shown exemplarily for C6:0Me.

9.1.1.7 Observation of droplet formation on SPME arrow surface

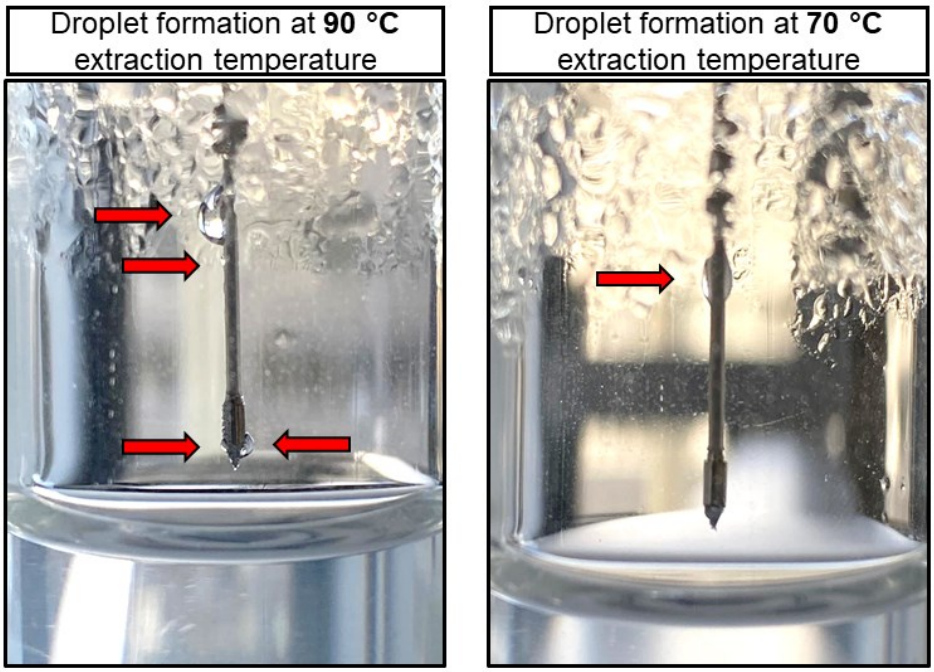

Figure 9.4 Observed increased droplet formation at SPME arrow surface at 90 °C compared to 70 °C extraction temperature. Droplets are indicated by red arrows.

9.1.1.8 Calibration plots and linear regression functions

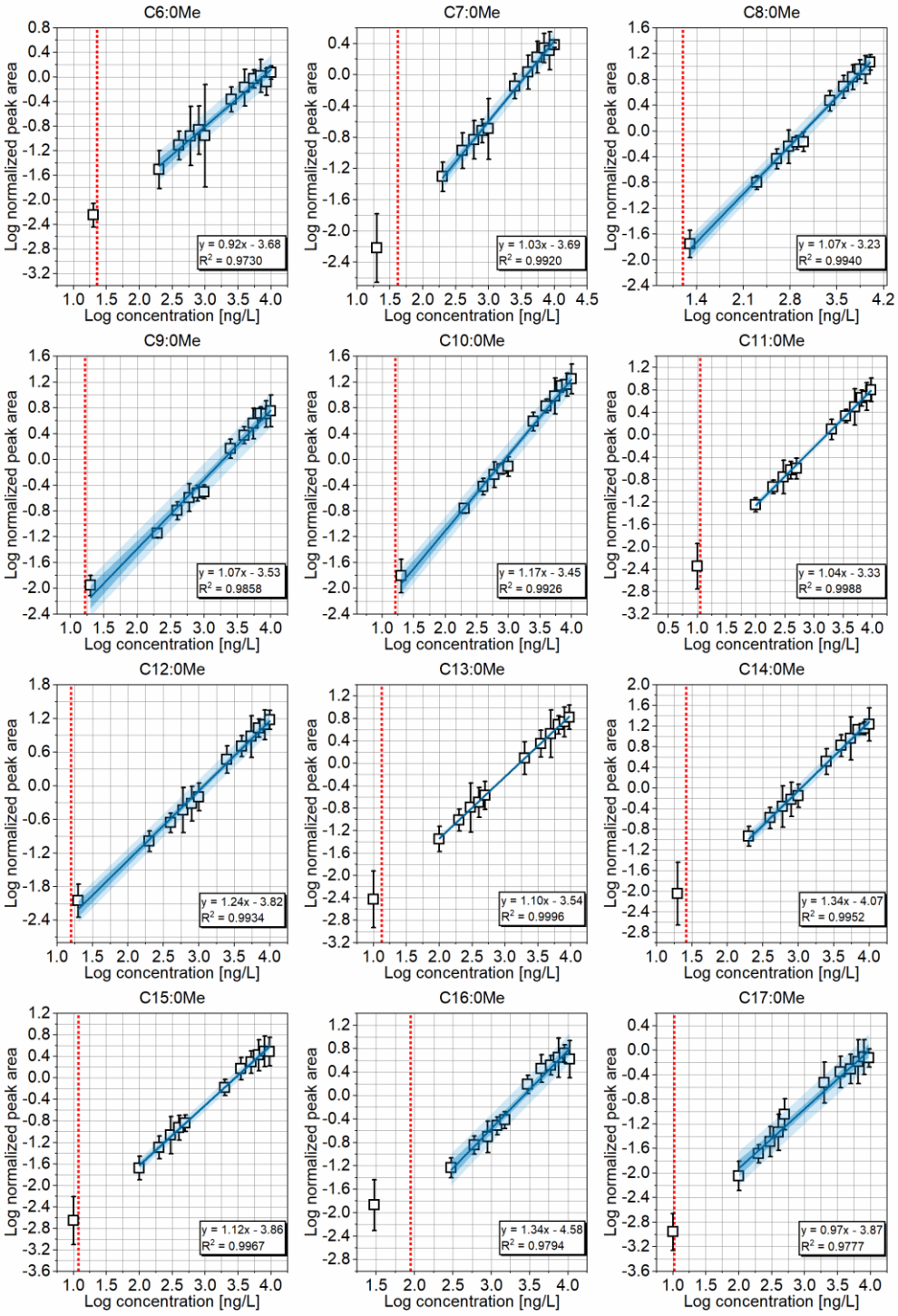

Figure 9.5 Double logarithmic visualized calibration plots for C6:0Me, C7:0Me, C8:0Me, C9:0Me, C10:0Me, C11:0Me, C12:0Me, C13:0Me, C14:0Me, C15:0Me, C16:0Me and C17:0Me. Light blue: 95% prognosis range, dark blue: 95% confidence range, red dotted line: MDL. Peak area was normalized to the internal standard C17:0dMe. Experimental parameters: n = 7; Sample: FAME mix with varying concentrations 1:400,000 diluted in bidistilled water; Extraction parameters: pH 2, DVB-PDMS, 70 °C, stirring rate: 1500 rpm, extraction time: 1200 s.

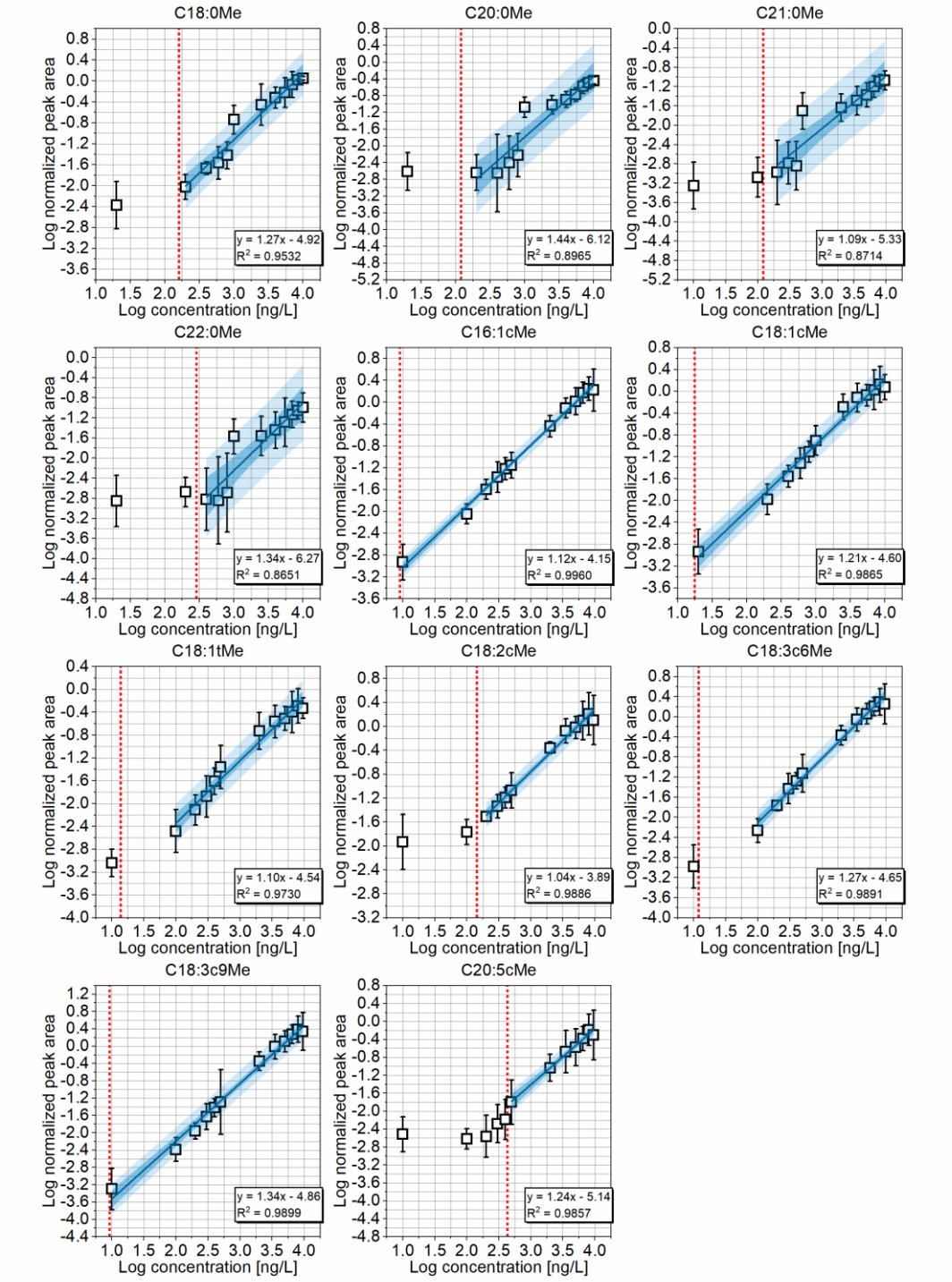

Figure 9.6 Double logarithmic visualized calibration plots for C18:0Me, C20:0Me, C21:0Me, C22:0Me, C16:1cMe, C18:1tMe, C18:1cMe, C18:2cMe, C18:3c6Me, C18:3c9Me, C20:5cMe. Light blue: 95% prognosis range, dark blue: 95% confidence range, red dotted line: MDL. Peak area was normalized to the internal standard C17:0dMe. Experimental parameters: n = 7; Sample: FAME mix with varying concentrations 1:400,000 diluted in bidistilled water; Extraction parameters: pH 2, DVB-PDMS, 70 °C, stirring rate: 1500 rpm, extraction time: 1200 s.

Table 9.4 Linear regression functions with slope m and y-intercept b from both calibrations, 1 and 2, and linearized extraction efficiency plots with correlation coefficient (m_E, b_E, R^2_E).

FAME	m_1	b_1	m_2	b_2	m_E	b_E	R^2_E
C6:0Me	$1.74 \cdot 10^{-4}$	$1.73 \cdot 10^{-3}$	$1.04 \cdot 10^{-4}$	$1.70 \cdot 10^{-1}$	$-1.4 \cdot 10^{-1}$	$2.0 \cdot 10^{-1}$	0.9231
C7:0Me	$2.39 \cdot 10^{-4}$	$3.80 \cdot 10^{-3}$	$2.46 \cdot 10^{-4}$	$1.18 \cdot 10^{-1}$	$-4.3 \cdot 10^{-1}$	$7.1 \cdot 10^{-1}$	0.9912
C8:0Me	$8.72 \cdot 10^{-4}$	$4.59 \cdot 10^{-3}$	$1.17 \cdot 10^{-3}$	$-6.92 \cdot 10^{-3}$	$-8.9 \cdot 10^{-1}$	$8.3 \cdot 10^{-1}$	0.9841
C9:0Me	$3.86 \cdot 10^{-4}$	$3.08 \cdot 10^{-3}$	$6.19 \cdot 10^{-4}$	$-2.65 \cdot 10^{-2}$	$-6.6 \cdot 10^{-1}$	$-9.5 \cdot 10^{-1}$	0.8100
C10:0Me	$9.23 \cdot 10^{-4}$	$-4.71 \cdot 10^{-4}$	$1.88 \cdot 10^{-3}$	$-7.90 \cdot 10^{-1}$	$-7.0 \cdot 10^{-1}$	$-1.52 \cdot 10^{0}$	0.7857
C11:0Me	$5.94 \cdot 10^{-4}$	$-2.09 \cdot 10^{-3}$	$6.60 \cdot 10^{-4}$	$-9.59 \cdot 10^{-2}$	$-6.4 \cdot 10^{-1}$	$-1.72 \cdot 10^{0}$	0.7581
C12:0Me	$6.15 \cdot 10^{-4}$	$-1.33 \cdot 10^{-2}$	$1.60 \cdot 10^{-3}$	$-1.05 \cdot 10^{0}$	$-6.3 \cdot 10^{-1}$	$-1.57 \cdot 10^{0}$	0.7920
C13:0Me	$5.24 \cdot 10^{-4}$	$-3.85 \cdot 10^{-3}$	$7.19 \cdot 10^{-4}$	$-1.49 \cdot 10^{-1}$	$-6.5 \cdot 10^{-1}$	$-1.38 \cdot 10^{0}$	0.8175
C14:0Me	$7.71 \cdot 10^{-4}$	$-2.60 \cdot 10^{-2}$	$1.86 \cdot 10^{-3}$	$-9.89 \cdot 10^{-1}$	$-6.4 \cdot 10^{-1}$	$-8.2 \cdot 10^{-1}$	0.8914
C15:0Me	$3.03 \cdot 10^{-4}$	$-5.63 \cdot 10^{-3}$	$3.56 \cdot 10^{-4}$	$9.75 \cdot 10^{-2}$	$-5.7 \cdot 10^{-1}$	$-3.2 \cdot 10^{-1}$	0.9274
C16:0Me	$2.45 \cdot 10^{-4}$	$-5.26 \cdot 10^{-3}$	$4.79 \cdot 10^{-4}$	$2.49 \cdot 10^{-1}$	$-4.3 \cdot 10^{-1}$	$-2.9 \cdot 10^{-1}$	0.9941
C17:0dMe	-	-	-	-	$-6.9 \cdot 10^{-1}$	$2.6 \cdot 10^{-1}$	0.9393
C17:0Me	$1.17 \cdot 10^{-4}$	$-1.63 \cdot 10^{-3}$	$7.48 \cdot 10^{-5}$	$1.27 \cdot 10^{-1}$	$-4.5 \cdot 10^{-1}$	$-2.7 \cdot 10^{-1}$	0.9464
C18:0Me	$4.36 \cdot 10^{-5}$	$2.48 \cdot 10^{-3}$	$1.09 \cdot 10^{-4}$	$6.08 \cdot 10^{-2}$	$-2.3 \cdot 10^{-1}$	$-5.0 \cdot 10^{-1}$	0.9964
C20:0Me	$4.51 \cdot 10^{-6}$	$1.57 \cdot 10^{-3}$	$3.40 \cdot 10^{-5}$	$3.30 \cdot 10^{-2}$	$-1.2 \cdot 10^{-1}$	$-3.4 \cdot 10^{-1}$	0.8054
C21:0Me	$2.63 \cdot 10^{-6}$	$5.79 \cdot 10^{-4}$	$8.10 \cdot 10^{-6}$	$8.97 \cdot 10^{-3}$	$-2.5 \cdot 10^{-1}$	$-1.8 \cdot 10^{-1}$	0.8570
C22:0Me	$3.18 \cdot 10^{-7}$	$1.58 \cdot 10^{-3}$	$9.11 \cdot 10^{-6}$	$7.94 \cdot 10^{-3}$	$-3.0 \cdot 10^{-1}$	$-5.0 \cdot 10^{-1}$	0.8199
C16:1cMe	$1.56 \cdot 10^{-4}$	$-3.78 \cdot 10^{-3}$	$1.98 \cdot 10^{-4}$	$3.66 \cdot 10^{-2}$	$-6.9 \cdot 10^{-1}$	$-3.3 \cdot 10^{-1}$	0.9393
C18:1tMe	$5.86 \cdot 10^{-5}$	$-1.88 \cdot 10^{-3}$	$4.89 \cdot 10^{-5}$	$6.92 \cdot 10^{-2}$	$-4.5 \cdot 10^{-1}$	-0.29	0.9464
C18:1cMe	$9.84 \cdot 10^{-5}$	$-6.62 \cdot 10^{-3}$	$1.22 \cdot 10^{-4}$	$1.63 \cdot 10^{-1}$	$-2.3 \cdot 10^{-1}$	0.26	0.9964
C18:2cMe	$1.38 \cdot 10^{-4}$	$6.20 \cdot 10^{-3}$	$1.51 \cdot 10^{-4}$	$1.68 \cdot 10^{-1}$	$-1.2 \cdot 10^{-1}$	-0.27	0.8409
C18:3c6Me	$1.39 \cdot 10^{-4}$	$-5.38 \cdot 10^{-3}$	$2.15 \cdot 10^{-4}$	$5.88 \cdot 10^{-2}$	$-2.5 \cdot 10^{-1}$	0.36	0.9939
C18:3c9Me	$9.68 \cdot 10^{-5}$	$-4.11 \cdot 10^{-3}$	$2.69 \cdot 10^{-4}$	$-1.68 \cdot 10^{-2}$	$-3.0 \cdot 10^{-1}$	0.45	0.9939
C20:5cMe	$1.01 \cdot 10^{-5}$	$1.96 \cdot 10^{-3}$	$6.57 \cdot 10^{-5}$	$-2.21 \cdot 10^{-2}$	$-5.4 \cdot 10^{-1}$	0.33	0.9887

9.1.1.9 Depletion curves obtained by extraction efficiency experiments

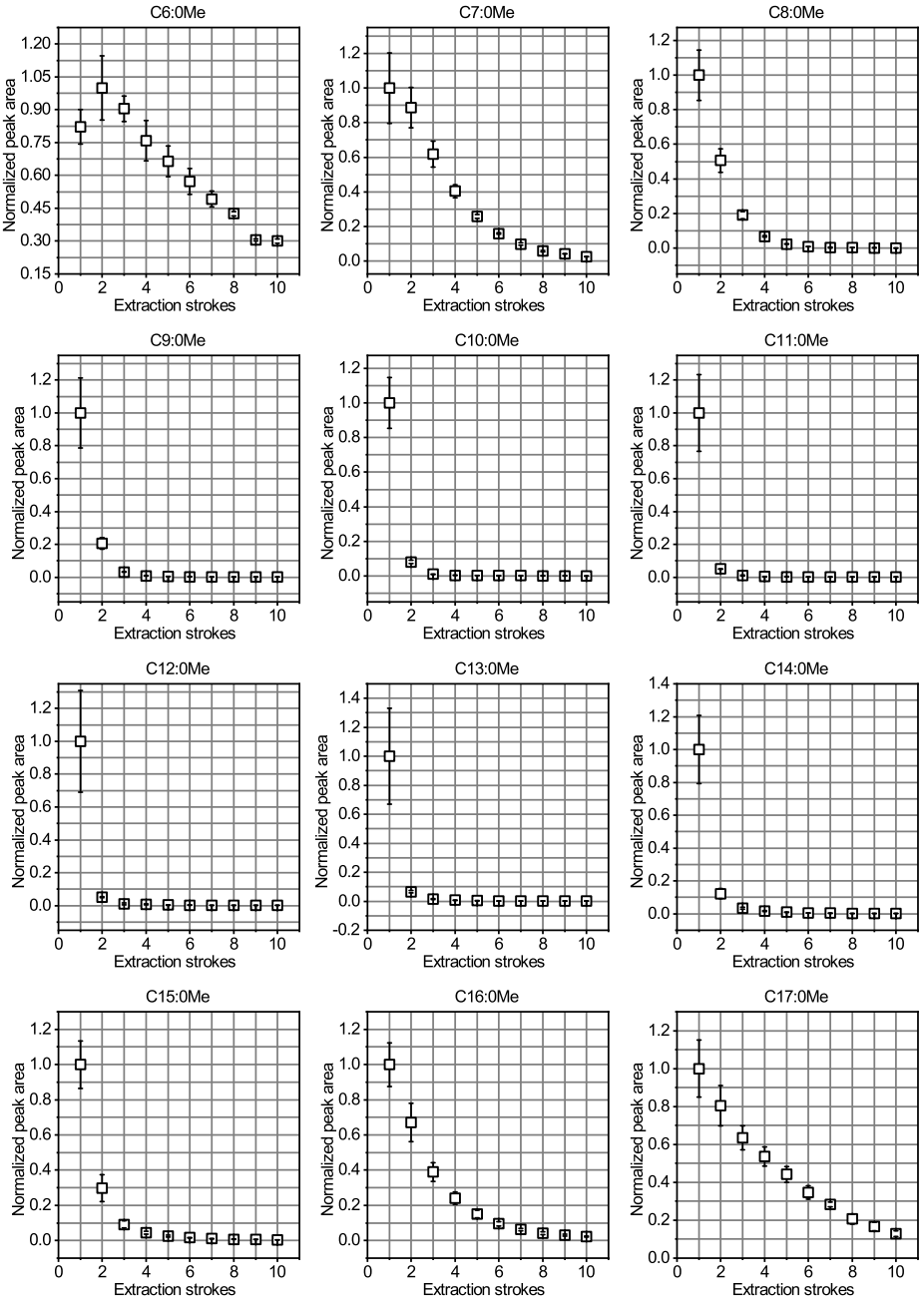

Figure 9.7 Depletion curve method plots for determination of extraction efficiency for C6:0Me, C7:0Me, C8:0Me, C9:0Me, C10:0Me, C11:0Me, C12:0Me, C13:0Me, C14:0Me, C15:0Me, C16:0Me and C17:0Me. Peak area was normalized to the highest value. Experimental parameters: n = 7; Sample: FAME mix with varying concentrations 1:400,000 diluted in bidistilled water; Extraction parameters: pH 2, DVB-PDMS, 70 °C, stirring rate: 1500 rpm, extraction time: 1200 s, 10 extraction strokes.

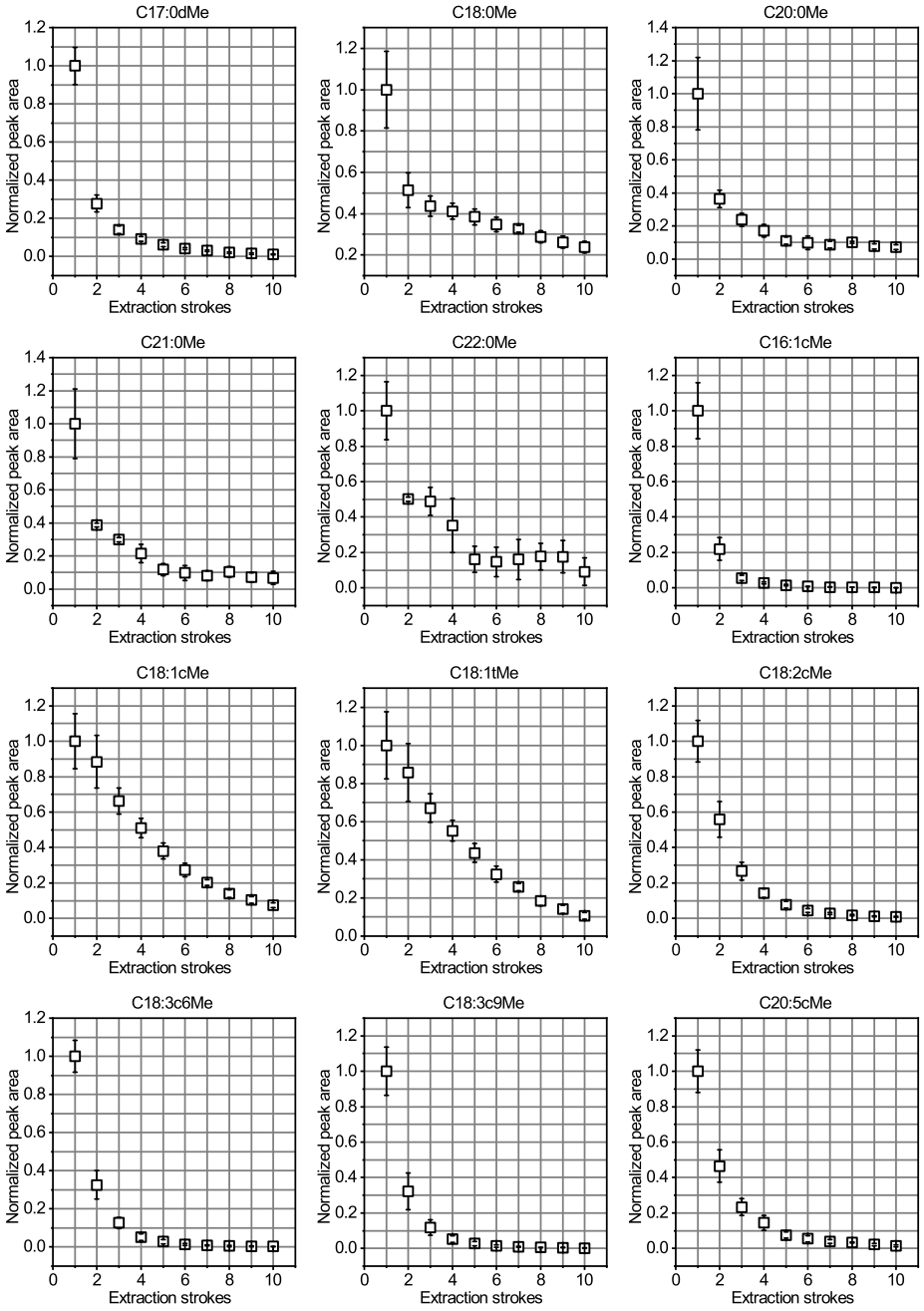

Figure 9.8 Depletion curve method plots for determination of extraction efficiency for C18:0Me, C20:0Me, C21:0Me, C22:0Me, C16:1cMe, C18:1tMe, C18:1cMe, C18:2cMe, C18:3c6Me, C18:3c9Me, C20:5cMe. Peak area was normalized to the highest value. Experimental parameters: n = 7; Sample: FAME mix with varying concentrations 1:400,000 diluted in bidistilled water; Extraction parameters: pH 2, DVB-PDMS, 70 °C, stirring rate: 1500 rpm, extraction time: 1200 s, 10 extraction strokes.

9.1.2 Supporting material for Chapter 5

9.1.2.1 MRM method

Table 9.5 MRM transitions from precursor to product ions with optimized collision energy and ion ratios for the determination of FAMEs and FAs. Time frame: chosen time frame for the given transitions; Abbr.: Abbreviation; *Quantifier ions; CE: Collision energy. For experimental conditions see the respective sections.

Time frame [min]	FAME/d_3-FAME	Abbr.	CAS No.	Retention time [min]	MRM Transitions Precursor ions > Product ions [*m/z*]	Optim. CE [eV]
5.00-8.25	Methyl hexanoate	C6:0Me	106-70-7	7.47	74>43* 87>55 101>59	5 10 5
	Methyl hexanoate-d_3	C6:0Me-d_3	-	7.43	77>44 90>55* 104>77	10 10 15
8.25-11.20	Methyl heptanoate	C7:0Me	106-73-0	9.82	74>43* 87>55 101>73	5 10 10
	Methyl heptanoate-d_3	C7:0Me-d_3	-	9.76	77>44* 90>55 104>77	10 10 15
11.20-12.70	Methyl octanoate	C8:0Me	111-11-5	11.94	74>43* 87>55 143>83	5 10 10
	Methyl octanoate-d_3	C8:0Me-d_3	-	11.91	77>44* 90>55 104>76	10 10 10
12.70-14.40	Methyl nonanoate	C9:0Me	1731-84-6	13.87	74>43* 87>55 143>101	5 10 5
	Methyl nonanoate-d_3	C9:0Me-d_3	-	13.84	77>44* 90>55 146>104	10 10 10
14.40-16.30	Methyl decanoate	C10:0Me	110-42-9	15.70	74>43 87>55* 143>83	5 10 10
	Methyl decanoate-d_3	C10:0Me-d_3	-	15.66	77>44 90>55* 146>83	10 10 10
16.30-18.00	Methyl undecanoate	C11:0Me	1731-86-8	17.35	74>43* 87>55 143>83	5 10 10
	Methyl undecanoate-d_3	C11:0Me-d_3	-	17.32	77>44* 90>55 146>83	10 10 10
18.00-19.30	Methyl dodecanoate	C12:0Me	111-82-0	18.91	74>43* 87>55 143>83	10 10 10
	Methyl dodecanoate-d_3	C12:0Me-d_3	-	18.88	77>44* 90>55 146>83	10 10 10
19.30-20.80	Methyl tridecanoate	C13:0Me	1731-88-0	20.39	74>43* 87>55 143>83	10 10 10

Time frame [min]	FAME/d_3-FAME	Abbr.	CAS No.	Retention time [min]	MRM Transitions Precursor ions > Product ions [*m/z*]	Optim. CE [eV]
	Methyl tridecanoate-d_3	C13:0Me-d_3	-	20.36	77>44* 90>55 146>104	10 10 10
20.80-22.20	Methyl tetradecanoate	C14:0Me	124-10-7	21.79	74>43* 87>55 143>83	10 10 10
	Methyl tetradecanoate-d_3	C14:0Me-d_3	-	21.77	77>44* 90>55 146>104	10 10 10
22.20-23.50	Methyl pentadecanoate	C15:0Me	7132-64-1	23.13	74>43* 87>55 143>83	10 10 10
	Methyl pentadecanoate-d_3	C15:0Me-d_3	-	23.10	77>44* 90>55 146>83	10 10 10
23.50-24.20	d_{31}-Isotope-labelled methyl hexadecanoate-d_3	d_{31}-C16:0Me-d_3		24.01	80>46* 159>110 304>110	10 10 15
24.20-24.70	Methyl hexadecanoate	C16:0Me	112-39-0	24.42	74>43* 87>55 143>83	10 10 10
	Methyl hexadecanoate-d_3	C16:0Me-d_3	-	24.39	77>44* 90>55 146>83	10 10 10
25.00-25.50	d_{33}-isotope-labeled methyl heptadecanoate	d_{33}-C17:0Me	1219804-81-5	25.33	317>107* 159>94 188>107	25 10 5
25.50-26.00	Methyl heptadecanoate	C17:0Me	1731-92-6	25.65	74>43* 87>55 143>83	10 10 10
	Methyl heptadecanoate-d_3	C17:0Me-d_3	-	25.63	77>44 90>55* 146>83	10 10 10
26.00-26.95	Methyl octadecanoate	C18:0Me	112-61-8	26.82	74>43* 87>55 143>55	10 10 15
	Methyl octadecanoate-d_3	C18:0Me-d_3	-	26.80	77>44* 90>55 146>83	10 10 10
28.90-29.50	Methyl eicosanoate	C20:0Me	1120-28-1	29.05	74>43* 87>55 143>55	10 10 15
	Methyl eicosanoate-d_3	C20:0Me-d_3	-	29.03	77>44* 90>55 146>104	10 10 10
29.50-30.50	Methyl heneicosanoate	C21:0Me	6064-90-0	30.12	74>43* 87>55 143>55	10 10 15
	Methyl heneicosanoate-d_3	C21:0Me-d_3	-	30.09	77>44* 90>55 146>104	10 10 10
30.50-31.30	Methyl docosanoate	C22:0Me	929-77-1	31.14	74>43* 87>55 143>55	10 10 15
	Methyl docosanoate-d_3	C22:0Me-d_3	-	31.12	77>44* 90>55	10 10

Time frame [min]	FAME/d_3-FAME	Abbr.	CAS No.	Retention time [min]	MRM Transitions Precursor ions > Product ions [*m/z*]	Optim. CE [eV]
					146>104	10
24.70-25.00	Methyl cis-9-hexadecenoate	C16:1cMe	1120-25-8	24.90	74>43* 101>59 115>55	10 5 10
	Methyl cis-9-hexadecenoate-d_3	C16:1cMe-d_3	-	24.88	77>44* 104>77 118>91	10 10 15
26.95-27.30	Methyl trans-9-octadecenoate	C18:1tMe	112-62-9	27.05	74>43* 87>55 101>59	10 10 5
	Methyl trans-9-octadecenoate-d_3	C18:1tMe-d_3	-	27.02	77>44 90>55* 118>91	15 10 15
26.95-27.30	Methyl cis-9-octadecenoate	C18:1cMe	2777-58-4	27.16	74>43* 87>55 101>59	10 10 5
	Methyl cis-9-octadecenoate-d_3	C18:1cMe-d_3	-	27.13	77>44 90>55* 118>91	20 10 15
27.30-28.00	Methyl cis,cis-9,12-octadecadienoate	C18:2cMe	112-63-0	27.87	74>43 87>55* 115>55	15 10 10
	Methyl cis,cis-9,12-octadecadienoate-d_3	C18:2cMe-d_3	-	27.85	77>44 90>55* 118>91	20 10 15
28.00-28.60	Methyl cis,cis,cis-6,9,12-octadecatrienoate	C18:3c6Me	16326-32-2	28.39	74>45* 115>55 157>130	15 10 10
	Methyl cis,cis,cis-6,9,12-octadecatrienoate-d_3	C18:3c6Me-d_3	-	28.37	77>44 104>77* 133>91	20 10 15
28.60-28.90	Methyl cis,cis,cis Methyl cis,cis,cis-9,12,15-octadecatrienoate	C18:3c9Me	301-00-8	28.76	74>45 101>59 115>59*	15 10 10
	Methyl cis,cis,cis Methyl cis,cis,cis-9,12,15-octadecatrienoate-d_3	C18:3c9Me-d_3	-	28.74	77>44 104>77* 133>91	20 10 15
31.30-31.80	Methyl cis,cis,cis,cis,cis-5,8,11,14,17-eicosapentaenoate	C20:5cMe	2734-47-6	31.61	74>45* 115>71 157>130	10 10 10
	Methyl cis,cis,cis,cis,cis-5,8,11,14,17-eicosapentaenoate-d_3	C20:5cMe-d_3	-	31.59	77>44 104>77* 159>88	10 15 10

9.1.2.2 Automation procedure

Table 9.6 List of the modules, tools, and suppliers used for the automation procedure.

Module/Unit/Tool	Supplier
Agitator	CTC Analytics
DeCapper	CTC Analytics
Fiber conditioning station	CTC Analytics
Heating and stirring plate with self-made heating block	IKA, Staufen, Germany
Wash station	CTC Analytics
Liquid tool 10 µL syringe	CTC Analytics
Liquid tool 100 µL syringe	CTC Analytics
Liquid tool 1000 µL syringe	CTC Analytics
SPME arrow tool	CTC Analytics

Table 9.7 Automation protocol displaying the different tasks, description of the tasks, and the involved objects of the task. Chronos (version 5.1.20, Axel Semrau, Sprockhoevel, Germany) was used as automation Software. FA-Mix: Fatty acid mix; FAME-Mix: 37-component FAME mix with varying concentration; M-FAME-Mix: FAME mix with missing components.

Number	Task	Description	Involved objects
1	ExecuteActivity	Set temperature of agitator	Agitator
2	DecapObject_PAL3	Remove cap from sample	DeCapper
3	Transfer	Transfer internal standard 10 µL to sample	Liquid tool 10 µL syringe
4	CleanSyringe	Cleaning syringe after IS transfer	Liquid tool 10 µL syringe; Wash station
5	Transfer	Transfer FA-Mix defined volume 1 to sample	Liquid tool 10 µL syringe or Liquid tool 100 µL syringe
6	CleanSyringe	Cleaning syringe after FA-Mix transfer	Liquid tool 10 µL syringe or Liquid tool 100 µL syringe; Wash station
7	Transfer	Transfer FAME-Mix defined volume 1 to sample	Liquid tool 10 µL syringe
8	Transfer	Transfer FAME-Mix defined volume 2 to sample	
9	CleanSyringe	Cleaning syringe after FAME-Mix transfer	Liquid tool 10 µL syringe; Wash station
10	Transfer	Transfer M-FAME-Mix defined volume 1 to sample	Liquid tool 10 µL syringe
11	Transfer	Transfer M-FAME-Mix defined volume 2 to sample	
12	CleanSyringe	Cleaning syringe after FAME-Mix transfer	Liquid tool 10 µL syringe, Wash station
13	Transfer	Transfer derivatization agent (CD_3OD) to sample	Liquid tool 1000 µL syringe
14	Transfer	Transfer H_2SO_4 (diluted in H2O) 28 µL to sample	Liquid tool 100 µL syringe
15	CapObject_PAL3	Put cap back on sample	DeCapper

Number	Task	Description	Involved objects
16	Transport	Put sample in agitator for derivatization time	Agitator
17	Wait	Wait for sample derivatization	
18	Transport	Put wash vial with MeOH in heating block	Stirring and heating plate
19	Transport	Put sample in heating block	Stirring and heating plate
20	WaitOverlapped	Wait for sample equilibrium	Agitator
21	FiberExposure	Move to MeOH vial and expose fiber in HS	SPME arrow tool; Stirring and heating plate
22	Wait	Chemical Fiber Cleaning	SPME arrow tool; Stirring and heating plate
23	FiberAspiration	Draw in fiber	SPME arrow tool
24	Transport	Put wash vial back to initial position	Stirring and heating plate
25	FiberExposure	Move to Conditioning Station and expose fiber	SPME arrow tool; Fiber conditioning station
26	Wait	Thermal fiber cleaning	
27	FiberAspiration	Draw in fiber	
28	FiberExposure	Start sample extraction	SPME arrow tool, Stirring and heating plate
29	Wait	Enrichment	
30	FiberAspiration	Draw in fiber	
31	WaitForStartSignal	Check GC Readiness before enrichment end	-
32	FiberExposure	Move to injector and expose fiber	SPME arrow tool, GC injector
33	Wait	Desorption in injector	
34	FiberAspiration	Draw in fiber	
35	Transport	Put sample 1 back to initial position	-
36	MoveToHome	Stay at this position till next job	-
37	WaitOverlapped	GC run time	-

9.1.2.3 Retention time prediction of deuterated molecules

Table 9.8 Calculation of predicted retention time of d_3-FAMEs using the averaged retention time shift per deuterium atom and the retention time of the non-deuterated FAME. Conformity states the accordance of the predicted and actual retention time for the d_3-FAMEs. Rt: Retention time; D: deuterium.

d_3-FAME/FAME	Rt d_3-FAME [min]	Rt FAME [min]	Rt shift per D atom [min]	Pred. Rt d_3-FAME [min]	Conformity [%]
C6:0Me-d_3/C6:0Me	7.43	7.47	0.014	7.44	99.82
d-C7:0Me-d_3/C7:0Me	9.76	9.82	0.020	9.79	99.68
d-C8:0Me-d_3/C8:0Me	11.91	11.94	0.010	11.91	99.98
d-C9:0Me-d_3/C9:0Me	13.84	13.87	0.009	13.84	100.00
d-C10:0Me-d_3/C10:0Me	15.66	15.70	0.010	15.67	99.98
d-C11:0Me-d_3/C11:0Me	17.32	17.35	0.010	17.32	99.99
d-C12:0Me-d_3/C12:0Me	18.88	18.91	0.009	18.88	100.01
d-C13:0Me-d_3/C13:0Me	20.36	20.39	0.010	20.36	99.99
d-C14:0Me-d_3/C14:0Me	21.77	21.79	0.008	21.76	100.01
d-C15:0Me-d_3/C15:0Me	23.10	23.13	0.009	23.10	100.00
d-C16:0Me-d_3/C16:0Me	24.39	24.42	0.010	24.39	99.99

d_3-FAME/FAME	Rt d_3-FAME [min]	Rt FAME [min]	Rt shift per D atom [min]	Pred. Rt d_3-FAME [min]	Conformity [%]
d-C16:1-c9Me-d_3/C16:1-c9Me	24.88	24.90	0.008	24.87	100.02
d-C17:0Me-d_3/C17:0Me	25.63	25.65	0.008	25.62	100.01
d-C18:0Me-d_3/C18:0Me	26.80	26.82	0.008	26.80	100.01
d-C18:1-t9Me-d_3/C18:1-t9Me	27.02	27.05	0.009	27.02	100.00
d-C18:1-c9Me-d_3/C18:1-c9Me	27.13	27.16	0.009	27.13	100.01
d-C18:2-c9-c12Me-d_3/C18:2-c9-12Me	27.85	27.87	0.008	27.84	100.01
d-C18:3-c6-9-12Me-d_3/C18:3-c6-9-12Me	28.37	28.39	0.007	28.36	100.02
d-C18:3-c9-12-15Me-d_3/C18:3-c9-12-15Me	28.74	28.76	0.007	28.73	100.03
d-C20:0Me-d_3/C20:0Me	29.03	29.05	0.007	29.03	100.02
d-C21:0Me-d_3/C21:0Me	30.09	30.12	0.009	30.09	100.00
d-C22:0Me-d_3/C22:0Me	31.12	31.14	0.007	31.11	100.02
d-C20:5-c-5-8-11-15-17Me-d_3/C20:5-c5-8-11-15-17Me	31.59	31.61	0.006	31.58	100.03
Mean	-	-	0.009	-	99.98

9.1.2.4 Mass spectral fragmentation patterns

Table 9.9 General mass spectral fragmentation patterns for identification of FAMEs adapted from Härtig et al. [134]. Precursors and product ions were selected based on known fragmentations. M: Molecular ion.

Fragments [m/z]	Identification	Derivate equivalent
43/57/71/85	Alkyl series	-
41/55/69/83	Alkenyl series	-
59	Methoxy carbonyl	62
74	McLafferty rearrangement ion	77
75	Dimethoxy methyl radical ion	
87	C3:0 Methyl ester	90
90	Cleavage at OH, H-rearrangement	
103	Cleavage at OH	
143	C7:0 methyl ester	146
199	Cleavage at C10 methyl branching site	-
M-15	Loss of methyl	-
M-18	Loss of water	-
M-29	Loss of ethyl	-
M-31	Loss of methoxy	M-34
M-32	Loss of methanol	M-35
M-43	Loss of propyl	-
M-46	Loss of ethyl + water	-
M-59	Loss of methoxy carbonyl	M-62
M-74	Loss of McLafferty fragement	M-77

9.1.2.4 Equations of DOE models

$$Y_{linear} = \beta_0 + \beta_1 p + \beta_2 t + \beta_3 T + \beta_4 d$$

$$Y_{linear+interactions} = \beta_0 + \beta_1 p + \beta_2 t + \beta_3 T + \beta_4 d + \beta_{12} pt + \beta_{13} pT + \beta_{14} pd + \beta_{23} tT + \beta_{24} Td + \beta_{34} Td$$

$$Y_{linear+squares} = \beta_0 + \beta_1 p + \beta_2 t + \beta_3 T + \beta_4 d + \beta_{11} p^2 + \beta_{22} t^2 + \beta_{33} T^2 + \beta_{44} d^2$$

$$Y_{full\ quadratic} = \beta_0 + \beta_1 p + \beta_2 t + \beta_3 T + \beta_4 d + \beta_{11} p^2 + \beta_{12} pt + \beta_{13} pT + \beta_{14} pd + \beta_{22} t^2 + \beta_{23} tT + \beta_{24} Td + \beta_{33} T^2 + \beta_{34} Td + \beta_{44} d^2$$

9.1.2.5 Optimal parameters and parameter dependencies obtained with DOE

Table 9.10 p-values of single and quadratic terms obtained by the full quadratic fit of the Box-Behnken model (DOE) of derivatization parameter optimization. Significant terms (<0.05) are displayed in green.

	p-values of single terms and quadratic terms												
FA	**pH**	**T**	**t**	**CD_3OD**	**pH*pH**	**t*t**	**CD_3OD *CD_3OD**	**pH*T**	**pH*t**	**pH*CD_3OD**	**T*t**	**T* CD_3OD**	**t*CD_3OD**
C6:0Me-d3	0.0191	0.8834	0.9718	0.1701	0.1593	0.8968	0.8301	0.2453	0.2100	0.0476	0.3531	1.0000	0.7681
C7:0Me-d3	0.0182	0.8120	0.2417	0.2706	0.0865	0.5528	0.9270	0.4999	0.0262	0.1178	0.8903	1.0000	0.7353
C8:0Me-d3	0.0213	0.8748	0.7028	0.1481	0.2556	0.6877	0.8926	0.1751	0.2194	0.0649	0.2924	0.8994	0.4680
C9:0Me-d3	0.0363	0.9603	0.4943	0.1788	0.3893	0.5763	0.9473	0.1510	0.3124	0.1359	0.2211	0.9863	0.4174
C10:0Me-d3	0.0517	0.8446	0.3808	0.2262	0.4846	0.5335	0.9650	0.1260	0.3692	0.1894	0.2311	0.9178	0.4212
C11:0Me-d3	0.0723	0.6114	0.2174	0.2662	0.5904	0.4729	0.9303	0.1002	0.4528	0.2573	0.3514	0.8434	0.3689
C12:0Me-d3	0.2571	0.0695	0.0085	0.4057	0.9792	0.0692	0.4502	0.2320	0.2492	0.2553	0.4602	0.5163	0.4335
C13:0Me-d3	0.4324	0.0063	0.0014	0.8689	0.5581	0.0210	0.2402	0.3659	0.1587	0.4385	0.0048	0.3731	0.9538
C14:0Me-d3	0.5601	0.0294	0.0048	0.4305	0.7721	0.0380	0.2390	0.3315	0.1762	0.4421	0.0095	0.7378	0.6312
C15:0Me-d3	0.4886	0.2651	0.0559	0.2454	0.6297	0.1138	0.3094	0.7004	0.2743	0.3491	0.1500	0.8844	0.4293
C16:0Me-d3	0.1622	0.7647	0.3637	0.4205	0.3550	0.2448	0.3519	0.9567	0.5500	0.3876	0.5490	0.9788	0.5500
C17:0Me-d3	0.0326	0.9276	0.7656	0.9478	0.1368	0.4237	0.8202	0.8631	0.1582	0.1364	0.8934	0.9855	0.6645
C18:0Me-d3	0.0212	0.9312	0.3556	0.3012	0.0945	0.8750	0.8183	0.7954	0.0705	0.0558	0.9888	0.9577	0.9380
C20:0Me-d3	0.0254	0.8924	0.3111	0.1955	0.1097	0.9945	0.8190	0.7932	0.0721	0.0476	0.9186	0.9725	0.9407
C21:0Me-d3	0.0332	0.9101	0.3393	0.2287	0.1627	0.8388	0.9109	0.7376	0.0688	0.0647	0.7525	0.9604	0.9418
C22:0Me-d3	0.0248	0.8353	0.2765	0.2357	0.1619	0.9421	0.9125	0.8218	0.0696	0.0550	0.7755	0.8992	0.9890
C16:1cMe-d3	0.4893	0.1608	0.0225	0.1951	0.9686	0.0518	0.3623	0.6275	0.1703	0.2379	0.0637	0.9716	0.3412
C18:1tMe-d3	0.0410	0.9134	0.5804	0.9547	0.1727	0.3709	0.9045	0.8086	0.0921	0.2098	0.9849	0.9776	0.6376
C18:1cMe-d3	0.0642	0.8798	0.9343	0.6670	0.2509	0.2953	0.8323	0.8551	0.1889	0.2961	0.9310	0.9374	0.4974
C18:2cMe-d3	0.2079	0.4018	0.1144	0.3807	0.5538	0.1430	0.3371	0.9000	0.7039	0.3926	0.3273	0.9075	0.4595
C18:3c6Me-d3	0.7151	0.1638	0.0768	0.6392	0.6493	0.0718	0.0554	0.9095	0.7068	0.5518	0.2897	0.8324	0.5899
C18:3c9Me-d3	0.4225	0.0151	0.0016	0.6811	0.5688	0.0147	0.1181	0.5147	0.4982	0.3107	0.0111	0.9818	0.6732
C20:5cMe-d3	0.0274	0.5512	0.9150	0.4183	0.5735	0.3005	0.9857	0.2934	0.1193	0.2628	0.0591	0.3936	0.7981
Total number significant terms	11	3	5	0	0	3	0	0	1	2	3	0	0
Percentage of significant terms [%]	48	13	22	0	0	13	0	0	4	9	13	0	0

Table 9.11 Optimal derivatization parameters for single FAs obtained with Box-Behnken model (DOE) and full quadratic fit. The parameters were averaged to determine the overall optimal parameters. pH values were averaged by the molar H^+ concentration.

FA	pH (H^+ conc. [M])	T [°C]	t [min]	CD_3OD [v/v%]
C6:0Me-d3	2.0 (10^{-2})	40.3	1.0	5.0
C7:0Me-d3	2.0 (10^{-2})	40.3	1.0	5.0
C8:0Me-d3	2.0 (10^{-2})	40.3	1.0	5.0
C9:0Me-d3	2.0 (10^{-2})	40.3	1.0	5.0
C10:0Me-d3	2.0 (10^{-2})	40.0	1.0	3.0
C11:0Me-d3	2.0 (10^{-2})	40.0	1.0	5.0
C12:0Me-d3	2.0 (10^{-2})	40.0	60.0	5.0
C13:0Me-d3	4.0 (10^{-4})	40.0	60.0	3.0
C14:0Me-d3	4.0 (10^{-4})	40.0	60.0	3.0
C15:0Me-d3	4.0 (10^{-4})	40.0	60.0	1.0
C16:0Me-d3	2.0 (10^{-4})	69.1	1.0	3.9
C17:0Me-d3	2.0 (10^{-2})	63.7	1.0	5.0
C18:0Me-d3	2.0 (10^{-2})	63.7	1.0	5.0
C20:0Me-d3	2.0 (10^{-2})	65.0	1.0	5.0
C21:0Me-d3	2.0 (10^{-2})	65.0	1.0	5.0
C22:0Me-d3	2.0 (10^{-2})	65.0	1.0	5.0
C16:1cMe-d3	2.0 (10^{-2})	40.0	60.0	1.0
C18:1tMe-d3	2.0 (10^{-2})	62.4	1.0	5.0
C18:1cMe-d3	2.0 (10^{-2})	62.4	1.0	5.0
C18:2cMe-d3	2.0 (10^{-2})	50.8	60.0	2.6
C18:3c6Me-d3	3.2 ($10^{-3.2}$)	40.0	60.0	2.6
C18:3c9Me-d3	3.6 ($10^{-3.6}$)	40.0	60.0	2.8
C20:5cMe-d3	2.0 (10^{-2})	90.0	1.0	5.0
Mean	2.1 ($10^{-2.1}$)	49.5	22.5	4.0
Final	2.1	50.0	20.0	4.0

9.1.2.6 Molar excess of derivatization reagents

Table 9.12 Calculation of the molar excess of the derivatization agents at different FA mix concentrations.

Parameter	4 µg L^{-1}	20 µg L^{-1}	40 µg L^{-1}	80 µg L^{-1}	120 µg L^{-1}
CD_3OD	$2{\cdot}10^6$	$5{\cdot}10^5$	$2{\cdot}10^5$	$1{\cdot}10^5$	$8{\cdot}10^4$
pH 2	$5{\cdot}10^4$	$1{\cdot}10^4$	$5{\cdot}10^3$	$2{\cdot}10^3$	$2{\cdot}10^3$
pH 3	$5{\cdot}10^3$	$1{\cdot}10^3$	$5{\cdot}10^2$	$2{\cdot}10^2$	$2{\cdot}10^2$
pH 4	$5{\cdot}10^2$	$1{\cdot}10^2$	$5{\cdot}10^1$	$2{\cdot}10^1$	$2{\cdot}10^1$
Final pH 2.1	$4{\cdot}10^4$	$8{\cdot}10^3$	$4{\cdot}10^3$	$2{\cdot}10^3$	$1{\cdot}10^3$

9.1.2.7 Calibration and method validation

Table 9.13 Linear regression functions with slope m and y-intercept b and R^2 for calibrations in ultrapure water (UW), surface water (SW), wastewater treatment plant outlet (WWTP), and bioreactor samples 1-3.

FA/FAME	UW		SW		WWTP		BR1		BR2		BR3	
	m	b	m	b	m	b	m	b	m	b	m	b
C6:0Me-d3	54	-22	34	40	20	104	103	1811	95	5002	147	4024
C7:0Me-d3	726	-3811	422	-1806	221	-672	139	754	214	1303	212	1880
C8:0Me-d3	1964	-2551	399	-1246	162	507	355	269	281	5846	284	13185
C9:0Me-d3	3072	-5217	591	-2990	181	387	183	3509	1043	2274	722	2334
C10:0Me-d3	2847	4301	279	1016	246	91	1106	-8190	1408	-412	1025	-99
C11:0Me-d3	4790	20132	688	-603	704	-2733	2915	-21827	3735	-11347	2614	-7550
C12:0Me-d3	3228	54574	585	5069	712	659	1636	9187	5465	5981	3649	7522
C13:0Me-d3	1406	41586	289	843	382	-1436	2616	-7934	3829	11923	3115	12857
C14:0Me-d3	1306	34769	236	3381	231	3971	2478	-7137	4551	19271	1835	25977
C15:0Me-d3	1088	28972	71	1200	702	-5930	1414	-5811	1911	4459	775	13135
C16:0Me-d3	725	99554	333	10975	1573	35582	4347	4365	2995	57178	1935	75478
C17:0Me-d3	333	40451	78	372	310	463	455	3818	392	5603	442	7035
C18:0Me-d3	817	26876	579	30125	924	24179	850	31610	828	25737	704	29142
C20:0Me-d3	118	8636	324	2563	304	2862	303	2758	285	3843	345	3548
C21:0Me-d3	40	3441	122	535	100	417	105	619	77	1194	74	1593
C22:0Me-d3	27	2217	34	1467	44	929	70	548	48	1236	41	1248
C16:1cMe-d3	97	3953	18	276	109	1666	204	1005	292	1341	110	1876
C18:1tMe-d3	77	1653	108	11393	130	10797	600	12418	122	8217	161	5437
C18:1cMe-d3	96	1876	124	8880	249	9654	334	13446	237	6988	61	6404
C18:2cMe-d3	10	314	15	542	16	600	16	1012	35	467	6	477
C18:3c6Me-d3	154	1756	253	-922	277	-709	374	-254	197	1570	183	948
C18:3c9Me-d3	114	1509	144	-225	176	-292	243	-164	140	861	116	56
C20:5cMe-d3	199	1492	349	-1277	384	-355	508	2985	274	1127	256	1295
C6:0Me	74522	-13598	13668	-280	38007	-6326	40284	5280	24718	13651	45772	14380
C7:0Me	190854	-49711	43002	-6118	43930	-5313	44512	-3524	34561	996	49237	-336
C8:0Me	910121	-214355	143411	-36670	105580	-21161	96915	-15944	145673	-31502	192200	-34372
C9:0Me	1277187	-378815	58894	-1290	83852	-13438	109625	-14799	74489	6110	274586	-34635
C10:0Me	2573034	-608102	260061	-51498	295350	-80551	359980	-82488	353606	-20904	1059000	-271590
C11:0Me	2595071	-488079	224383	-18760	240033	-27255	398650	-51783	451136	11742	944228	-135170
C12:0Me	5041930	40064	854617	-142067	573596	-89854	1491383	-368915	1981750	-192491	3176328	-692281
C13:0Me	2553019	-144874	341121	-26796	344352	-57136	644638	-100542	970756	-7917	2196993	-297747
C14:0Me	4158998	-530539	484693	-97755	366521	-221537	272964	-13687	2291116	-347033	2859870	-582170

FA/FAME	UW		SW		WWTP		BR1		BR2		BR3	
	m	b	m	b	m	b	m	b	m	b	m	b
C15:0Me	2075896	-83723	144649	-2037	228906	-26970	181459	-6142	1362398	-135417	1459012	-83230
C16:0Me	2978994	778075	473901	-80049	227445	-7961	4780543	-1787611	3421533	-908045	3295656	-591603
C17:0Me	1443219	27969	180510	-8909	1099476	-200284	1348535	-114952	1011604	-15997	930768	55860
C18:0Me	733757	387908	1172843	-92084	1273026	-109655	1453330	-119332	1248796	-71904	1202588	3815
C20:0Me	116298	202982	379496	-4804	505759	-51747	436946	-13395	371786	2830	315299	28671
C21:0Me	32277	47097	85639	8097	81684	8443	82333	13409	84269	8410	66155	13277
C22:0Me	35020	27327	68833	5774	88864	-2545	54837	17267	64696	5010	62146	4793
C16:1cMe	268452	-28214	27514	-1288	14559	163	364408	-65452	254833	-32441	233617	-18084
C18:1tMe	115233	23434	269364	-7140	298589	-6072	357878	-10989	284194	144	218485	33651
C18:1cMe	222875	41309	248913	-31423	275725	-32812	330101	-42694	262765	-25612	242005	-5365
C18:2cMe	20073	-2031	18069	-1887	21153	-2102	26076	-2481	16954	-954	14984	340
C18:3c6Me	1805	693	41576	35170	40330	46559	74261	53804	40894	57883	40299	34877
C18:3c9Me	1483	-5	4559	-752	2679	-68	3997	-276	3212	-121	2971	-141
C20:5cMe	773	340	1452	237	1761	-36	1849	25	1121	74	1242	207

Table 9.14 Results of method validation in different matrices with the method detection limit (MDL) in µg L^{-1}, Recovery (R), and linear calibration curve correlation coefficient (R^2). FA: Fatty acid; FAME: Fatty acid methyl ester; UW: Ultra pure water; SW: Surface water; WWTP: Wastewater treatment plant effluent; BR1-3: Bioreactor water 1-3.

FA/FAME	UW			SW			WWTP			BR1			BR2			BR3		
	MDL	R [%]	R^2	MDL	R [%]	R^2	MDL	R [%]	R^2	MDL	R [%]	R^2	MDL	R [%]	R^2	MDL	R [%]	R^2
C6:0Me-d_3	2	115	0.9966	5	108	0.9276	1	91	0.9682	10	101	0.9849	3	97	0.9547	8	99	0.9877
C7:0Me-d_3	2	90	0.9829	6	108	0.9516	6	103	0.9856	12	92	0.9948	7	95	0.9868	20	81	0.9554
C8:0Me-d_3	1	87	0.9971	8	110	0.9248	12	101	0.9829	8	112	0.8854	10	85	0.9032	27	79	0.8719
C9:0Me-d_3	3	81	0.9961	8	112	0.8962	1	98	0.9898	19	98	0.9891	3	99	0.9910	5	99	0.9859
C10:0Me-d_3	1	85	0.9989	4	99	0.9843	11	99	0.9785	8	75	0.9886	3	102	0.9903	3	105	0.9786
C11:0Me-d_3	2	83	0.9954	3	88	0.9906	6	105	0.9730	8	77	0.9965	4	107	0.9608	7	104	0.9843
C12:0Me-d_3	4	83	0.9724	3	94	0.9969	2	101	0.9780	4	70	0.9983	5	103	0.9816	7	100	0.9874
C13:0Me-d_3	10	85	0.9599	3	90	0.9848	11	107	0.9592	6	109	0.9345	6	95	0.9956	5	90	0.9766
C14:0Me-d_3	18	90	0.9965	2	81	0.9727	9	83	0.9356	4	105	0.9682	14	94	0.9850	3	92	0.9530
C15:0Me-d_3	3	101	0.9940	2	101	0.9496	12	116	0.9576	5	103	0.9710	10	90	0.9985	8	90	0.9119
C16:0Me-d_3	5	103	0.9775	5	98	0.9227	0.4	98	0.9958	0.2	84	0.9820	9	93	0.9752	5	107	0.9961
C17:0Me-d_3	2	116	0.9469	5	91	0.9191	3	91	0.9183	3	94	0.9629	8	93	0.9544	1	135	0.9364
C18:0Me-d_3	2	105	0.9324	6	97	0.9948	3	106	0.9132	5	124	0.9026	15	95	0.9961	14	97	0.9636

FA/FAME	UW			SW			WWTP			BR1			BR2			BR3		
	MDL	R [%]	R^2	MDL	R [%]	R^2	MDL	R [%]	R^2	MDL	R [%]	R^2	MDL	R [%]	R^2	MDL	R [%]	R^2
C20:0Me-d_3	3	93	0.9674	3	109	0.9787	2	84	0.9745	3	83	0.9455	5	130	0.9004	5	105	0.9867
C21:0Me-d_3	4	93	0.9635	6	84	0.7699	8	72	0.9535	14	139	0.9168	21	93	0.9304	10	121	0.9707
C22:0Me-d_3	5	86	0.9367	7	95	0.9345	10	86	0.9250	14	122	0.9172	3	91	0.9060	2	89	0.9156
C16:1cMe-d_3	30	90	0.9968	7	108	0.9452	23	89	0.9089	9	91	0.9340	9	95	0.9951	2	92	0.9397
C18:1tMe-d_3	2	114	0.9234	10	92	0.9553	16	101	0.9769	4	100	0.9989	23	121	0.9807	10	99	0.9969
C18:1cMe-d_3	2	111	0.9170	8	94	0.9386	11	79	0.9559	7	99	0.9907	17	104	0.9836	23	91	0.8495
C18:2cMe-d_3	1	90	0.9527	20	95	0.9862	4	91	0.9191	9	94	0.9570	3	95	0.9986	16	91	0.9232
C18:3c6Me-d_3	1	85	0.9686	6	108	0.9982	4	103	0.9842	6	103	0.9843	16	92	0.9881	6	94	0.9837
C18:3c9Me-d_3	1	89	0.9731	7	109	0.9881	7	104	0.9857	6	102	0.9918	5	91	0.9497	2	100	0.9970
C20:5cMe-d_3	1	83	0.9847	5	109	0.9387	4	104	0.9844	3	92	0.9931	9	98	0.9803	9	93	0.9990
Mean	5	94	0.9709	6	99	0.9500	7	96	0.9610	7	99	0.9647	9	98	0.9690	9	98	0.9587
C6:0Me	0.09	105	0.9908	0.10	97	0.9987	0.18	108	0.9525	0.06	91	0.9886	0.14	112	0.9545	0.03	80	0.9928
C7:0Me	0.18	84	0.9610	0.20	112	0.9337	0.14	106	0.9741	0.12	102	0.9910	0.03	97	0.9899	0.05	94	0.9809
C8:0Me	0.07	82	0.9748	0.29	116	0.8893	0.29	114	0.9115	0.28	66	0.8879	0.27	111	0.9340	0.20	101	0.9638
C9:0Me	0.06	75	0.9683	0.23	90	0.9939	0.18	111	0.9402	0.16	109	0.9549	0.12	96	0.9733	0.16	108	0.9682
C10:0Me	0.10	81	0.9861	0.29	110	0.9466	0.33	115	0.8939	0.29	109	0.9424	0.11	111	0.9731	0.30	113	0.9136
C11:0Me	0.19	119	0.9928	0.28	101	0.9884	0.18	106	0.9625	0.17	107	0.9664	0.04	101	0.9797	0.20	110	0.9516
C12:0Me	0.27	80	0.9931	0.29	104	0.9719	0.25	97	0.9444	0.27	110	0.9288	0.23	106	0.9681	0.33	107	0.9516
C13:0Me	0.27	90	0.9964	0.20	104	0.9815	0.24	110	0.9452	0.17	109	0.9478	0.16	105	0.9774	0.21	106	0.9727
C14:0Me	0.25	56	0.9930	0.31	111	0.9357	0.08	123	0.8862	0.09	107	0.9475	0.35	108	0.9639	0.37	107	0.9608
C15:0Me	0.03	92	0.9987	0.17	97	0.9990	0.14	65	0.9216	0.05	103	0.9699	0.20	107	0.9735	0.15	103	0.9931
C16:0Me	0.05	89	0.9479	0.38	89	0.9192	0.17	118	0.7926	0.38	112	0.8770	0.42	112	0.9203	0.34	103	0.9620
C17:0Me	0.05	95	0.9453	0.17	86	0.9847	0.21	103	0.9336	0.26	103	0.9888	0.11	106	0.9798	0.07	93	0.9896
C18:0Me	0.10	91	0.9655	0.13	100	0.9861	0.23	97	0.9676	0.19	99	0.9834	0.17	105	0.9843	0.16	100	0.9859
C20:0Me	0.29	83	0.9269	0.04	96	0.9765	0.29	86	0.9585	0.19	106	0.9800	0.15	103	0.9810	0.14	90	0.9709
C21:0Me	0.44	76	0.9567	0.14	90	0.9860	0.15	83	0.9437	0.04	84	0.9562	0.05	97	0.9667	0.06	79	0.9466
C22:0Me	0.57	62	0.9525	0.003	96	0.9923	0.32	90	0.9745	0.04	107	0.9793	0.12	100	0.9617	0.24	99	0.9851
C16:1cMe	0.15	85	0.9945	0.13	86	0.9853	0.01	102	0.9617	0.18	110	0.9462	0.17	110	0.9504	0.16	103	0.9911
C18:1tMe	0.08	95	0.9708	0.08	103	0.9950	0.11	99	0.9947	0.11	101	0.9957	0.10	105	0.9869	0.02	85	0.9559
C18:1cMe	0.07	91	0.9489	0.19	105	0.9799	0.22	101	0.9782	0.22	103	0.9770	0.21	107	0.9730	0.18	102	0.9806
C18:2cMe	0.05	94	0.9720	0.14	110	0.9497	0.15	105	0.9802	0.13	105	0.9809	0.16	108	0.9704	0.07	100	0.9893
C18:3c6Me	0.72	81	0.9518	0.59	105	0.9277	0.10	98	0.9417	0.09	96	0.9585	0.03	100	0.9432	0.11	92	0.9567
C18:3c9Me	0.04	92	0.9744	0.24	107	0.9591	0.09	103	0.9932	0.34	108	0.9640	0.25	106	0.9791	0.15	103	0.9900
C20:5cMe	0.10	83	0.9312	0.11	94	0.9510	0.49	108	0.9640	0.31	103	0.9673	0.40	90	0.9821	0.33	90	0.9712
Mean	0.18	86	0.9693	0.20	100	0.9666	0.20	102	0.9442	0.18	102	0.9600	0.17	104	0.9681	0.18	99	0.9706

9.1.2.8 Quantification of FAs and FAMEs in real samples

Table 9.15 Results of analyte quantification in real samples.

FA/FAME	SW	WWTP	BR1	BR2	BR3
	c [µg L^{-1}]				
C6:0Me-d_3	Nd	5	175	526	274
C7:0Me-d_3	Nd	Nd	Nd	Nd	Nd
C8:0Me-d_3	Nd	Nd	Nd	208	465
C9:0Me-d_3	Nd	2	Nd	Nd	Nd
C10:0Me-d_3	Nd	Nd	Nd	Nd	Nd
C11:0Me-d_3	Nd	Nd	Nd	Nd	Nd
C12:0Me-d_3	9	Nd	56	Nd	Nd
C13:0Me-d_3	Nd	Nd	Nd	Nd	Nd
C14:0Me-d_3	14	17	Nd	Nd	142
C15:0Me-d_3	17	Nd	Nd	Nd	169
C16:0Me-d_3	33	23	10	191	390
C17:0Me-d_3	Nd	Nd	84	143	159
C18:0Me-d_3	52	26	372	311	414
C20:0Me-d_3	8	9	91	135	103
C21:0Me-d_3	Nd	Nd	Nd	Nd	215
C22:0Me-d_3	43	21	Nd	256	305
C16:1cMe-d_3	15	Nd	Nd	Nd	170
C18:1tMe-d_3	105	83	207	674	338
C18:1cMe-d_3	72	39	402	294	1056
C18:2cMe-d_3	36	38	653	134	741
C18:3c6Me-d_3	Nd	Nd	Nd	Nd	Nd
C18:3c9Me-d_3	Nd	Nd	Nd	62	Nd
C20:5cMe-d_3	Nd	Nd	59	Nd	Nd
Sum c [µg L^{-1}]	404	263	2109	2934	4941
C6:0Me	Nd	Nd	1.3	5.5	3.1
C7:0Me	Nd	Nd	Nd	0.29	Nd
C8:0Me	Nd	Nd	Nd	Nd	Nd
C9:0Me	Nd	Nd	Nd	Nd	Nd
C10:0Me	Nd	Nd	Nd	Nd	Nd
C11:0Me	Nd	Nd	Nd	Nd	Nd
C12:0Me	Nd	Nd	Nd	Nd	Nd
C13:0Me	Nd	Nd	Nd	Nd	Nd
C14:0Me	Nd	Nd	Nd	Nd	Nd
C15:0Me	Nd	Nd	Nd	Nd	Nd
C16:0Me	Nd	Nd	Nd	Nd	Nd
C17:0Me	Nd	Nd	Nd	Nd	Nd
C18:0Me	Nd	Nd	Nd	Nd	Nd
C20:0Me	Nd	Nd	Nd	Nd	Nd
C21:0Me	Nd	Nd	1.6	1.0	2.0
C22:0Me	0.08	Nd	3.1	Nd	Nd
C16:1cMe	Nd	0.01	Nd	Nd	Nd
C18:1tMe	Nd	Nd	Nd	Nd	Nd
C18:1cMe	Nd	Nd	Nd	Nd	Nd
C18:2cMe	Nd	Nd	Nd	Nd	Nd
C18:3c6Me	0.85	1.15	7.2	14	8.7
C18:3c9Me	Nd	Nd	Nd	Nd	Nd
C20:5cMe	0.16	Nd	Nd	Nd	Nd
Sum c [µg L^{-1}]	1.1	1.2	13	21	14

9.1.3 Supporting material for Chapter 6

9.1.3.1 MRM method

Table 9.16 MRM transitions of selected analytes with optimized collision energy and quantifier ions. Time frame: chosen time frame for the given transitions; *Quantifier ions; CE: Collision energy. For experimental conditions see the respective sections.

Time frame [min]	Analyte	CAS No.	Retention time [min]	MRM Transitions Precursor ions > Product ions [m/z]	Optim. CE [eV]
4.00-6.00	Toluene	108-88-3	4.52	91>39 91>65* 91>51 65>39	30 20 30 20
6.00-9.00	*o*-Xylene	95-47-6	8.25	91>39 91>65* 105>51	30 20 30
	2-Heptanone	110-43-0	8.30	43>15 43>39 58>43*	20 10 10
9.00-11.50	Anisole	100-66-3	9.88	108>65 108>39 108>78* 78>51 78>39 78>63	20 30 10 20 20 20
11.50-14.50	Phenol	108-95-2	12.39	94>65 94>39 94>51	20 20 30
	Heptanoic acid methyl ester	106-73-0	12.50	74>43 74>31 43>15	10 10 20
14.50-17.00	n-Dodecane	112-40-3	15.96	57>39 57>27 57>41* 43>27 43>39 43>15	20 10 10 10 10 20
17.00-18.75	Naphtalene	91-20-3	17.83	128>102 128>77* 128>52 128>52 64>51 64>27	20 20 30 10 10 20
18.75-21.00	Indole	120-72-9	19.40	117>89* 117>64 117>51 117>51 90>39 90>51	20 30 20 20 20 30
21.00-24.33	Lindane	58-89-9	21.73	181>109 181>146* 181>74 219>147 219>109 219>85	30 20 30 20 30 30

9.1.3.2 Partitioning constants

Table 9.17 Calculated theoretical extracted equilibrium fractions f_f and distribution constants $log\ K_{aw}$ (25 °C), $log\ K_{ow}$ (25 °C) and $log\ K_{fa}$ (25 °C, PDMS) from literature data. LSER descriptors and partitioning constants were taken from the database from the UFZ Helmholz Center for environmental research [135]. E: excess molar refraction; S: polarizability/dipolarity; A: solute hydrogen bond acidity; B: solute hydrogen bond basicity; V: McGowan's molar volume; L: logarithmic gas-hexane partition coefficient.

Analyte	E	S	A	B	V	L	$\log K_{aw}$	$\log K_{ow}$
Toluene	0.60	0.52	0.00	0.14	0.86	3.33	0.62	2.62
Indole	1.20	1.26	0.44	0.18	0.95	5.31	4.60	2.43
Phenol	0.81	0.89	0.6	0.30	0.78	3.77	4.81	1.43
Anisole	0.71	0.75	0.00	0.29	0.92	3.89	-2.00	2.16
o-Xylene	0.66	0.56	0.00	0.16	1.00	3.94	0.74	3.10
Naphthalene	1.34	0.92	0.00	0.20	1.09	5.16	2.16	3.19
2-Heptanone	0.12	0.68	0.00	0.51	1.11	3.76	2.30	1.92
n-Dodecane	0.00	0	0.00	0.00	1.80	5.70	2.55	7.13
Lindane	1.45	0.91	0.00	0.68	1.58	7.47	4.10	3.73
Heptanoic acid methyl ester	0.08	0.6	0.00	0.45	1.31	4.36	1.70	2.97

9.1.3.3 Calculation of optimal extraction parameters

Table 9.18 Averaged optimal extraction parameters determined with DOE. T: Extraction temperature; t: Exraction time.

Analyte	T [°C]	t [min]	Material	R^2	Adj. R^2
Toluene	40	1	HLB 5+30 µm arrow	0.8845	0.8538
Indole	70	30	HLB 5+30 µm arrow	0.8742	0.8406
Anisole	58	1	HLB 5+30 µm arrow	0.9157	0.8932
o-Xylene	40	1	HLB 5+30 µm arrow	0.9062	0.8812
Naphthalene	70	27	HLB 5+30 µm arrow	0.8360	0.7923
2-Heptanone	70	16	HLB 5+30 µm arrow	0.9283	0.9092
n-Dodecane	70	30	HLB 5+30 µm arrow	0.8661	0.8304
Lindane	70	30	HLB 5 µm arrow	0.7804	0.7219
Average	61	17	HLB 5+30 µm arrow	0.8739	0.8403

9.1.3.4 Calibration results

Table 9.19 Results of the calibration of the observed analytes. The calibration was done at quadruplicates in a concentration range of 5-70 µg L^{-1} with eight calibration points.

Analyte	m	b	R^2
Toluene	28721	84625	0.9899
Indole	11463	16013	0.9941
Anisole	24831	77153	0.9917
o-Xylene	128183	659477	0.9919
Naphthalene	166919	3084223	0.9765
2-Heptanone	16803	-12618	0.9982
n-Dodecane	198412	1271703	0.9915
Lindane	1158	169	0.9956

9.1.4 Supporting material for Chapter 7

9.1.4.1 Chemical ionization procedure

For CI, H_2 was let through a plasma at 13 mbar to produce H_3^+. For the generation of CI reagent ions such as $[N_2H]^+/[N_4H]^+$, N_2 gas was added subsequently to the H_2 gas stream. For the generation of reagent ions such as $[H_3O]^+$ and $[NH_4]^+$, the N_2 gas stream was enriched with water and a 30% ammonia in water mixture using a permeation tube setup, respectively [197]. Both $[N_2H]^+/[N_4H]^+$ and $[H_3O]^+$ reagent ions usually create protonated or deprotonated molecular ions ($[M+H]^+$ or $[M-H]^+$) whereas the $[NH_4]^+$ reagent ion rarely creates the protonated or deprotonated molecular ions and instead produces $[M+NH_4]^+$ adduct ions.

9.1.4.2 Workflow

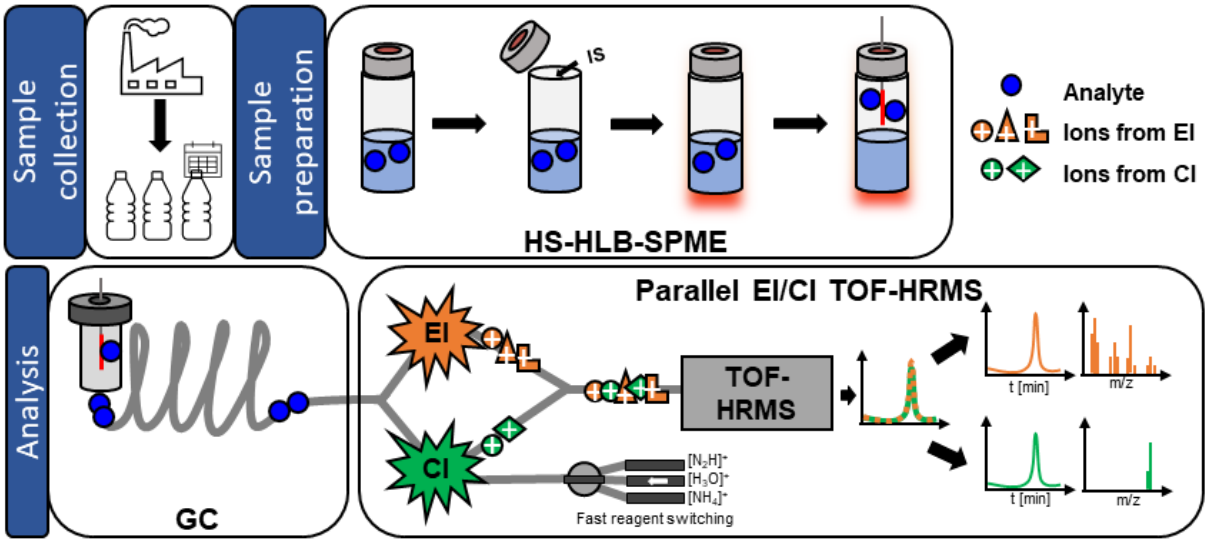

Figure 9.9 Workflow including sample collection from the industrial production plant, sample preparation using solid-phase microextraction (SPME), and GC-TOF-HRMS analysis with parallel CI and EI. IS: Internal standards; HS: headspace; HLB: hydrophilic-lipophilic-balanced.

9.1.4.3 Data processing parameters

Table 9.20 Data processing parameters in Analyzer Pro XD. For chromatographic peaks that were not properly separated by the deconvolution algorithm different settings for "scan window" of 3 and 5 were applied.

Processing parameters	Settings	Comments
Minimum no. of masses	2	
Reject masses	414, 57, 69, 58, 131, 219, 264	Rejection of masses only applied for CI data
Mass range	30-350	
Area threshold	1	
Height threshold	0	
Scan window	3 or 5	
Signal to noise	1	
Smoothing	7	
Width [min]	0.01	

Processing parameters	Settings	Comments
Temporal resolution	Minimum	
Fronting [%]	0	
Tailing [%]	0	
Data channel grouping window [scans]	± 2	For grouping of CI and EI data
Forward threshold	650	
Reverse threshold	650	
Confidence threshold	60	
Confidence ratio	70:30	
Match targets using	Retention time	
Retention time window [min]	0.2	

9.1.4.4 Mass spectra of example 2

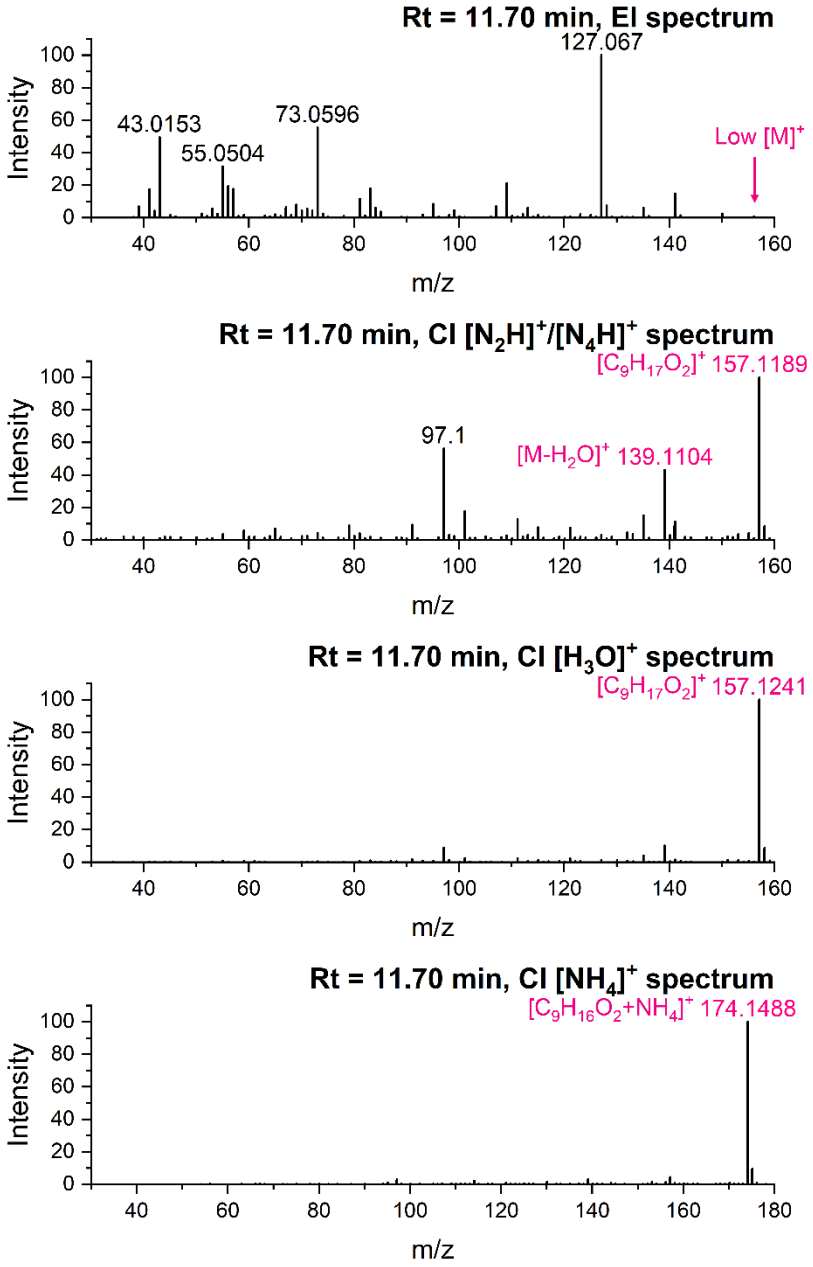

Figure 9.10 EI (A), CI $[N_2H^+/[N_4H]^+$ reagent (B), CI $[H_3O]^+$ reagent (C), and CI $[NH_4]^+$ reagent (D) mass spectra for a compound detected at a retention time of 11.70 min.

9.1.4.5 Identification parameters and identification confidence levels

The results of the identification parameters were treated as follows:

- Obtained RI vs. Database RI: allowed deviation ± 20 (green), >20 (red)
- NIST Database Match and R.Match >800 (very good, green), >700 <800 (satisfactory, yellow), >600 <700 (unsatisfactory, orange), <600 (not acceptable, red)
- Mass accuracy error: <5 ppm (very good, green), >5 <10 ppm (satisfactory, yellow), >10 <15 ppm (unsatisfactory, orange), >15 ppm (not acceptable, red)

The results were categorized into different identification confidence levels based on Schymanski et al. [203], which were interpreted as follows using CI and EI data:

Level 1 (confirmed structure):

- Very good results for each category and confirmation with a reference standard

Level 2a (probable structure):

- RI fits, EI hit(s) fit(s), minimum 1x CI with <5 ppm mass accuracy error

Level 2b (probable structure):

- EI hit(s) off, structural investigation with hybrid similarity search
- or CI off, structural investigation with hybrid similarity search

Level 3 (no exact structure):

- RI off, EI hit(s) fit(s), minimum 1x CI with <5 ppm mass accuracy error
- or EI fits, EI hit(s) off, minimum 1x CI with <5 ppm mass accuracy error
- or RI and EI hit(s) fit, CI is off

Level 4 (only molecular formula and exact mass):

- Only CI fits
- or only EI hit(s) fit(s)
- or only RI fits

Level 5 (only exact mass):

- Every category is off, but CI gives an exact mass but the accurate mass error is off (the sum formula is wrong)

Table 9.21 List of identified substances and their identification parameters for EI and CI data. *: affected through Co-elution, [a]Discussed as an example; [b]different substances with the same retention time, that were found in different samples; [c]compounds identified with NIST hybrid search (HSS), which are not included in the database do not have a database RI, the stated match factor yielded by using HSS; X: Undefined rests that could not be fully identified. Compound names or sum formulas marked in red had unacceptable identification results (e.g. both NIST matches <700), and should be interpreted with caution. Possible isomers that gave the same database hit are marked with isomer x and only the hit with the better identification level and/or retention index was included in further data evaluation.

	General information						Electron ionization data				Chemical ionization data					
No.	Retention time [min]	NIST name	Sum formula	Molar exact mass [Da]	Identification level	Peak size	Obtained RI	Database RI	Match	Reversed Match	Molecular ion in $[N_2H]^+/[N_4H]^+$	Exact mass ± mass acc. error $[N_2H]^+/[N_4H]^+$	Molecular ion in $[H_3O]^+$	Exact mass ± mass acc. error $[H_3O]^+$	Molecular ion in $[NH_4]^+$	Exact mass ± mass acc. error $[NH_4]^+$
1	6.26	Phenylethyne	C_8H_6	102.0470	3	+	860	834	933	938	$[M+H]^+$	103.0542 +6.8 ppm	$[M+H]^+$	103.0542 +2.3 ppm	$[M+NH_4]^+$	120.0808 +2.4 ppm
2	6.36[b]	2,6-Lutidine	C_7H_9N	107.0735	2a	+	855	834	818	904	$[M+H]^+$	108.0808 +2.2 ppm	$[M+H]^+$	108.0808 +1.6 ppm	$[M+H]^+$	108.0808 +5.0 ppm
3	6.36[b]	Cyclohexanol	$C_6H_{12}O$	100.0888	3	o	874	880	795	882	-	-	-	-	-	-
4	6.37*	2-Heptanone	$C_7H_{14}O$	114.1045	2a	+	891	875	601	811	$[M+H]^+$	115.1117 +6.5 ppm	$[M+H]^+$	115.1117 +0.1 ppm	$[M+NH_4]^+$	132.1383 -4.7 ppm
5	6.46*	Cyclohexanone	$C_6H_{10}O$	98.0732	3	o	887	894	657	749	$[M+H]^+$	99.0804 +5.3 ppm	$[M+H]^+$	99.0804 +1.2 ppm	$[M+NH_4]^+$	116.1070 -4.2 ppm
6	6.52	1,3-Dioxolane, 2-(chloromethyl)-	$C_4H_7ClO_2$	122.0135	4	o	896	894 (est)	593	774	-	-	-	-	-	-
7	6.66	-	$C_5H_{10}OS_2$	150.0173	4	-	-	-	-	-	$[M+H]^+$	151.0246 -2.4 ppm	$[M+H]^+$	151.0246 -3.6 ppm	-	-
8	6.76	Cyclohexane, (1-methylethyl)-	C_9H_{18}	126.1409	2a	+	919	924	863	906	$[M-H]^+$	125.1325 -2.3 ppm	$[M-H]^+$	125.1325 +2.6 ppm	-	-
9	6.89	2-Heptanone, 3-methyl-	$C_8H_{16}O$	128.1201	2a	-	930	937	869	914	$[M+H]^+$	129.1274 +11.0 ppm	$[M+H]^+$	129.1274 -3.4 ppm	$[M+NH_4]^+$	146.1539 +1.3 ppm

	General information						Electron ionization data				Chemical ionization data					
No.	Retention time [min]	NIST name	Sum formula	Molar exact mass [Da]	Identification level	Peak size	Obtained RI	Database RI	Match	Reversed Match	Molecular ion in $[N_2H]^+/[N_4H]^+$	Exact mass ± mass acc. error $[N_2H]^+/[N_4H]^+$	Molecular ion in $[H_3O]^+$	Exact mass ± mass acc. error $[H_3O]^+$	Molecular ion in $[NH_4]^+$	Exact mass ± mass acc. error $[NH_4]^+$
10	6.91	Pyridine, 2,5-dimethyl-	C_7H_9N	107.0735	2a	o	932	922	802	803	$[M+H]^+$	108.0808 +6.8 ppm	$[M+H]^+$	108.0808 -0.7 ppm	-	-
11	6.99	3,4-Dimethyl-3-hexanol	$C_8H_{18}O$	130.1358	3	o	939	920 (est)	874	921	-	-	-	-	-	-
12	7.02	3-Heptanone, 5-methyl-	$C_8H_{16}O$	128.1201	2a	o	942	944	800	825	$[M+H]^+$	129.1274 +3.3 ppm	$[M+H]^+$	129.1274 +4.3 ppm	$[M+NH_4]^+$	146.1539 +1.7 ppm
13	7.05	2-Heptanone, 3-methyl-	$C_8H_{16}O$	128.1201	2a	o	944	937	789	824	$[M+H]^+$	129.1274 +1.9 ppm	$[M+H]^+$	129.1274 -1.4 ppm	$[M+NH_4]^+$	146.1539 -2.3 ppm
14	7.43	5,5-Dimethyl-2-isopropyl-1,3-dioxane	$C_9H_{18}O_2$	158.1307	2a	+	980	968	815	872	$[M-H]^+$	157.1223 –3.1 ppm	$[M+H]^+$	159.1380 +0.2 ppm	$[M+NH_4]^+$	176.1645 +1.9 ppm
15	7.56	-	$C_5H_8O_2S$	132.0245	5	-	990	-	-	-	$[M+H]^+$	133.0318 -5.4 ppm	$[M+H]^+$	133.0318 +22.5 ppm	-	-
16	7.57*	2-Octanone	$C_8H_{16}O$	128.1201	3	-	991	991	746	779	$[M+H]^+$	129.1274 -2.8 ppm	$[M+H]^+$	129.1274 +1.0 ppm	$[M+NH_4]^+$	146.1539 -0.8 ppm
17	7.61	-	C_9H_8	116.0626	4	o	995	-	-	-	$[M+H]^+$	117.0699 +2.8 ppm	$[M+H]^+$	117.0699 +4.2 ppm	-	-
18	7.82	Cycloheptanone	$C_7H_{12}O$	112.0888	2a	+	1013	1012	808	938	$[M+H]^+$	113.0961 +0.1 ppm	$[M+H]^+$	113.0961 +3.2 ppm	$[M+NH_4]^+$	130.1226 +3.7 ppm
19	7.90	-	C_7H_9N	107.0735	4	-	1019	-	-	-	$[M+H]^+$	108.0808 -4.5 ppm	-	-	-	-
20	7.93	2-Isopropyl-5,5-Dimethyl-[1,3]Dioxane	$C_9H_{18}O_2$	158.1307	3	-	1022	968	720	820	$[M-H]^+$	157.1223 +1.9 ppm	$[M+H]^+$	159.1380 +12.6 ppm	$[M+NH_4]^+$	176.1645 +2.4 ppm

	General information						Electron ionization data				Chemical ionization data					
No.	Retention time [min]	NIST name	Sum formula	Molar exact mass [Da]	Identification level	Peak size	Obtained RI	Database RI	Match	Reversed Match	Molecular ion in $[N_2H]^+/[N_4H]^+$	Exact mass ± mass acc. error $[N_2H]^+/[N_4H]^+$	Molecular ion in $[H_3O]^+$	Exact mass ± mass acc. error $[H_3O]^+$	Molecular ion in $[NH_4]^+$	Exact mass ± mass acc. error $[NH_4]^+$
21	8.00	1-hexanol, 2 ethyl-	$C_8H_{18}O$	130.1357	2a	o	1027	1030	880	929	$[M-H]^+$	129.1274 +4.0 ppm	$[M-H]^+$	129.1274 -0.5 ppm	$[M+NH_4]^+$	148.1696 +3.4 ppm
22	8.16	Cyclohexanone, 3,3,5-trimethyl-	$C_9H_{16}O$	140.1201	3	-	1040	1059 (est)	631	758	$[M+H]^+$	141.1274 +4.4 ppm	$[M+H]^+$	141.1274 +0.7 ppm	$[M+NH_4]^+$	158.1539 +9.3 ppm
23	8.24	Indene	C_9H_8	116.0626	2a	-	1047	1041	814	901	$[M+H]^+$	117.0699 +3.8 ppm	$[M+H]^+$	117.0699 +0.1 ppm	-	-
24	8.33	7-Oxabicyclo[4.3.0]nonane, cis-	$C_8H_{14}O$	126.1045	2a	o	1054	1062 (est)	743	855	$[M+H]^+$	127.1117 +8.8 ppm	$[M+H]^+$	127.1117 +5.0 ppm	$[M+NH_4]^+$	144.1383 +9.1 ppm
25	8.34	Bis(2-chloroisopropyl) ether	$C_6H_{12}Cl_2O$	170.0265	1	+	1055	1061	804	817	-	-	-	-	$[M+NH_4]^+$	188.0603 +2.1 ppm
26	8.44	Benzene, 1-propynyl-	C_9H_8	116.0626	2a	-	1063	1052	802	855	$[M+H]^+$	117.0699 +6.6 ppm	$[M+H]^+$	117.0699 -0.0 ppm	-	-
27	8.49	7-Oxabicyclo[4.3.0]nonane, cis-	$C_8H_{14}O$	126.1045	2a	+	1067	1062 (est)	911	924	$[M-H]^+$	125.0961 +3 ppm	$[M+H]^+$	127.1117 +1 ppm	$[M+NH_4]^+$	144.1383 -3.0 ppm
28	8.55	1,4-Diethynylbenzene	$C_{10}H_6$	126.0470	3	-	1072	1020 (est)	758	839	$[M+H]^+$	127.0542 +0.7 ppm	$[M+H]^+$	127.0542 +3.1 ppm	-	-
29	8.60	-	$C_{10}H_8$	128.0626	5	-	1076	-	-	-	$[M-H]^+$	127.0542 +1.5 ppm	$[M-H]^+$	127.0542 +5.1 ppm	-	-
30	8.69[c]	X-butyl-5,5-Dimethyl-[1,3]Dioxane X: iso-, n-, etc.	$C_{10}H_{20}O_2$	172.1463	2b	o	1083	-	895	915	$[M-H]^+$	171.1380 +0.5 ppm	$[M+H]^+$	173.1536 +8.0 ppm	$[M+NH_4]^+$	190.1802 +4.5 ppm
31	8.71	Benzaldehyde, 3-methyl-	C_8H_8O	120.0575	3	-	1084	1071	551	792	$[M+H]^+$	121.0648 -4.4 ppm	$[M+H]^+$	121.0648 +1.3 ppm	-	-

	General information						Electron ionization data				Chemical ionization data					
No.	Retention time [min]	NIST name	Sum formula	Molar exact mass [Da]	Identification level	Peak size	Obtained RI	Database RI	Match	Reversed Match	Molecular ion in $[N_2H]^+/[N_4H]^+$	Exact mass ± mass acc. error $[N_2H]^+/[N_4H]^+$	Molecular ion in $[H_3O]^+$	Exact mass ± mass acc. error $[H_3O]^+$	Molecular ion in $[NH_4]^+$	Exact mass ± mass acc. error $[NH_4]^+$
32	8.75[b]	Benzenemethanol, α,α-dimethyl-	$C_9H_{12}O$	136.0888	4	-	1088	1090	812	843	-	-	-	-	-	-
33	8.75[b]	1-Pentanol, 4-methyl-2-propyl-	$C_9H_{20}O$	144.1514	3	+	1088	1091	705	762	$[M-H]^+$	143.1430 +4.8 ppm	$[M-H]^+$	143.1430 -1.8 ppm	$[M+NH_4]^+$	162.1852 +2.9 ppm
34	8.81*	Verbenol	$C_{10}H_{16}O$	152.1201	5	+	1093	1140	605	635	$[M+H]^+$	153.1274 -0.5 ppm	$[M+H]^+$	153.1274 +4.4 ppm	$[M+NH_4]^+$	170.1539 -1.8 ppm
35	8.86	Cyclohexanol, 1-propyl-	$C_9H_{18}O$	142.1358	4	-	1096	1118 (est)	737	830	-	-	-	-	-	-
36	8.90	Undecane	$C_{11}H_{24}$	156.1878	1	o	1100	1100	852	886	$[M-H]^+$	155.1794 +2.9 ppm	-	-	-	-
37	8.95	-	$C_{10}H_{22}O_3$	190.1569	5	-	1103	-	-	-	$[M-H]^+$	189.1485 -12.6 ppm	-	-	-	-
38	8.99	X-Octanol, X-methyl- (Isomer 1)	$C_9H_{20}O$	144.1514	3	-	1106	1119	809	837	$[M-H]^+$	143.1430 +6.7 ppm	$[M-H]^+$	143.1430 +5.8 ppm	$[M+NH_4]^+$	162.1852 +9.3 ppm
39	9.09	-	$C_{10}H_{20}O$	156.1514	4	-	1113	-	-	-	$[M+H]^+$	157.1587 +19.2 ppm	$[M+H]^+$	157.1587 +0.5 ppm	-	-
40	9.13	X-Octanol, X-methyl- (Isomer 2)	$C_9H_{20}O$	144.1514	2a	-	1116	1119	807	825	$[M-H]^+$	143.1434 -2.1 ppm	$[M-H]^+$	143.1434 -1.3 ppm	$[M+NH_4]^+$	162.1852 + 5.9 ppm
41	9.16	Methyl 2-fluorobenzoate	$C_8H_7FO_2$	154.0430	2a	-	1117	1124	606	815	$[M+H]^+$	155.0503 -3.0 ppm	$[M+H]^+$	155.0503 -1.1 ppm	$[M+NH_4]^+$	172.1006 -16.6 ppm
42	9.23	Cyclooctanone	$C_8H_{14}O$	126.1045	2a	o	1122	1115	842	880	$[M+H]^+$	127.1117 +2.2 ppm	$[M+H]^+$	127.1117 +5.5 ppm	$[M+NH_4]^+$	144.1383 +1.3 ppm
43	9.47	Cyclohexanol, 1-methyl-4-	$C_{10}H_{20}O$	156.1514	4	-	1138	1138	744	777	-	-	-	-	-	-

	General information						Electron ionization data				Chemical ionization data					
No.	Retention time [min]	NIST name	Sum formula	Molar exact mass [Da]	Identification level	Peak size	Obtained RI	Database RI	Match	Reversed Match	Molecular ion in $[N_2H]^+/[N_4H]^+$	Exact mass ± mass acc. error $[N_2H]^+/[N_4H]^+$	Molecular ion in $[H_3O]^+$	Exact mass ± mass acc. error $[H_3O]^+$	Molecular ion in $[NH_4]^+$	Exact mass ± mass acc. error $[NH_4]^+$
		(1-methylethyl)-, cis-														
44	9.60	Cyclohexanol, 4-(1-methylethyl)-	$C_9H_{18}O$	142.1358	2a	-	1147	1166 (est)	808	856	$[M-H]^+$	141.1274 +7.7 ppm	$[M-H]^+$	141.1274 +1.6 ppm	$[M+NH_4]^+$	160.1696 +3.9 ppm
45	9.72	Benzene, 1,4-bis(1-methylethyl)-	$C_{12}H_{18}$	162.1409	4	o	1155	1168	618	655	-	-	-	-	-	-
46	9.76	2-Nonen-1-ol, (Z)-	$C_9H_{18}O$	142.1358	4	o	1157	1167 (est)	590	681	-	-	-	-	-	-
47	9.80	Cyclohexanol, 1-methyl-4-(1-methylethyl)-, cis-	$C_{10}H_{20}O$	156.1514	4	o	1167	1160	625	740	-	-	-	-	-	-
48	10.20	2-Heptenal, 2-propyl-	$C_{10}H_{18}O$	154.1358	2a	o	1186	1189 (est)	871	879	$[M+H]^+$	155.1430 +3.2 ppm	$[M+H]^+$	155.1430 +2.0 ppm	$[M+NH_4]^+$	172.1696 +3.1 ppm
49	10.27	Naphthalene	$C_{10}H_8$	128.0626	1	o	1191	1182	892	924	$[M+H]^+$	129.0699 +1.4 ppm	$[M+H]^+$	129.0699 +6.0 ppm	-	-
50	10.34	L-α-Terpineol	$C_{10}H_{18}O$	154.1358	3	-	1196	1192	515	550	$[M-H]^+$	153.1274 +4.1 ppm	$[M+H]^+$	155.1430 +4.8 ppm	$[M+NH_4]^+$	172.1696 +4.2 ppm
51	10.41	Dodecane	$C_{12}H_{26}$	170.2035	1	-	1200	1200	660	755	-	-	-	-	-	-
52	10.50	Cyclohexanol, 1-butyl-	$C_{10}H_{20}O$	156.1514	3	+	1205	1229 (est)	910	949	$[M-H]^+$	155.1430 +8.1 ppm	$[M-H]^+$	155.1430 +4.4 ppm	$[M+NH_4]^+$	174.1852 +12.1 ppm
53	10.61	5-Isopropenyl-2-methyl-7-	$C_{10}H_{16}O_2$	168.1150	4	+	1211	1169 (est)	734	754	$[M-H]^+$	167.1067 -0.8 ppm	$[M+H]^+$	169.1223 -4.0 ppm	$[M+H]^+$	169.1223 -2.5 ppm

	General information						Electron ionization data				Chemical ionization data					
No.	Retention time [min]	NIST name	Sum formula	Molar exact mass [Da]	Identification level	Peak size	Obtained RI	Database RI	Match	Reversed Match	Molecular ion in $[N_2H]^+/[N_4H]^+$	Exact mass ± mass acc. error $[N_2H]^+/[N_4H]^+$	Molecular ion in $[H_3O]^+$	Exact mass ± mass acc. error $[H_3O]^+$	Molecular ion in $[NH_4]^+$	Exact mass ± mass acc. error $[NH_4]^+$
		oxabicyclo[4.1.0]heptan-2-ol														
54	10.64[b]	5-Ethoxy-cycloocten e	$C_{10}H_{18}O$	154.1358	4	+	1213	1186 (est)	591	661	$[M+H]^+$	155.1430 -2.4 ppm	$[M+H]^+$	155.1430 +3.2 ppm	$[M-H]^+$	153.1274 -0.9 ppm
55	10.64[b]	Heptanol, 2-propyl	$C_{10}H_{22}O$	158.1671	2a	-	1213	1206 (est)	816	854	$[M-H]^+$	157.1587 +4.5 ppm	$[M-H]^+$	157.1587 +10.3 ppm	$[M+NH_4]^+$	176.2009 +4.6 ppm
56	10.67	Cyclohexene, 1-hexyl-	$C_{12}H_{22}$	166.1722	3	-	1214	1244	734	748	$[M-H]^+$	165.1638 +2.3 ppm	$[M+H]^+$	167.1794 +8.8 ppm	-	-
57	10.71[b]	4,4-Dimethylcyclohexadienone	$C_8H_{10}O$	122.0732	4	o	1217	1078	676	781	$[M+H]^+$	123.0804 -2.1 ppm	$[M+H]^+$	123.0804 -4.9 ppm	$[M+NH_4]^+$	140.1070 -4.0 ppm
58	10.71[b]	1-Butanone, 1-cyclohexyl-	$C_{10}H_{18}O$	154.1358	2a	+	1217	1215 (est)	792	832	$[M+H]^+$	155.1430 +3.5 ppm	$[M+H]^+$	155.1430 +2.8 ppm	$[M+NH_4]^+$	172.1696 +2.6 ppm
59	10.85	Cyclononanone	$C_9H_{16}O$	140.1201	4	-	1224	1252	733	792	$[M+H]^+$	141.1274 +4.9 ppm	$[M+H]^+$	141.1274 +4.1 ppm	$[M+NH_4]^+$	158.1539 +3.6 ppm
60	10.95	-	C_7H_7NS	137.0299	4	o	1230	-	-	-	$[M-H]^+$	136.0215 -2.1 ppm	$[M-H]^+$	136.0215 +2.3 ppm	-	-
61	11.00	-	$C_9H_{14}O$	138.1045	4	o	1233	-	-	-	$[M+H]^+$	139.1117 -2.1 ppm	$[M+H]^+$	139.1117 -2.1 ppm	$[M+H]^+$	139.1117 -3.0 ppm
62	11.26	1-Phenoxypropan-2-ol	$C_9H_{12}O_2$	152.0837	2a	+	1246	1251	879	951	$[M-H]^+$	151.0754 +2.6 ppm	$[M+H]^+$	151.0754 -6.2 ppm	$[M+NH_4]^+$	170.1176 +4.8 ppm
63	11.42	-	$C_{10}H_{16}O$	152.1201	4	+	1256	-	-	-	$[M+H]^+$	153.1274 1.3 ppm	$[M+H]^+$	153.1274 -2.1 ppm	$[M+H]^+$	153.1274 +2.2 ppm
64	11.47	Cyclohexene, 1-butyl-	$C_{10}H_{18}$	138.1409	4	+	1258	1001	685	704	$[M-H]^+$	137.1325 +4.0 ppm	$[M+H]^+$	139.1481 +4.5 ppm	-	-

	General information						Electron ionization data				Chemical ionization data					
No.	Retention time [min]	NIST name	Sum formula	Molar exact mass [Da]	Identification level	Peak size	Obtained RI	Database RI	Match	Reversed Match	Molecular ion in $[N_2H]^+/[N_4H]^+$	Exact mass ± mass acc. error $[N_2H]^+/[N_4H]^+$	Molecular ion in $[H_3O]^+$	Exact mass ± mass acc. error $[H_3O]^+$	Molecular ion in $[NH_4]^+$	Exact mass ± mass acc. error $[NH_4]^+$
65	11.53[c]	Cyclopentacarboxylic acid, pentyl ester	$C_{11}H_{20}O_2$	184.1463	2b	+	1262	-	801	844	$[M-H]^+$	183.1380 +0.4 ppm	$[M+H]^+$	185.1536 -2.3 ppm	$[M+NH_4]^+$	202.1802 +0.7 ppm
66	11.57	Isoquinoline	C_9H_7N	129.0578	2a	o	1264	1261	818	930	$[M+H]^+$	130.0651 -1.0 ppm	$[M+H]^+$	130.0651 +0.1 ppm	$[M+H]^+$	130.0651 +0.2 ppm
67	11.70[ac]	5-ethyl-4,4,5-trimethyloxolan-2-one	$C_9H_{16}O_2$	156.1150	2b	+	1271	-	864	889	$[M+H]^+$	157.1223 +1.3 ppm	$[M+H]^+$	157.1223 +1.2 ppm	$[M+NH_4]^+$	174.1489 +3.8 ppm
68	11.74	-	$C_{10}H_{16}O$	152.1201	4	-	1274	-	-	-	$[M-H]^+$	151.1117 -0.4 ppm	$[M+H]^+$	153.1274 -4.1 ppm	$[M+H]^+$	153.1274 +2.5 ppm
69	11.81	Carbonimidodithioic acid, methyl-, dimethyl ester	$C_4H_9NS_2$	135.0176	3	+	1277	1282	677	738	$[M+H]^+$	136.0249 -1.4 ppm	$[M+H]^+$	136.0249 +3.2 ppm	$[M+H]^+$	136.0249 -2.5 ppm
70	12.09	-	$C_9H_{17}O_2$	156.1150	4	-	1293	-	-	-	$[M+H]^+$	157.1223 +10.2 ppm	$[M+H]^+$	157.1223 +11.7 ppm	$[M+NH4]^+$	174.1475 + 2.1 ppm
71	12.10	-	$C_{10}H_{16}O$	152.1201	4	-	1293	-	-	-	$[M+H]^+$	153.1274 +1.9 ppm	$[M+H]^+$	153.1274 +7.4 ppm	$[M+H]^+$	153.1274 +3.6 ppm
72	12.21	cis-Hexahydrophthalide	$C_8H_{12}O_2$	140.0837	3	+	1299	1355 (est)	837	897	$[M-H]^+$	139.0754 -3.3 ppm	$[M+H]^+$	141.0910 +2.1 ppm	$[M+NH_4]^+$	158.1176 +2.3 ppm
73	12.23	Naphthalene, 2-methyl-	$C_{11}H_{10}$	142.0783	2a	-	1300	1297	892	910	$[M+H]^+$	143.0855 +4.4 ppm	$[M+H]^+$	143.0855 +2.0 ppm	$[M+H]^+$	143.0855 +11.8 ppm
74	12.43	1,1'-Bicyclohexyl	$C_{12}H_{22}$	166.1722	3	-	1310	1301	756	848	$[M-H]^+$	165.1638 +7.8 ppm	-	-	-	-

	General information						Electron ionization data				Chemical ionization data					
No.	Retention time [min]	NIST name	Sum formula	Molar exact mass [Da]	Identification level	Peak size	Obtained RI	Database RI	Match	Reversed Match	Molecular ion in $[N_2H]^+/[N_4H]^+$	Exact mass ± mass acc. error $[N_2H]^+/[N_4H]^+$	Molecular ion in $[H_3O]^+$	Exact mass ± mass acc. error $[H_3O]^+$	Molecular ion in $[NH_4]^+$	Exact mass ± mass acc. error $[NH_4]^+$
75	12.56	Cyclododecene	$C_{12}H_{22}$	166.1722	3	+	1316	1306	909	947	$[M-H]^+$	165.1638 +13.2 ppm	$[M+H]^+$	167.1794 +6.7 ppm	-	-
76	12.57	1H-Indene, 1-ethylidene-	$C_{11}H_{10}$	142.0783	2a	o	1317	1315	847	890	$[M+H]^+$	143.0855 +1.1 ppm	$[M+H]^+$	143.0855 -1.6 ppm	-	-
77	12.63	-	$C_{10}H_{18}O$	154.1358	4	-	1320	-	-	-	$[M+H]^+$	155.1430 +1.7 ppm	$[M+H]^+$	155.1430 -1.4 ppm	$[M+NH_4]^+$	172.1696 +14.8 ppm
78	12.87	Cyclododecane	$C_{12}H_{24}$	168.1878	2a	+	1332	1330	931	938	$[M-H]^+$	167.1794 -1.8 ppm	$[M+H]^+$	169.1951 +2.4 ppm	$[M+NH_4]^+$	186.2216 +4.7 ppm
79	13.02	1,4-Ethanonaphthalene, 1,2,3,4-tetrahydro-	$C_{12}H_{14}$	158.1095	3	o	1339	1374 (est)	779	861	$[M+H]^+$	159.1168 -0.0 ppm	-	-	-	-
80	13.13	5,6,7,8,9,10-Hexahydrobenzocyclooctene	$C_{12}H_{16}$	160.1252	2a	+	1344	1364 (est)	888	918	$[M-H]^+$	159.1168 +2.0 ppm	$[M+H]^+$	161.1325 -0.5 ppm	-	-
81	13.26	1(3H)-Isobenzofuranone	$C_8H_6O_2$	134.0368	2a	o	1351	1350 (est)	831	930	$[M+H]^+$	135.0441 +4 ppm	$[M+H]^+$	135.0441 +0.9 ppm	$[M+NH_4]^+$	152.0706 +2 ppm
82	13.59	-	$C_{11}H_{13}N$	159.1048	4	-	1367	-	-	-	$[M+H]^+$	160.1121 -3.2 ppm	$[M+H]^+$	160.1121 +1.0 ppm	$[M+H]^+$	160.1094 -2.7 ppm
83	13.83	Naphthalene, 5-ethyl-1,2,3,4-tetrahydro-	$C_{12}H_{16}$	160.1252	3	-	1379	1362	697	777	$[M+H]^+$	161.1325 -2 ppm	$[M+H]^+$	161.1325 +10.4 ppm	-	-
84	13.91	Biphenyl	$C_{12}H_{10}$	154.0783	2a	+	1383	1381	887	937	$[M+H]^+$	155.0855 +5 ppm	$[M+H]^+$	155.0855 +0.9 ppm	-	-
85	14.21	Phenol, 4-(1,1-	$C_{11}H_{16}O$	164.1201	2a	+	1398	1400	894	923	$[M+H]^+$	165.1274 +2.9 ppm	$[M+H]^+$	165.1274 +3.9 ppm	-	-

	General information						Electron ionization data				Chemical ionization data					
No.	Retention time [min]	NIST name	Sum formula	Molar exact mass [Da]	Identification level	Peak size	Obtained RI	Database RI	Match	Reversed Match	Molecular ion in $[N_2H]^+/[N_4H]^+$	Exact mass ± mass acc. error $[N_2H]^+/[N_4H]^+$	Molecular ion in $[H_3O]^+$	Exact mass ± mass acc. error $[H_3O]^+$	Molecular ion in $[NH_4]^+$	Exact mass ± mass acc. error $[NH_4]^+$
		dimethylpropyl)-														
86	14.26	Tetradecane	$C_{14}H_{30}$	198.2348	1	+	1400	1400	809	900	$[M-H]^+$	197.2255 +4.2 ppm	-	-	-	-
87	14.40	Quinoline, 2,3-dimethyl-	$C_{11}H_{11}N$	157.0891	4	-	1407	1435	489	739	$[M+H]^+$	158.0964 +1.0 ppm	$[M+H]^+$	158.0964 +3.3 ppm	$[M+H]^+$	158.0964 -4.8 ppm
88	14.57	Cycloundecanone	$C_{11}H_{24}O$	168.1514	4	o	1415	1486	827	851	$[M+H]^+$	169.1587 -3.6 ppm	$[M+H]^+$	169.1587 -0.3 ppm	$[M+NH_4]^+$	186.1852 -1.7 ppm
89	14.69	1(2H)-Naphthalenone, octahydro-3,8a-dimethyl-, (3α,4aβ,8aα)-	$C_{12}H_{20}O$	180.1150	4	+	1420	1449 (est)	751	788	$[M+H]^+$	181.1587 +1.0 ppm	$[M+H]^+$	181.1587 +4.0 ppm	$[M+H]^+$	181.1587 +0.9 ppm
90	14.76	Naphthalene, 1, 7-dimethyl-	$C_{12}H_{12}$	156.0939	2a	-	1423	1419	681	882	$[M+H]^+$	157.1012 -0.9 ppm	$[M+H]^+$	157.1012 -7.5 ppm	-	-
91	14.81	-	$C_8H_{10}O_2$	138.0692	4	-	1426	-	-	-	$[M+H]^+$	139.0754 +3.1 ppm	$[M+H]^+$	139.0765 -0.1 ppm	$[M+H]^+$	156.1019 -2.8 ppm
92	14.95	-	$C_{12}H_{17}N$	175.1361	4	-	1432	-	-	-	$[M+H]^+$	176.1441 -4.4 ppm	$[M+H]^+$	176.1441 +1.0 ppm	$[M+H]^+$	176.1441 +5.5 ppm
93	15.17	Naphthalene, 1,5-dimethyl-	$C_{12}H_{12}$	156.0939	2a	-	1442	1440	813	847	$[M+H]^+$	157.1012 +0.7 ppm	$[M+H]^+$	157.1012 +7.3 ppm	-	-
94	15.27	-	$C_{11}H_{20}O_2$	184.1463	4	-	1447	-	-	-	$[M+H]^+$	185.1536 +2.1 ppm	$[M+H]^+$	185.1536 +0.5 ppm	$[M+NH_4]^+$	202.1802 +2.2 ppm
95	15.28[c]	Cyclohexanone, 2 hexyl	$C_{12}H_{22}O$	182.1671	2b	o	1448	-	909	935	$[M+H]^+$	183.1743 -1.9 ppm	$[M+H]^+$	183.1743 -6.0 ppm	$[M+NH_4]^+$	200.2009 +1.3 ppm
96	15.39	(8R,8aS)-8,8a-	$C_{12}H_{18}O$	178.1358	2a	+	1452	1440	722	803	$[M+H]^+$	179.1430 +0.1 ppm	$[M+H]^+$	179.1430 +3.0 ppm	$[M+NH_4]^+$	196.1696 -2.9 ppm

	General information						Electron ionization data				Chemical ionization data					
No.	Retention time [min]	NIST name	Sum formula	Molar exact mass [Da]	Identification level	Peak size	Obtained RI	Database RI	Match	Reversed Match	Molecular ion in $[N_2H]^+/[N_4H]^+$	Exact mass ± mass acc. error $[N_2H]^+/[N_4H]^+$	Molecular ion in $[H_3O]^+$	Exact mass ± mass acc. error $[H_3O]^+$	Molecular ion in $[NH_4]^+$	Exact mass ± mass acc. error $[NH_4]^+$
		Dimethyl-3,4,6,7,8,8a-he-ahydronaphthalen-2(1H)-one														
97	15.46	Oxacyclododecan-2-one	$C_{11}H_{20}O_2$	184.1463	3	-	1456	1440	555	631	$[M+H]^+$	185.1536 -0.8 ppm	$[M+H]^+$	185.1536 +4.2 ppm	$[M+NH_4]^+$	202.1802 +1.3 ppm
98	15.67	2(1H)-Naphthalenone, octahydro-4a,5-dimethyl-, (4aα,5α,8aβ)-	$C_{12}H_{20}O$	180.1514	3	+	1465	1476 (est)	743	774	$[M-H]^+$	179.1430 +1.2 ppm	$[M+H]^+$	181.1587 +4.4 ppm	$[M+H]^+$	181.1587 +0.8 ppm
99	15.69	-	$C_{12}H_{20}O_2$	196.1463	4	+	1467	-	-	-	$[M-H]^+$	195.1380 +4.8 ppm	$[M-H]^+$	195.1380 +4.2 ppm	$[M+H]^+$	197.1536 +2.0 ppm
100	15.79	cis,trans-5,9-Cyclododecadiene-cis-1,2-diol	$C_{12}H_{20}O_2$	196.1463	4	+	1471	1718 (est)	610	634	$[M-H]^+$	195.1380 +0.7 ppm	$[M-H]^+$	195.1380 +1.6 ppm	$[M+H]^+$	197.1536 -2.1 ppm
101	15.84	2,6-Di-tert-butyl-4-hydroxy-4-methylcyclohexa-2,5-dien-1-one	$C_{15}H_{24}O_2$	236.1776	4	+	1474	1475	735	767	$[M-H]^+$	235.1693 +2.8 ppm	$[M+H]^+$	237.1847 +1.4 ppm	$[M+H]^+$	237.1847 -2.1 ppm
102	15.99	-	$C_{12}H_{21}N$	179.1674	5	+	1480	-	-	-	$[M+H]^+$	180.1747 +0.2 ppm	$[M+H]^+$	180.1747 +1.3 ppm	$[M+H]^+$	180.1720 +9.1 ppm
103	16.12	12-Methyl-oxa-	$C_{12}H_{20}O_2$	196.1463	4	-	1487	1512 (est)	679	698	$[M-H]^+$	195.1380 +4.8 ppm	$[M-H]^+$	195.1380 +0.2 ppm	$[M+H]^+$	197.1536 +2.8 ppm

	General information						Electron ionization data				Chemical ionization data					
No.	Retention time [min]	NIST name	Sum formula	Molar exact mass [Da]	Identification level	Peak size	Obtained RI	Database RI	Match	Reversed Match	Molecular ion in $[N_2H]^+/[N_4H]^+$	Exact mass ± mass acc. error $[N_2H]^+/[N_4H]^+$	Molecular ion in $[H_3O]^+$	Exact mass ± mass acc. error $[H_3O]^+$	Molecular ion in $[NH_4]^+$	Exact mass ± mass acc. error $[NH_4]^+$
		cyclododec-6-en-2-one														
104	16.14	Acenaphthene	$C_{12}H_{10}$	154.0783	1	+	1487	1482	811	891	$[M+H]^+$	155.0855 +1.3 ppm	$[M+H]^+$	155.0855 +0.1 ppm	-	-
105	16.41	Pentadecane	$C_{15}H_{32}$	212.2504	1	-	1500	1500	678	794	$[M-H]^+$	211.2420 -1.3 ppm	$[M-H]^+$	211.2420 +11.2 ppm	-	-
106	16.49[c]	Cyclohexanone, 3-(5-oxobutyl)-	$C_{12}H_{20}O_2$	196.1463	2b	o	1504	-	905	910	$[M+H]^+$	197.1536 -3.3 ppm	$[M+H]^+$	197.1536 -0.7 ppm	$[M+NH_4]^+$	214.1802 +2.7 ppm
107	16.64	Cyclododecane, 1,2-epoxy-	$C_{12}H_{22}O$	182.1671	3	+	1510	1475 (est)	888	891	$[M+H]^+$	183.1743 +0.2 ppm	$[M+H]^+$	183.1743 +0.1 ppm	$[M+NH_4]^+$	200.2009 +2.5 ppm
108	16.68*	2,4-Di-tert-butylphenol	$C_{14}H_{22}O$	206.1671	2a	+	1513	1514	798	823	$[M-H]^+$	205.1587 +4.3 ppm	$[M-H]^+$	205.1587 +3.3 ppm	-	-
109	16.70	Cyclododecanone	$C_{12}H_{22}O$	182.1671	2a	o	1514	1524	879	892	$[M+H]^+$	183.1743 +0.8 ppm	$[M+H]^+$	183.1743 -2.0 ppm	$[M+NH_4]^+$	200.2009 +4.1 ppm
110	16.75*	Phenol, 2,6-bis(1,1-dimethylethyl)-4-methyl-	$C_{15}H_{24}O$	220.1827	2a	o	1516	1516	758	808	$[M-H]^+$	219.1743 +2.7 ppm	$[M+H]^+$	221.1900 +4.2 ppm	$[M]^+$	220.1822 -0.3 ppm
111	16.80	Spiro[5.6]dodecan-7-one	$C_{12}H_{20}O$	180.1514	2a	+	1518	1523 (est)	844	845	$[M+H]^+$	181.1587 -4.5 ppm	$[M+H]^+$	181.1587 -3.4 ppm	$[M+NH_4]^+$	198.1852 +5.9 ppm
112	17.06	Benzene, 1-methyl-3-(phenylmethyl)-	$C_{14}H_{14}$	182.1096	3	-	1530	1571	861	892	$[M-H]^+$	181.1012 -7.9 ppm	-	-	$[M]^+$	182.1090 -0.9 ppm
113	17.14	Benzene, 1-methyl-2-(phenylmethyl)-	$C_{14}H_{14}$	182.1096	3	+	1534	1570	923	924	$[M-H]^+$	181.1012 -3.8 ppm	-	-	$[M+NH_4]^+$	200.1434 -12.4 ppm

	General information						Electron ionization data				Chemical ionization data					
No.	Retention time [min]	NIST name	Sum formula	Molar exact mass [Da]	Identification level	Peak size	Obtained RI	Database RI	Match	Reversed Match	Molecular ion in $[N_2H]^+/[N_4H]^+$	Exact mass ± mass acc. error $[N_2H]^+/[N_4H]^+$	Molecular ion in $[H_3O]^+$	Exact mass ± mass acc. error $[H_3O]^+$	Molecular ion in $[NH_4]^+$	Exact mass ± mass acc. error $[NH_4]^+$
114	17.19	Cyclododecane, 1,2-epoxy-	$C_{12}H_{22}O$	182.1671	3	+	1536	1576 (est)	876	876	$[M-H]^+$	181.1587 +1.7 ppm	$[M+H]^+$	183.1743 +0.8 ppm	$[M+NH_4]^+$	200.2009 +2.4 ppm
115	17.20*	1(2H)-Naphthalenone, 3,4-dihydro-5,8-dimethyl-	$C_{12}H_{14}O$	174.1045	3	-	1536	1564 (est)	757	831	$[M-H]^+$	173.0961 +3.1 ppm	$[M+H]^+$	175.1117 +6.2 ppm	$[M+NH_4]^+$	192.1383 -4.5 ppm
116	17.25	Benzene, (1-butylhexyl)-	$C_{16}H_{26}$	218.2035	3	+	1539	1535	849	858	-	-	-	-	-	-
117	17.31[a]	Benzene, 1-methyl-3-(phenylmethyl)-	$C_{14}H_{14}$	182.1096	3	+	1541	1571	916	917	$[M-H]^+$	181.1012 +3.1 ppm	$[M-H]^+$	181.1012 +0.4 ppm	$[M+NH_4]^+$	200.1434 +4.7 ppm
118	17.35	Spiro[5.6]dodecan-7-one (Isomer 1)	$C_{12}H_{20}O$	180.1514	4	+	1543	1525 (est)	747	758	$[M-H]^+$	179.1430 +0.4 ppm	$[M+H]^+$	181.158 -3.3 ppm	$[M+NH_4]^+$	198.1852 +6.9 ppm
119	17.43	Benzene, (1-propylheptyl)-	$C_{16}H_{26}$	218.2035	2a	+	1547	1546	870	895	$[M-H]^+$	217.1951 +4.7 ppm	-	-	-	-
120	17.51	2H-Benzocyclohepten-2-one, decahydro-9a-methyl-, trans- (Isomer 2)	$C_{12}H_{20}O$	180.1514	3	+	1551	1544 (est)	689	742	$[M-H]^+$	179.1430 +3.0 ppm	$[M+H]^+$	181.1587 -2.7 ppm	$[M+NH_4]^+$	198.1852 -0.2 ppm
121	17.64	-	$C_{12}H_{12}O$	172.0888	4	-	1557	-	-	-	$[M+H]^+$	173.0961 +4.7 ppm	$[M+H]^+$	173.0961 -4.8 ppm	$[M+NH_4]^+$	190.1226 -1.2 ppm

	General information						Electron ionization data				Chemical ionization data					
No.	Retention time [min]	NIST name	Sum formula	Molar exact mass [Da]	Identification level	Peak size	Obtained RI	Database RI	Match	Reversed Match	Molecular ion in $[N_2H]^+/[N_4H]^+$	Exact mass ± mass acc. error $[N_2H]^+/[N_4H]^+$	Molecular ion in $[H_3O]^+$	Exact mass ± mass acc. error $[H_3O]^+$	Molecular ion in $[NH_4]^+$	Exact mass ± mass acc. error $[NH_4]^+$
122	17.83	Benzene, (1-ethyloctyl)-	$C_{16}H_{26}$	218.2035	3	+	1565	1568	857	894	-	-	-	-	-	-
123	17.92*	2H-Benzocyclohepten-2-one, decahydro-4a-methyl-, trans-	$C_{12}H_{20}O$	180.1514	2a	+	1570	1526 (est)	724	802	$[M+H]^+$	181.1587 +4.8 ppm	$[M+H]^+$	181.1587 -3.8 ppm	$[M+NH_4]^+$	198.1852 -1.0 ppm
124	18.22	Fluorene	$C_{13}H_{10}$	166.0783	1	o	1584	1583	813	850	$[M+H]^+$	167.0855 +3.4 ppm	$[M+H]^+$	167.0855 -1.6 ppm	-	-
125	18.28	-	$C_{12}H_{18}O_2$	194.1307	4	o	1586	-	-	-	$[M+H]^+$	195.1380 -1.7 ppm	$[M+H]^+$	195.1380 -3.3 ppm	$[M+H]^+$	195.1380 +4.0 ppm
126	18.34	Ketone	$C_{12}H_{18}O$	178.1358	3	o	1589	1569	695	749	$[M+H]^+$	179.1430 +0.4 ppm	$[M+H]^+$	179.1430 -2.3 ppm	$[M+NH_4]^+$	196.1696 +0.0 ppm
127	18.50	-	$C_{12}H_{18}O$	178.1358	4	-	1596	-	-	-	$[M+H]^+$	179.1430 +0.4 ppm	$[M+H]^+$	179.1430 +0.5 ppm	$[M+NH_4]^+$	196.1696 -3.1 ppm
128	18.57	-	$C_{16}H_{34}$	226.2661	5	-	1599	1572	694	716	$[M-H]^+$	225.2577 +14.1 ppm	$[M-H]^+$	225.2577 +12.3 ppm	-	-
129	18.61	Benzene, (1-methylnonyl)-	$C_{16}H_{26}$	218.2035	3	-	1601	1616	926	929	$[M-H]^+$	217.1951 +8.0 ppm	-	-	-	-
130	18.80	-	$C_{12}H_{18}O$	178.1358	4	-	1611	-	-	-	$[M+H]^+$	179.1430 -6.0 ppm	$[M+H]^+$	179.1430 +2.2 ppm	$[M+H]^+$	179.1430 +5.5 ppm
131	19.24*	Benzophenone	$C_{13}H_{10}O$	182.0732	2a	o	1631	1635	769	938	$[M+H]^+$	183.0804 +0.7 ppm	$[M+H]^+$	183.0804 -4.3 ppm	$[M+NH_4]^+$	200.1056 -2.6 ppm
132	19.29	Benzene, (1-pentylhexyl)-	$C_{17}H_{28}$	232.2191	2a	-	1633	1628	905	908	$[M-H]^+$	231.2107 +2.9 ppm	$[M-H]^+$	231.2107 -0.7 ppm	$[M+NH_4]^+$	250.2529 +1.2 ppm

	General information						Electron ionization data				Chemical ionization data					
No.	Retention time [min]	NIST name	Sum formula	Molar exact mass [Da]	Identification level	Peak size	Obtained RI	Database RI	Match	Reversed Match	Molecular ion in $[N_2H]^+/[N_4H]^+$	Exact mass ± mass acc. error $[N_2H]^+/[N_4H]^+$	Molecular ion in $[H_3O]^+$	Exact mass ± mass acc. error $[H_3O]^+$	Molecular ion in $[NH_4]^+$	Exact mass ± mass acc. error $[NH_4]^+$
133	19.36	Benzene, (1-butylheptyl)-	$C_{17}H_{28}$	232.2191	2a	-	1637	1632	933	938	$[M-H]^+$	231.2107 +4.6 ppm	$[M-H]^+$	231.2107 +4.8 ppm	$[M+NH_4]^+$	250.2529 -4.1 ppm
134	19.51	1,4-Cyclododecanedione (Isomer 1)	$C_{12}H_{20}O_2$	196.1463	3	-	1643	1764 (est)	809	812	$[M+H]^+$	197.1536 +1.3 ppm	$[M+H]^+$	197.1536 -2.0 ppm	$[M+NH_4]^+$	214.1802 +1.4 ppm
135	19.57	Benzene, (1-propyloctyl)-	$C_{17}H_{28}$	232.2191	2a	-	1646	1643	900	905	$[M-H]^+$	231.2107 +2.9 ppm	$[M-H]^+$	231.2107 +2.4 ppm	$[M+NH_4]^+$	250.2529 +0.3 ppm
136	19.83	1,4-Cyclododecanedione (Isomer 2)	$C_{12}H_{20}O_2$	196.1463	3	+	1658	1764 (est)	753	760	$[M-H]^+$	195.1380 +0.2 ppm	$[M-H]^+$	195.1380 -4.5 ppm	$[M+NH_4]^+$	214.1802 +1.9 ppm
137	20.01	Benzene, (1-ethylnonyl)-	$C_{17}H_{28}$	232.2191	2a	-	1667	1670	904	904	$[M-H]^+$	231.2107 +1.2 ppm	$[M-H]^+$	231.2107 -0.6 ppm	$[M+NH_4]^+$	250.2529 +3.6 ppm
138	20.07	1,3,5-Triazine-2,4,6(1H,3H,5H)-trione, 1,3,5-tri-2-propenyl-	$C_{12}H_{15}N_3O_3$	249.1113	3	-	1670	1661	606	733	$[M+H]^+$	250.1186 -2.8 ppm	$[M+H]^+$	250.1186 +0.1 ppm	$[M+H]^+$	250.1186 +7.3 ppm
139	20.58	Dodecyl acrylate	$C_{15}H_{28}O_2$	240.2089	3	o	1693	1697	825	869	-	-	-	-	-	-
140	20.71*	Heptadecane	$C_{17}H_{36}$	240.2817	1	-	1700	1700	646	857	-	-	-	-	-	-
141	20.78	Benzene, (1-methyldecyl)-	$C_{17}H_{28}$	232.2191	2a	-	1704	1708	888	898	$[M-H]^+$	231.2107 +3.2 ppm	$[M-H]^+$	231.2107 +3.3 ppm	$[M+NH_4]^+$	250.2529 +14.9 ppm

	General information						Electron ionization data				Chemical ionization data					
No.	Retention time [min]	NIST name	Sum formula	Molar exact mass [Da]	Identification level	Peak size	Obtained RI	Database RI	Match	Reversed Match	Molecular ion in $[N_2H]^+/[N_4H]^+$	Exact mass ± mass acc. error $[N_2H]^+/[N_4H]^+$	Molecular ion in $[H_3O]^+$	Exact mass ± mass acc. error $[H_3O]^+$	Molecular ion in $[NH_4]^+$	Exact mass ± mass acc. error $[NH_4]^+$
142	20.95	Cyclododecanone, oxime	$C_{12}H_{23}NO$	197.1780	2a	+	1715	1721 (est)	891	896	$[M-H]^+$	198.1852 -2.1 ppm	$[M+H]^+$	198.1852 -1.8 ppm	$[M+H]^+$	198.1852 +1.0 ppm
143	21.27	Benzene, (1-pentylheptyl)-	$C_{18}H_{30}$	246.2348	2a	-	1735	1726	903	920	$[M-H]^+$	245.2264 +3.1 ppm	$[M-H]^+$	245.2264 5.2 ppm	$[M+NH_4]^+$	264.2686 +10.9 ppm
144	21.35	Benzene, (1-butyloctyl)-	$C_{18}H_{30}$	246.2348	2a	-	1740	1730	908	910	$[M-H]^+$	245.2264 -4.7 ppm	$[M-H]^+$	245.2264 +2.8 ppm	$[M+NH_4]^+$	264.2686 +5.5 ppm
145	21.45	Cyclododecanemethanol	$C_{13}H_{26}O$	198.1984	3	-	1747	1743	829	847	-	-	-	-	-	-
146	21.54	Benzene, (1-propylnonyl)-	$C_{18}H_{30}$	246.2348	2a	-	1752	1742	870	884	$[M-H]^+$	245.2264 +1.9 ppm	$[M-H]^+$	245.2264 -5.2 ppm	$[M+NH_4]^+$	264.2686 +4.5 ppm
147	21.86	Benzene, (1-ethyldecyl)-	$C_{18}H_{30}$	246.2348	2a	-	1773	1766	854	890	$[M-H]^+$	245.2264 +2.6 ppm	$[M-H]^+$	245.2264 -4.4 ppm	$[M+NH_4]^+$	264.2686 +2.1 ppm
148	22.00	Phenanthrene	$C_{14}H_{10}$	178.0783	1	o	1782	1776	830	941	$[M+H]^+$	179.0855 +1.4 ppm	$[M+H]^+$	179.0855 -4.0 ppm	-	-
149	22.07	Benzenesulfonamide, N-butyl-	$C_{10}H_{15}NO_2S$	213.0824	2a	+	1796	1786	885	892	$[M+H]^+$	214.0896 +3.4 ppm	$[M+H]^+$	214.0896 +4.6 ppm	$[M+NH_4]^+$	231.1162 +4.8 ppm
150	22.11	Azacyclotridecan-2-one	$C_{12}H_{23}NO$	197.1780	2a	+	1789	1782	911	926	[M+H]+	198.1852 +2.9 ppm	[M+H]+	198.1852 +1.6 ppm	[M+H]+	198.1852 -4.9 ppm
151	22.15	-	$C_{15}H_{28}O_2$	240.2089	4	+	1791	-	-	-	$[M+H]^+$	241.2162 +2.6 ppm	$[M+H]^+$	241.2162 -1.5 ppm	$[M+NH_4]^+$	258.2428 -3.0 ppm
152	22.21	-	$C_{15}H_{28}O_2$	240.2089	4	o	1795	-	-	-	$[M+H]^+$	241.2162 +3.3 ppm	$[M+H]^+$	241.2162 +2.2 ppm	$[M+NH_4]^+$	258.2428 -0.8 ppm
153	22.33	-	$C_{12}H_{21}NO_2$	211.1572	4	+	-	-	-	-	$[M+H]^+$	212.1645 -2 ppm	$[M+H]^+$	212.1645 +4.9 ppm	$[M+NH_4]^+$	299.1911 +3.6 ppm

	General information						Electron ionization data				Chemical ionization data					
No.	Retention time [min]	NIST name	Sum formula	Molar exact mass [Da]	Identification level	Peak size	Obtained RI	Database RI	Match	Reversed Match	Molecular ion in $[N_2H]^+/[N_4H]^+$	Exact mass ± mass acc. error $[N_2H]^+/[N_4H]^+$	Molecular ion in $[H_3O]^+$	Exact mass ± mass acc. error $[H_3O]^+$	Molecular ion in $[NH_4]^+$	Exact mass ± mass acc. error $[NH_4]^+$
154	22.40[b]	-	$C_{15}H_{28}O_2$	240.2089	4	+	1809	-	-	-	$[M+H]^+$	241.2162 -0.0 ppm	$[M+H]^+$	241.2162 -1.4 ppm	$[M+NH_4]^+$	258.2428 -0.4 ppm
155	22.40[b]	Benzene, (1-methylundecyl)-	$C_{18}H_{30}$	246.2348	2a	+	1809	1808	809	877	$[M-H]^+$	245.2264 -3 ppm	$[M-H]^+$	245.2264 +1.6 ppm	$[M+NH_4]^+$	264.2686 -0.8 ppm
156	22.51[a]	-	$C_{15}H_{28}O_2$	240.2089	4	+	1818	-	-	-	$[M+H]^+$	241.2162 +0.1 ppm	$[M+H]^+$	241.2162 +2.1 ppm	$[M+NH_4]^+$	258.2428 -5.3 ppm
157	22.64*	3,4'-Diisopropyl biphenyl (Isomer 1)	$C_{18}H_{22}$	238.1722	4	o	1829	1921	671	767	$[M+H]^+$	239.1794 -0.5 ppm	$[M+H]^+$	239.1794 -0.0 ppm	-	-
158	22.66*	Benzene, (1-pentyloctyl)-	$C_{19}H_{32}$	260.2504	2a	+	1819	1830	789	809	$[M-H]^+$	259.2420 -3.9 ppm	$[M-H]^+$	259.2420 +4.0 ppm	-	-
159	22.74	Benzene, (1-butylnonyl)-	$C_{19}H_{32}$	260.2504	2a	o	1826	1838	843	888	$[M-H]^+$	259.2420 +2.5 ppm	$[M-H]^+$	259.2420 +3.1 ppm	-	-
160	22.89	Benzene, (1-propyldecyl)-	$C_{19}H_{32}$	260.2504	2a	o	1851	1840	803	836	$[M-H]^+$	259.2420 -3.9 ppm	$[M-H]^+$	259.2420 +0.1 ppm	-	-
161	23.05	Diisopropy biphenyl (Isomere 2)	$C_{18}H_{22}$	238.1722	2a	o	1864	1859 (est)	803	864	$[M+H]^+$	239.1794 +2.5 ppm	$[M+H]^+$	239.1794 +4.7 ppm	-	-
162	23.17	Benzene, (1-ethylundecyl)-	$C_{19}H_{32}$	260.2504	4	-	1874	1865	788	799	$[M-H]^+$	259.2420 +7.2 ppm	$[M-H]^+$	259.2420 +31.2 ppm	-	-
163	23.59	3,4-Diisopropyl biphenyl (Isomer 3)	$C_{18}H_{22}$	238.1722	2a	o	1911	1921	838	852	$[M+H]^+$	239.1793 +0.5 ppm	$[M+H]^+$	238.1794 -3.4 ppm	-	-

	General information						Electron ionization data				Chemical ionization data					
No.	Retention time [min]	NIST name	Sum formula	Molar exact mass [Da]	Identification level	Peak size	Obtained RI	Database RI	Match	Reversed Match	Molecular ion in $[N_2H]^+/[N_4H]^+$	Exact mass ± mass acc. error $[N_2H]^+/[N_4H]^+$	Molecular ion in $[H_3O]^+$	Exact mass ± mass acc. error $[H_3O]^+$	Molecular ion in $[NH_4]^+$	Exact mass ± mass acc. error $[NH_4]^+$
164	23.62	Benzene, (1-methyldodecyl)-	$C_{19}H_{32}$	260.2504	2a	o	1913	1916	808	859	$[M-H]^+$	259.2420 +1.8 ppm	-	-	-	-
165	23.80	Diphenyl sulfone	$C_{12}H_{10}O_2S$	218.0402	4	o	1931	1926	546	686	-	-	-	-	-	-
166	23.98	4,4'-Diisopropyl biphenyl	$C_{18}H_{22}$	238.1722	2a	o	1948	1963	853	898	$[M+H]^+$	239.1794 -3 ppm	$[M+H]^+$	239.1794 +7.7 ppm	-	-
167	24.90	Chromone, 5-hydroxy-8-isopentyl-7-methoxy-2-methyl-	$C_{16}H_{20}O_4$	276.1362	2a	o	2037	2255 (est)	453	827	$[M+H]^+$	277.1434 +9.7 ppm	$[M+H]^+$	277.1434 +1.9 ppm	-	-
168	27.28	Benzene, 1-phenylmethyl), 4-methyl-(phenyldimethyl)-	$C_{21}H_{20}$	272.1565	2a	-	2300	2294 (est)	903	939	$[M-H]^+$	271.1481 -0.4 ppm	$[M+H]^+$	273.1638 +3.0 ppm	$[M+NH_4]^+$	290.1903 -4.0 ppm

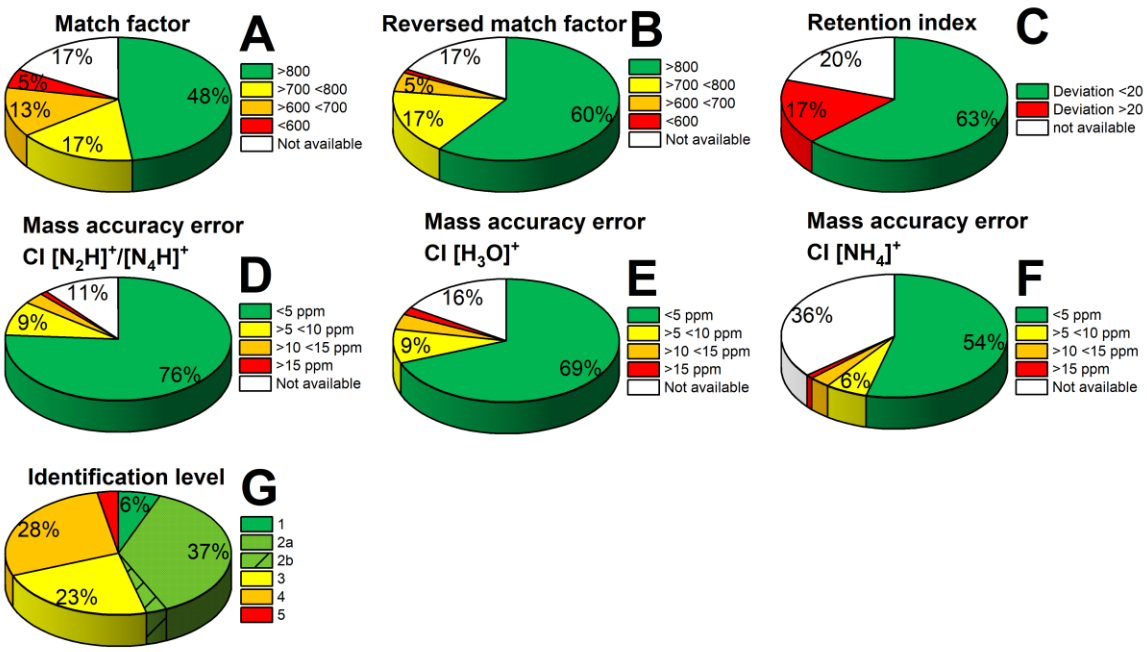

Figure 9.11 Cake plots with the percentual distribution of the identification parameters quality with match factor (A), reversed match factor (B), retention index (C), mass accuracy errors of CI reagent ions $[N_2H]^+/[N_4H]^+$ (D), $[H_3O]^+$ (E) and $[NH_4]^+$ (F) and the identification levels according to [203] (G).

9.1.4.6 Partitioning constants of found substances

The following equations were used for the calculation of partitioning constants between air and water K_{aw} and octanol and water K_{ow} by the online database for polyparameter linear free energy relationships (pp-LFERs) from the UFZ Helmholtz Centre for Environmental Research [135]. The pp-LFER descriptors were polarizability/dipolarity S, solute hydrogen bond acidity A, solute hydrogen bond basicity B; McGowan's molar volume V, logarithmic gas-hexane partition coefficient L and excess molar refraction E. [216]

$$\log K_{wa} = -0.99 + 2.55\,S + 3.81\,A + 4.84\,B - 0.87\,V + 0.58\,E \qquad 13$$

$$\log K_{ow} = -0.09 - 1.05\,S + 0.03\,A - 3.46\,B + 3.81\,V + 0.56\,E \qquad 14$$

Table 9.22 Partitioning constants $log\,K_{wa}$ and $log\,K_{0w}$ and LSER descriptors were taken from the database of the UFZ Helmholtz Centre for Environmental Research [135]. S: polarizability/dipolarity; A: solute hydrogen bond acidity; B: solute hydrogen bond basicity; V: McGowan's molar volume; L: logarithmic gas-hexane partition coefficient; E: excess molar refraction.

Compound	S	A	B	V	L	E	$\log K_{wa}$ (25 °C)	$\log K_{ow}$ (25 °C)
Phenylethyne	0.58	0.12	0.24	0.9122	3.692	0.68	1.71	2.51
2,6-Lutidine	0.70	0.00	0.62	0.9571	3.760	0.61	3.32	1.20
Cyclohexanol	0.54	0.32	0.57	0.9041	3.758	0.46	3.85	1.27

Compound	S	A	B	V	L	E	$\log K_{wa}$ (25 °C)	$\log K_{ow}$ (25 °C)
2-Heptanone	0.68	0.00	0.51	1.1106	3.760	0.12	2.32	1.91
Cyclohexanone	0.86	0.00	0.56	0.8611	3.792	0.4	3.40	0.76
Cyclohexane, (1-methylethyl)-	0.07	0.00	0.00	1.2681	4.292	0.28	-1.75	5.01
2-Heptanone, 3-methyl-	0.66	0.00	0.51	1.2515	4.218	0.11	2.14	2.47
Pyridine, 2,5-dimethyl-	0.74	0.00	0.62	0.9571	3.986	0.63	3.43	1.17
3-Heptanone, 5-methyl-	0.65	0.00	0.52	1.2515	4.089	0.11	2.16	2.44
2-Octanone	0.68	0.00	0.51	1.2515	4.257	0.11	2.19	2.44
Cycloheptanone	0.86	0.00	0.56	1.002	4.376	0.44	3.30	1.32
Indene	0.77	0.00	0.20	0.9875	4.559	1.00	1.66	2.92
Benzaldehyde, 3-methyl-	0.97	0.00	0.42	1.0139	4.548	0.84	3.12	1.96
Benzenemethanol, α,α-dimethyl-	0.85	0.32	0.65	1.1978	4.520	0.85	4.99	2.00
Undecane	0.00	0.00	0.00	1.6585	5.191	0.00	-2.43	6.41
Methyl 2-fluorobenzoate	0.89	0.00	0.46	1.0903	4.719	0.58	2.89	2.05
Cyclooctanone	0.86	0.00	0.56	1.1429	4.981	0.47	3.19	1.87
Benzene, 1,4-bis(1-methylethyl)-	0.47	0.00	0.20	1.5618	5.315	0.62	0.18	5.21
Naphthalene	0.92	0.00	0.20	1.0854	5.161	1.34	2.16	3.32
Cyclononanone	0.86	0.00	0.56	1.2838	5.537	0.49	3.08	2.42
Isoquinoline	1.00	0.00	0.54	1.0443	5.595	1.21	3.97	1.83
Naphthalene, 2-methyl-	0.90	0.00	0.20	1.2263	5.743	1.22	1.91	3.81
1,1'-Bicyclohexyl	0.45	0.00	0.04	1.5822	6.047	0.52	-0.72	5.80
Cyclododecane	0.10	0.00	0.00	1.6908	6.190	0.56	-1.88	6.75
1(3H)-Isobenzofuranone	1.84	0.00	0.45	0.964	5.390	0.95	5.59	0.81
Biphenyl	0.99	0.00	0.26	1.3242	6.014	1.36	2.43	3.96
Phenol, 4-(1,1-dimethylpropyl)-	0.89	0.56	0.42	1.4796	6.200	0.81	4.63	3.82
Tetradecane	0.00	0.00	0.00	2.0812	6.705	0.00	-2.80	8.03
Quinoline, 2,3-dimethyl-	1.01	0.00	0.56	1.3261	6.330	1.33	3.91	2.90
Naphthalene, 1,5-dimethyl-	1.05	0.00	0.18	1.3672	6.545	1.40	2.18	4.36
Acenaphthene	1.04	0.00	0.20	1.2586	6.469	1.60	2.46	4.00
Pentadecane	0.00	0.00	0.00	2.2221	7.209	0.00	-2.92	8.56
2,4-Di-tert-butylphenol	0.90	0.45	0.50	1.9023	7.879	0.83	4.27	5.15
Cyclododecanone	0.86	0.00	0.56	1.7065	7.222	0.59	2.77	4.09
Benzene, 1-methyl-3-(phenylmethyl)-	1.01	0.00	0.33	1.606	6.771	1.22	2.49	4.70
Benzene, 1-methyl-2-(phenylmethyl)-	1.01	0.00	0.33	1.606	6.812	1.22	2.49	4.70
Fluorene	1.03	0.00	0.20	1.3565	6.922	1.59	2.35	4.38
Benzophenone	1.50	0.00	0.50	1.4808	6.955	1.45	4.81	3.25
Dodecyl acrylate	0.62	0.00	0.42	2.2535	7.675	0.14	0.75	6.66
Heptadecane	0.00	0.00	0.00	2.5039	8.218	0.00	-3.17	9.64
Phenanthrene	1.29	0.00	0.29	1.4544	7.632	2.06	3.63	4.43
Diphenyl sulfone	2.10	0.00	0.71	1.6051	8.65	1.57	7.32	2.43
Dodecane	0.00	0.00	0.00	1.7994	5.696	0.00	-2.55	6.95

9.2 List of abbreviations

Table 9.23 List of abbreviations used in this work.

Abbreviation	Definition
AGREE	Analytical GREEnness Metric Approach
AGREEprep	Analytical GREEnness Metric Approach for sample preparation
CE	Collision energy
CI	Chemical ionization
CWR	Carbon wide range
DLLME	Dispersive liquid-liquid microextraction
DOE	Design of experiment
DVB	Divinylbenzene
EEG	ger: Erneuerbare-Energien-Gesetz, eng: Renewable Energy Sources Act
EI	Electron ionization
EME	Electromembrane extraction
ESI	Electron spray ionization
FA	Fatty acid
FAME	Fatty acid methyl ester
FID	Flame ionization detector
GAC	Green analytical chemistry
GAPI	Green Analytical Procedure Index
GC	Gas chromatography
HF-LPME	Hollow-fiber liquid-phase microextraction
HLB	Hydrophilic-lipophilic balance
HPLC	High-performance liquid-chromatography
HRMS	High-resolution mass spectrometry
ISO	International Organization for Standardization
ITEX	In-tube extraction
ITEX-DHS	In-tube extraction dynamic headspace
LC	Liquid chromatography
LE	Liquid extraction
LLE	Liquid-liquid extraction
LPME	Liquid-phase microextraction
(pp-)LSER	(Poly parameter) linear solvation energy relationship
MDL	Method detection limit
MD-LPME	Microfluidic device liquid-phase microextraction
MEPS	Microextraction by packed sorbent
MS	Mass spectrometry
MS/MS	Tandem mass spectrometry
MRM	Multiple reaction monitoring
NEMI	National Environmental Method Index
NTA	Non-target analysis
NTD	Needle-trap device
NTE	Needle-trap extraction
OFAT	One-factor-at-a-time
PA	Polyacrylate
PALME	parallel artificial liquid membrane extraction
PBT	Persistent Bioaccumulative Toxic
PDMS	Polydimethylsiloxane
pp-LFER	Polyparameter linear free energy relationships
RGB	Red-green-blue color model
RSD	Relative standard deviation
RTC PAL	Robotic tool change prep and load autosampler
SBSE	Stir bar sorptive extraction
SDME	Single-drop microextraction
SFODME	Solidified floating organic droplet microextraction
SPDE	Solid-phase dynamic extraction
SPE	Solid-phase extraction
SPME	Solid-phase microextraction

Abbreviation	Definition
TDU	Thermal desorption unit
TF-SPME	Thin-film solid-phase microextraction
TOFMS	Time-of-flight mass spectrometer
USEPA	United States Environmental Protection Agency
USGS	United States Geological Survey
VALLME	Vortex-assisted liquid-liquid microextraction

9.3 List of figures

9.4 List of tables

9.5 References

1. Dimzon IKD, Morata AS, Müller J, Yanela RK, Lebertz S, Weil H, Perez TR, Müller J, Dayrit FM, Knepper TP. Trace organic chemical pollutants from the lake waters of San Pablo City, Philippines by targeted and non-targeted analysis. Sci Total Environ. 2018;639:588-95.
2. Beckers L-M, Brack W, Dann JP, Krauss M, Müller E, Schulze T. Unraveling longitudinal pollution patterns of organic micropollutants in a river by non-target screening and cluster analysis. Sci Total Environ. 2020;727:138388.
3. Rethmeier J, Neumann G, Stumpf C, Rabenstein A, Vogt C. Determination of low thiourea concentrations in industrial process water and natural samples using reversed-phase high-performance liquid chromatography. J Chromatogr A. 2001;934:129-34.
4. Gago-Ferrero P, Schymanski EL, Bletsou AA, Aalizadeh R, Hollender J, Thomaidis NS. Extended Suspect and Non-Target Strategies to Characterize Emerging Polar Organic Contaminants in Raw Wastewater with LC-HRMS/MS. Environ Sci Technol. 2015;49:12333-41.
5. Directive 2000/60/EC of the European Parliament and of the Council of 23 October 2000 establishing a framework for Community action in the field of water policy. 2000.
6. Directive 2010/75/EU of the European Parliament and of the Council of 24 November 2010 on industrial emissions (integrated pollution prevention and control). 2010.
7. Menon A, Lyng JG. Circular bioeconomy solutions: driving anaerobic digestion of waste streams towards production of high value medium chain fatty acids. Rev Environ Sci Biotechnol. 2021;20:189-208.
8. Hassan AH, Mietzel T, Brunstermann R, Schmuck S, Schoth J, Küppers M, Widmann R. Fermentative hydrogen production from low-value substrates. World J Microbiol Biotechnol. 2018;34:1-11.
9. Lourenço ND, Lopes JA, Almeida CF, Sarraguça MC, Pinheiro HM. Bioreactor monitoring with spectroscopy and chemometrics: a review. Anal Bioanal Chem. 2012;404:1211-37.
10. Farris RD. Methyl-Esters in the Fatty-Acid Industry. J Am Oil Chem Soc. 1979;56:770-73.
11. Suresh A, Praveenkumar R, Thangaraj R, Oscar FL, Baldev E, Dhanasekaran D, Thajuddin N. Microalgal fatty acid methyl ester a new source of bioactive compounds with antimicrobial activity. Asian Pac J Trop Dis. 2014;4:979-84.
12. Zonta Ž, Alves MM, Flotats X, Palatsi J. Modelling inhibitory effects of long chain fatty acids in the anaerobic digestion process. Water Res 2013;47:1369-80.
13. Alves MM, Pereira MA, Sousa DZ, Cavaleiro AJ, Picavet M, Smidt H, Stams AJ. Waste lipids to energy: how to optimize methane production from long-chain fatty acids (LCFA). Microb Biotechnol. 2009;2:538-50.
14. United States Environmental Protection Agency. Method 8272: Parent and alkyl polycyclic aromatics in sediment pore water by solid-phase microextraction and gas chromatography/mass spectrometry in selected ion monitoring mode. 2007
15. Water Quality - Determination of short-chain polychlorinated alkanes (SCCP) in water - Method using gas chromatography-mass spectrometry (GC-MS) and negative-ion chemical ionization (NCI) - (ISO 12010:2019), (2019).
16. Arthur CL, Pawliszyn J. Solid phase microextraction with thermal desorption using fused silica optical fibers. Anal Chem. 1990;62:2145-8.

17. Tobiszewski M, Mechlińska A, Zygmunt B, Namieśnik J. Green analytical chemistry in sample preparation for determination of trace organic pollutants. TrAC Trends Anal Chem. 2009;28:943-51.
18. Tobiszewski M, Mechlinska A, Namiesnik J. Green analytical chemistry-theory and practice. Chem Soc Rev. 2010;39:2869-78.
19. Kokosa JM, Przyjazny A. Green microextraction methodologies for sample preparations. Green Anal Chem. 2022;3:100023.
20. Lorenzo-Parodi N, Kaziur W, Stojanović N, Jochmann MA, Schmidt TC. Solventless microextraction techniques for water analysis. TrAC Trends Anal Chem. 2019;113:321-31.
21. Trujillo-Rodríguez MJ, Pacheco-Fernández I, Taima-Mancera I, Díaz JHA, Pino V. Evolution and current advances in sorbent-based microextraction configurations. J Chromatogr A. 2020;1634
22. Souza ID, Oliveira IGC, Queiroz MEC. Innovative extraction materials for fiber-in-tube solid phase microextraction: A review. Anal Chim Acta. 2021;1165
23. Piri-Moghadam H, Alam MN, Pawliszyn J. Review of geometries and coating materials in solid phase microextraction: Opportunities, limitations, and future perspectives. Anal Chim Acta. 2017;984:42-65.
24. Loussala HM, Feng J, Han S, Sun M, Ji X, Li C, Fan J, Pei M. Carbon nanotubes functionalized mesoporous silica for in-tube solid-phase microextraction of polycyclic aromatic hydrocarbons. J Sep Sci. 2020;43:3275-84.
25. Juanjuan F, Xiangping J, Chunying L, Mingxia S, Sen H, Jiaqing F, Haili S, Yang F, Minw S. Recent advance of new sample preparation materials in the analysis and detection of environmental pollutants. Chin J Chromatogr (Se Pu). 2021;39:781-801.
26. Feng J, Han S, Ji X, Li C, Wang X, Tian Y, Sun M. A green extraction material - natural cotton fiber for in-tube solid-phase microextraction. J Sep Sci. 2019;42:1051-7.
27. Feng J, Feng J, Loussala HM, Han S, Ji X, Li C, Sun H, Sun M. Dendritic mesoporous silica nanospheres@porous carbon for in-tube solid-phase microextraction to detect polycyclic aromatic hydrocarbons in tea beverages. Food Chem. 2021;364
28. Zhang YP, Luan CC, Lu ZY, Chen N, Zhang YJ, Cui CX. Brass wires with different surface wettability used for in-tube solid-phase microextraction. J Chromatogr A. 2022;1670
29. Pereira I, Rodrigues MF, Chaves AR, Vaz BG. Molecularly imprinted polymer (MIP) membrane assisted direct spray ionization mass spectrometry for agrochemicals screening in foodstuffs. Talanta. 2018;178:507-14.
30. Ouyang G, Vuckovic D, Pawliszyn J. Nondestructive Sampling of Living Systems Using in Vivo Solid-Phase Microextraction. Chem Rev. 2011;111:2784-814.
31. Yu J, Xu X-B, Murtada K, Pawliszyn J. Untargeted analysis of microbial metabolites and unsaturated fatty acids in salmon via hydrophilic-lipophilic balanced solid-phase microextraction arrow. Food Chem. 2022;380:132219.
32. Brereton RG, Jansen J, Lopes J, Marini F, Pomerantsev A, Rodionova O, Roger JM, Walczak B, Tauler R. Chemometrics in analytical chemistry—part I: history, experimental design and data analysis tools. Anal Bioanal Chem. 2017;409:5891-9.
33. Ferreira SLC, Bruns RE, Ferreira HS, Matos GD, David JM, Brandão GC, da Silva EGP, Portugal LA, dos Reis PS, Souza AS, dos Santos WNL. Box-Behnken design: An alternative for the optimization of analytical methods. Anal Chim Acta. 2007;597:179-86.
34. Anastas P, Warner JTC. Green chemistry: theory and practice. Oxford University Press; 1998. 1394013941 p.

35. Anastas PT. Green chemistry and the role of analytical methodology development. Crit Rev Anal Chem. 1999;29:167-75.
36. Koel M, Kaljurand M. Application of the principles of green chemistry in analytical chemistry. Pure Appl Chem. 2006;78:1993-2002.
37. Welch CJ, Wu N, Biba M, Hartman R, Brkovic T, Gong X, Helmy R, Schafer W, Cuff J, Pirzada Z. Greening analytical chromatography. TrAC Trends Anal Chem. 2010;29:667-80.
38. Spietelun A, Marcinkowski Ł, de la Guardia M, Namieśnik J. Recent developments and future trends in solid phase microextraction techniques towards green analytical chemistry. J Chromatogr A. 2013;1321:1-13.
39. Pena-Pereira F, Lavilla I, Bendicho C. Liquid-phase microextraction techniques within the framework of green chemistry. TrAC Trends Anal Chem. 2010;29:617-28.
40. Gałuszka A, Migaszewski Z, Namieśnik J. The 12 principles of green analytical chemistry and the SIGNIFICANCE mnemonic of green analytical practices. TrAC Trends Anal Chem. 2013;50:78-84.
41. Armenta S, Garrigues S, de la Guardia M. Green analytical chemistry. TrAC Trends Anal Chem. 2008;27:497-511.
42. Keith LH, Gron LU, Young JL. Green analytical methodologies. Chem Rev. 2007;107:2695-708.
43. Gałuszka A, Migaszewski ZM, Konieczka P, Namieśnik J. Analytical Eco-Scale for assessing the greenness of analytical procedures. TrAC Trends Anal Chem. 2012;37:61-72.
44. Płotka-Wasylka J. A new tool for the evaluation of the analytical procedure: Green Analytical Procedure Index. Talanta. 2018;181:204-9.
45. Płotka-Wasylka J, Wojnowski W. Complementary green analytical procedure index (ComplexGAPI) and software. Green Chem. 2021;23:8657-65.
46. Pena-Pereira F, Wojnowski W, Tobiszewski M. AGREE—Analytical GREEnness metric approach and software. Anal Chem. 2020;92:10076-82.
47. Pena-Pereira F, Tobiszewski M, Wojnowski W, Psillakis E. A Tutorial on AGREEprep an Analytical Greenness Metric for Sample Preparation. Adv Sample Prep
2022;3:100025.
48. Wojnowski W, Tobiszewski M, Pena-Pereira F, Psillakis E. AGREEprep – Analytical greenness metric for sample preparation. TrAC Trends Anal Chem. 2022;149:116553.
49. Koel M. Do we need Green Analytical Chemistry? Green Chem. 2016;18:923-31.
50. Nowak PM, Kościelniak P. What Color Is Your Method? Adaptation of the RGB Additive Color Model to Analytical Method Evaluation. Anal Chem 2019;91:10343-52.
51. Nowak PM, Wietecha-Posłuszny R, Pawliszyn J. White Analytical Chemistry: An approach to reconcile the principles of Green Analytical Chemistry and functionality. TrAC Trends Anal Chem. 2021;138:116223.
52. Batt WG, Alber HK. Systematic Qualitative Organic Microanalysis. Ind Eng Chem Anal Ed. 1941;13:127-32.
53. Pawliszyn J. Applications of solid phase microextraction. Royal Society of Chemistry; 1999.
54. Pawliszyn J. Solid phase microextraction: theory and practice. Wiley-VCH; 1997.
55. Sarafraz-Yazdi A, Amiri A. Liquid-phase microextraction. TrAC Trends Anal Chem. 2010;29:1-14.

56. Psillakis E. The effect of vacuum: an emerging experimental parameter to consider during headspace microextraction sampling. Anal Bioanal Chem. 2020;412:5989-97.
57. Williams DBG, George MJ, Meyer R, Marjanovic L. Bubbles in Solvent Microextraction: The Influence of Intentionally Introduced Bubbles on Extraction Efficiency. Anal Chem. 2011;83:6713-6.
58. Mascrez S, Purcaro G. Exploring multiple-cumulative trapping solid-phase microextraction for olive oil aroma profiling. J Sep Sci. 2020;43:1934-41.
59. Fu C, Li Z, Sun Z, Xie S. A review of salting-out effect and sugaring-out effect: driving forces for novel liquid-liquid extraction of biofuels and biochemicals. Front Chem Sci Eng. 2021;15:854-71.
60. Endo S, Pfennigsdorff A, Goss K-U. Salting-out effect in aqueous NaCl solutions: trends with size and polarity of solute molecules. Environ Sci Technol. 2012;46:1496-503.
61. Zimmermann T, Ensinger WJ, Schmidt TC. Depletion solid-phase microextraction for the evaluation of fiber-sample partition coefficients of pesticides. J Chromatogr A. 2006;1102:51-9.
62. Płotka-Wasylka J, Rutkowska M, Owczarek K, Tobiszewski M, Namieśnik J. Extraction with environmentally friendly solvents. TrAC Trends Anal Chem. 2017;91:12-25.
63. Tobiszewski M. Analytical chemistry with biosolvents. Anal Bioanal Chem. 2019;411:4359-64.
64. Chen Y, Mu T. Revisiting greenness of ionic liquids and deep eutectic solvents. Green Chem Eng. 2021;2:174-86.
65. Winterton N. The green solvent: a critical perspective. Clean Technol Environ Policy. 2021;23:2499-522.
66. Alexovič M, Horstkotte B, Solich P, Sabo J. Automation of static and dynamic non-dispersive liquid phase microextraction. Part 1: Approaches based on extractant drop-, plug-, film- and microflow-formation. Anal Bioanal Chem. 2016;906:22-40.
67. Alexovic M, Horstkotte B, Solich P, Sabo J. Automation of static and dynamic non-dispersive liquid phase microextraction. Part 2: Approaches based on impregnated membranes and porous supports. Anal Chim Acta. 2016;907:18-30.
68. Alexovič M, Horstkotte B, Šrámková I, Solich P, Sabo J. Automation of dispersive liquid–liquid microextraction and related techniques. Approaches based on flow, batch, flow-batch and in-syringe modes. TrAC Trends Anal Chem. 2017;86:39-55.
69. Carasek E, Merib J, Mafra G, Spudeit D. A recent overview of the application of liquid-phase microextraction to the determination of organic micro-pollutants. TrAC Trends Anal Chem. 2018;108:203-9.
70. Jeannot MA, Cantwell FF. Solvent Microextraction into a Single Drop. Anal Chem. 1996;68:2236-40.
71. Liu S, Dasgupta PK. Liquid Droplet. A Renewable Gas Sampling Interface. Anal Chem. 1995;67:2042-9.
72. Wang X, Yuan K, Liu H, Lin L, Luan T. Fully automatic exposed and in-syringe dynamic single-drop microextraction with online agitation for the determination of polycyclic musks in surface waters of the Pearl River Estuary and South China Sea. J Sep Sci. 2014;37:1842-9.
73. Mafra G, Vieira AA, Merib J, Anderson JL, Carasek E. Single drop microextraction in a 96-well plate format: A step toward automated and high-throughput analysis. Anal Chim Acta. 2019;1063:159-66.

74. Giordano BC, Burgi DS, Hart SJ, Terray A. On-line sample pre-concentration in microfluidic devices: A review. Anal Chim Acta. 2012;718:11-24.
75. Carasek E, Merib J. Membrane-based microextraction techniques in analytical chemistry: A review. Anal Chim Acta. 2015;880:8-25.
76. Mafra G, Birk L, Scheid C, Eller S, Brognoli R, de Oliveira TF, Carasek E, Merib J. A straightforward and semiautomated membrane-based method as efficient tool for the determination of cocaine and its metabolites in urine samples using liquid chromatography coupled to quadrupole time-of-flight-mass spectrometry. J Chromatogr A. 2020;1621:461088.
77. Gjelstad A, Rasmussen KE, Parmer MP, Pedersen-Bjergaard S. Parallel artificial liquid membrane extraction: micro-scale liquid–liquid–liquid extraction in the 96-well format. Bioanalysis. 2013;5:1377-85.
78. Hansen FA, Pedersen-Bjergaard S. Electromembrane extraction – looking closer into the liquid membrane. Adv Sample Prep. 2022;2
79. Lemos VA, Barreto JA, Santos LB, de Assis RDS, Novaes CG, Cassella RJ. In-syringe dispersive liquid-liquid microextraction. Talanta. 2022;238:123002.
80. Viñas P, Campillo N, Andruch V. Recent achievements in solidified floating organic drop microextraction. TrAC Trends Anal Chem. 2015;68:48-77.
81. Jalili V, Barkhordari A, Ghiasvand A. A comprehensive look at solid-phase microextraction technique: A review of reviews. Microchem J. 2020;152:104319.
82. Ouyang G, Pawliszyn J. A critical review in calibration methods for solid-phase microextraction. Anal Chim Acta. 2008;627:184-97.
83. Maruya KA, Zeng EY, Tsukada D, Bay SM. A passive sampler based on solid-phase microextraction for quantifying hydrophobic organic contaminants in sediment pore water. Environ Toxicol Chem. 2009;28:733-40.
84. Helin A, Ronkko T, Parshintsev J, Hartonen K, Schilling B, Laubli T, Riekkola ML. Solid phase microextraction Arrow for the sampling of volatile amines in wastewater and atmosphere. J Chromatogr A. 2015;1426:56-63.
85. Raynie D. New Sample Preparation Products and Accessories. LC GC N Am. 2019;37
86. Wilcockson JB, Gobas FA. Thin-film solid-phase extraction to measure fugacities of organic chemicals with low volatility in biological samples. Environ Sci Technol. 2001;35:1425-31.
87. Baltussen E, Sandra P, David F, Cramers C. Stir bar sorptive extraction (SBSE), a novel extraction technique for aqueous samples: theory and principles. J Microcolumn Sep. 1999;11:737-47.
88. Godage NH, Gionfriddo E. A critical outlook on recent developments and applications of matrix compatible coatings for solid phase microextraction. TrAC Trends Anal Chem. 2019;111:220-8.
89. Kędziora-Koch K, Wasiak W. Needle-based extraction techniques with protected sorbent as powerful sample preparation tools to gas chromatographic analysis: Trends in application. J Chromatogr A. 2018;1565:1-18.
90. Moein MM, Abdel-Rehim A, Abdel-Rehim M. Microextraction by packed sorbent (MEPS). TrAC Trends Anal Chem. 2015;67:34-44.
91. Abdel-Rehim M. Microextraction by packed sorbent (MEPS): a tutorial. Anal Chim Acta. 2011;701:119-28.
92. Yang L, Said R, Abdel-Rehim M. Sorbent, device, matrix and application in microextraction by packed sorbent (MEPS): a review. J Chrom B. 2017;1043:33-43.
93. Trefz P, Kischkel S, Hein D, James ES, Schubert JK, Miekisch W. Needle trap micro-extraction for VOC analysis: Effects of packing materials and desorption parameters. J Chromatogr A. 2012;1219:29-38.

94. Jochmann MA, Yuan X, Schilling B, Schmidt TC. In-tube extraction for enrichment of volatile organic hydrocarbons from aqueous samples. J Chromatogr A. 2008;1179:96-105.
95. Laaks J, Jochmann MA, Schilling B, Schmidt TC. Optimization strategies of in-tube extraction (ITEX) methods. Anal Bioanal Chem. 2015;407:6827-38.
96. Xu L, Basheer C, Lee HK. Developments in single-drop microextraction. J Chromatogr A. 2007;1152:184-92.
97. Ouyang G, Zhao W, Pawliszyn J. Automation and optimization of liquid-phase microextraction by gas chromatography. J Chromatogr A. 2007;1138:47-54.
98. Paul S, Moon H. Drop-to-drop liquid-liquid extraction of DNA in an electrowetting-on-dielectric digital microfluidics. Biomicrofluidics. 2021;15:034110.
99. Zgoła-Grześkowiak A, Grześkowiak T. Dispersive liquid-liquid microextraction. TrAC Trends Anal Chem. 2011;30:1382-99.
100. Bruheim I, Liu X, Pawliszyn J. Thin-film microextraction. Anal Chem. 2003;75:1002-10.
101. Piri-Moghadam H, Gionfriddo E, Grandy JJ, Alam MN, Pawliszyn J. Development and validation of eco-friendly strategies based on thin film microextraction for water analysis. J Chromatogr A. 2018;1579:20-30.
102. Camino-Sánchez FJ, Rodríguez-Gómez R, Zafra-Gómez A, Santos-Fandila A, Vílchez JL. Stir bar sorptive extraction: Recent applications, limitations and future trends. Talanta. 2014;130:388-99.
103. Gilart N, Marcé RM, Borrull F, Fontanals N. New coatings for stir-bar sorptive extraction of polar emerging organic contaminants. TrAC Trends Anal Chem. 2014;54:11-23.
104. Musshoff F, Lachenmeier DW, Kroener L, Madea B. Automated headspace solid-phase dynamic extraction for the determination of amphetamines and synthetic designer drugs in hair samples. J Chromatogr A. 2002;958:231-8.
105. Lipinski J. Automated solid phase dynamic extraction - Extraction of organics using a wall coated syringe needle. Anal Bioanal Chem. 2001;369:57-62.
106. Zeinali S, Khalilzadeh M, Pawliszyn J. The evolution of needle-trap devices with focus on aerosol investigations. TrAC Trends Anal Chem. 2022;153:116643.
107. Betz JM, Brown PN, Roman MC. Accuracy, precision, and reliability of chemical measurements in natural products research. Fitoterapia. 2011;82:44-52.
108. United States Environmental Protection Agency. Method 604: Phenols. 1984
109. Buchholz KD, Pawliszyn J. Determination of phenols by solid-phase microextraction and gas chromatographic analysis. Environ Sci Technol. 1993;27:2844-8.
110. United States Environmental Protection Agency. Method 556: Determination of Carbonyl Compounds in Drinking Water by Pentafluorobenylhydroxylamine Derivatization and Capillary Gas Chromatography with Electron Capture Detection, Revision 1. 1998
111. Cancho B, Ventura F, Galceran T. Determination of aldehydes in drinking water using pentafluorobenzylhydroxylamine derivatization and solid-phase microextraction. J Chromatogr A. 2002;943:1-13.
112. United States Environmental Protection Agency. Method 552.3: Determination of Haloacetic Acids and Dalapon in Drinking Water by Liquid-Liquid Microextraction, Derivatization, and Gas Chromatography with Electron Capture Detection, Revision 1. 2003
113. Casas Ferreira AM, Fernández Laespada ME, Pérez Pavón JL, Moreno Cordero B. In situ derivatization coupled to microextraction by packed sorbent and gas

chromatography for the automated determination of haloacetic acids in chlorinated water. J Chromatogr A. 2013;1318:35-42.
114. Supriyadi, Suzuki M, Wu S, Tomita N, Fujita A, Watanabe N. Biogenesis of volatile methyl esters in snake fruit (Salacca edulis, Reinw) cv. Pondoh. Biosci Biotechnol Biochem. 2003;67:1267-71.
115. Seo EJ, Yeon YJ, Seo JH, Lee JH, Bongol JP, Oh Y, Park JM, Lim SM, Lee CG, Park JB. Enzyme/whole-cell biotransformation of plant oils, yeast derived oils, and microalgae fatty acid methyl esters into n-nonanoic acid, 9-hydroxynonanoic acid, and 1,9-nonanedioic acid. Bioresource Technol. 2018;251:288-94.
116. Yu GW, Wang XJ, Wang P, Zhao YP, Nie J, Li ZG, Fang XG, Lee MR. Dispersive Liquid-Liquid Microextraction Combined with Microwave Demulsification for Determination of FAME Residuals in Biodiesel Wastewater. J Chromatogr Sci. 2020;58:976-84.
117. Stavarache C, Vinatoru M, Nishimura R, Maeda Y. Fatty acids methyl esters from vegetable oil by means of ultrasonic energy. Ultrason Sonochem. 2005;12:367-72.
118. Musharraf SG, Ahmed MA, Zehra N, Kabir N, Choudhary MI, Rahman AU. Biodiesel production from microalgal isolates of southern Pakistan and quantification of FAMEs by GC-MS/MS analysis. Chem Cent J. 2012;6:149.
119. Quezada M, Buitron G, Moreno-Andrade I, Moreno G, Lopez-Marin LM. The use of fatty acid methyl esters as biomarkers to determine aerobic, facultatively aerobic and anaerobic communities in wastewater treatment systems. FEMS Microbiol Lett. 2007;266:75-82.
120. Pardo VL, Fagundes CAM, Caldas SS, Kurz MH, Clementin RM, D'Oca MGM, Primel EG. Development and Validation of a Method for the Determination of Fatty Acid Methyl Ester Contents in Tung Biodiesel and Blends. J Am Oil Chem Soc. 2012;89:631-37.
121. Yang Z, Hollebone BP, Wang Z, Yang C, Landriault M. Method development for fingerprinting of biodiesel blends by solid-phase extraction and gas chromatography-mass spectrometry. J Sep Sci. 2011;34:3253-64.
122. Lu Y, Harrington PB. Classification of bacteria by simultaneous methylation–solid phase microextraction and gas chromatography/mass spectrometry analysis of fatty acid methyl esters. Anal Bioanal Chem. 2010;397:2959-66.
123. Choi M, Lee S, Bae S. Analysis of fatty acid methyl ester in bio-liquid by hollow fiber-liquid phase microextraction. Anal Sci Technol. 2017;30:174-81.
124. Kremser A, Jochmann MA, Schmidt TC. PAL SPME Arrow-evaluation of a novel solid-phase microextraction device for freely dissolved PAHs in water. Anal Bioanal Chem. 2016;408:943-52.
125. Barreira LMF, Duporte G, Ronkko T, Parshintsev J, Hartonen K, Hyrsky L, Heikkinen E, Jussila M, Kulmala M, Riekkola ML. Field measurements of biogenic volatile organic compounds in the atmosphere using solid-phase microextraction Arrow. Atmos Meas Tech. 2018;11:881-93.
126. Song NE, Lee JY, Lee YY, Park JD, Jang HW. Comparison of headspace-SPME and SPME-Arrow-GC-MS methods for the determination of volatile compounds in Korean salt-fermented fish sauce. Appl Biol Chem. 2019;62:16.
127. Kaziur-Cegla W, Salemi A, Jochmann MA, Schmidt TC. Optimization and validation of automated solid-phase microextraction arrow technique for determination of phosphorus flame retardants in water. J Chromatogr A. 2020;1626:461349.
128. Armenta S, Garrigues S, Esteve-Turrillas FA, de la Guardia M. Green extraction techniques in green analytical chemistry. TrAC Trends Anal Chem. 2019;116:248-53.

129. Lorenzo-Parodi N, Kaziur W, Stojanovic N, Jochmann MA, Schmidt TC. Solventless microextraction techniques for water analysis. Trac-Trend Anal Chem. 2019;113:321-31.
130. Feldberg L, Schuster O, Elhanany E, Laskar O, Yitzhaki S, Gura S. Rapid and sensitive identification of ricin in environmental samples based on lactamyl agarose beads using LC-MS/MS (MRM). J Mass Spectrom. 2020;55:4482.
131. Commission Decision of 12 August 2002 implementing Council Directive 96/23/EC concerning the performance of analytical methods and the interpretation of results. Off J Eur Union. 2002.
132. OriginLab Corporation, Origin(Pro). 2020-9.7.0.188 ed. Northhampton, MA, USA, 2020.
133. United States Environmental Protection Agency. Definition and Procedure for the Determination of the Method Detection Limit, Revision 2. 2016
134. Hartig C. Rapid identification of fatty acid methyl esters using a multidimensional gas chromatography-mass spectrometry database. J Chromatogr A. 2008;1177:159-69.
135. Ulrich N, Endo S, Brown TN, Watanabe N, Bronner G, Abraham MH, Goss KU. UFZ-LSER database v 3.2.1 2017 http://www.ufz.de/lserd.
136. Mezcua M, Martinez-Uroz MA, Wylie PL, Fernandez-Alba AR. Simultaneous screening and target analytical approach by gas chromatography-quadrupole-mass spectrometry for pesticide residues in fruits and vegetables. J AOAC Int. 2009;92:1790-806.
137. Rayne S, Forest K. Carboxylic acid ester hydrolysis rate constants for food and beverage aroma compounds. Flavour Frag J. 2016;31:385-94.
138. Cha D, Liu M, Zeng Z, Hu X, Guan W. Analysis of fatty acids in sputum from patients with pulmonary tuberculosis using gas chromatography–mass spectrometry preceded by solid-phase microextraction and post-derivatization on the fiber. J Chromatogr A. 2009;1216:1450-7.
139. Lotti C, Rubert J, Fava F, Tuohy K, Mattivi F, Vrhovsek U. Development of a fast and cost-effective gas chromatography–mass spectrometry method for the quantification of short-chain and medium-chain fatty acids in human biofluids. Anal Bioanal Chem. 2017;409:5555-67.
140. Emrich J, Sprung R, Sammler J, Remberg G. Identification of fatty acid methyl esters (FAMEs) in postmortem tissue. A new marker of alcohol abuse? Forensic Sci Int. 1997;85:41-9.
141. Chowdhury TR, Dick RP. Standardizing methylation method during phospholipid fatty acid analysis to profile soil microbial communities. J Microbiol Methods. 2012;88:285-91.
142. Dong T, Yu L, Gao D, Yu X, Miao C, Zheng Y, Lian J, Li T, Chen S. Direct quantification of fatty acids in wet microalgal and yeast biomass via a rapid in situ fatty acid methyl ester derivatization approach. Appl Microbiol Biotechnol. 2015;99:10237-47.
143. Kindler R, Miltner A, Thullner M, Richnow H-H, Kästner M. Fate of bacterial biomass derived fatty acids in soil and their contribution to soil organic matter. Org Geochem. 2009;40:29-37.
144. Nawabi P, Bauer S, Kyrpides N, Lykidis A. Engineering Escherichia coli for biodiesel production utilizing a bacterial fatty acid methyltransferase. Appl Environ Microbiol. 2011;77:8052-61.
145. Yaşar D, Şevket G. α-tocopherol and Fatty acids of Spirulina platensis biomass in Glass panel bioreactor. Pak J Biol Sci. 2006;9:2901-4.

146. La Nasa J, Modugno F, Aloisi M, Lluveras-Tenorio A, Bonaduce I. Development of a GC/MS method for the qualitative and quantitative analysis of mixtures of free fatty acids and metal soaps in paint samples. Anal Chim Acta. 2018;1001:51-8.
147. Mkhize NT, Msagati TA, Mamba BB, Momba M. Determination of volatile fatty acids in wastewater by solvent extraction and gas chromatography. Phys Chem Earth. 2014;67:86-92.
148. Dunkel T, de León Gallegos EL, Schoensee CD, Hesse T, Jochmann M, Wingender J, Denecke M. Evaluating the influence of wastewater composition on the growth of Microthrix parvicella by GCxGC/qMS and real-time PCR. Water Res 2016;88:510-23.
149. Aleryani SL, Cluette-Brown JE, Khan ZA, Hasaba H, Lopez de Heredia L, Laposata M. Fatty acid methyl esters are detectable in the plasma and their presence correlates with liver dysfunction. Clin Chim Acta. 2005;359:141-9.
150. Guo L, Zeng X-Y, Wang D-Y, Li G-Q. Methanol metabolism in the Asian corn borer, Ostrinia furnacalis (Guenée)(Lepidoptera: Pyralidae). J Insect Physiol. 2010;56:260-5.
151. Desbois AP, Smith VJ. Antibacterial free fatty acids: activities, mechanisms of action and biotechnological potential. Appl Microbiol Biotechnol. 2010;85:1629-42.
152. Miao X, Wu Q. Biodiesel production from heterotrophic microalgal oil. Bioresour Technol. 2006;97:841-6.
153. Zhang H, Wang Z, Liu O. Development and validation of a GC–FID method for quantitative analysis of oleic acid and related fatty acids. J Pharm Anal. 2015;5:223-30.
154. Ferreira AMC, Laespada MEF, Pavón JLP, Cordero BM. In situ aqueous derivatization as sample preparation technique for gas chromatographic determinations. J Chromatogr A. 2013;1296:70-83.
155. Sarrión M, Santos F, Galceran M. In situ derivatization/solid-phase microextraction for the determination of haloacetic acids in water. Anal Chem. 2000;72:4865-73.
156. Araujo L, Wild J, Villa N, Camargo N, Cubillan D, Prieto A. Determination of anti-inflammatory drugs in water samples, by in situ derivatization, solid phase microextraction and gas chromatography–mass spectrometry. Talanta. 2008;75:111-5.
157. Li N, Deng C, Zhang X. Determination of methylmalonic acid and glutaric acid in urine by aqueous-phase derivatization followed by headspace solid-phase microextraction and gas chromatography-mass spectrometry. J Sep Sci. 2007;30:266-71.
158. Cartoni G, Liberti A, Pela A. Gas chromatographic separation of polar isotopic molecules. Anal Chem. 1967;39:1618-22.
159. Shi B, Davis BH. Gas chromatographic separation of pairs of isotopic molecules. J Chromatogr A. 1993;654:319-25.
160. Thakur N, Aslani S, Armstrong DW. Evaluation of gas chromatography for the separation of a broad range of isotopic compounds. Anal Chim Acta. 2021;1165:338490.
161. Meier-Augenstein W. Stable isotope analysis of fatty acids by gas chromatography–isotope ratio mass spectrometry. Anal Chim Acta. 2002;465:63-79.
162. Scheiner S. Calculation of isotope effects from first principles. Biochim Biophys Acta Bioenerg. 2000;1458:28-42.
163. Tintrop LK, Jochmann MA, Beesley T, Küppers M, Brunstermann R, Schmidt TC. Optimization and automation of rapid and selective analysis of fatty acid methyl

esters from aqueous samples by headspace SPME arrow extraction followed by GC–MS/MS analysis. Anal Bioanal Chem. 2022
164. Liu Y, Lotero E, Goodwin Jr JG. Effect of carbon chain length on esterification of carboxylic acids with methanol using acid catalysis. J Catal. 2006;243:221-8.
165. Musharraf SG, Ahmed MA, Zehra N, Kabir N, Choudhary MI, Rahman A-u. Biodiesel production from microalgal isolates of southern Pakistan and quantification of FAMEs by GC-MS/MS analysis. 2012;6:149.
166. Tintrop LK, Salemi A, Jochmann MA, Engewald WR, Schmidt TC. Improving greenness and sustainability of standard analytical methods by microextraction techniques: A critical review. Anal Chim Acta. 2023:341468.
167. López-Lorente ÁI, Pena-Pereira F, Pedersen-Bjergaard S, Zuin VG, Ozkan SA, Psillakis E. The ten principles of green sample preparation. TrAC Trends Anal Chem. 2022;148:116530.
168. Souza-Silva ÉA, Jiang R, Rodríguez-Lafuente A, Gionfriddo E, Pawliszyn J. A critical review of the state of the art of solid-phase microextraction of complex matrices I. Environmental analysis. TrAC Trends Anal Chem. 2015;71:224-35.
169. Souza-Silva ÉA, Gionfriddo E, Pawliszyn J. A critical review of the state of the art of solid-phase microextraction of complex matrices II. Food analysis. TrAC Trends Anal Chem. 2015;71:236-48.
170. Souza-Silva ÉA, Reyes-Garcés N, Gómez-Ríos GA, Boyacı E, Bojko B, Pawliszyn J. A critical review of the state of the art of solid-phase microextraction of complex matrices III. Bioanalytical and clinical applications. TrAC Trends Anal Chem. 2015;71:249-64.
171. Ventanas S, Ruiz J. On-site analysis of volatile nitrosamines in food model systems by solid-phase microextraction coupled to a direct extraction device. Talanta. 2006;70:1017-23.
172. Reichardt C, Welton T. Solvents and solvent effects in organic chemistry. John Wiley & Sons; 2011.
173. Katritzky AR, Fara DC, Yang H, Tämm K, Tamm T, Karelson M. Quantitative Measures of Solvent Polarity. Chem Rev. 2004;104:175-98.
174. Junior VRA, Goméz-Ríos GA, Tascon M, Queiroz MEC, Pawliszyn J. Analysis of endocannabinoids in plasma samples by biocompatible solid-phase microextraction devices coupled to mass spectrometry. Anal Chim Acta. 2019;1091:135-45.
175. Murtada K, Nazdrajić E, Pawliszyn J. Performance Evaluation of Extraction Coatings with Different Sorbent Particles and Binder Composition. Anal Chem. 2023;95:12745-53.
176. Buchholz KD, Pawliszyn J. Optimization of solid-phase microextraction conditions for determination of phenols. Anal Chem. 1994;66:160-7.
177. Llompart Ma, Lourido M, Landín P, García-Jares C, Cela R. Optimization of a derivatization–solid-phase microextraction method for the analysis of thirty phenolic pollutants in water samples. J Chromatogr A. 2002;963:137-48.
178. MacBean C. Lindane. e-Pesticide manual. 2010
179. McManus S-L, Coxon CE, Richards KG, Danaher M. Quantitative solid phase microextraction – Gas chromatography mass spectrometry analysis of the pesticides lindane, heptachlor and two heptachlor transformation products in groundwater. J Chromatogr A. 2013;1284:1-7.
180. Directive 2013/39/EU of the European Parliament and the Council of 12. August 2013 amending Directives 2000/60/EC and 2008/105/EC as regards priority substances in the field of water policy. Off J Eur Union. 2013
181. United States Environmental Protection Agency. United States Code - Clean Water Act - Title 33: Navigation and navigable waters. 2021.

182. United States Environmental Protection Agency. Code of Federal Regulations - 401.15 Toxic pollutants. 2023.
183. Daughton CG. Non-regulated water contaminants: emerging research. Environ Impact Assess Rev. 2004;24:711-32.
184. Brunner AM, Bertelkamp C, Dingemans MML, Kolkman A, Wols B, Harmsen D, Siegers W, Martijn BJ, Oorthuizen WA, ter Laak TL. Integration of target analyses, non-target screening and effect-based monitoring to assess OMP related water quality changes in drinking water treatment. Sci Total Environ. 2020;705:135779.
185. Schollée JE, Bourgin M, von Gunten U, McArdell CS, Hollender J. Non-target screening to trace ozonation transformation products in a wastewater treatment train including different post-treatments. Water Res. 2018;142:267-78.
186. Xu H, Jia Y, Sun Z, Su J, Liu QS, Zhou Q, Jiang G. Environmental pollution, a hidden culprit for health issues. Eco Environ Health. 2022;1:31-45.
187. González-Gaya B, Lopez-Herguedas N, Bilbao D, Mijangos L, Iker A, Etxebarria N, Irazola M, Prieto A, Olivares M, Zuloaga O. Suspect and non-target screening: the last frontier in environmental analysis. Anal Methods. 2021;13:1876-904.
188. Hollender J, Schymanski EL, Ahrens L, Alygizakis N, Béen F, Bijlsma L, Brunner AM, Celma A, Fildier A, Fu Q, Gago-Ferrero P, Gil-Solsona R, Haglund P, Hansen M, Kaserzon S, Kruve A, Lamoree M, Margoum C, Meijer J, Merel S, Rauert C, Rostkowski P, Samanipour S, Schulze B, Schulze T, Singh RR, Slobodnik J, Steininger-Mairinger T, Thomaidis NS, Togola A, Vorkamp K, Vulliet E, Zhu L, Krauss M. NORMAN guidance on suspect and non-target screening in environmental monitoring. Environ Sci Eur. 2023;35:75.
189. Menger F, Gago-Ferrero P, Wiberg K, Ahrens L. Wide-scope screening of polar contaminants of concern in water: A critical review of liquid chromatography-high resolution mass spectrometry-based strategies. Trends Environ Anal Chem. 2020;28:e00102.
190. Lee S, Kim K, Jeon J, Moon H-B. Optimization of suspect and non-target analytical methods using GC/TOF for prioritization of emerging contaminants in the Arctic environment. Ecotoxicol Environ Saf. 2019;181:11-7.
191. Jiang J, Zhao J, Zhao G, Liu L, Song H, Liao S. Recognition, possible source, and risk assessment of organic pollutants in surface water from the Yongding River Basin by non-target and target screening. Environ Pollut. 2023;331:121895.
192. Domínguez I, Arrebola FJ, Martínez Vidal JL, Garrido Frenich A. Assessment of wastewater pollution by gas chromatography and high resolution Orbitrap mass spectrometry. J Chromatogr A. 2020;1619:460964.
193. Wei J, Xiang L, Cai Z. Emerging environmental pollutants hydroxylated polybrominated diphenyl ethers: From analytical methods to toxicology research. Mass Spectrom Rev. 2021;40:255-79.
194. The NIST Mass Spectral Search Program for the NIST/EPA/NIH EI and NIST Tandem Mass Spectral Library, Standard Reference Database 1. Gaithersburg, MD, USA: National Institute of Standards and Technology; 2020.
195. Hejazi L, Ebrahimi D, Hibbert DB, Guilhaus M. Compatibility of electron ionization and soft ionization methods in gas chromatography/orthogonal time-of-flight mass spectrometry. Rapid Commun Mass Spectrom. 2009;23:2181-9.
196. Bräkling S, Kroll K, Stoermer C, Rohner U, Gonin M, Benter T, Kersten H, Klee S. Parallel Operation of Electron Ionization and Chemical Ionization for GC–MS Using a Single TOF Mass Analyzer. Anal Chem. 2022;94:6057-64.
197. Bräkling S, Hinterleitner C, Cappellin L, Vetter M, Mayer I, Benter T, Klee S, Kersten H. Gas chromatography coupled to time-of-flight mass spectrometry using parallel electron and chemical ionization with permeation tube facilitated reagent ion

control for material emission analysis. Rapid Commun Mass Spectrom. 2023;37:e9461.
198. Kloskowski A, Chrzanowski W, Pilarczyk M, Namiesnik J. Modern Techniques of Sample Preparation for Determination of Organic Analytes by Gas Chromatography. Crit Rev Anal Chem. 2007;37:15-38.
199. Domínguez I, Arrebola FJ, Romero-González R, Nieto-García A, Martínez Vidal JL, Garrido Frenich A. Solid phase microextraction and gas chromatography coupled to magnetic sector high resolution mass spectrometry for the ultra-trace determination of contaminants in surface water. J Chromatogr A. 2017;1518:15-24.
200. Ochiai N, Ieda T, Sasamoto K, Takazawa Y, Hashimoto S, Fushimi A, Tanabe K. Stir bar sorptive extraction and comprehensive two-dimensional gas chromatography coupled to high-resolution time-of-flight mass spectrometry for ultra-trace analysis of organochlorine pesticides in river water. J Chromatogr A. 2011;1218:6851-60.
201. Grandy JJ, Singh V, Lashgari M, Gauthier M, Pawliszyn J. Development of a Hydrophilic Lipophilic Balanced Thin Film Solid Phase Microextraction Device for Balanced Determination of Volatile Organic Compounds. Anal Chem. 2018;90:14072-80.
202. Purschke K, Vosough M, Leonhardt J, Weber M, Schmidt TC. Evaluation of Nontarget Long-Term LC–HRMS Time Series Data Using Multivariate Statistical Approaches. Anal Chem. 2020;92:12273-81.
203. Schymanski EL, Jeon J, Gulde R, Fenner K, Ruff M, Singer HP, Hollender J. Identifying Small Molecules via High Resolution Mass Spectrometry: Communicating Confidence. Environ Sci Technol. 2014;48:2097-8.
204. Rebryk A, Haglund P. Non-targeted screening workflows for gas chromatography–high-resolution mass spectrometry analysis and identification of biomagnifying contaminants in biota samples. Anal Bioanal Chem. 2021;413:479-501.
205. European Chemicals Agency - Information on Chemicals European Union. https://echa.europa.eu.
206. Munson B. Encyclopedia of Analytical Chemistry - Chemical Ionization Mass Spectrometry: Theory and Applications.
207. Hunter EPL, Lias SG. Evaluated Gas Phase Basicities and Proton Affinities of Molecules: An Update. J Phys Chem Ref. 1998;27:413-656.
208. Thoben C, Werres T, Henning I, Simon PR, Zimmermann S, Schmidt TC, Teutenberg T. Towards a miniaturized on-site nano-high performance liquid chromatography electrospray ionization ion mobility spectrometer with online enrichment. Green Anal Chem. 2022;1:100011.
209. Chen J, Zou J, Zeng J, Song X, Ji J, Wang Y, Ha J, Chen X. Preparation and evaluation of graphene-coated solid-phase microextraction fiber. Anal Chim Acta. 2010;678:44-9.
210. Dias AN, Simão V, Merib J, Carasek E. Cork as a new (green) coating for solid-phase microextraction: Determination of polycyclic aromatic hydrocarbons in water samples by gas chromatography–mass spectrometry. Anal Chim Acta. 2013;772:33-9.
211. Zhu W, Qin P, Han L, Zhang X, Li D, Li M, Wang Y, Zhang X, Lu M, Cai Z. Gas-cycle-assisted headspace solid-phase microextraction coupled with gas chromatography for rapid analysis of organic pollutants. Chem Comm. 2021;57:8810-3.
212. Poole JJ, Grandy JJ, Gómez-Ríos GA, Gionfriddo E, Pawliszyn J. Solid Phase Microextraction On-Fiber Derivatization Using a Stable, Portable, and Reusable

Pentafluorophenyl Hydrazine Standard Gas Generating Vial. Anal Chem. 2016;88:6859-66.
213. Sajid M, Płotka-Wasylka J. “Green” nature of the process of derivatization in analytical sample preparation. TrAC Trends Anal Chem. 2018;102:16-31.
214. Goss KU. Predicting the equilibrium partitioning of organic compounds using just one linear solvation energy relationship (LSER). Fluid Phase Equilibr. 2005;233:19-22.
215. Sprunger L, Proctor A, Acree WE, Abraham MH. Characterization of the sorption of gaseous and organic solutes onto polydimethyl siloxane solid-phase microextraction surfaces using the Abraham model. J Chromatogr A. 2007;1175:162-73.
216. Abraham MH, Andonian-Haftvan J, Whiting GS, Leo A, Taft RS. Hydrogen bonding. Part 34. The factors that influence the solubility of gases and vapours in water at 298 K, and a new method for its determination. J Chem Soc. 1994:1777-91.
217. Haynes WM. CRC Handbook of Chemistry and Physics; 2017.

9.6 Publications and presentations

9.6.1 List of publications in peer-reviewed journals

Ziefuß, A.R., Hupfeld, T., Meckelmann, S.W., Meyer, M., Schmitz, O.J., Kaziur-Cegla W., Tintrop, L. K., Schmidt, T. C., Gökce, B., Barcikowski, S. Ultrafast cold-brewing of coffee by picosecond-pulsed laser extraction. npj Science of Food. 2022.

Tintrop, L.K., Jochmann, M.A., Beesley, T., Küppers, M., Brunstermann, R., Schmidt, T.C. Optimization and automation of rapid and selective analysis of fatty acid methyl esters from aqueous samples by headspace SPME arrow extraction followed by GC-MS/MS analysis. Analytical and Bioanalytical Chemistry. 2022.

Fromme, T., Tintrop, L.K., Reichenberger, S., Schmidt, T.C., Barcikowski, S. Impact of Chemical and Physical Properties of Organic Solvents on the Gas and Hydrogen Formation during Laser Synthesis of Gold Nanoparticles. ChemPhysChem. 2023.

Tintrop, L.K., Salemi, A., Jochmann, M.A., Engewald, W.R., Schmidt, T.C. Improving greenness and sustainability of standard analytical methods by microextraction techniques: A critical review. Analytica Chimica Acta. 2023.

Tintrop, L.K., Lieske-Overgrand, J.R., Wickneswaran, K., Abis, R., Brunstermann, R., Jochmann, M.A., Schmidt, T.C. Isotope-labeling in situ derivatization and HS-SPME arrow GC-MS/MS for simultaneous determination of fatty acids and fatty acid methyl esters in aqueous matrices. Analytical and Bioanalytical Chemistry. 2023.

Tintrop, L. K., Solazzo, L., Salemi, A., Jochmann, M.A., Schmidt, T. C. Characterization of a hydrophilic-lipophilic balanced SPME material for enrichment of analytes with different polarities from aqueous samples. Advances in Sample Preparation. 2023.

9.6.2 List of publications in non-peer-reviewed journals

Tintrop, L.K., Engewald, W., Jochmann, M.A., Schmidt T.C. Schneller, grüner, besser - Trends in der Probenvorbereitung. Nachrichten aus der Chemie. 2022.

9.6.3 List of oral presentations

Tintrop, L. K., Jochmann, M. A., Schmidt, T. C., Optimization and automation of a rapid and selective analysis of fatty acid methyl esters from aqueous samples by headspace SPME arrow extraction followed by GC-MS/MS analysis. 32. Doktorandenseminar AK Separation Science, online, 01/11/2022

Tintrop, L. K., Bräkling, S., Vetter, M., Klee, S., Schmidt T. C., Non-target analysis of industrial wastewater samples by using GC-ecTOFMS. ec-TOF VIP-Tag TOFWERK, Thun, Switzerland, 11/05/2023

Tintrop, L.K., Lieske-Overgrand, J. R., Wickneswaran, K., Abis, R., Brunstermann, R., Jochmann, M., Schmidt, T. C., How to analyze fatty acids and fatty acid methyl esters in water samples simultaneously. 25th International Symposium on Advances in Extraction Technologies, Teneriffe, Spain, 20/07/2023

Tintrop, L. K., Bräkling, S., Vetter, M., Klee, S., Schmidt T. C., Non-target analysis of industrial wastewater samples by using GC-ecTOFMS. ec-TOF VIP-Tag TOFWERK, Bergische Universität Wuppertal, Germany, 28/09/2023

Tintrop, L. K., Bräkling, S., Vetter, M., Eßer, W., Drees, F., Salemi, A., Jochmann, M., Klee, S., Schmidt, T. C., Non-target analysis of industrial wastewater samples using HS-SPME and GC-TOFMS with parallel chemical and electron ionization. International Conference on Non-Target Screening, Erding, Germany, 18/10/2023

9.6.4 List of poster presentations

Tintrop, L. K., Jochmann, M. A., Schmidt, T. C., Optimization and automation of a rapid and selective analysis of fatty acid methyl esters from aqueous samples by headspace SPME arrow extraction followed by GC-MS/MS analysis. 1st European Sample Preparation e-conference, online, 11-12/03/2021

Tintrop, L.K., Lieske-Overgrand, J. R., Wickneswaran, K., Abis, R., Jochmann, M., Schmidt, T. C., Simultaneous Determination of Fatty Acids and Fatty Acid Methyl Esters by HS-SPME arrow GC-MS/MS. Mülheimer Wasseranalytisches Seminar, Mülheim, Germany, 14-15/09/2022

Tintrop, L.K., Lieske-Overgrand, J. R., Jochmann, M., Schmidt, T. C., Simultaneous Determination of Fatty Acids and Fatty Acid Methyl Esters by HS-SPME arrow GC-MS/MS. International Symposium on Chromatography, Budapest, Hungary, 18-22/09/2022

Tintrop, L.K., Lieske-Overgrand, J. R., Wickneswaran, K., Abis, R., Brunstermann, R., Jochmann, M., Schmidt, T. C., How to analyze fatty acids and fatty acid methyl esters in water samples simultaneously. ANAKON, Vienna, Austria, 11-14/04/2023

9.7 Declaration of scientific contribution

This thesis includes works that have been prepared, processed and written in collaboration with co-authors, hence the scientific contribution of each author is stated in the form of the Contributor Roles Taxonomy (CRediT).

Chapter 3

Lucie K. Tintrop, Amir Salemi, Maik A. Jochmann, Werner R. Engewald, Torsten C. Schmidt. Improving greenness and sustainability of standard analytical methods by microextraction techniques: A critical review. Analytica Chimica Acta. 2023.

CRediT: *Lucie K. Tintrop*: Conceptualization, Methodology, Software, Validation, Formal analysis, Investigation, Visualization, Writing – Original draft; *Amir Salemi, Maik A. Jochmann, Werner R. Engewald*: Resources, Writing – Review & editing; *Torsten C. Schmidt*: Resources, Supervision, Writing -Review & Editing, Project administration

Chapter 4

Lucie K. Tintrop, Maik A. Jochmann, Thomas Beesley, Marco Küppers, Ruth Brunstermann, Torsten C. Schmidt. Optimization and automation of rapid and selective analysis of fatty acid methyl esters from aqueous samples by headspace SPME arrow extraction followed by GC-MS/MS analysis. Analytical and Bioanalytical Chemistry. 2022.

CRediT: *Lucie K. Tintrop*: Conceptualization, Methodology, Software, Validation, Formal analysis, Investigation, Visualization, Writing – Original draft; *Maik A. Jochmann*: Resources, Writing – Review & editing; *Thomas Beesley*: Investigation, Formal analysis; *Marco Küppers*: Resources, Writing -Review & Editing; *Ruth*

Brunstermann: Supervision, Writing -Review & Editing; *Torsten C. Schmidt*: Supervision, Writing -Review & Editing, Project administration

Chapter 5

Lucie K. Tintrop, Jana R. Lieske-Overgrand, Kaliyani Wickneswaran, Rukiyye Abis, Ruth Brunstermann, Maik A. Jochmann, Torsten C. Schmidt. Isotope-labeling in situ derivatization and HS-SPME arrow GC-MS/MS for simultaneous determination of fatty acids and fatty acid methyl esters in aqueous matrices. Analytical and Bioanalytical Chemistry. 2023.

CRediT: *Lucie K. Tintrop*: Conceptualization, Methodology, Software, Validation, Formal analysis, Investigation, Visualization, Writing - original draft; *Jana R. Lieske-Overgrand*: Methodology, Software, Formal analysis, Investigation; *Kaliyani Wickneswaran*: Validation, Formal analysis, Investigation; *Rukiyye Abis*: Investigation; *Ruth Brunstermann*: Resources, Writing - review and editing; *Maik A. Jochmann*: Resources, Writing - review and editing; *Torsten C. Schmidt*: Supervision, Writing - review and editing, Project administration.

Chapter 6

Lucie K. Tintrop, Leonardo Solazzo, Amir Salemi, Maik A. Jochmann, Torsten C. Schmidt. Characterization of a hydrophilic-lipophilic balanced SPME material for enrichment of analytes with different polarities from aqueous samples. Advances in Sample Preparation. 2023.

CRediT: *Lucie K. Tintrop*: Conceptualization, Methodology, Software, Validation, Investigation, Visualization, Writing - Original draft; *Leonardo Solazzo*: Software, Formal analysis, Validation, Investigation, Visualization; *Amir Salemi, Maik A. Jochmann*: Resources, Writing - review and editing; *Torsten C. Schmidt*: Supervision, Writing - review and editing, Project administration.

Chapter 7

Lucie K. Tintrop, Steffen Bräkling, Marleen Vetter, Willi Eßer, Felix Drees, Amir Salemi, Maik A. Jochmann, Sonja Klee, Torsten C. Schmidt. Evaluation of GC-EI&CI-TOFMS for non-target analysis of wastewater using hydrophilic-lipophilic balanced SPME. Submitted to Analytical Chemistry. 2023.

CRediT: *Lucie K. Tintrop*: Conceptualization, Methodology, Software, Validation, Formal analysis, Investigation, Visualization, Writing - Original draft; *Steffen Bräkling*, *Marleen Vetter*: Conceptualization, Methodology, Software, Formal analysis, Validation, Investigation, Writing - review, and editing; *Willi Eßer*: Methodology, Software, Formal analysis, Validation, Investigation; *Felix Drees, Amir Salemi*: Resources, Writing - review and editing; *Maik A. Jochmann, Sonja Klee, Torsten C. Schmidt*: Supervision, Writing - review and editing, Project administration.

9.8 Curriculum vitae

Der Lebenslauf ist in der Online-Version aus Gründen des Datenschutzes nicht enthalten.

Der Lebenslauf ist in der Online-Version aus Gründen des Datenschutzes nicht enthalten.

9.9 Declaration

Hiermit versichere ich, dass ich die vorliegende Arbeit mit dem Titel

„Development of green sample preparation methods for the analysis of organic substances in aqueous matrices with gas chromatography mass spectrometry”

selbst verfasst, keine außer den angegebenen Hilfsmitteln und Quellen benutzt habe, alle wörtlich oder inhaltlich übernommenen Stellen als solche gekennzeichnet sind und die Arbeit in dieser oder ähnlicher Form noch bei keiner anderen Universität eingereicht wurde.

Essen, den 13.10.2023
Lucie Katharina Tintrop